frontiers | Research Topics

The mechanism of tumor evolution and microenvironmental changes of genitourinary oncology in clinical diagnosis and treatment

Edited by
Wen-Hao Xu, Housheng Hansen He, Philippe E. Spiess, Dingwei Ye and Hailiang Zhang

Published in
Frontiers in Oncology
Frontiers in Immunology

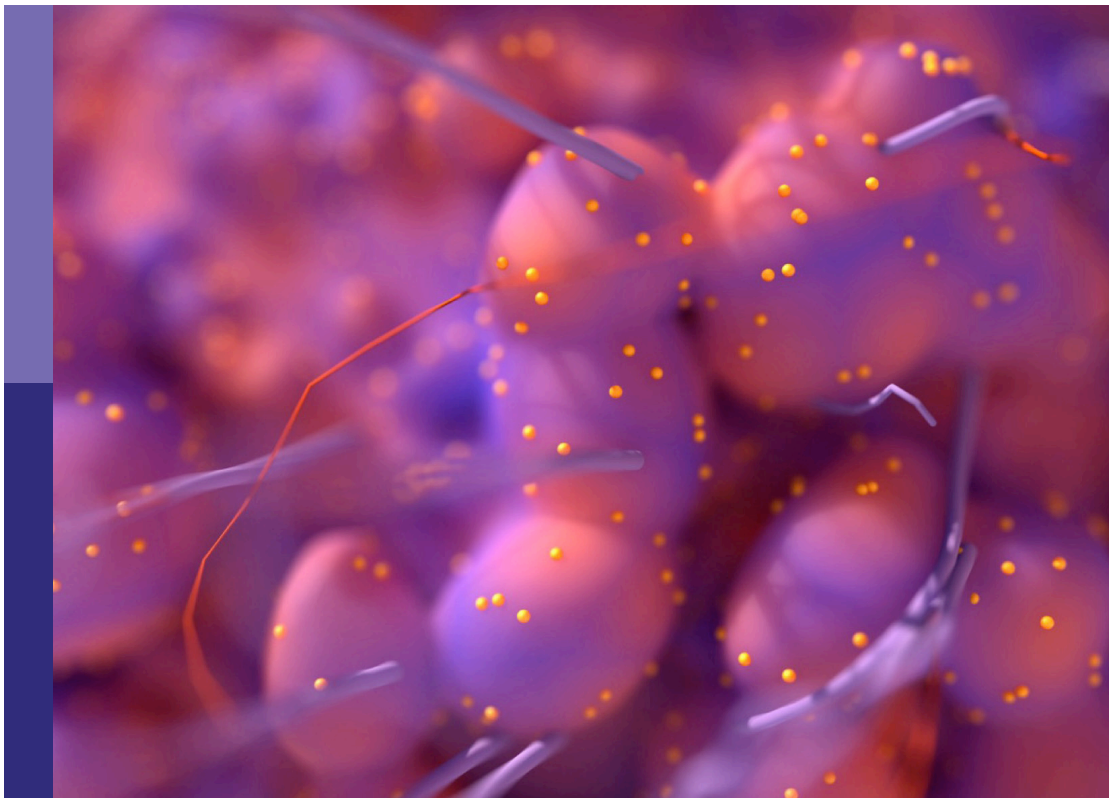

ISSN 1664-8714
ISBN 978-2-8325-3470-0
DOI 10.3389/978-2-8325-3470-0

About Frontiers

Frontiers is more than just an open access publisher of scholarly articles: it is a pioneering approach to the world of academia, radically improving the way scholarly research is managed. The grand vision of Frontiers is a world where all people have an equal opportunity to seek, share and generate knowledge. Frontiers provides immediate and permanent online open access to all its publications, but this alone is not enough to realize our grand goals.

Frontiers journal series

The Frontiers journal series is a multi-tier and interdisciplinary set of open-access, online journals, promising a paradigm shift from the current review, selection and dissemination processes in academic publishing. All Frontiers journals are driven by researchers for researchers; therefore, they constitute a service to the scholarly community. At the same time, the *Frontiers journal series* operates on a revolutionary invention, the tiered publishing system, initially addressing specific communities of scholars, and gradually climbing up to broader public understanding, thus serving the interests of the lay society, too.

Dedication to quality

Each Frontiers article is a landmark of the highest quality, thanks to genuinely collaborative interactions between authors and review editors, who include some of the world's best academicians. Research must be certified by peers before entering a stream of knowledge that may eventually reach the public - and shape society; therefore, Frontiers only applies the most rigorous and unbiased reviews. Frontiers revolutionizes research publishing by freely delivering the most outstanding research, evaluated with no bias from both the academic and social point of view. By applying the most advanced information technologies, Frontiers is catapulting scholarly publishing into a new generation.

What are Frontiers Research Topics?

Frontiers Research Topics are very popular trademarks of the *Frontiers journals series*: they are collections of at least ten articles, all centered on a particular subject. With their unique mix of varied contributions from Original Research to Review Articles, Frontiers Research Topics unify the most influential researchers, the latest key findings and historical advances in a hot research area.

Find out more on how to host your own Frontiers Research Topic or contribute to one as an author by contacting the Frontiers editorial office: frontiersin.org/about/contact

The mechanism of tumor evolution and microenvironmental changes of genitourinary oncology in clinical diagnosis and treatment

Topic editors

Wen-Hao Xu — Fudan University, China
Housheng Hansen He — University Health Network (UHN), Canada
Philippe E. Spiess — Moffitt Cancer Center, United States
Dingwei Ye — Fudan University, China
Hailiang Zhang — Fudan University, China

Citation

Xu, W.-H., He, H. H., Spiess, P. E., Ye, D., Zhang, H., eds. (2023). *The mechanism of tumor evolution and microenvironmental changes of genitourinary oncology in clinical diagnosis and treatment*. Lausanne: Frontiers Media SA.
doi: 10.3389/978-2-8325-3470-0

Table of contents

frontiers | Frontiers in Oncology

TYPE Editorial
PUBLISHED 29 August 2023
DOI 10.3389/fonc.2023.1272984

OPEN ACCESS

EDITED AND REVIEWED BY
Ronald M Bukowski,
Cleveland Clinic, United States

*CORRESPONDENCE
Hailiang Zhang
zhanghl918@alu.fudan.edu.cn
Dingwei Ye
dwyelie@163.com

RECEIVED 05 August 2023
ACCEPTED 11 August 2023
PUBLISHED 29 August 2023

CITATION
Lu J, Xu W-H, Zhang H and Ye D (2023) Editorial: The mechanism of tumor evolution and microenvironmental changes of genitourinary oncology in clinical diagnosis and treatment.
Front. Oncol. 13:1272984.
doi: 10.3389/fonc.2023.1272984

Editorial: The mechanism of tumor evolution and microenvironmental changes of genitourinary oncology in clinical diagnosis and treatment

Jiahe Lu[1,2,3], Wen-Hao Xu[1,2,3], Hailiang Zhang[1,2,3]* and Dingwei Ye[1,2,3]*

[1]Department of Urology, Fudan University Shanghai Cancer Center, Shanghai, China, [2]Department of Oncology, Shanghai Medical College, Fudan University, Shanghai, China, [3]Shanghai Genitourinary Cancer Institute, Shanghai, China

KEYWORDS

the tumor microenvironment (TME), genitourinary (GU), renal cell carcinoma (RCC), prostate adenocarcinoma (PRAD), bladder cancer (BCa)

Editorial on the Research Topic
The mechanism of tumor evolution and microenvironmental changes of genitourinary oncology in clinical diagnosis and treatment

The tumor microenvironment (TME) encompasses the immediate surroundings in which tumor cells undergo formation and progression. This includes the peritumoral blood vessels, immune cells, fibroblasts, bone marrow-derived inflammatory cells, diverse signaling chemicals, and extracellular matrix (ECM) (1). The tumor microenvironment is closely related to tumorigenesis and immune escape. Consequently, there has been a paradigm shift in cancer research and treatment, transitioning from a focus solely on cancer cells to a more comprehensive approach centered upon the TME. This Research Topic aims to have a thorough examination of the numerous interactions occurring between genitourinary tumor cells and their adjacent microenvironment in order to comprehend the diverse underlying mechanisms affecting genitourinary tumor diagnosis and treatment.

Renal cell carcinoma (RCC)

One of the defining characteristics of clear cell RCC (ccRCC) is the occurrence of deletion, mutation, and/or promoter methylation on chromosome 3p, resulting in the functional inactivation of the Von Hippel-Lindau (VHL) tumor suppressor gene. This inactivation subsequently leads to the abnormal accumulation of hypoxia-inducible factor (HIF) and the activation of the angiogenic pathway (2). Several additional genomic abnormalities have been identified in relation to disease progression and invasiveness. These include mutations in genes associated with the 3p region, namely PBRM1, SETD2, and BAP1. Additionally, deletions at the 9p21 locus can lead to the loss of CDKN2A and

CDKN2B genes. Furthermore, alterations in KDM5C, TP53, MTOR, or PTEN have also been found to be associated with the extent of disease progression and invasiveness (3). Pharmacological interventions for RCC encompass many approaches such as cytokines, molecularly targeted therapeutics, and innovative immunosuppressive agents. Notably, these treatments mostly focus on modulating the tumor microenvironment rather than directly targeting the RCC tumor cells. ccRCC is a tumor form that exhibits significant inflammation, as evidenced by its high immune infiltration score in pan-cancer analysis (4).

The presence of unique yet fluctuating levels of vascular density, immune cell infiltration, and PD-L1 expression in ccRCC necessitates the use of inhibitors targeting the vascular endothelial growth factor (VEGF) pathway and the PD-L1 axis. Administering these inhibitors, either individually or in combination, has been shown to greatly enhance the clinical results of patients with advanced RCC. Nevertheless, there are instances where certain individuals exhibit a lack of response to this particular treatment, and it is worth noting that these treatments are accompanied by notable levels of toxicity. Hence, it is imperative to acquire a more comprehensive comprehension of the molecular underpinnings that contribute to the clinical variability observed in individuals with advanced RCC. Such understanding is crucial for devising effective treatment regimens and elucidating the mechanisms underlying resistance to therapies.

Due to its insensitivity to radiotherapy and chemotherapy, the primary treatment options for advanced ccRCC, which is the most prevalent and malignant subtype of RCC, are palliative tumor resection, targeted therapy, and immunotherapy (5). Fan et al. identified a novel immune subtyperelated prognostic signature of ccRCC associated with the expression of vacuole membrane protein 1. Guo et al. focused on a rare type of RCC, Xp11.2 translocation RCC, and investigated the clinical and pathological heterogeneity of its different fusion subtypes. Liu et al. showed that not only are sarcopenia and inflammation associated with tumor progression, leading to poor survival of RCC patients, but tumormediated inflammation may in turn exacerbate muscle wasting and further create a tumor-penetrating vicious cycle between sarcopenia and inflammation. Zhang et al. showed that patients with a high claudinTME related (CTR) risk signature may be more sensitive to immune checkpoint blockade.

It is noteworthy that the majority of the literature indicates a lack of correlation between RCC and immunodeficiency generated by the human immunodeficiency virus (HIV). Zhu et al. comprehensively reviewed the epidemiology, risk factors, and diagnostic approaches pertaining to RCC in individuals affected by HIV. Additionally, the authors offered significant perspectives on the management strategies for RCC patients with HIV.

Prostate adenocarcinoma (PRAD)

PRAD is predominantly a hormone-mediated disease with androgen receptor (AR) signaling driving cell proliferation. The standard of care for PRAD is castration therapy or androgen deprivation therapy (ADT). However, ADT-treated patients will inevitably develop treatment resistance. Combining ADT with other therapeutic agents is therefore of considerable interest. Wang et al. conducted a systematic review of doublet and triplet therapies for hormone-sensitive metastatic prostate cancer and concluded that both showed a significant increase in overall survival, although triplet therapies may be less safe. Post-transcriptional modifications may affect the initiation and progression of tumors. The prognostic value of N6-methyladenosine (m6A) regulators in patients with metastatic prostate cancer was demonstrated by Liu et al. and Guo et al. examined the targeting mechanism of the ubiquitin-specific protease family as potential PRAD therapies.

The homeostasis and growth of the TME are governed by the complex intercellular communication, which includes extracellular metabolites. Using byproducts of sugar metabolism, cancer cells can co-opt tumorinfiltrating immune cells (6). Liu et al. developed a metabolic prediction model with a 12-mRNA signature that predicts the progression of PRAD patients. In addition, they discover that the metabolic enzyme myo-inositol oxygenase is associated with the DNA damage repair process in PRAD and plays a significant role in the aberrant immune infiltration of the TME.

Bladder cancer (BCa)

BCa has the highest incidence rate among genitourinary malignancies. Chemotherapy is currently the mainstay treatment for advanced BCa. As with other malignancies, numerous immunotherapy clinical trials for BCa are currently ongoing. However, the TME of BCa and the immune signature within it remain unclear, making it difficult to predict the efficacy of immunotherapy. Yang et al. discovered that adenylate cyclase 2 methylation is a reliable biomarker for the diagnosis and immunotherapy of patients with BCa. Integrins, a class of cell surface adhesion molecules with signal transduction functions, serve a crucial role in virtually every phase of tumor proliferation and metastasis. Recent research indicates that homoharringtonine may inhibit the growth of bladder cancer by inactivating the integrin 5/1-FAK/Src axis (7). Collagen induces senescence in tumor cells by activating the p53/p21 pathway via the integrin 1/AKT axis (8). Tu et al. identified three integrin subunit genes that may serve as bladder cancer prognostic markers. Overall, the complex effects of integrins and other adhesion factors in the tumor microenvironment, such as the equilibrium between the formation of a protective tumor shield and the recruitment of immune cells, require further investigation.

Other genitourinary cancers

Systemic inflammation has prognostic value for patient overall survival, as mentioned previously. Wang et al. hypothesized that the same holds true for testicular germ cell tumor. Neutrophil-to-lymphocyte ratio (NLR) and systemic immune-inflammation

index (SII) may be cost-effective and more accessible future markers.

In numerous forms of cancer, including penile cancer, cancer-associated fibroblasts (CAFs) are a vital component of the tumor microenvironment. CAFs contribute significantly to tumor progression, angiogenesis, invasion, and metastasis. Cury et al. demonstrated that a drug that targets matrix metalloproteinases can modulate CAFs, thereby expanding treatment options for penile cancer.

Author contributions

JL: Writing – original draft. WX: Writing – original draft. HZ: Writing – review & editing. DY: Writing – review & editing.

Funding

This work was supported by grants from the National Natural Science Foundation of China (No. 821172817, and 82172741), the Natural Science Foundation of Shanghai (No. 20ZR1413100), the Shanghai Anticancer Association EYAS PROJECT (No. SACA-CY21A06), and Shanghai Municipal Health Bureau (No.2020CXJQ03).

Conflict of interest

The authors declare that the research was conducted in the absence of any commercial or financial relationships that could be construed as a potential conflict of interest.

Publisher's note

References

1. Joyce JA, Fearon DT. T cell exclusion, immune privilege, and the tumor microenvironment. *Science* (2015) 348:74–80. doi: 10.1126/science.aaa6204

2. Sato Y, Yoshizato T, Shiraishi Y, Maekawa S, Okuno Y, Kamura T, et al. Integrated molecular analysis of clear-cell renal cell carcinoma. *Nat Genet* (2013) 45:860–7. doi: 10.1038/ng.2699

3. Motzer RJ, Banchereau R, Hamidi H, Powles T, McDermott D, Atkins MB, et al. Molecular subsets in renal cancer determine outcome to checkpoint and angiogenesis blockade. *Cancer Cell* (2020) 38:803–17. doi: 10.1016/j.ccell.2020.10.011

4. Vuong L, Kotecha RR, Voss MH, Hakimi AA. Tumor microenvironment dynamics in clear-cell renal cell carcinoma. *Cancer Discov* (2019) 9:1349–57. doi: 10.1158/2159-8290.CD-19-0499

5. Atkins MB, Tannir NM. Current and emerging therapies for first-line treatment of metastatic clear cell renal cell carcinoma. *Cancer Treat Rev* (2018) 70:127–37. doi: 10.1016/j.ctrv.2018.07.009

6. Vander Heiden MG, Cantley LC, Thompson CB. Understanding the warburg effect: the metabolic requirements of cell proliferation. *science* (2009) 324:1029–33. doi: 10.1126/science.1160809

7. He H, Ma J, Xiong C, Wei T, Tang A, Chen Y, et al. Development and validation of a nomogram to predict the risk of lumbar disk reherniation within 2 years after percutaneous endoscopic lumbar discectomy. *World Neurosurg* (2023) 172:e349–56. doi: 10.1016/j.wneu.2023.01.026

8. Deng L, Jin K, Zhou X, Zhang Z, Ge L, Xiong X, et al. Blockade of integrin signaling reduces chemotherapy-induced premature senescence in collagen cultured bladder cancer cells. *Precis Clin Med* (2022) 5:pbac007. doi: 10.1093/pcmedi/pbac007

frontiers | Frontiers in Oncology

REVIEW
published: 01 April 2022
doi: 10.3389/fonc.2022.872438

Renal Cell Carcinoma Associated With HIV/AIDS: A Review of the Epidemiology, Risk Factors, Diagnosis, and Treatment

Zhiqiang Zhu[1,2†], *Yihang Zhang*[3†], *Hu Wang*[3], *Taiyi Jiang*[3], *Mengmeng Zhang*[2], *Yu Zhang*[2], *Bin Su*[3*] and *Ye Tian*[1*]

[1] Department of Urology, Beijing Friendship Hospital, Capital Medical University, Beijing, China, [2] Department of Urology, Beijing Youan Hospital, Capital Medical University, Beijing, China, [3] Beijing Key Laboratory for HIV/AIDS Research, Clinical and Research Center for Infectious Diseases, Beijing Youan Hospital, Capital Medical University, Beijing, China

OPEN ACCESS

Edited by:
Wen-Hao Xu,
Fudan University, China

Reviewed by:
An Zhao,
University of Chinese Academy of Sciences, China
Yushi Zhang,
Peking Union Medical College Hospital (CAMS), China

***Correspondence:**
Ye Tian
tianye166@126.com
Bin Su
binsu@ccmu.edu.cn

[†]These authors contributed equally to this work

Specialty section:
This article was submitted to Genitourinary Oncology, a section of the journal Frontiers in Oncology

Received: 09 February 2022
Accepted: 07 March 2022
Published: 01 April 2022

Citation:
Zhu Z, Zhang Y, Wang H, Jiang T, Zhang M, Zhang Y, Su B and Tian Y (2022) Renal Cell Carcinoma Associated With HIV/AIDS: A Review of the Epidemiology, Risk Factors, Diagnosis, and Treatment. Front. Oncol. 12:872438. doi: 10.3389/fonc.2022.872438

Renal cell carcinoma (RCC), one of the most common genitourinary tumors, is induced by many factors, primarily smoking, obesity, and hypertension. As a non-acquired immunodeficiency syndrome (AIDS)-defining cancer, human immunodeficiency virus (HIV) may also play a critical role in the incidence and progression of RCC. It is evident that individuals who are infected with HIV are more likely than the general population to develop RCC. The age of RCC diagnosis among HIV-positive patients is younger than among HIV-negative individuals. However, many other characteristics remain unknown. With the increase in RCC incidence among HIV-infected patients, more research is being conducted to discover the relationship between RCC and HIV, especially with regard to HIV-induced immunodeficiency, diagnosis, and treatment. Unexpectedly, the majority of the literature suggests that there is no relationship between RCC and HIV-induced immunodeficiency. Nonetheless, differences in pathology, symptoms, or treatment in HIV-positive patients diagnosed with RCC are a focus. In this review, we summarize the association of RCC with HIV in terms of epidemiology, risk factors, diagnosis, and treatment.

Keywords: renal cell carcinoma, HIV, AIDS, risk factors, diagnosis, treatment

INTRODUCTION

Globally, renal cell carcinoma (RCC) is the 9th most common cancer in men and the 14th most common cancer in women (1). RCC derived from tubular epithelial cells is the most common cancer of the kidney, accounting for approximately 80% (2). The etiology of RCC remains unknown, and there are more than ten pathological classifications. In general, clear cell RCC (ccRCC) and nonclear cell RCC (nccRCC) are used to pathologically divide RCC into two main parts: ccRCC is the most common, accounting for 70%~75% of cases; nccRCC represents 15%~30% of cases (3). Risk factors for RCC are tobacco smoking, high body mass index (BMI, especially obesity), hypertension, occupational exposure, diet, and drug use (4). With the development of

ultrasonography and imaging technology, many methods are used to detect renal tumors. Ultrasound (US), computed tomography (CT) and magnetic resonance imaging (MRI) are critical means of detection, and each has different clinical advantages and disadvantages. Surgery is the pillar of treatment for localized or locally advanced RCC and is the only curative treatment. Partial nephrectomy (PN) and radical nephrectomy (RN) are the main operations (5). Since 2005, multiple new drugs have been approved, including tyrosine kinase inhibitors (TKIs) and immune checkpoint inhibitors (ICIs). Hence, the overall survival (OS) of patients with metastatic RCC (mRCC) has increased from 1 year in the cytokine era to approximately 2.5~3 years in the TKI and immunotherapy eras (6). Despite major advances in exploring the molecular basis of RCC carcinogenesis, the selection of therapy is still based on clinical presentation and patient body status. Moreover, there are a number of concerns that should be considered for different populations, such as those with coinfection with human immunodeficiency virus (HIV).

HIV is responsible for human immunodeficiency syndrome (AIDS), which was discovered in 1983 (7). According to the UNAIDS, there were 1.5 million individuals in 2020 who were newly infected with HIV and 680,000 who died from AIDS-related illnesses. There are 37.7 million HIV-positive patients worldwide (8). Before the era of antiretroviral therapy (ART), people living with HIV/AIDS (PLWH) were at high risk of AIDS-related events, such as opportunistic infections and AIDS-defining malignancies, resulting in a short survival time. With the advent of ART, the lifespan of PLWH was prominently increased and even closed to that of HIV-negative populations, and the incidence of AIDS-defining cancers (ADCs) decreased dramatically (9–11). Nevertheless, non-AIDS-defining cancers (NADCs), including but not limited to lung, liver, kidney, anal and skin tumors, have gradually emerged (9, 12, 13). At present, RCC is regarded as an NADC and has partially different features in HIV-positive and HIV-negative populations. In this review, we focus on the epidemiology, risk factors, diagnosis and treatment of RCC patients with and without HIV.

MORBIDITY AND MORTALITY

During the last 2 decades, there has been an annual increase of 2% in the incidence of RCC worldwide and in Europe. Indeed, nearly 99,200 new RCC cases and 39,100 kidney cancer-related deaths were reported in the European Union in 2018 (5). As reported in 2022, the newest total estimated numbers of new kidney and pelvis cancer cases and deaths were 79,000 and 13,920, respectively, in the United States (14). There are no detailed data on how many RCC patients are coinfected with HIV or how many HIV-positive patients are diagnosed with RCC. Nevertheless, early literature reported that the HIV-positive population has an 8.5-fold greater chance of developing RCC than the general population and that the average age of occurrence is approximately 15 years younger (15). Other studies found the same conclusions, namely, that the HIV-positive population has a high incidence of RCC (16, 17). One meta-analysis of seven studies including 444,172 HIV/AIDS patients reported that the standardized incidence ratio of kidney cancer in people with HIV/AIDS was 1.50 (18). Overall, it is clear that HIV-positive patients are at a high risk of being diagnosed with RCC and that the age of these individuals is younger than that of the general population.

RISK FACTORS

To date, the well-known risk factors for RCC are cigarette smoking, obesity, hypertension and the von Hippel-Lindau (VHL) mutation. Alcohol, occupational exposure, diet, drugs and caffeine have controversial effects in RCC (2, 19).

Smoking, especially cigarette smoking, is confirmed to promote the carcinogenesis of many tumors, including RCC. Tobacco smoke includes a mixture of carcinogens implicated in the etiology of RCC. In 2016, Cumberbatch et al. reported that the risk of developing RCC was significantly higher for all smokers than for nonsmokers. Among them, current smokers had a greater risk than former smokers (20). A meta-analysis of 24 studies reported a strong dose-dependent increase in the risk of RCC in both sexes. In addition, RCC patients who had quit smoking for >10 years had better outcomes than those who had quit smoking for 1-10 years (21). Some studies reported that smokers had worse outcomes in RCC than nonsmokers not only with respect to surgery but also targeted treatment (22–25). A recent cohort study indicated that heavy smoking (more than 40 pack-years) was associated with a significant increase in RCC incidence (26). Of course, smoking also has a negative effect on HIV/AIDS. The prevalence of smoking in individuals infected with HIV is higher than that in the general population. Additionally, these individuals are less likely to quit smoking than the general population (27, 28). Hence, smoking puts HIV-positive patients at risk of many of the known health consequences, and these patients evidently have increased morbidity and mortality related to smoking (29). Although the prevalence of RCC patients with HIV is unknown, we find that HIV-positive patients who are current smokers or ever smokers have a greater tendency to be diagnosed with RCC. As smoking cessation is less likely, HIV-positive patients might have a worse outcome than HIV-negative patients diagnosed with RCC. Therefore, encouraging PLWH to stop smoking will affect the prognosis of these individuals, especially with cessation of smoking for more than 10 years.

Obesity is another evident risk factor for RCC at present (30). BMI, defined as weight (kg) divided by the square of body height (m), is often used to assess body mass. Obesity is defined as BMI of 30 kg/m^2 or greater in non-Asian populations and 25 kg/m^2 or greater in Asian populations. A meta-analysis including 17 epidemiological studies estimated a 24% increase in the risk of developing RCC in men and a 34% increase in women for each 5-point increase in BMI (31). Another meta-analysis showed a significant association between excess body weight and increased risk of RCC in both men and women, with a slightly higher risk

in women. In addition, the researchers found that each 1-kg/m^2 increase in BMI corresponded to a 4% increase in the risk of RCC (32). However, among studies about RCC and obesity, there were some viewpoints regarding obesity as a protective factor called the "obesity paradox" (33). One clinical-based cohort and meta-analysis of 1,543 patients who underwent nephrectomy for RCC in Korea indicated that high BMI prior to renal surgery was associated with improved OS, cancer-specific survival (CSS) and recurrence-free survival (RFS) when compared with low BMI (34). Recent studies similarly reported that high BMI might play a positive role in RCC compared with normal or low BMI (35–37). Turco et al. reviewed this phenomenon and offered an explanation, suggesting that these studies considering BMI as a protective factor in RCC had some limitations. BMI is used to assess body weight conveniently, but it does not accurately reflect the respective weight of fat, muscle, and bone mass. Similarly, it also does not assess fat in the subcutaneous area or viscera. Some studies define obesity as BMI of more than 25 kg/m^2 instead of 30 kg/m^2, amplifying the inclusion criteria. Other possible reasons, such as nutrition and genetic and molecular features, might be associated with the obesity paradox (33). For HIV-positive patients, obesity is also a factor to focus on due to ART use, and unhealthy diet and low exercise might affect body weight. A recent report indicated that obesity and overweight were common in older patients with HIV and associated with the presence of metabolic disease and multimorbidity (38). Overall, obesity is regarded as a risk factor in multiple diseases. HIV patients should maintain strict control of their body weight to not only prevent the development of RCC but also to reduce the risk of other metabolic diseases.

Hypertension is a significant risk factor for both kidney cancer incidence and mortality in men, as revealed by multivariable regression analysis (39). In the VITAL study involving a prospective cohort of more than 77,000 US residents, hypertension was independently associated with the risk of RCC (40). In addition, there was evidence indicating that hypertension might have a dose-dependent effect on kidney cancer risk. A recent meta-analysis of 18 prospective studies showed that each 10-mmHg increase in blood pressure was associated with a 10%~22% increase in the risk of kidney cancer (41). The prevalence of hypertension in HIV-infected patients is higher (42), and there are many factors that induce hypertension. A recent meta-analysis showed that exposure to ART was associated with a significantly increased risk of hypertension (43). Given that ART is used throughout the life of HIV-infected patients, blood pressure should be examined regularly, especially in older patients. Controlling blood pressure within a certain range is an effective way to reduce morbidity and mortality in HIV-infected patients with RCC. However, the optimal blood pressure range and which antihypertensive drugs should be chosen need further investigation.

For HIV-positive patients, $CD4^+$ T cell count is an extremely important factor. ADCs are strongly associated with immunosuppression (17), especially when $CD4^+$ T cell counts decrease by 200 cells/μL. However, not all NADCs are associated with immunosuppression (44), and HIV-induced immunosuppression appears to play a lesser role than lifestyle habits and viral coinfection compared with those in ADCs (45). Some related reports are described below. In 1990, Adjiman et al. reported a 25-year-old patient diagnosed with RCC associated with advanced malignant lymphoma, which is known to be directly related to immune depression (46). Azon-Masoliver et al. also reported a patient with both Kaposi's sarcoma and renal cell adenocarcinoma. These two cases seem to indicate that RCC may have an association with immunodeficiency. However, given that only two patients were described, it is not possible to determine whether a relationship between immunodeficiency and RCC exists. In 1997, Stephen A. Baynham et al. reported that RCC may occur in individuals with higher CD4 T cell counts and that the occurrence of RCC might not be only due to nonspecific immunosuppression, as seen with AIDS-related lymphoma (15). In 2008, Bruce J. Dezube et al. reported nine HIV-positive patients who were diagnosed with RCC, 7 of whom had mild-to-moderate immunosuppression (CD4 T cell count: 62~731 cells/μL). The authors concluded that HIV-related immunosuppression might not play an important role in RCC. Instead, HIV infection and ART might result in nephropathy and diabetes, both of which are potential risk factors for RCC (45). In the same year, Annah B. Layman et al. reported no association between CD4 T cell count at AIDS onset and the risk of RCC during the incidence period (47). In 2016, Wee Loon ONG et al. reported seven HIV-positive patients diagnosed with RCC; most had a mild-to-moderate immunodeficiency ($CD4^+$ T cell counts: 178~1,352 cells/μL). Additionally, five of the patients had viral loads below 50 copies/mL (48). These reports appear to suggest no association between RCC and HIV-induced immunosuppression. A similar conclusion was reached in 2021. Zhang and Zhu et al. from Beijing Youan Hospital reported 19 HIV-infected patients diagnosed with RCC. They concluded that there was no evidence to support a relationship between immune deficiency and tumor progression, even though some patients did not undergo regular ART (49). Overall, recent studies have tended to consider that there is insufficient evidence to prove an association between HIV-induced immunodeficiency and RCC. However, there were many limitations in these studies. First, the number of RCC patients with HIV infection was relatively low. Second, most of the patients were men. Third, we suspect that RCC has an association with HIV-induced immunodeficiency, but patients with low CD4 T cell counts tend to be diagnosed with ADC and have a worse prognosis; thus, they may die because of ADCs and opportunistic infections at a younger age before they develop RCC. Fourth, there was a lack of different ranges of CD4 T cell counts to evaluate the association with immunodeficiency and RCC. Therefore, further studies are needed.

The VHL gene, located at chromosome 3p, is a tumor-suppressor gene that plays an important role in the development of RCC (50). VHL is not only the most frequently studied gene but also has the highest mutation prevalence, accounting for 64% (51). Mutant VHL lacks the ability to target hypoxia-inducible factor (HIF) involved in angiogenesis and mitogenesis for destruction by the pVHL-E3 ligase complex ubiquitin-proteasome pathway (52). Interestingly, stabilization and increased transcription and expression of HIF-1 are clearly affected by human oncogenic

viruses by disrupting degradation of HIF-1 (53). Moreover, one study indicated that proper pVHL increased HIV-1 replication and gene expression. Researchers have also found that the Cul2/VHL-mediated degradation pathway promoted integrase (a key enzyme in the HIV integration process) stabilization in RCC4 cells (54). Hence, HIV might actually participate in the development of RCC. Besides, we speculate that in RCC patients with VHL gene mutation, HIV replication can, to some degree, be influenced by a reduction in pVHL expression *in vivo*. That may become a new target of treatment to diminish HIV after we know for sure how pVHL functions in HIV replication. In addition, other modifiable risk factors, including alcohol consumption, caffeine, diet, occupational exposure and drugs, are more or less associated with RCC. Further investigations are needed.

DIAGNOSIS

Clinical Presentation

The major clinical presentations, or classical triad, described in RCC are hematuria, flank pain and abdominal or flank mass, but they are only seen in a few individuals. Other clinical presentations, such as weight loss, acute varicocele and symptoms due to metastasis, are found in some patients (55). HIV-positive populations with RCC, in addition to having parallel symptoms, may exhibit some AIDS-related clinical manifestations, such as opportunistic infections and ADCs, especially in those who have low $CD4^+$ T cell counts.

Imaging

US, CT, and MRI are used to screen for RCC (56). US is one of the first methods used for the diagnostic imaging of renal lesions, as it is easily repeatable, does not require radiation and is cost-effective. Hence, US is a readily available, fast and easy method of evaluation for clinicians. However, it requires operator experience, and the kidneys cannot always be satisfactorily imaged (57). Moreover, the use of US to screen for renal cancer in asymptomatic patients is controversial, as the rate of incidental malignant findings has been found to be very low, at only 0.2% (58). One study found that CT was a better choice than US when the diameters of renal lesions were 0 to 5 mm (the detection rates were 47% and 0%, respectively), and the detection rate increased with an increase in lesion diameter. For instance, in large lesions (10 to 35 mm), the detection rates were 80% for CT and 82% for US (59). Despite its limited sensitivity for small lesions, US may be useful to determine whether a lesion is likely to be cystic in nature but appears hyperdense on a CT scan in patients in whom contrast agents are contraindicated. Regardless, US is still an important method for the detection and diagnosis of RCC. CT has been the gold standard for cross-sectional RCC imaging since the 1990s. Due to the increased vascularity in RCC, it might be better visualized with contrast-enhanced CT (57). Nevertheless, CT has some limitations that restrict its wide use. Contrast-enhanced CT is not recommended for patients who are allergic to contrast agents, those who are pregnant, and those who are undergoing renal dialysis. MRI has played an increasingly important role in imaging patients with RCC, particularly those who are intolerant to CT (57). According to the American College of Radiology, MRI is comparable to CT for RCC staging and post-treatment follow-up and for the evaluation of indeterminate renal masses (60). There is an evidence that MRI may better evaluate renal masses previously deemed indeterminate on CT imaging or US (61). In addition, a report showed that MRI imaging has a sensitivity of 92.3% and a specificity of 86.4% in the diagnosis of inferior vena cava thrombus before surgery (62). Regardless, MRI has some limitations, such as high cost, inconvenience, and a long examination time. Each imaging technique has different advantages and shortcomings for the diagnosis of RCC. If patients have symptoms or renal masses found through certain examinations, excluding any contraindications, CT as the gold standard is strongly recommended. CT is more sensitive than US, especially in the detection of small renal masses. If patients have contraindications for CT, MRI is another method that can be used. Considering the advantages and disadvantages of each imaging technique, multiple imaging methods have been combined in the field of RCC diagnosis, thus improving the sensitivity and accuracy.

Histological Diagnosis

According to the WHO classification of tumors of the kidney in 2016, renal cell carcinoma is divided into 16 subtypes. The most common subtype is ccRCC, accounting for 70%~75% of cases. Papillary RCC (pRCC) is the most common non-ccRCC subtype, accounting for 15%~20% of cases. Chromophobe RCC (chRCC) and other pathological types account for 5% each (3). There are considerable differences in tumor stage, grade, and CSS between each type. Each pathological type has different molecular features and immunohistochemistry profiles. For example, ccRCC is characterized by cells with clear cytoplasm and a delicate capillary network. However, infiltrative growth, eosinophilic cytoplasm or globules, poorly differentiated adenocarcinoma-like morphology, rare papillary formation, giant multinucleated tumor cells, and sarcomatoid/rhabdoid morphology are characteristics of ccRCC subtypes. Some of them are related to a worse prognosis and may serve as biomarkers of prognosis (63). With the use of more imaging techniques, early-stage RCC can be detected incidentally, improving the cure rate and survival time of patients. Some case reports showed that there were no marked differences in pathology between RCC with and without HIV (45, 48, 49). In 2008, Gaughan et al. reported nine RCC patients with HIV, six of whom had ccRCC (45). In 2016, Wee Loon ONG et al. reported 7 RCC patients diagnosed with HIV, and five had ccRCC (48). In 2021, Zhang and Zhu et al. reported nineteen patients diagnosed with RCC and HIV; seventeen of these patients were diagnosed with ccRCC, accounting for 89%. One patient had partial ccRCC and partial pRCC, and another had chRCC (49). According to these case reports, ccRCC is still a dominant pathological type in HIV-infected patients.

TREATMENT

Currently, localized RCC can be treated by PN or RN (5). As a refractory tumor, the optimal treatment of mRCC has been constantly explored. Given the poor response of RCC to radiation and chemotherapy, targeted treatment and immunotherapy are commonly used for mRCC, with good results for the majority of patients (2, 64, 65). In addition, the combination of cabozantinib and nivolumab is now recommended as the first-line treatment of advanced disease, bringing new hope to RCC patients (66).

Zhang and Zhu et al. reported that the treatment approaches appear to be the same for HIV-positive and HIV-uninfected RCC patients, and their prognosis following PN is no worse than that of patients undergoing RN. In a retrospective study of 19 patients, 12 with varying degrees of immunodeficiency ($CD4^+$ T cell counts < 400 cells/μL) were alive at the 34-month posttreatment follow-up, with only one case of metastasis. In general, additional trials are still needed to evaluate the effect of immunodeficiency on RCC recurrence and metastasis in HIV-positive individuals (49). Similar to the aforementioned study, an article from Australia suggested that patients with RCC and HIV infection should be given the same treatment measures as the general population (48). However, neither study found an association between immunodeficiency and tumor progression in HIV-infected patients.

RCC is an immune-responsive tumor, and with the emergence of ICIs, there is new hope for the treatment of advanced RCC (67–69). Recently, the phase III KEYNOTE-426 study showed that pembrolizumab (targeting PD-1) plus axitinib continues to result in superior clinical outcomes versus sunitinib, and these results provide further evidence that using pembrolizumab plus axitinib as first-line therapy as the standard of care for advanced RCC is an option that benefits patients (70). In fact, the immune checkpoint PD-1 not only serves as a therapeutic target for RCC but also plays a role in the body's fight against HIV. More interestingly, studies have demonstrated that PD-1 expression and exhaustion occur in HIV-specific $CD4^+$ and $CD8^+$ T cells and that PD-1 expression is associated with viral load, CD4 T cell count, and cytotoxic function of $CD8^+$ T cells (71–74). This PD-1 expression and T cell depletion can be reduced by ART but not to pre-HIV infection levels (75). Therefore, ART should not be interrupted during RCC treatment. More recently, Li et al. noted that $CD8^+$ T cell activity can be restored by targeting the adenosine and PD-1 signaling pathways together. Further study revealed that targeting both the CD39/adenosine and PD-1 pathways improved $CD8^+$ T cell antiviral effectiveness more than targeting only one immune checkpoint pathway, which can be a potential strategy for treating HIV (76). Similarly, other immune checkpoints may play an important role during HIV infection, such as CTLA-4, TIM-3, TIGIT, and LAG-3, which are all associated with changes in some patient indicators during HIV infection (74, 77–80). In a recent study, investigators evaluated the effect of intravenous pembrolizumab every 3 weeks on HIV latency in 32 PLWH and patients with cancer. The findings support the use of anti-PD-1 therapy in combination with other therapeutic approaches to reduce the HIV viral reservoir, with fresh perspectives on ICI use for HIV infection (81).

For advanced cancer patients with HIV, both the feasibility and safety of ICIs have been demonstrated in two clinical investigations. In the phase I study Cancer Immunotherapies Network Study-12 (CITN-12), the investigators recruited HIV-infected patients with advanced cancer who had CD4 T cell counts greater than or equal to 100 cells/μL, underwent ART for 4 weeks or more, and had an HIV viral load less than 200 copies/mL. Interestingly, the clinical benefit rate (defined as tumor shrinkage or stabilization at 24 weeks) for pembrolizumab was 17%, and the toxicity profile of the ICIs was similar to that of HIV-uninfected individuals (82). In addition, the phase 2 DURVAST study, which aimed to assess the feasibility and safety of durvalumab for the treatment of solid tumors in PLWH, observed partial responses in 4 of 16 evaluable patients (25%). Five patients (31%) had stable disease, and 4 of them had durable stable disease (50% disease control) without unexpected toxicity (83).

PD-1 inhibitors have great potential in the management of mRCC and at the same time modulate potential immunosuppression in PLWH. However, most clinical trials on ICI treatment for cancer have not included PLWH (84), which prevents them from acquiring the same cancer treatment opportunities as those who are not infected with HIV, despite their higher risk of developing cancer and their higher cancer-specific mortality (85, 86). Initially, PLWH were excluded from clinical trials, possibly due to the lack of consistent evidence-based guidelines for the development of relevant clinical trials and concerns about some potential risks arising from interactions between ICIs or other drugs and ART drugs (87). However, with growing evidence that ICIs have similar efficacy and tolerability in PLWH compared to the general population in advanced cancer treatment (88, 89), in 2020, the Food and Drug Administration (FDA) recommended that PLWH with acceptable immune function be included in cancer trials. In the future, more clinical trials, such as NCT04514484, which includes PLWH with advanced RCC, should be conducted to bring more survival possibilities to this group of patients.

Of course, some kinds of conventional drugs for HIV/AIDS may have effects on ccRCC when combined with anti-ccRCC drugs. For example, non-nucleoside reverse transcriptase inhibitors such as efavirenz and nevirapine can either induce reversible downregulation of cell proliferation or enhance cell differentiation in human renal carcinoma cells (90). Moreover, the protease inhibitors lopinavir and nelfinavir used for HIV/AIDS treatment substantially improve the activity of carfilzomib in ccRCC cell lines and primary cells at therapeutically relevant drug concentrations (91). These studies provide a different view that traditional drugs for both HIV/AIDS and RCC may have synergistic effects and even become proper regimens.

CONCLUSIONS

RCC is one of the most common kidney cancers. People with the risk factors smoking, obesity, and hypertension are at high risk of RCC. The symptoms of RCC are not obvious in the majority of

patients, especially in the early stage of the tumor. Hence, regular examinations are needed in high-risk groups. Three methods are most commonly used clinically for detection: US, CT and MRI. Each of them has advantages and shortcomings. Their combination can improve the sensitivity and accuracy of the diagnosis of RCC. To date, surgery is still the only way to cure RCC. However, with the development of understanding of etiology, targeted treatments and immunotherapies have continued to emerge. Moreover, there is an increasing number of treatments for RCC, especially mRCC. PLWH are at high risk of RCC as well, with a younger age of onset. We still do not understand why these special groups tend to develop RCC. According to some case reports, there are no differences in pathological type, clinical presentation, screening method, and treatment compared with the general population. Interestingly, most reports indicate that no association between RCC and HIV-induced immunodeficiency. Therefore, imaging examinations in HIV-infected patients are critically needed, even in those with high $CD4^+$ T cell counts. Surgical treatment is strongly recommended for patients with localized RCC with HIV/AIDS. RN tends to be offered to patients with lower $CD4^+$ T cell counts. Although the combination of targeted treatment and immunotherapy has emerged, bringing new hope for mRCC patients, there is no clear evidence of the optimal treatment for mRCC patients with HIV/AIDS. Consequently, advanced investigations are urgently needed, and more treatments need to be developed.

AUTHOR CONTRIBUTIONS

BS and YT conceived and supervised the whole study, TYJ, MMZ, and YZ. searched the literature, selected studies and provided important scientific input, ZQZ, YHZ, HW, and BS wrote the draft of the manuscript. All authors listed, have made a substantial, direct, and intellectual contribution to the work. All authors read and approved the final manuscript.

FUNDING

This work was supported by the National Natural Science Foundation of China (NSFC, 81974303 and 81772165), the "Climbing the peak (Dengfeng)" Talent Training Program of Beijing Hospitals Authority (DFL20191701), the National 13th Five-Year Grand Program on Key Infectious Disease Control (2017ZX10202102-005-003 and 2017ZX10202101-004-001), and the Beijing Key Laboratory for HIV/AIDS Research (BZ0089). The funders had no role in study design, data collection and analysis, decision to publish, or preparation of the manuscript.

REFERENCES

1. Znaor A, Lortet-Tieulent J, Laversanne M, Jemal A, Bray F. International Variations and Trends in Renal Cell Carcinoma Incidence and Mortality. *Eur Urol* (2015) 67(3):519–30. doi: 10.1016/j.eururo.2014.10.002
2. Escudier B, Porta C, Schmidinger M, Rioux-Leclercq N, Bex A, Khoo V, et al. Renal Cell Carcinoma: ESMO Clinical Practice Guidelines for Diagnosis, Treatment and Follow-Updagger. *Ann Oncol* (2019) 30(5):706–20. doi: 10.1093/annonc/mdz056
3. Moch H, Cubilla AL, Humphrey PA, Reuter VE, Ulbright TM. The 2016 WHO Classification of Tumours of the Urinary System and Male Genital Organs-Part A: Renal, Penile, and Testicular Tumours. *Eur Urol* (2016) 70 (1):93–105. doi: 10.1016/j.eururo.2016.02.029
4. Cho E, Adami HO, Lindblad P. Epidemiology of Renal Cell Cancer. *Hematol Oncol Clin North Am* (2011) 25(4):651–65. doi: 10.1016/j.hoc.2011.04.002
5. Ljungberg B, Albiges L, Abu-Ghanem Y, Bensalah K, Dabestani S, Fernandez-Pello S, et al. European Association of Urology Guidelines on Renal Cell Carcinoma: The 2019 Update. *Eur Urol* (2019) 75(5):799–810. doi: 10.1016/j.eururo.2019.02.011
6. Gong J, Maia MC, Dizman N, Govindarajan A, Pal SK. Metastasis in Renal Cell Carcinoma: Biology and Implications for Therapy. *Asian J Urol* (2016) 3 (4):286–92. doi: 10.1016/j.ajur.2016.08.006
7. Barre-Sinoussi F, Chermann JC, Rey F, Nugeyre MT, Chamaret S, Gruest J, et al. Isolation of a T-Lymphotropic Retrovirus From a Patient at Risk for Acquired Immune Deficiency Syndrome (AIDS). *Science* (1983) 220 (4599):868–71. doi: 10.1126/science.6189183
8. Joint United Nations Programme on HIV/AIDS. *FACT SHEET – WORLD AIDS DAY 2021* (2021). Available at: https://www.unaids.org/en/resources/fact-sheet (Accessed 09 February 2022).
9. Lee LK, Dinneen MD, Ahmad S. The Urologist and the Patient Infected With Human Immunodeficiency Virus or With Acquired Immunodeficiency Syndrome. *BJU Int* (2001) 88(6):500–10. doi: 10.1046/j.1464-410X.2001.02376.x
10. Hogg RS, Yip B, Kully C, Craib KJ, O'Shaughnessy MV, Schechter MT, et al. Improved Survival Among HIV-Infected Patients After Initiation of Triple-Drug Antiretroviral Regimens. *CMAJ* (1999) 160(5):659–65.
11. Cobucci RN, Lima PH, de Souza PC, Costa VV, Cornetta Mda C, Fernandes JV, et al. Assessing the Impact of HAART on the Incidence of Defining and Non-Defining AIDS Cancers Among Patients With HIV/AIDS: A Systematic Review. *J Infect Public Health* (2015) 8(1):1–10. doi: 10.1016/j.jiph.2014.08.003
12. Deeken JF, Tjen ALA, Rudek MA, Okuliar C, Young M, Little RF, et al. The Rising Challenge of Non-AIDS-Defining Cancers in HIV-Infected Patients. *Clin Infect Dis* (2012) 55(9):1228–35. doi: 10.1093/cid/cis613
13. Powles T, Robinson D, Stebbing J, Shamash J, Nelson M, Gazzard B, et al. Highly Active Antiretroviral Therapy and the Incidence of Non-AIDS-Defining Cancers in People With HIV Infection. *J Clin Oncol* (2009) 27 (6):884–90. doi: 10.1200/JCO.2008.19.6626
14. Siegel RL, Miller KD, Fuchs HE, Jemal A. Cancer Statistics, 2022. *CA Cancer J Clin* (2022) 72(1):7–33. doi: 10.3322/caac.21708
15. Baynham SA, Katner HP, Cleveland KB. Increased Prevalence of Renal Cell Carcinoma in Patients With HIV Infection. *AIDS Patient Care STDS* (1997) 11(3):161–5. doi: 10.1089/apc.1997.11.161
16. Hyun G, Lowe FC. AIDS and the Urologist. *Urol Clin North Am* (2003) 30 (1):101–9. doi: 10.1016/S0094-0143(02)00124-6
17. Patel P, Hanson DL, Sullivan PS, Novak RM, Moorman AC, Tong TC, et al. Incidence of Types of Cancer Among HIV-Infected Persons Compared With the General Population in the United States, 1992-2003. *Ann Intern Med* (2008) 148(10):728–36. doi: 10.7326/0003-4819-148-10-200805200-00005
18. Grulich AE, van Leeuwen MT, Falster MO, Vajdic CM. Incidence of Cancers in People With HIV/AIDS Compared With Immunosuppressed Transplant Recipients: A Meta-Analysis. *Lancet* (2007) 370(9581):59–67. doi: 10.1016/S0140-6736(07)61050-2
19. Al-Bayati O, Hasan A, Pruthi D, Kaushik D, Liss MA. Systematic Review of Modifiable Risk Factors for Kidney Cancer. *Urol Oncol* (2019) 37(6):359–71. doi: 10.1016/j.urolonc.2018.12.008
20. Cumberbatch MG, Rota M, Catto JW, La Vecchia C. The Role of Tobacco Smoke in Bladder and Kidney Carcinogenesis: A Comparison of Exposures and Meta-Analysis of Incidence and Mortality Risks. *Eur Urol* (2016) 70 (3):458–66. doi: 10.1016/j.eururo.2015.06.042

21. Hunt JD, van der Hel OL, McMillan GP, Boffetta P, Brennan P. Renal Cell Carcinoma in Relation to Cigarette Smoking: Meta-Analysis of 24 Studies. *Int J Cancer* (2005) 114(1):101–8. doi: 10.1002/ijc.20618
22. Macleod LC, Dai JC, Holt SK, Bassett JC, Wright JL, Gore JL. Underuse and Underreporting of Smoking Cessation for Smokers With a New Urologic Cancer Diagnosis. *Urol Oncol* (2015) 33(12):504.e501–507. doi: 10.1016/j.urolonc.2015.07.008
23. Parker A, Lohse C, Cheville J, Leibovich B, Igel T, Blute M. Evaluation of the Association of Current Cigarette Smoking and Outcome for Patients With Clear Cell Renal Cell Carcinoma. *Int J Urol* (2008) 15(4):304–8. doi: 10.1111/j.1442-2042.2008.01994.x
24. Keizman D, Gottfried M, Ish-Shalom M, Maimon N, Peer A, Neumann A, et al. Active Smoking may Negatively Affect Response Rate, Progression-Free Survival, and Overall Survival of Patients With Metastatic Renal Cell Carcinoma Treated With Sunitinib. *Oncologist* (2014) 19(1):51–60. doi: 10.1634/theoncologist.2012-0335
25. Kroeger N, Li H, De Velasco G, Donskov F, Sim HW, Stuhler V, et al. Active Smoking Is Associated With Worse Prognosis in Metastatic Renal Cell Carcinoma Patients Treated With Targeted Therapies. *Clin Genitourin Cancer* (2019) 17(1):65–71. doi: 10.1016/j.clgc.2018.09.006
26. Minami T, Inoue M, Sawada N, Yamaji T, Iwasaki M, Tsugane S. Alcohol Consumption, Tobacco Smoking, and Subsequent Risk of Renal Cell Carcinoma: The JPHC Study. *Cancer Sci* (2021) 112(12):5068–77. doi: 10.1111/cas.15129
27. Mdodo R, Frazier EL, Dube SR, Mattson CL, Sutton MY, Brooks JT, et al. Cigarette Smoking Prevalence Among Adults With HIV Compared With the General Adult Population in the United States: Cross-Sectional Surveys. *Ann Intern Med* (2015) 162(5):335–44. doi: 10.7326/M14-0954
28. Regan S, Meigs JB, Grinspoon SK, Triant VA. Determinants of Smoking and Quitting in HIV-Infected Individuals. *PloS One* (2016) 11(4):e0153103. doi: 10.1371/journal.pone.0153103
29. Shirley DK, Kaner RJ, Glesby MJ. Effects of Smoking on Non-AIDS-Related Morbidity in HIV-Infected Patients. *Clin Infect Dis* (2013) 57(2):275–82. doi: 10.1093/cid/cit207
30. Scelo G, Larose TL. Epidemiology and Risk Factors for Kidney Cancer. *J Clin Oncol* (2018) 2018:JCO2018791905. doi: 10.1200/JCO.2018.79.1905
31. Renehan AG, Tyson M, Egger M, Heller RF, Zwahlen M. Body-Mass Index and Incidence of Cancer: A Systematic Review and Meta-Analysis of Prospective Observational Studies. *Lancet* (2008) 371(9612):569–78. doi: 10.1016/S0140-6736(08)60269-X
32. Wang F, Xu Y. Body Mass Index and Risk of Renal Cell Cancer: A Dose-Response Meta-Analysis of Published Cohort Studies. *Int J Cancer* (2014) 135(7):1673–86. doi: 10.1002/ijc.28813
33. Turco F, Tucci M, Di Stefano RF, Samuelly A, Bungaro M, Audisio M, et al. Renal Cell Carcinoma (RCC): Fatter Is Better? A Review on the Role of Obesity in RCC. *Endocr Relat Cancer* (2021) 28(7):R207–16. doi: 10.1530/ERC-20-0457
34. Choi Y, Park B, Jeong BC, Seo SI, Jeon SS, Choi HY, et al. Body Mass Index and Survival in Patients With Renal Cell Carcinoma: A Clinical-Based Cohort and Meta-Analysis. *Int J Cancer* (2013) 132(3):625–34. doi: 10.1002/ijc.27639
35. Liu Z, Wang H, Chen Y, Jin J, Yu W. Obesity: An Independent Protective Factor for Localized Renal Cell Carcinoma in a Systemic Inflammation State. *Int Braz J Urol* (2020) 46(4):585–98. doi: 10.1590/s1677-5538.ibju.2019.0228
36. Darbas T, Forestier G, Leobon S, Pestre J, Jesus P, Lachatre D, et al. Impact of Body Composition in Overweight and Obese Patients With Localised Renal Cell Carcinoma. *In Vivo* (2020) 34(5):2873–81. doi: 10.21873/invivo.12115
37. Plonski JJS, Fernandez-Pello S, Jimenez LR, Rodriguez IG, Calvar LA, Villamil LR. Impact of Body Mass Index on Survival of Metastatic Renal Cancer. *J Kidney Cancer VHL* (2021) 8(2):49–54. doi: 10.15586/jkcvhl.v8i2.169
38. Mazzitelli M, Isabel Pereira B, Moyle G, Asboe D, Pozniak A, Boffito M, et al. Factors Associated With Overweight/Obesity in a Cohort of People Living With HIV Over 50 Years of Age. *AIDS Care* (2021) 2021:1–3. doi: 10.1080/09540121.2021.1935438
39. Huang J, Leung DK, Chan EO, Lok V, Leung S, Wong I, et al. A Global Trend Analysis of Kidney Cancer Incidence and Mortality and Their Associations With Smoking, Alcohol Consumption, and Metabolic Syndrome. *Eur Urol Focus* (2021) 8(1):200–9. doi: 10.1016/j.euf.2020.12.020
40. Macleod LC, Hotaling JM, Wright JL, Davenport MT, Gore JL, Harper J, et al. Risk Factors for Renal Cell Carcinoma in the VITAL Study. *J Urol* (2013) 190(5):1657–61. doi: 10.1016/j.juro.2013.04.130
41. Hidayat K, Du X, Zou SY, Shi BM. Blood Pressure and Kidney Cancer Risk: Meta-Analysis of Prospective Studies. *J Hypertens* (2017) 35(7):1333–44. doi: 10.1097/HJH.0000000000001286
42. van Zoest RA, van den Born BH, Reiss P. Hypertension in People Living With HIV. *Curr Opin HIV AIDS* (2017) 12(6):513–22. doi: 10.1097/COH.0000000000000406
43. Nduka CU, Stranges S, Sarki AM, Kimani PK, Uthman OA. Evidence of Increased Blood Pressure and Hypertension Risk Among People Living With HIV on Antiretroviral Therapy: A Systematic Review With Meta-Analysis. *J Hum Hypertens* (2016) 30(6):355–62. doi: 10.1038/jhh.2015.97
44. Burgi A, Brodine S, Wegner S, Milazzo M, Wallace MR, Spooner K, et al. Incidence and Risk Factors for the Occurrence of Non-AIDS-Defining Cancers Among Human Immunodeficiency Virus-Infected Individuals. *Cancer* (2005) 104(7):1505–11. doi: 10.1002/cncr.21334
45. Gaughan EM, Dezube BJ, Aboulafia D, Bower M, Stebbing J, Powles T, et al. Human Immunodeficiency Virus–Associated Renal Cell Carcinoma: A Transatlantic Case Series. *Clin Genitourin Cancer* (2008) 6(2):86–90. doi: 10.3816/CGC.2008.n.013
46. Adjiman S, Zerbib M, Flam T, Brochard M, Desligneres S, Boissonnas A, et al. Genitourinary Tumors and HIV1 Infection. *Eur Urol* (1990) 18(1):61–3. doi: 10.1159/000463869
47. Layman AB, Engels EA. Kidney and Bladder Cancers Among People With AIDS in the United States. *J Acquir Immune Defic Syndr* (2008) 48(3):365–7. doi: 10.1097/QAI.0b013e31817ae5da
48. Ong WL, King K, Koh TL, Chipman M, Royce P, Hoy J, et al. HIV and Renal Cell Carcinoma: Experience in an Australian Statewide HIV Center. *Asia Pac J Clin Oncol* (2016) 12(2):188–93. doi: 10.1111/ajco.12487
49. Zhang M, Zhu Z, Xue W, Liu H, Zhang Y. Human Immunodeficiency Virus-Related Renal Cell Carcinoma: A Retrospective Study of 19 Cases. *Infect Agent Cancer* (2021) 16(1):26. doi: 10.1186/s13027-021-00362-7
50. Gnarra JR, Tory K, Weng Y, Schmidt L, Wei MH, Li H, et al. Mutations of the VHL Tumour Suppressor Gene in Renal Carcinoma. *Nat Genet* (1994) 7(1):85–90. doi: 10.1038/ng0594-85
51. Bui TO, Dao VT, Nguyen VT, Feugeas JP, Pamoukdjian F, Bousquet G. Genomics of Clear-Cell Renal Cell Carcinoma: A Systematic Review and Meta-Analysis. *Eur Urol* (2022) S0302-2838(21):02219–3. doi: 10.1016/j.eururo.2021.12.010
52. Kondo K, Klco J, Nakamura E, Lechpammer M, Kaelin WGJr. Inhibition of HIF Is Necessary for Tumor Suppression by the Von Hippel-Lindau Protein. *Cancer Cell* (2002) 1(3):237–46. doi: 10.1016/S1535-6108(02)00043-0
53. Mthembu NN, Mbita Z, Hull R, Dlamini Z. Abnormalities in Alternative Splicing of Angiogenesis-Related Genes and Their Role in HIV-Related Cancers. *HIV AIDS (Auckl)* (2017) 9:77–93. doi: 10.2147/HIV.S124911
54. Mousnier A, Kubat N, Massias-Simon A, Segeral E, Rain JC, Benarous R, et al. Von Hippel Lindau Binding Protein 1-Mediated Degradation of Integrase Affects HIV-1 Gene Expression at a Postintegration Step. *Proc Natl Acad Sci USA* (2007) 104(34):13615–20. doi: 10.1073/pnas.0705162104
55. Yadlapalli SB, Shi D, Vaishampayan U. Renal Cell Carcinoma: Clinical Presentation, Staging, and Prognostic Factors. *Kidney Cancer: Springer* (2015) 105–21. doi: 10.1007/978-3-319-17903-2_7
56. Coll DM, Smith RC. Update on Radiological Imaging of Renal Cell Carcinoma. *BJU Int* (2007) 99(5 Pt B):1217–22. doi: 10.1111/j.1464-410X.2007.06824.x
57. Sankineni S, Brown A, Cieciera M, Choyke PL, Turkbey B. Imaging of Renal Cell Carcinoma. *Urol Oncol* (2016) 34(3):147–55. doi: 10.1016/j.urolonc.2015.05.020
58. Haliloglu AH, Gulpinar O, Ozden E, Beduk Y. Urinary Ultrasonography in Screening Incidental Renal Cell Carcinoma: Is It Obligatory? *Int Urol Nephrol* (2011) 43(3):687–90. doi: 10.1007/s11255-010-9843-3
59. Jamis-Dow CA, Choyke PL, Jennings SB, Linehan WM, Thakore KN, Walther MM. Small (< or = 3-Cm) Renal Masses: Detection With CT Versus US and Pathologic Correlation. *Radiology* (1996) 198(3):785–8. doi: 10.1148/radiology.198.3.8628872
60. American College of Radiology. *ACR Appropriateness Criteria. Post-Treatment Follow-Up and Active Surveillance of Clinically Localized Renal*

Cell Carcinoma (2021). Available at: https://acsearch.acr.org/docs/69365/Narrative/ (Accessed 09 February 2022).
61. Willatt JM, Hussain HK, Chong S, Kappil M, Azar SF, Liu PS, et al. MR Imaging in the Characterization of Small Renal Masses. *Abdom Imaging* (2014) 39(4):761–9. doi: 10.1007/s00261-014-0109-x
62. Adams LC, Ralla B, Bender YY, Bressem K, Hamm B, Busch J, et al. Renal Cell Carcinoma With Venous Extension: Prediction of Inferior Vena Cava Wall Invasion by MRI. *Cancer Imaging* (2018) 18(1):17. doi: 10.1186/s40644-018-0150-z
63. Trpkov K, Hes O, Williamson SR, Adeniran AJ, Agaimy A, Alaghehbandan R, et al. New Developments in Existing WHO Entities and Evolving Molecular Concepts: The Genitourinary Pathology Society (GUPS) Update on Renal Neoplasia. *Mod Pathol* (2021) 34(7):1392–424. doi: 10.1038/s41379-021-00779-w
64. Chowdhury N, Drake CG. Kidney Cancer: An Overview of Current Therapeutic Approaches. *Urol Clin North Am* (2020) 47(4):419–31. doi: 10.1016/j.ucl.2020.07.009
65. Onufrey V, Mohiuddin M. Radiation Therapy in the Treatment of Metastatic Renal Cell Carcinoma. *Int J Radiat Oncol Biol Phys* (1985) 11(11):2007–9. doi: 10.1016/0360-3016(85)90285-8
66. Powles T. Recent Eupdate to the ESMO Clinical Practice Guidelines on Renal Cell Carcinoma on Cabozantinib and Nivolumab for First-Line Clear Cell Renal Cancer: Renal Cell Carcinoma: ESMO Clinical Practice Guidelines for Diagnosis, Treatment and Follow-Up. *Ann Oncol* (2021) 32(3):422–3. doi: 10.1016/j.annonc.2020.11.016
67. Massari F, Santoni M, Ciccarese C, Santini D, Alfieri S, Martignoni G, et al. PD-1 Blockade Therapy in Renal Cell Carcinoma: Current Studies and Future Promises. *Cancer Treat Rev* (2015) 41(2):114–21. doi: 10.1016/j.ctrv.2014.12.013
68. Powles T. Re: Nivolumab Plus Ipilimumab Versus Sunitinib in Advanced Renal-Cell Carcinoma. *Eur Urol* (2018) 74(5):679–80. doi: 10.1016/j.eururo.2018.07.019
69. Santoni M, Massari F, Di Nunno V, Conti A, Cimadamore A, Scarpelli M, et al. Immunotherapy in Renal Cell Carcinoma: Latest Evidence and Clinical Implications. *Drugs Context* (2018) 7:1–8. doi: 10.7573/dic.212528
70. Powles T, Plimack ER, Soulières D, Waddell T, Stus V, Gafanov R, et al. Pembrolizumab Plus Axitinib Versus Sunitinib Monotherapy as First-Line Treatment of Advanced Renal Cell Carcinoma (KEYNOTE-426): Extended Follow-Up From a Randomised, Open-Label, Phase 3 Trial. *Lancet Oncol* (2020) 21(12):1563–73. doi: 10.1016/S1470-2045(20)30436-8
71. Blackburn SD, Shin H, Haining WN, Zou T, Workman CJ, Polley A, et al. Coregulation of CD8+ T Cell Exhaustion by Multiple Inhibitory Receptors During Chronic Viral Infection. *Nat Immunol* (2009) 10(1):29–37. doi: 10.1038/ni.1679
72. D'Souza M, Fontenot AP, Mack DG, Lozupone C, Dillon S, Meditz A, et al. Programmed Death 1 Expression on HIV-Specific CD4+ T Cells Is Driven by Viral Replication and Associated With T Cell Dysfunction. *J Immunol* (2007) 179(3):1979–87. doi: 10.4049/jimmunol.179.3.1979
73. Day CL, Kaufmann DE, Kiepiela P, Brown JA, Moodley ES, Reddy S, et al. PD-1 Expression on HIV-Specific T Cells Is Associated With T-Cell Exhaustion and Disease Progression. *Nature* (2006) 443(7109):350–4. doi: 10.1038/nature05115
74. Kaufmann DE, Kavanagh DG, Pereyra F, Zaunders JJ, Mackey EW, Miura T, et al. Upregulation of CTLA-4 by HIV-Specific CD4+ T Cells Correlates With Disease Progression and Defines a Reversible Immune Dysfunction. *Nat Immunol* (2007) 8(11):1246–54. doi: 10.1038/ni1515
75. El-Far M, Halwani R, Said E, Trautmann L, Doroudchi M, Janbazian L, et al. T-Cell Exhaustion in HIV Infection. *Curr HIV/AIDS Rep* (2008) 5(1):13–9. doi: 10.1007/s11904-008-0003-7
76. Li J, Huang HH, Tu B, Zhou MJ, Hu W, Fu YL, et al. Reversal of the CD8(+) T-Cell Exhaustion Induced by Chronic HIV-1 Infection Through Combined Blockade of the Adenosine and PD-1 Pathways. *Front Immunol* (2021) 12:687296. doi: 10.3389/fimmu.2021.687296
77. Jones RB, Ndhlovu LC, Barbour JD, Sheth PM, Jha AR, Long BR, et al. Tim-3 Expression Defines a Novel Population of Dysfunctional T Cells With Highly Elevated Frequencies in Progressive HIV-1 Infection. *J Exp Med* (2008) 205 (12):2763–79. doi: 10.1084/jem.20081398
78. Rallón N, García M, García-Samaniego J, Cabello A, Álvarez B, Restrepo C, et al. Expression of PD-1 and Tim-3 Markers of T-Cell Exhaustion Is Associated With CD4 Dynamics During the Course of Untreated and Treated HIV Infection. *PloS One* (2018) 13(3):e0193829. doi: 10.1371/journal.pone.0193829
79. Tian X, Zhang A, Qiu C, Wang W, Yang Y, Qiu C, et al. The Upregulation of LAG-3 on T Cells Defines a Subpopulation With Functional Exhaustion and Correlates With Disease Progression in HIV-Infected Subjects. *J Immunol* (2015) 194(8):3873–82. doi: 10.4049/jimmunol.1402176
80. Chew GM, Fujita T, Webb GM, Burwitz BJ, Wu HL, Reed JS, et al. TIGIT Marks Exhausted T Cells, Correlates With Disease Progression, and Serves as a Target for Immune Restoration in HIV and SIV Infection. *PloS Pathog* (2016) 12(1):e1005349. doi: 10.1371/journal.ppat.1005349
81. Uldrick TS, Adams SV, Fromentin R, Roche M, Fling SP, Gonçalves PH, et al. Pembrolizumab Induces HIV Latency Reversal in People Living With HIV and Cancer on Antiretroviral Therapy. *Sci Transl Med* (2022) 14(629): eabl3836. doi: 10.1126/scitranslmed.abl3836
82. Uldrick TS, Gonçalves PH, Abdul-Hay M, Claeys AJ, Emu B, Ernstoff MS, et al. Assessment of the Safety of Pembrolizumab in Patients With HIV and Advanced Cancer—A Phase 1 Study. *JAMA Oncol* (2019) 5(9):1332. doi: 10.1001/jamaoncol.2019.2244
83. Gonzalez-Cao M, Morán T, Dalmau J, Garcia-Corbacho J, Bracht JWP, Bernabe R, et al. Assessment of the Feasibility and Safety of Durvalumab for Treatment of Solid Tumors in Patients With HIV-1 Infection: The Phase 2 DURVAST Study. *JAMA Oncol* (2020) 6(7):1063–7. doi: 10.1001/jamaoncol.2020.0465
84. Reuss JE, Stern D, Foster JC, Ramaswami R, Lurain K, Chen HX, et al. Assessment of Cancer Therapy Evaluation Program Advocacy and Inclusion Rates of People Living With HIV in Anti-PD1/PDL1 Clinical Trials. *JAMA Netw Open* (2020) 3(12):e2027110. doi: 10.1001/jamanetworkopen.2020.27110
85. Coghill AE, Shiels MS, Suneja G, Engels EA. Elevated Cancer-Specific Mortality Among HIV-Infected Patients in the United States. *J Clin Oncol* (2015) 33(21):2376–83. doi: 10.1200/JCO.2014.59.5967
86. Coghill AE, Pfeiffer RM, Shiels MS, Engels EA. Excess Mortality Among HIV-Infected Individuals With Cancer in the United States. *Cancer Epidemiol Biomark Prev* (2017) 26(7):1027–33. doi: 10.1158/1055-9965.EPI-16-0964
87. Vora KB, Ricciuti B, Awad MM. Exclusion of Patients Living With HIV From Cancer Immune Checkpoint Inhibitor Trials. *Sci Rep* (2021) 11(1):1–6. doi: 10.1038/s41598-021-86081-w
88. Cook MR, Kim C. Safety and Efficacy of Immune Checkpoint Inhibitor Therapy in Patients With HIV Infection and Advanced-Stage Cancer: A Systematic Review. *JAMA Oncol* (2019) 5(7):1049–54. doi: 10.1001/jamaoncol.2018.6737
89. Luo L, Xu Y, Li T. Immune Checkpoint Inhibitor Therapy for Cancer Patients Infected With HIV: A Systematic Review. *Asia Pac J Clin Oncol* (2020) 1–6. doi: 10.1111/ajco.13320
90. Landriscina M, Altamura SA, Roca L, Gigante M, Piscazzi A, Cavalcanti E, et al. Reverse Transcriptase Inhibitors Induce Cell Differentiation and Enhance the Immunogenic Phenotype in Human Renal Clear-Cell Carcinoma. *Int J Cancer* (2008) 122(12):2842–50. doi: 10.1002/ijc.23197
91. Abt D, Besse A, Sedlarikova L, Kraus M, Bader J, Silzle T, et al. Improving the Efficacy of Proteasome Inhibitors in the Treatment of Renal Cell Carcinoma by Combination With the Human Immunodeficiency Virus (HIV)-Protease Inhibitors Lopinavir or Nelfinavir. *BJU Int* (2018) 121(4):600–9. doi: 10.1111/bju.14083

Conflict of Interest: The authors declare that the research was conducted in the absence of any commercial or financial relationships that could be construed as a potential conflict of interest.

frontiers | Frontiers in Oncology

ORIGINAL RESEARCH
published: 20 May 2022
doi: 10.3389/fonc.2022.899861

Transcriptome Profiles Reveal a 12-Signature Metabolic Prediction Model and a Novel Role of Myo-Inositol Oxygenase in the Progression of Prostate Cancer

Wangrui Liu[1,2†], Jianfeng Xiang[1†], Xinrui Wu[2†], Shiyin Wei[3†], Haineng Huang[3], Yu Xiao[3], Bo Zhai[1,4*] and Tao Wang[1*]*

[1] Department of Interventional Oncology, Renji Hospital, Shanghai Jiao Tong University School of Medicine, Shanghai, China, [2] Department of Clinical Medicine, Medical School of Nantong University, Nantong, China, [3] Affiliated Hospital of Youjiang Medical University for Nationalities, Baise, China, [4] State Key Laboratory of Oncogenes and Related Genes, Shanghai Cancer Institute, Renji Hospital, School of Medicine, Shanghai Jiao Tong University, Shanghai, China

Prostate adenocarcinoma (PRAD) is an extremely common type of cancer in the urinary system. Here, we aimed to establish a metabolic signature to identify novel targets in a predictive model of PRAD patients. A total of 133 metabolic differentially expressed genes (MDEGs) were identified with significant prognostic value. Least absolute shrinkage and selection operator (LASSO) regression analysis was used to construct a 12-mRNA signature model, a metabolic prediction model (MPM), in 491 PRAD patients. The risk score of the MPM significantly predicted the progression of PRAD patients ($p < 0.001$, area under the curve (AUC) = 0.745). Furthermore, myo-inositol oxygenase (MIOX), the most prominently upregulated metabolic enzyme and hub gene in the protein–protein interaction network of the MPM, showed significant prognostic implications. Next, MIOX expression in normal prostate tissues was lower than in PRAD tissues, and high MIOX expression was significantly associated with disease progression ($p = 0.005$, HR = 2.274) in 81 PRAD patients undergoing first-line androgen receptor signaling inhibitor treatment from the Renji cohort. Additionally, MIOX was significantly involved in the abnormal immune infiltration of the tumor microenvironment and associated with the DNA damage repair process of PRAD. In conclusion, this study provides the first opportunity to comprehensively elucidate the landscape of prognostic MDEGs, establish novel prognostic modeling of MPM using large-scale PRAD transcriptomic data, and identify MIOX as a potential prognostic target in PRAD patients from multiple cohorts. These findings help manage risk assessment and provide valuable insights into treatment strategies for PRAD.

Keywords: prostate adenocarcinoma, metabolic prediction models, myo-inositol oxygenase, progression, machine learning

OPEN ACCESS

Edited by:
Hailiang Zhang,
Fudan University, China

Reviewed by:
Jian-Yuan Zhao,
Fudan University, China
Anwaier Aihetaimujiang,
Fudan University, China

***Correspondence:**
Yu Xiao
yjxiaoyushennei@163.com
Bo Zhai
zhaiboshi@sina.com
Tao Wang
13061931996@163.com

†These authors have contributed equally to this work

Specialty section:
This article was submitted to Genitourinary Oncology, a section of the journal Frontiers in Oncology

Received: *19 March 2022*
Accepted: *04 April 2022*
Published: *20 May 2022*

Citation:
Liu W, Xiang J, Wu X, Wei S, Huang H, Xiao Y, Zhai B and Wang T (2022) Transcriptome Profiles Reveal a 12-Signature Metabolic Prediction Model and a Novel Role of Myo-Inositol Oxygenase in the Progression of Prostate Cancer. Front. Oncol. 12:899861. doi: 10.3389/fonc.2022.899861

INTRODUCTION

Prostate adenocarcinoma (PRAD) is primarily a hormone-driven disease mediated by cell growth that is driven by androgen receptor (AR) signaling. Elevated serum concentrations of the AR downstream target prostate-specific antigen (PSA) are evidence in support of this AR-mediated tumor growth. However, the therapeutic effect of castration therapy for PRAD patients is still not known to clinicians (1). The main reason is the presence of an AR amplification, mutation, or splice variant, which can eventually lead to castration-resistant prostate cancer. The prognosis of such patients remains unclear (2). In addition to those "AR-dependent" castration-resistant adenocarcinomas, a subset of patients was found to progress in AR-independent cancer biology, with short-term responses to hormone therapy, early and widespread metastases, and poor outcomes. Notably, this aggressive variant of prostate cancer is frequently associated with low PSA production and therefore cannot be identified by PSA monitoring, which presents a great challenge for clinicians and an extremely poor prognosis for patients (3). Therefore, early screening and diagnosis of PRAD remain challenging.

Numerous studies have identified many factors that may contribute to altered prostate cancer development, but these do not accurately predict tumor aggressiveness (4). Identifying the genomic alterations that cause cancer cells to transition from benign to malignant is critical (5). The genomic alterations observed in this transition include DNA damage repair capacity, telomerase activity, and loss of p53, among others (6, 7).

In recent years, novel immunotherapies represented by programmed cell death-1/programmed cell death-ligand (PD-1/PD-L1) inhibitors have rapidly emerged in the field of PRAD treatment (8), and their efficacy largely depends on interactions with the tumor microenvironment (TME) (9, 10). Accumulating studies have found that the efficacy of immunotherapy and targeted therapy is inseparable from the individual TME (11, 12). Therefore, exploring the underlying mechanisms of the occurrence and development of TME-driven PRAD, improving the efficiency of various existing treatments, and developing models that can accurately predict the disease are critical to advancing the understanding of the biology and developing better treatments (13, 14).

Homeostasis and evolution of the TME are controlled by close connections between all involved cells. This complex interaction often involves extracellular metabolites, which not only constitute a source of energy supply but also act as communication signals between different cellular compartments (15, 16). Cancer cells can use byproducts of sugar metabolism to hijack the functions of tumor-infiltrating immune cells for their benefit. All of these nutrient limitations can shape the metabolism of the developing tumor and thus act as a prominent invasive force (17).

This study aimed to first establish and validate an efficient prognostic metabolic prediction model (MPM) that recruits large-scale transcriptome metabolic genes in PRAD patients. We hypothesized that the MPM classifier could facilitate risk management and treatment strategies for PRAD patients and identify new targets in the combined network of MPMs, providing clinicians with a precise prognostic model for treating PRAD with new insights into precise treatment directions.

Abbreviations: PRAD, prostate adenocarcinoma; CTPAC, Clinical Proteomic Tumor Analysis Consortium; GSEA, Gene Set Enrichment Analysis; ICGC, International Cancer Genome Consortium; KEGG, Kyoto Encyclopedia of Genes and Genomes; MDEGs, metabolic differentially expressed genes; MPMs, metabolic prediction models; OS, overall survival; PFS, progression-free survival; PPI, protein–protein interaction; TCGA, The Cancer Genome Atlas; MIOX, myo-inositol oxygenase; AR, androgen receptor; PSA, prostate-specific antigen; TME, tumor microenvironment; AUC, area under the curve; ROC, receiver operating characteristic.

MATERIALS AND METHODS

Data Collection

This study used publicly available mRNA expression and clinical data from the PRAD cohort. Consent and ethical approval from registered patients are available in the relevant original article where the dataset was published. A total of 495 PRAD patients from the online dataset were obtained from The Cancer Genome Atlas (TCGA) database (https://portal.gdc.cancer.gov/).

Identification of Differentially Expressed Genes About Metabolism

Overall, 41 metabolic pathways were selected according to the Kyoto Encyclopedia of Genes and Genomes (KEGG) pathway atlas. The 133 metabolic genes were utilized to identify significant metabolic differentially expressed genes (MDEGs) using the Limma R package (Version 3.6.5) with false discovery rate (FDR) < 0.05 and $|\log FC| > 0.5$.

Metabolic Prediction Models

Univariate Cox regression analysis was used to identify prognostic implications of significant MDEGs, which were presented in a forest plot using the survival R package (18). Least absolute shrinkage and selection operator (LASSO) regression analysis was performed to construct the 12-mRNA signature model and MPMs in PRAD patients from TCGA cohorts with the glmnet and survival R packages (19).

Cox Regression Analysis and Receiver Operating Characteristic Curve Construction

All PRAD patients from TCGA cohorts were included for subsequent analysis. Univariate and multivariable Cox regression analyses were used to evaluate the independent prognostic value of the metabolic clusters using a forest plot. The receiver operating characteristic (ROC) curve was constructed for traditional clinical pathologic parameters and the risk score of MPMs in TCGA cohorts. The area under the curve (AUC) was utilized to assess the predictive value of these prognostic signatures.

Tumor Microenvironment Purity Assessment

The ESTIMATE algorithm was utilized to evaluate total and immune scores using the estimate package (http://r-forge.rproject.org; repos=rforge, dependencies=TRUE) in patients from TCGA cohort. Associations between TME purity and risk score of MPMs or myo-inositol oxygenase (MIOX) expression were assessed using Pearson's r test.

Differential Myo-Inositol Oxygenase mRNA Expression and Survival Analysis

Differentially expressed MIOX levels were evaluated between PRAD and normal samples from TCGA cohort using a Student's t-test. The Kaplan–Meier (KM) method with 95% CIs and a log-rank test was used for survival analysis in the Renji cohort. All analyses were performed in R (Version 4.0.1) and GraphPad Prism 8.0. Results were considered statistically significant when $p = 0.05$.

RESULTS

Identification of Metabolic Differentially Expressed Genes in Both The Cancer Genome Atlas Cohorts

The expression levels of 133 metabolic genes were collected from 495 PRAD samples in TCGA cohort. Then, these 133 metabolic genes were utilized for further analysis, where 46 significant MDEGs were identified and visualized in a volcano plot (**Figure 1A**). Hierarchical partitioning of significant MDEGs

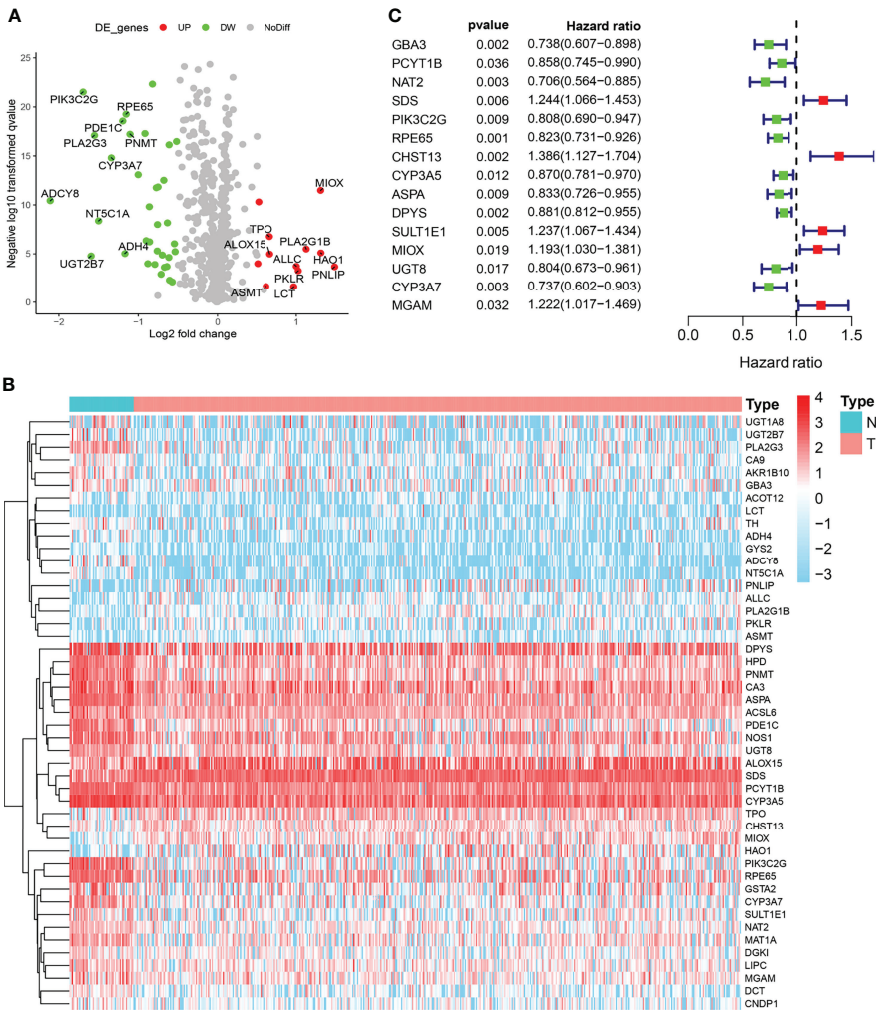

FIGURE 1 | Identification of metabolic differentially expressed genes (MDEGs) in both The Cancer Genome Atlas (TCGA) cohorts. **(A)** Identification of significant MDEGs from 133 metabolic genes. **(B)** Hierarchical partitioning of significant MDEGs was acquired from DNA microarrays based on TCGA cohort. **(C)** Univariate Cox regression analysis of 46 significant MDEGs ($p < 0.05$) in TCGA cohort was performed in a forest plot.

was acquired from DNA microarrays based on TCGA cohort (**Figure 1B**). The mRNA expression levels of these genes were examined across 495 PRAD patients and normal controls, with high expression shown in red and low expression shown in green. Additionally, a univariate Cox regression analysis of 58 significant MDEGs ($p < 0.05$) in TCGA cohort was performed in a forest plot (**Figure 1C**). Markedly, LASSO regression analysis was used to construct a 12-mRNA signature model and MPMs in PRAD patients of TCGA cohort. By comparing the p-value and hazard ratio, we analyzed the impact of each key gene on the survival of PRAD patients, and we selected MIOX as a hub gene regulating PRAD metabolic disorders ($p = 0.019$, HR = 1.193).

Survival Risk Assessment of Metabolic Prediction Models in The Cancer Genome Atlas Cohort

KM survival analysis showed the significant predictive value of the risk score depending on MPMs in TCGA cohort (**Figure 2A**). The prediction effect of the 12-mRNA signature model is statistically significant for 491 PRAD patients ($p < 0.001$). The high-risk group is marked in red, and the low-risk group is marked in blue. A survival risk assessment of MPMs consisting of the metabolic 12-mRNA signature was performed. The distributions of survival time, status (**Figure 2B**), risk score (**Figure 2C**), and hierarchical partitioning (**Figure 2D**) of MPMs in tumor and normal samples are shown in TCGA cohort ($p < 0.001$).

Cox Regression Analysis, Receiver Operating Characteristic Analysis, and Nomogram of Independent Prognostic Factors and Metabolic Prediction Models in Prostate Adenocarcinoma Patients

Univariate and multivariate Cox regression analyses enrolling clinical pathologic parameters and MPMs are illustrated using forest plots (**Figures 3A, B**). The risk score of MPMs significantly predicts the prognosis for PRAD patients in TCGA ($p < 0.001$, HR = 2.251). In addition, ROC analysis showed a robust predictive value of MPMs in TCGA (AUC = 0.745) cohorts (**Figure 3C**). A nomogram was constructed based on four independent prognostic factors, including Gleason score, pathologic N stage, pathologic T stage, and risk score of MPMs in PRAD patients (**Figure 3D**).

Gene Ontology, Kyoto Encyclopedia of Genes and Genomes, and Gene Set Enrichment Analysis

MIOX, a hub gene in the protein–protein interaction (PPI) network of MPMs, shows significant prognostic value in 495 PRAD patients from TCGA cohorts. The PPI network was constructed in 20 metabolic mRNA signatures in MPMs (**Figure 4A**). Gene Ontology (GO) term analysis showed that the genes that were significantly correlated with MIOX are involved in sulfur metabolism, retinol metabolism, and oxygen binding (**Figure 4B**). Gene Set Enrichment Analysis (GSEA)

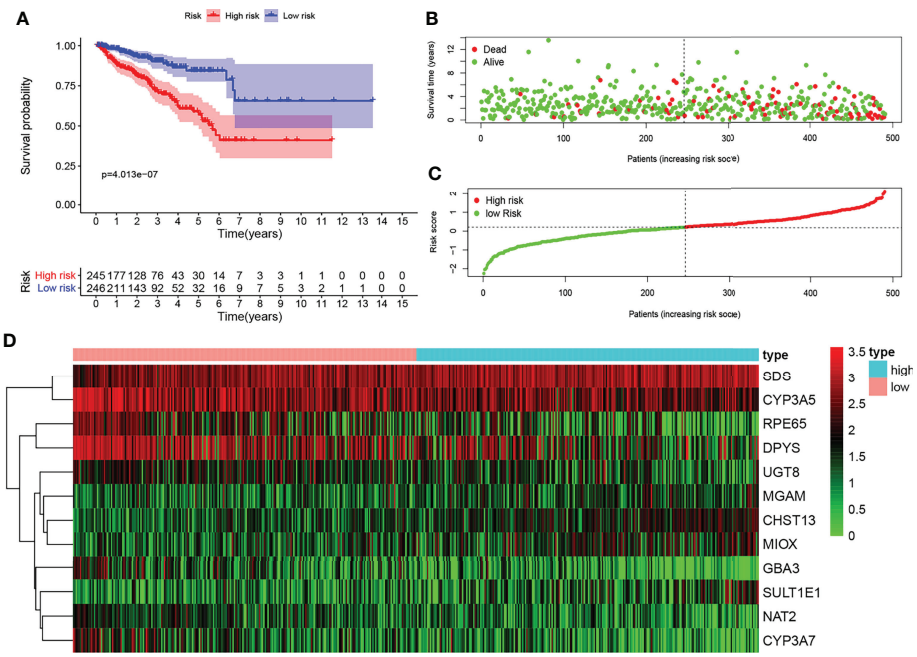

FIGURE 2 | Survival risk assessment of metabolic prediction models (MPMs) consists of a metabolic 12-mRNA signature in The Cancer Genome Atlas (TCGA) and the Clinical Proteomic Tumor Analysis Consortium (CTPAC) cohorts. **(A)** The 12-mRNA signature model (MPMs) in prostate adenocarcinoma (PRAD) patients was calculated using least absolute shrinkage and selection operator (LASSO) regression analysis. Kaplan–Meier survival analysis showed significant predictive value of the risk score depending on MPMs in TCGA cohort. **(B–D)** The distribution of survival time, **(B)** status, **(C)** risk score, and **(D)** hierarchical partitioning of 12 signatures in tumor and normal samples is shown in TCGA cohort.

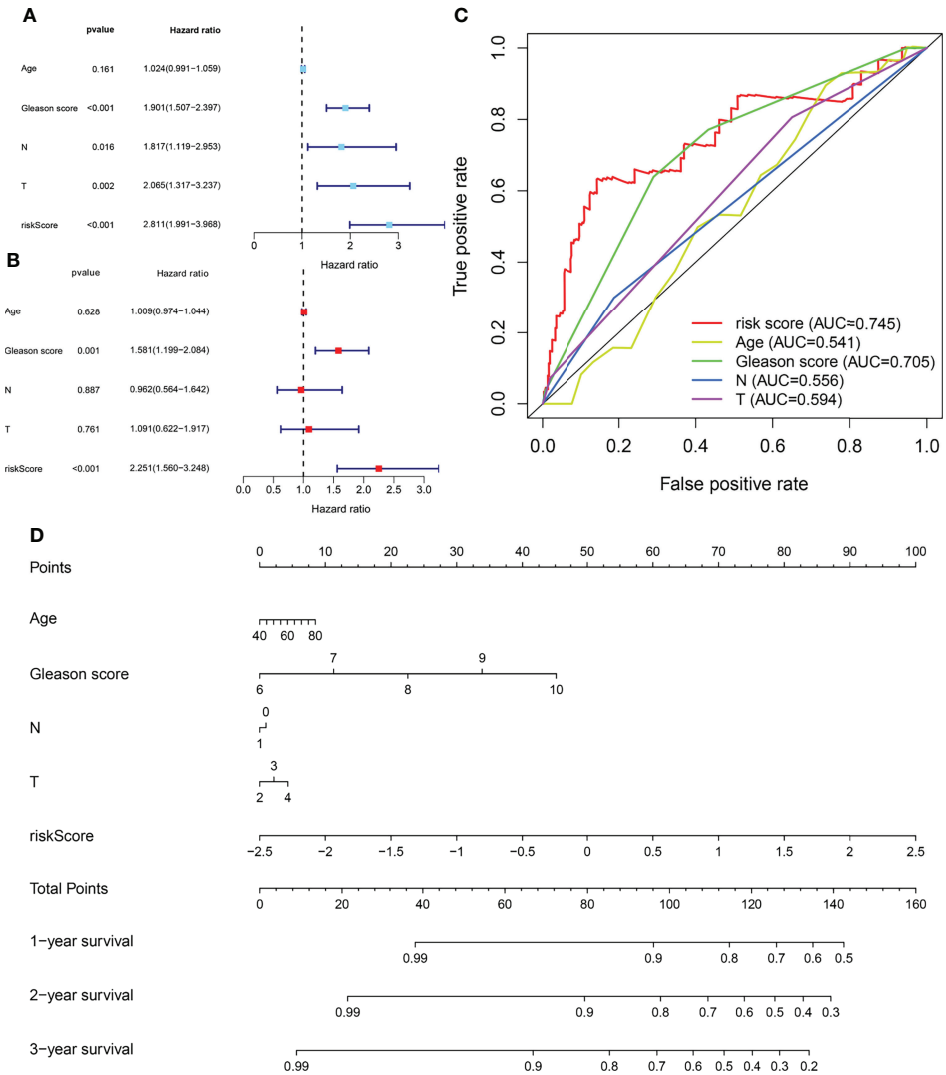

FIGURE 3 | Cox regression analysis, receiver operating characteristic (ROC) analysis, and nomogram of independent prognostic factors and metabolic prediction models (MPMs) in prostate adenocarcinoma (PRAD) patients. **(A, B)** Univariate and multivariate Cox regression analyses enrolling clinical pathologic parameters and MPMs are illustrated in The Cancer Genome Atlas (TCGA) cohort using forest plots. Risk score of MPMs significantly predict prognosis for PRAD patients in TCGA. **(C)** ROC analysis shows robust predictive value of MPMs in TCGA cohort (area under the curve (AUC) = 0.745). **(D)** A nomogram was constructed based on four independent prognostic factors in PRAD patients.

indicated significantly altered KEGG pathways based on differential risk scores of MPMs in PRAD patients with available transcriptomics data from TCGA and Clinical Proteomic Tumor Analysis Consortium (CTPAC) cohorts. The top five significantly altered KEGG pathways in high- or low-risk PRAD patients were examined in TCGA (**Figures 4C, D**) cohort. We found that the pathways involving the PRAD-related genes are mainly related to the Cell cycle, Homologous recombination, Lysine degradation, Amino sugar and nucleotide sugar metabolism, Arginine and proline metabolism, and Butanoate metabolism. This indicates that MIOX, as a key gene, is involved in the regulation of the cell cycle and metabolic pathways of tumor cells in PRAD.

Myo-Inositol Oxygenase Promotes an Immune-Infiltrated Tumor Microenvironment and Glycolytic Effects of Prostate Adenocarcinoma

Next, based on the CIBERSORT algorithm, we characterized the immune cell composition of complex tissues using their gene expression profiles of PRAD from TCGA. As shown in **Figure 5A**, we found significant enrichment in T-cell regulatory and T-cell CD4+ memory activated, while decreased naive B cells and myeloid dendritic cells activated in the high MIOX expression group. Next, we examined the percentage of immune cells expressing MIOX-high PRAD, with T cells

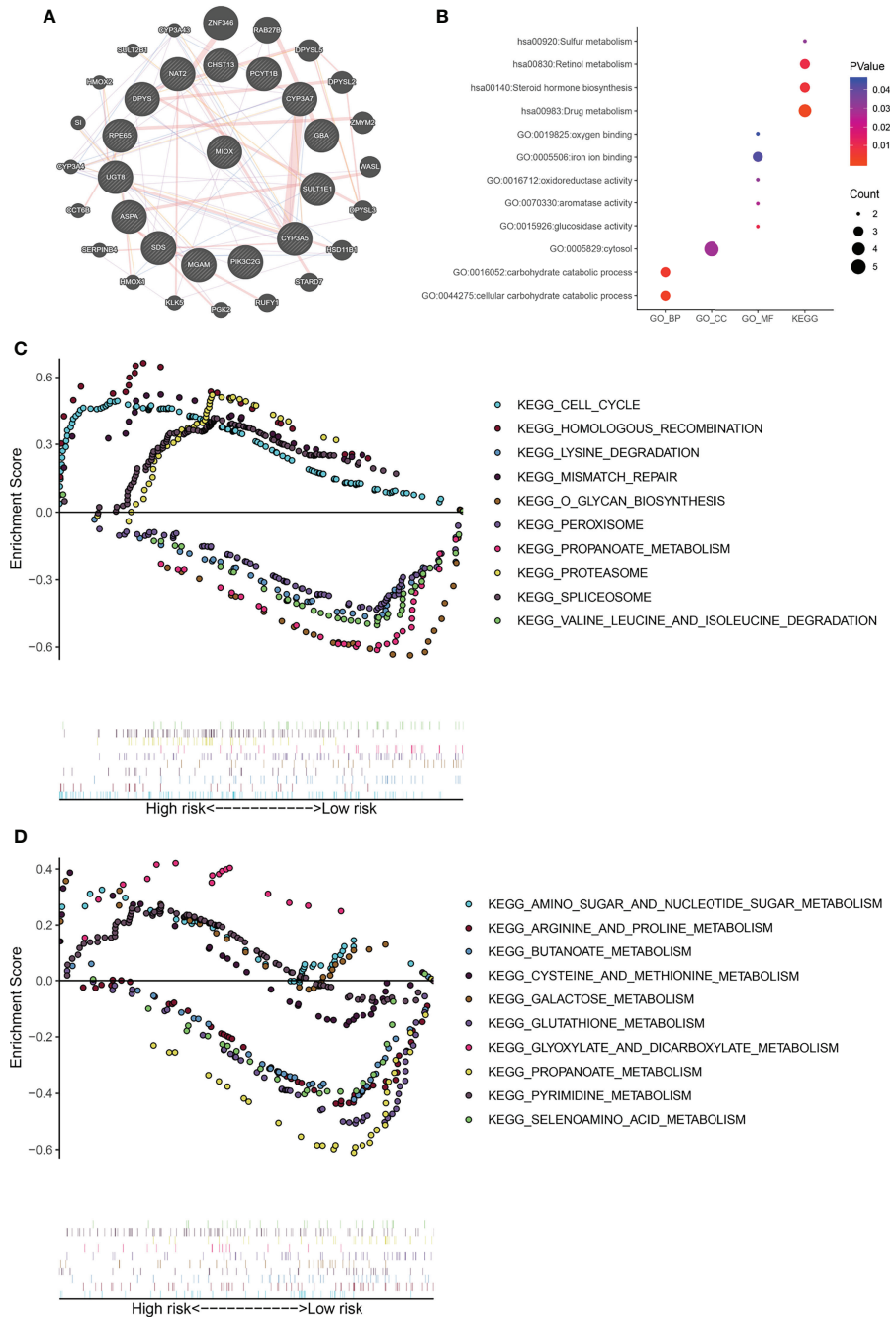

FIGURE 4 | Gene Set Enrichment Analysis (GSEA) indicated significantly altered Gene Ontology (GO) and Kyoto Encyclopedia of Genes and Genomes (KEGG) pathways based on differential risk scores of metabolic prediction models (MPMs) in prostate adenocarcinoma (PRAD) patients. **(A)** A protein–protein interaction (PPI) network was constructed in 12 metabolic mRNA signatures in MPMs. **(B)** GO analysis in high- or low-risk PRAD patients in The Cancer Genome Atlas (TCGA) cohort. **(C)** The top five significantly altered KEGG pathways in high- or low-risk PRAD patients in TCGA cohort. **(D)** The top five significantly altered KEGG pathways in high- or low-risk PRAD patients of the Clinical Proteomic Tumor Analysis Consortium (CTPAC) cohort.

accounting for a large proportion (**Figure 5B**). Additionally, for patients with higher MIOX expression, the expression levels of most immune checkpoint genes were significantly increased, including CTLA-4, LAG-3, PD-1, PD-L2, and SIGLEC15 (**Figure 5C**).

Elevated Myo-Inositol Oxygenase Expression Predicts Progression in the Renji Cohort

MIOX mRNA expression was examined across PRAD patients and normal controls. The MIOX expression difference between

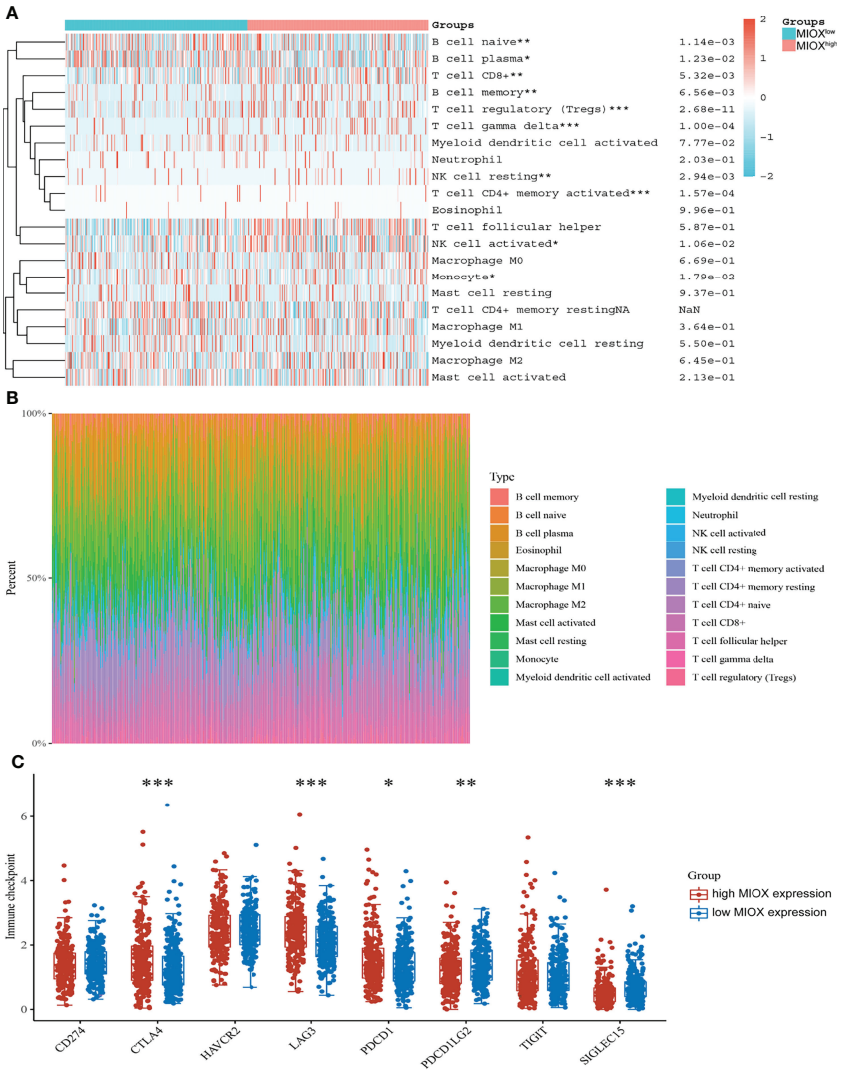

FIGURE 5 | Myo-inositol oxygenase (MIOX) promotes an immune-infiltrated tumor immune microenvironment (TIME) and glycolytic effects of prostate adenocarcinoma (PRAD). **(A)** The CIBERSORT algorithm was performed to characterize the immune cell composition of complex tissues from their gene expression profiles of PRAD in The Cancer Genome Atlas (TCGA). **(B)** The percentage of immune cells in PRAD with high MIOX expression. **(C)** Expression of immune checkpoint molecules was assessed using unpaired t-tests. *$p < 0.05$, **$p < 0.01$, ***$p < 0.001$.

tumor and normal tissues is very significant (**Figure 6A**, $p < 0.001$). KM survival analysis showed a significant predictive value of the risk score depending on MPMs in TCGA (**Figure 6B**). The high-risk group is marked in red, and the low-risk group is marked in blue. To validate the increased expression of MIOX in PRAD samples compared with normal prostate tissues using immunohistochemistry staining analysis (**Figure 6C**), we first collected samples and explored the prognostic implications of MIOX expression in 81 PRAD patients undergoing first-line AR signaling inhibitor from the Renji cohort. The nuclear MIOX protein expression levels were significantly higher in patients with worse prognoses compared with those with better prognoses in the Renji cohorts (**Figure 6D**). Additionally, the results suggested that increased MIOX protein expression was closely associated with worse PFS ($p = 0.005$, HR = 2.274). We then calculated mRNAsi, the stemness index score, of MIOX in PRAD. Although its association with mRNAsi was not significant, we found that the association between MIOX and the DNA damage repair process was statistically significant ($p < 0.001$) (**Figures 6E, F**).

DISCUSSION

Tumors can phenotypically and functionally damage the blood vessels of the original target organ during development, but tumor growth usually requires neovascularization. In turn, the TME typically exhibits some degree of hypoxia, which favors the

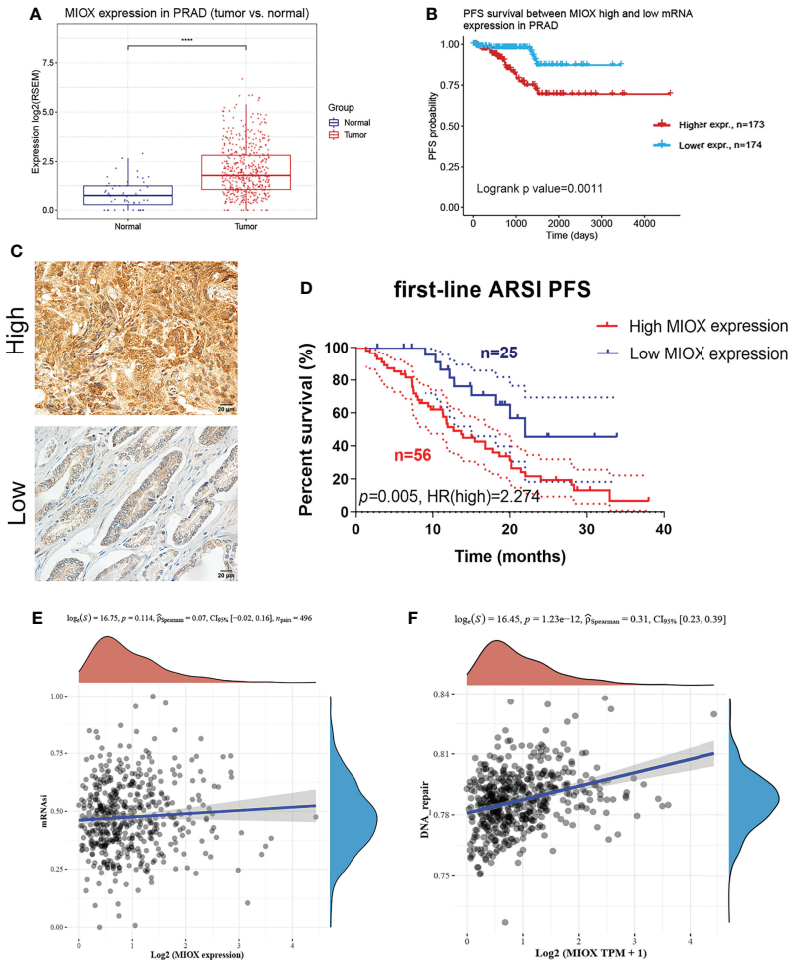

FIGURE 6 | Differential myo-inositol oxygenase (MIOX) expression predicts outcomes in 81 prostate adenocarcinoma (PRAD) patients from Renji cohorts. **(A)** MIOX was expressed at lower levels in normal prostate tissues. **(B)** In PRAD samples from The Cancer Genome Atlas (TCGA) cohort, higher MIOX expression was associated with worse progression-free survival (PFS) in patients. **(C, D)** High MIOX expression was significantly correlated with poor prognosis (p = 0.005, HR = 2.274) in 81 PRAD patients from the Renji cohort. **(E, F)** Dryness Index Score for MIOX in PRAD.

upregulation of solute carrier family 40 members and apolipoprotein 2, improves iron uptake by malignant cells, and promotes further proliferative activation (20). Moreover, in different *in vivo* mouse tumor models, metabolism leads to DNA damage-induced upregulation of transcript 4, which is also consistent with our study. The abovementioned processes lead to increased oxidative metabolism with a concomitant reduction in glucose uptake, ultimately leading to endothelial hyperactivation, resulting in increased glucose availability in the TME leading to neovascularization and metastasis (21).

The development of precise and accurate predictive biomarkers to clinically benefit prostate cancer patients remains an urgent and unmet clinical need. Promising predictive biomarkers being investigated by our group are precisely associated with reduced sensitivity to endocrine therapy and DNA repair defects (22, 23). However, this has not been without challenges. The significance of MIOX testing can only be fully realized when studies are conducted with active metabolically targeted therapies, converting MIOX from negative to positive predictive biomarkers (24, 25). Second, not all DNA repair deficiencies respond to treatment, with a recent study showing that men with ATM mutations have poorer treatment outcomes as compared with men with BRCA1/2 mutations. Further research is important to determine the best predictive biomarker suite for PRAD to provide the greatest clinical benefit for patients with lethal prostate cancer (26). Elucidating the pathogenesis of DNA repair proteins in prostate cancer could help identify strategies that may have therapeutic benefits, and a metabolic perspective would be even stronger. Taken together, these data demonstrate how detailed studies of protein function can lead to laboratory findings that can potentially impact the management and treatment of prostate cancer.

MIOX is a 32-kDa cytoplasmic enzyme that is expressed in the proximal renal tubule and is upregulated in hyperglycemia

(27, 28). A previous study showed that phosphorylation of serine/threonine residues of MIOX can enhance its enzymatic activity (29). Interestingly, the MIOX promoter includes osmotic pressure, carbohydrates, sterols, and oxidative-antioxidative response elements, and thus its transcription is regulated by organic osmotic regulators, high sugar, fatty acids, and oxidative stress (30, 31). We can argue that the upregulation of MIOX is associated with changes in cellular redox, as its promoter contains oxidative response elements. Previous studies have shown that the upregulation of MIOX in acute tubular injury is mediated by oxidants and endoplasmic reticulum stress. The latest research also shows that high blood sugar can lead to increased oxidative and endoplasmic reticulum stress while promoting each other's activities (32). Therefore, we believe that MIOX plays a key role in the TME of PRAD. As a core gene of aerobic metabolism and glucose metabolism in the TME, it can affect the prognosis of PRAD patients.

There are some limitations of this work. Our study is a single-center study, and in the future, we will conduct a multicenter prospective study to verify the conclusions. In addition, we will conduct *in vitro* and *in vivo* experiments to explore the potentially effective functions of MIOX and reveal the underlying mechanisms.

CONCLUSION

Overall, this study comprehensively elucidated the prognostic MDEGs landscape, established novel prognostic MPMs using large-scale PRAD transcriptome data, and identified MIOX as a potential prognostic target in PRAD patients from multiple cohorts. These findings could assist in managing risk assessment and provide valuable insight into treatment strategies for PRAD.

DATA AVAILABILITY STATEMENT

The original contributions presented in the study are included in the article/**Supplementary Material**. Further inquiries can be directed to the corresponding authors.

ETHICS STATEMENT

Study ethics procedures were approved by Renji Hospital, Shanghai Jiao Tong University School of Medicine.

AUTHOR CONTRIBUTIONS

The work was performed in cooperation with all authors. TW, BZ, and YX defined research topics, discussed analysis, supervise studies, provided funding, and revised manuscript. WL, XW, and SW drafted the manuscript, analyzed the data, and interpreted and validated the results. JX, WL, and TW assisted in performing data collection, statistical analysis, and reference collection. XW and WL helped in IHC analysis and patients' information collection from FUSCC. All authors read and approved the final manuscript.

FUNDING

This work is supported by the National Key Research and Development Program: 2020YFC0122305 and General Program from the National Natural Science Foundation of China: 82070619.

ACKNOWLEDGMENTS

We thank TCGA database for survival data and gene expressions. We thank J. Iacona, Ph.D., from Liwen Bianji (Edanz) (www.liwenbianji.cn), for editing the English text of a draft of this manuscript.

SUPPLEMENTARY MATERIAL

The Supplementary Material for this article can be found online at: https://www.frontiersin.org/articles/10.3389/fonc.2022.899861/full#supplementary-material

REFERENCES

1. Xu WH, Wang J, Sheng HY, Qu YY, Wang HK, Zhu Y, Shi GH, et al. Prognostic Implication and Functional Annotations of Rad50 Expression in Patients With Prostate Cancer. *J Cell Biochem* (2020) 121(5-6):3124–34. doi: 10.1002/jcb.29580
2. Wang J, Xu WH, Wei Y, Zhu Y, Qin XJ, Zhang HL, et al. Elevated MRE11 Expression Associated With Progression and Poor Outcome in Prostate Cancer. *J Cancer* (2019) 10(18):4333–40. doi: 10.7150/jca.31454
3. Moon YE, Joo MA, Joo J. Effects of Esmolol Continuous Infusion on Blood Loss in Patients Undergoing Posterior Lumbar Internal Fixation Surgery: A Prospective Randomized Study. *J Int Med Res* (2022) 50(3):3000605 221078705. doi: 10.1177/03000605221078705
4. Miyahira AK, Sharp A, Ellis L, Jones J, Kaochar S, Larman HB, et al. Prostate Cancer Research: The Next Generation; Report From the 2019 Coffey-Holden Prostate Cancer Academy Meeting. *Prostate* (2020) 80(2):113–32. doi: 10.1002/pros.23934
5. Graham MK, Meeker A. Telomeres and Telomerase in Prostate Cancer Development and Therapy. *Nat Rev Urol* (2017) 14(10):607–19. doi: 10.1038/nrurol.2017.104
6. Liu D, Takhar M, Alshalalfa M, Erho N, Shoag J, Jenkins RB, et al. Impact of the SPOP Mutant Subtype on the Interpretation of Clinical Parameters in Prostate Cancer. *JCO Precis Oncol* (2018) 2018. doi: 10.1200/PO.18.00036
7. Augello MA, Liu D, Deonarine LD, Robinson BD, Huang D, Stelloo S, et al. CHD1 Loss Alters AR Binding at Lineage-Specific Enhancers and Modulates Distinct Transcriptional Programs to Drive Prostate Tumorigenesis. *Cancer Cell* (2019) 35(5):817–9. doi: 10.1016/j.ccell.2019.04.012
8. Wu J, Xu WH, Wei Y, Qu YY, Zhang HL, Ye DW. An Integrated Score and Nomogram Combining Clinical and Immunohistochemistry Factors to

Predict High ISUP Grade Clear Cell Renal Cell Carcinoma. *Front Oncol* (2018) 8:634. doi: 10.3389/fonc.2018.00634
9. Egan BM, Hennes MM, Stepniakowski KT, O'Shaughnessy IM, Kissebah AH, Goodfriend TL. Obesity Hypertension is Related More to Insulin's Fatty Acid Than Glucose Action. *Hypertension* (1996) 27(3 Pt 2):723–8. doi: 10.1161/01.HYP.27.3.723
10. Gonias SL, Karimi-Mostowfi N, Murray SS, Mantuano E, Gilder AS. Expression of LDL Receptor-Related Proteins (LRPs) in Common Solid Malignancies Correlates With Patient Survival. *PloS One* (2017) 12(10): e0186649. doi: 10.1371/journal.pone.0186649
11. Lu X, Li C, Xu W, Wu Y, Wang J, Chen S, et al. Malignant Tumor Purity Reveals the Driven and Prognostic Role of CD3E in Low-Grade Glioma Microenvironment. *Front Oncol* (2021) 11:676124. doi: 10.3389/fonc.2021.676124
12. Xu W, Anwaier A, Ma C, Liu W, Tian X, Palihati M, et al. Multi-Omics Reveals Novel Prognostic Implication of SRC Protein Expression in Bladder Cancer and its Correlation With Immunotherapy Response. *Ann Med* (2021) 53(1):596–610. doi: 10.1080/07853890.2021.1908588
13. Xu W, Anwaier A, Liu W, Tian X, Zhu W-K, Wang J, et al. Systematic Genome-Wide Profiles Reveal Alternative Splicing Landscape and Implications of Splicing Regulator DExD-Box Helicase 21 in Aggressive Progression of Adrenocortical Carcinoma. *Phenomics* (2021) 1(6):243–56. doi: 10.1007/s43657-021-00026-x
14. Yang H, Xu F, Xiao K, Chen Y, Tian Z. N-Glycoproteomics Study of Putative N-Glycoprotein Biomarkers of Drug Resistance in MCF-7/ADR Cells. *Phenomics* (2021) 1(6):269–84. doi: 10.1007/s43657-021-00029-8
15. Wu Q, Huang Q-X, Zeng H-l, Ma S, Lin H-D, Xia M-F, et al. Prediction of Metabolic Disorders Using NMR-Based Metabolomics: The Shanghai Changfeng Study. *Phenomics* (2021) 1(4):186–98. doi: 10.1007/s43657-021-00021-2
16. Nieman KM, Kenny HA, Penicka CV, Ladanyi A, Buell-Gutbrod R, Zillhardt MR, et al. Adipocytes Promote Ovarian Cancer Metastasis and Provide Energy for Rapid Tumor Growth. *Nat Med* (2011) 17(11):1498–503. doi: 10.1038/nm.2492
17. Krauß D, Fari O, Sibilia M. Lipid Metabolism Interplay in CRC-An Update. *Metabolites* (2022) 12(3):213. doi: 10.3390/metabo12030213
18. Teng B, Xie C, Zhao Y, Wang Z. Studies Related to Ruptured Abdominal Aortic Aneurysms in the Past 10 Years (2011-2020): A Bibliometric Analysis. *Med Sci Monit* (2022) 28:e935006. doi: 10.12659/MSM.935006
19. Sun C, Zhu B, Zhu S, Zhang L, Du X, Tan X. Risk Factors Analysis of Bone Mineral Density Based on Lasso and Quantile Regression in America During 2015-2018. *Int J Environ Res Public Health* (2021) 19(1):355. doi: 10.3390/ijerph19010355
20. Mertens C, Akam EA, Rehwald C, Brüne B, Tomat E, Jung M. Intracellular Iron Chelation Modulates the Macrophage Iron Phenotype With Consequences on Tumor Progression. *PloS One* (2016) 11(11):e0166164. doi: 10.1371/journal.pone.0166164
21. Wenes M, Shang M, Di Matteo M, Goveia J, Martín-Prez R, Serneels J, et al. Macrophage Metabolism Controls Tumor Blood Vessel Morphogenesis and Metastasis. *Cell Metab* (2016) 24(5):701–15. doi: 10.1016/j.cmet.2016.09.008
22. Armenia J, Wankowicz SAM, Liu D, Gao J, Kundra R, Reznik E, et al. The Long Tail of Oncogenic Drivers in Prostate Cancer. *Nat Genet* (2018) 50 (5):645–51. doi: 10.1038/s41588-018-0078-z
23. Sharp A, Coleman I, Yuan W, Sprenger C, Dolling D, Rodrigues DN, et al. Androgen Receptor Splice Variant-7 Expression Emerges With Castration Resistance in Prostate Cancer. *J Clin Invest* (2019) 129(1):192–208. doi: 10.1172/JCI122819
24. Sharp A, Porta N, Lambros MBK, Welti JC, Paschalis A, Raj GV, et al. Dissecting Prognostic From Predictive Utility: Circulating AR-V7 Biomarker Testing for Advanced Prostate Cancer. *J Clin Oncol* (2019) 37(24):2182–4. doi: 10.1200/JCO.19.01104
25. Armstrong AJ, Halabi S, Luo J, Nanus DM, Scher HI, Antonarakis ES, et al. Reply to L. Dirix, B. De Laere Et Al and A. Sharp Et al. *J Clin Oncol* (2019) 37 (24):2184–6. doi: 10.1200/JCO.19.01230
26. Mateo J, Lord CJ, Serra V, Tutt A, Balmaña J, Castroviejo-Bermejo M, et al. A Decade of Clinical Development of PARP Inhibitors in Perspective. *Ann Oncol* (2019) 30(9):1437–47. doi: 10.1093/annonc/mdz192
27. Nayak B, Xie P, Akagi S, Yang Q, Sun L, Wada J, et al. Modulation of Renal-Specific Oxidoreductase/Myo-Inositol Oxygenase by High-Glucose Ambience. *Proc Natl Acad Sci USA* (2005) 102(50):17952–7. doi: 10.1073/pnas.0509089102
28. Chang HH, Chao HN, Walker CS, Choong SY, Phillips A, Loomes KM. Renal Depletion of Myo-Inositol is Associated With its Increased Degradation in Animal Models of Metabolic Disease. *Am J Physiol Renal Physiol* (2015) 309 (9):F755–63. doi: 10.1152/ajprenal.00164.2015
29. Nayak B, Kondeti VK, Xie P, Lin S, Viswakarma N, Raparia K, et al. Transcriptional and Post-Translational Modulation of Myo-Inositol Oxygenase by High Glucose and Related Pathobiological Stresses. *J Biol Chem* (2011) 286(31):27594–611. doi: 10.1074/jbc.M110.217141
30. Prabhu KS, Arner RJ, Vunta H, Reddy CC. Up-Regulation of Human Myo-Inositol Oxygenase by Hyperosmotic Stress in Renal Proximal Tubular Epithelial Cells. *J Biol Chem* (2005) 280(20):19895–901. doi: 10.1074/jbc.M502621200
31. Tominaga T, Dutta RK, Joladarashi D, Doi T, Reddy JK, Kanwar YS, et al. Transcriptional and Translational Modulation of Myo-Inositol Oxygenase (Miox) by Fatty Acids: Implications in Renal Tubular Injury Induced in Obesity and Diabetes. *J Biol Chem* (2016) 291(3):1348–67. doi: 10.1074/jbc.M115.698191
32. Sharma I, Deng F, Liao Y, Kanwar YS. Myo-Inositol Oxygenase (MIOX) Overexpression Drives the Progression of Renal Tubulointerstitial Injury in Diabetes. *Diabetes* (2020) 69(6):1248–63. doi: 10.2337/db19-0935

Conflict of Interest: The authors declare that the research was conducted in the absence of any commercial or financial relationships that could be construed as a potential conflict of interest.

Publisher's Note: All claims expressed in this article are solely those of the authors and do not necessarily represent those of their affiliated organizations, or those of the publisher, the editors and the reviewers. Any product that may be evaluated in this article, or claim that may be made by its manufacturer, is not guaranteed or endorsed by the publisher.

frontiers | Frontiers in Oncology

ORIGINAL RESEARCH
published: 22 June 2022
doi: 10.3389/fonc.2022.914692

Molecular Characterization and Clinical Relevance of N^6-Methyladenosine Regulators in Metastatic Prostate Cancer

Qiwei Liu[1,2†], Zhen Li[3,4†], Lizhao He[1†], Ke Li[1], Chen Hu[1], Jialiang Chen[1], Fangjian Zhou[3,4], Jun Wang[3,4], Yonghong Li[3,4*] and Hengjun Xiao[1*]*

[1] Department of Urology, the Third Affiliated Hospital of Sun Yat-Sen University, Guangzhou, China, [2] Plastic Surgery Institute, Chinese Academy of Medical Sciences and Peking Union Medical College, Beijing, China, [3] State Key Laboratory of Oncology in South China, Collaborative Innovation Center for Cancer Medicine, Sun Yat-sen University Cancer Center, Guangzhou, China, [4] Department of Urology, Sun Yat-sen University Cancer Center, Guangzhou, China

OPEN ACCESS

Edited by:
Hailiang Zhang,
Fudan University, China

Reviewed by:
Wangrui Liu,
Shanghai Jiao Tong University, China
Lin Shan,
Capital Medical University, China

***Correspondence:**
Jun Wang
Wangjun2@sysucc.org.cn
Yonghong Li
liyongh@sysucc.org.cn
Hengjun Xiao
hjxiao555@126.com

[†]These authors have contributed equally to this work

Specialty section:
This article was submitted to Genitourinary Oncology, a section of the journal Frontiers in Oncology

Received: 07 April 2022
Accepted: 20 May 2022
Published: 22 June 2022

Citation:
Liu Q, Li Z, He L, Li K, Hu C, Chen J, Zhou F, Wang J, Li Y and Xiao H (2022) Molecular Characterization and Clinical Relevance of N^6-Methyladenosine Regulators in Metastatic Prostate Cancer. Front. Oncol. 12:914692. doi: 10.3389/fonc.2022.914692

Prostate cancer is a leading malignancy in the male population globally. N6-methylation of adenosine (m6A) is the most prevalent mRNA modification and plays an essential role in various biological processes *in vivo*. However, the potential roles of m6A in metastatic prostate cancer are largely unknown. In this study, we evaluated and identified two m6A modification patterns based on 21 m6A regulators in four public metastatic prostate cancer datasets. Different modification patterns correlated with distinct molecular characteristics. According to m6A-associated genes, we constructed a prognostic model, called m6Ascore, to predict the outcomes of patients with metastatic prostate cancer. We found that high m6A score level was related to dismal prognosis and characterized by higher cell cycle, DNA repair and mismatch repair pathway score. *In vitro* experiments confirmed that upregulation of METTL14, an m6A writer, enhanced the invasion, metastasis, and sensitivity of prostate cancer cells to poly (ADP-ribose) polymerase inhibitor. Conversely, down-regulation of potential target genes of m6A had the opposite effect. Finally, we validated that a higher m6A score was associated with a worse prognosis and a higher Gleason score in The Cancer Genome Atlas Program (TCGA) cohort. This work illustrated the nonnegligible role of m6A modification in multiple biological processes of metastatic prostate cancer. Evaluating the m6A risk scores of individual tumours will guide more effective judgement of prognosis as well as treatments for metastatic prostate cancer in clinical practice.

Keywords: metastatic prostate cancer, m6A, regulator, prognosis, treatment

INTRODUCTION

Prostate cancer (PCa) is the most prevalently diagnosed malignancy in men. There are, however, limited effective treatments for advanced prostate cancer, especially metastatic prostate cancer (1). Although multiple treatments, including surgery, chemotherapy, radiotherapy, and targeted therapy, have improved the outcomes of prostate cancer to some extent, some adverse effects, such as resistance and toxicity, still exist (2). Thus, burrowing prognostic and therapeutic molecular biomarkers is urgent.

To date, more than 150 kinds of posttranscriptional modifications in RNA have been identified (3). N6-methyladenosine (m6A) is the most common RNA modification in mammalian cells (4) and has been suggested to be involved in various aspects of RNA metabolism and to play essential roles in different biological processes in mammals (5, 6). m6A methylation is achieved by recognition proteins (readers) and methyltransferases (writers), and the demethylation process is conducted by demethyltransferases (erasers). "Readers" include YTHDF1/2/3, YTHDC1/2, FMR1 and HNRNPA2B1; "writers" include METTL3, METTL5, METTL14, METTL16, WTAP, KIAA1429, ZC3H13 and RBM15; and "erasers" include FTO and ALKBH5.

Accumulated studies have highlighted tight connections between m6A methylation and tumour initiation and progression (6). In glioblastoma, downregulation of FTO or upregulation of METTL3 was involved in the poor prognosis of glioblastoma by promoting the proliferation and self-renewal of glioblastoma stem cells (7). High expression of METTL3 or METTL4 was also essential for the maintenance and self-renewal of leukaemia stem cells, thus aggravating acute myeloid leukaemia (8). Upregulation of METTL3 and downregulation of METTL14 can both lead to progression of hepatocellular carcinoma by facilitating cell proliferation and invasion (9, 10). YTHDF2 not only enhances cell proliferation by the AKT/GSK3β/cyclin D1 signalling axis but also inhibits migration and invasion by destabilizing the m6A sites of YAP (11). Huang et al. constructed a prognostic model for colon cancer basing on seven m6A regulators, and characterized three distinct subtypes of colon cancer, one of which was recognized as immunosuppressive (12). Similarly, Zhang et al. characterized tumor microenvironment characteristics through evaluating the m6A modification patterns (13). Wang et al. constructed a prognostic model for prostate cancer based on MRTTL14 and YTHDF2 (14). However, the mode of action of m6A methylation in metastatic prostate cancer remains largely unknown. Herein, we used published sequencing data to investigate the exact role of m6A methylation with respect to metastatic prostate cancer. This m6Ascore group-based model may facilitate the more effective judgement of prognosis for patients with metastatic prostate cancer and offer more valuable information for personalized precise pharmacy therapy.

MATERIALS AND METHODS

Prostate Cancer Dataset

Public gene expression data and relative clinical information were gathered from the TCGA database (https://xenabrowser.net/datapages/). Patients without detailed survival information were removed. In addition, four eligible metastatic prostate cancer cohorts were acquired from https://www.cbioportal.org/, which include mRNA expression data, somatic mutation data and copy number variation (CNV). Clinical annotations were downloaded by the *R* package cgdsr, and somatic mutation data were collected using the R package TCGAbiolinks (15). Specific collected data are shown in **Table 1**, and more detailed information about the samples is presented in **Supplementary Table 1**.

TABLE 1 | Specimen information.

	mRNA	SNP	CNV
TCGA_PRAD	481	503	502
nepc_wcm_2016	49	114	107
prad_mich	31	61	60
prad_su2c_2015	118	150	150
prad_su2c_2019	212	442	443

For data consistency, the original data from https://www.cbioportal.org/were normalized by the z-score function, and the FPKM data from TCGA were transformed into the zscore normalized dataset. Finally, batch effects were corrected using the *R* package *sva*.

Unsupervised Clustering for 21 m6A Regulators

Altogether, 21 m6A regulators were extracted from four eligible metastatic prostate cancer cohorts downloaded from the cBioPortal website to discern distinct m6A regulator-mediated modification patterns. These regulators consisted of 8 writers (METTL3, METTL14, RBM15, RBM15B, WTAP, KIAA1429, CBLL1, ZC3H13), 2 erasers (ALKBH5, FTO) and 11 readers (YTHDC1, YTHDC2, YTHDF1, YTHDF2, YTHDF3, IGF2BP1, HNRNPA2B1, HNRNPC, FMR1, LRPPRC, ELAVL1). Based on the different expression patterns of m6A regulators, unsupervised clustering was performed to identify various m6A modification patterns and classify patients. We applied the consensus clustering algorithm (ConsensusClusterPlus package, 1000 repetitions) to determine cluster numbers and their stability (16).

Gene Set Variation Analysis and Functional Annotation

To further investigate the biological significance of different m6A modification patterns, we conducted GSVA enrichment analysis with the "GSVA" R package. GSVA is a nonparametric and unsupervised technique that is commonly used to estimate changes in biological processes and signal pathways in samples (17). The annotated gene sets of "c2.cp.kegg.v6.2.-symbols" were collected from the MSigDB database (https://www.gsea-msigdb.org/gsea/index.jsp). Adjusted P <0.5 was viewed as statistically significant. To carry out functional annotation for m6A-related genes, the clusterProfiler R package was used (FDR cut-off of < 0.05).

Identification of Differentially Expressed Genes Between Distinct m6A Phenotypes

Referring to distinctly expressed m6A regulators, we classified four eligible metastatic prostate cancer cohorts collected from the cBioPortal website into two different m6A modification patterns. DEGs between the two distinct modification patterns were determined by the R package limma (18). Genes with p<0.5 and 1.5<fold-change (or fold-change <0.667) were regarded as differentially expressed genes.

m6Ascore Calculation

Redundant genes of DEGs were removed using the random forest approach (19), and the remaining genes were selected for survival

analysis ($p<0.05$). Genes were classified into two clusters utilizing the Cox regression model. Based on the above genes, we construct a prognostic model, called m6Ascore.We then calculated m6Ascore referring to the following GGI method (20): m6Ascore=scale(ΣX-ΣY), where x or y is the gene expression value when the Cox coefficient is positive or negative, respectively. Based on the median value of m6Ascore, samples were divided into m6Ascore-high and m6Ascore-low. Subsequently, prognostic analysis was performed between the two samples.

Correlation Between the m6A Gene Signature and Other Related Biological Processes

Mariathasan et al. constructed a series of gene sets involved in specific biological processes, including immune checkpoints; epithelial mesenchymal transition (EMT) markers such as EMT1 and EMT2; and DNA mismatch repair (21). We subsequently carried out correction analysis to uncover the relationships between m6Ascore and relative biological pathways.

Copy Number Variation Analysis

According to SNP6 CopyNumber segment data, the shared changing areas of copy number among all the samples were detected utilizing the GISTIC method. Relative parameters were set as follows: $Q \leq 0.05$, confidence level was 0.95. The above analysis was performed using the corresponding MutSigCV module of GenePattern (https://cloud.genepattern.org/gp/pages/index.jsf, an online analytical tool developed by the Broad Research Institute.

Cell Culture and Cell Transfection

Human prostate cancer cell lines DU145 and PC3 were obtained from ATCC (USA). Cells were kept in RPMI-1640 medium supplemented with 10% FBS at 37°C in a humidified incubator with 5% CO_2.

After reaching 80% confluency, cells were transfected with the following lentiviral plasmids using Lipofectamine® 2000 (Invitrogen): short hairpin (sh)RNA-NC (5 nM), pLVSO2-METTL14 (5 nM), pLKOG-shRNA-CSNK1D-ABC (5 nM), pLKOG-shRNA- METTL14-AB (5 nM), and pLKOG-shRNA-SLC35E1-ABC (5 nM). Twenty-four hours after transfection, subsequent experiments were performed.

Western Blot Analysis

Western blotting was conducted as previously described (22). Briefly, protein concentrations were measured with a BCA Kit. Protein lysates were resolved using SDS–PAGE and transferred onto PVDF membranes (Millipore). The membrane was subsequently incubated overnight (4°C) with the following primary antibodies: anti-METTL14 (Norvus), anti-CSNK1D (Norvus), anti-SLC35E1 (Norvus) and β-actin (Invitrogen). After washing, the membranes were further subjected to the appropriate secondary antibodies (Invitrogen). Blots were visualized by a ChemiDoc XRS system, followed by quantification using Image Lab software (Bio–Rad).

Transwell Assay

Matrigel was defrosted at 4°C overnight and diluted with serum-free medium (dilution, 1:6). Transwells were inserted in a 24-well culture plate, 40 μl of prediluted Matrigel was inoculated into each Transwell chamber, followed by 2 hours in a 37°C incubator to coagulate. Stably transfected cells were previously seeded in 6-well plates and cultured to 90% confluence. After digestion, a total of 200 μl cell suspension (8×10^4 cells/well) was dispensed to the upper chamber, and 800 μl medium containing 30% FBS was dispensed to the lower chamber. After 24 hours of incubation at 37°C, cells in the upper layer of the Transwell were removed with sterile cotton swabs, followed by PBS washing and fixation with methanol for 20 min. Subsequently, cells were further stained with crystal violet dye for 5 min, washed with distilled water, imaged and counted under an inverted microscope.

Wound Healing Assay

Transfected cells were plated into a 6-well plate. Before scratching, the culture medium was replaced with serum-free medium containing 1 μg/ml mitomycin C to obtain monolayer cells. Scratches were generated using 200 μl pipette tips, followed by washing three times with PBS. Migrated cells were counted and photographed by a microscope at 0 and 24 hours after scratching.

CCk-8 Assay

When the cell confluency reached 70%, drugs were added for 72 hours. DMSO was added to the control groups, and the experimental groups were administered olaparib for 72 hours. Cells were cultured to 90% confluence and then subjected to digestion, centrifugation and resuspension. Cells were further seeded in 96-well plates at a density of 4×103 cells/well. Cell proliferation was detected with a CCK-8 assay following the manufacturer instructions after culture for 24, 48 and 96 hours. The absorbance was measured at 45 nm wavelength.

Statistical Analyses

The bioinformatics differences between the two groups were analysed using the Wilcox test. Referring to the relevance between m6Ascore and patient survival, the cut-off values of different subgroups were identified by the survminer R package. Survival curves were generated using Kaplan–Meier analysis, and significant differences were determined by log-rank tests. The predictive value of m6Ascore for metastatic samples was evaluated *via* receiver operating characteristic (ROC) curve analysis, and the area under the curve (AUC) was calculated utilizing the pROC R package. The maftools R package was applied to plot the mutation atlas of patients with high and low m6Ascore. The R package RCircos was used to depict the location of m6A regulators on chromosomes. ns represents $P > 0.05$, *$P \leq 0.05$, ** $P \leq 0.01$, *** $P \leq 0.001$, **** $P \leq 0.0001$.

For the experimental data, a two-tailed t test was used with PRISM software. A P value < 0.05 was viewed as statistically significant.

RESULTS

The Genetic Variation of m6A Regulators

Altogether, 21 m6A regulators (8 writers, 2 erasers and 11 readers) were identified. We first analysed the mRNA

expression levels of m6A regulators between metastatic and nonmetastatic samples and found that few genes were differentially expressed, such as FMR1 and FTO (**Figure 1**). Subsequently, we summarized the incidence of CNV and somatic mutations of 21 m6A regulators in metastatic, nonmetastatic and NEPC samples. Except for the prevalent missing frequency of CNV in a few regulators, such as FTO, RBM15B and YTHDC2, most regulators experienced an amplification in copy number (**Figures 1B–E**; **Supplementary Table 2**). Among these samples, mutations of m6A regulators rarely occurred (**Figures 1F, G**). The distribution of m6A regulators on chromosomes is presented in **Figure 1H**.

Unsupervised Clustering for m6A Regulators in Metastatic Prostate Cancer

We performed consensus clustering and univariate Cox analysis utilizing m6A gene expression matrix and patient's survival information from the prad_su2c_2019 dataset. The m6A regulation network in **Figure 2A** (**Supplementary Table 3**) revealed that the interaction and junction of m6A regulators and their impacts on the prognosis of metastatic prostate cancer. We found that not only the same functional categories of m6A regulators but also the distinct functional categories of m6A regulators displayed significant correlations in expression.

The above results illustrated that the interactions between distinct functional categories of m6A regulators may play important roles in various m6A modification patterns. We characterized the different expression patterns of 21 m6A regulators in four eligible metastatic prostate cancer cohorts downloaded from the cBioPortal website and performed unsupervised clustering analysis using the ConsensusClusterPlus R package, which led to the identification of two distinct subclusters (**Figure 2B**, **Supplementary Table 4**). We termed these patterns m6A Clusters.A and m6A Clusters.B, respectively.

To investigate biological behaviours among different subgroups, we performed gene set enrichment analysis (GSEA) (**Supplementary Table 5**). As shown in **Figure 2D**, m6A Cluster.A was significantly enriched in lysine degradation and the mTOR signalling pathway. m6A Cluster.B was mainly enriched in arachidonic acid metabolism and steroid hormone biosynthesis (**Supplementary Table 6**).

Furthermore, we evaluated the expression and mutation atlas of specific genes between m6A Cluster.A and m6A Cluster.B (**Figure 2E, F**, **Supplementary Tables 7, 8**). Particularly, in the prad_su2c_2019 datasets, the ARV7 score and ARscore between these two clusters showed significant differences (**Figure 3**, **Supplementary Table 9**). Further prognosis analysis revealed that the prognosis between these two clusters was significantly different (**Figure 2C**). Subsequently, we performed GSVA based on the gene sets constructed by Mariathasan et al. (**Figure 3C**, **Supplementary Table 10**). The activities of matrix molecules were markedly increased in m6A Cluster.B, such as the activation of epithelial mesenchymal transition, transforming growth factor-β and angiogenesis signalling pathways. In addition, the expression levels of m6A regulators in the m6A cluster.A were higher than in m6A Cluster.B (**Figure 3D**, **Supplementary Table 11**).

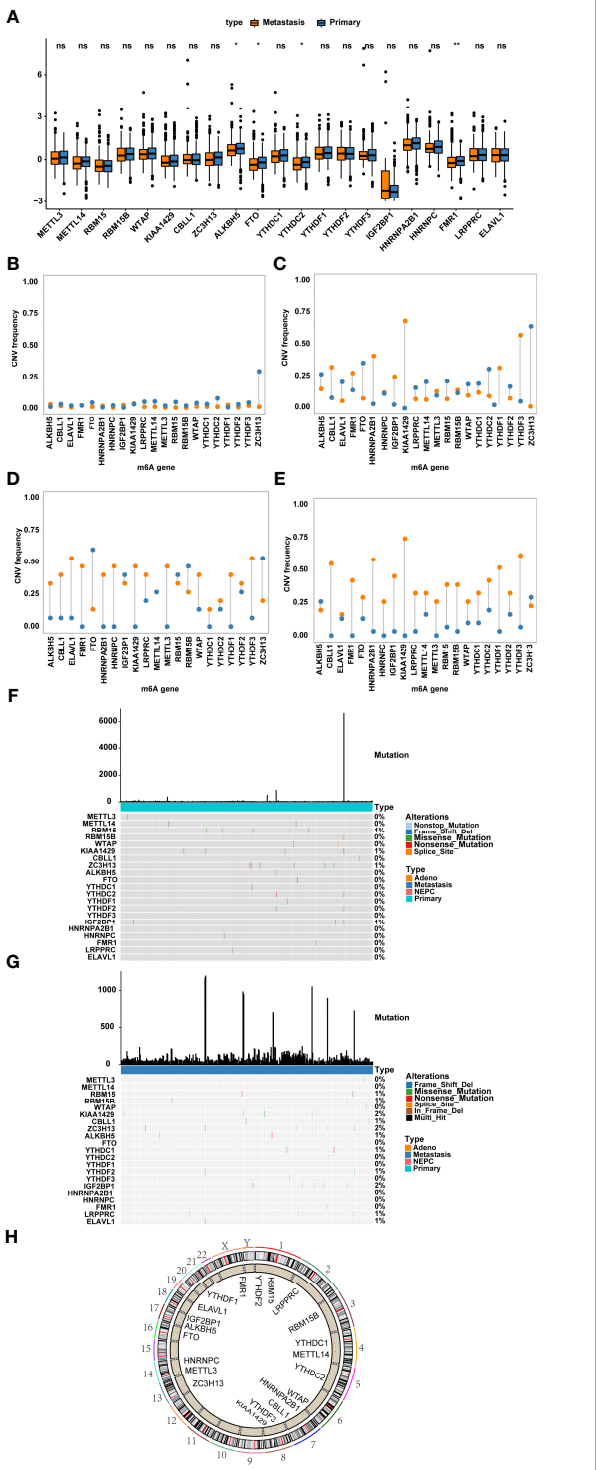

FIGURE 1 | Genetic variants of m6A regulators. **(A)** The expression of m6A regulator genes in nonmetastatic and metastatic prostate cancers; Frequency of CNV in m6A regulator genes in primary tumour **(B)**, metastatic tumour **(C)**, neuroendocrine prostate cancer **(D)** and prostate adenoma **(E)** were shown. Blue represents deletion, orange represents amplification. **(F, G)** The location of somatic mutations of m6A regulator genes in **(F)** primary tumour and **(G)** metastatic tumour. **(H)** The location of m6A regulator genes on chromosomes. ns represents P > 0.05, *P ≤ 0.05, **P ≤ 0.01.

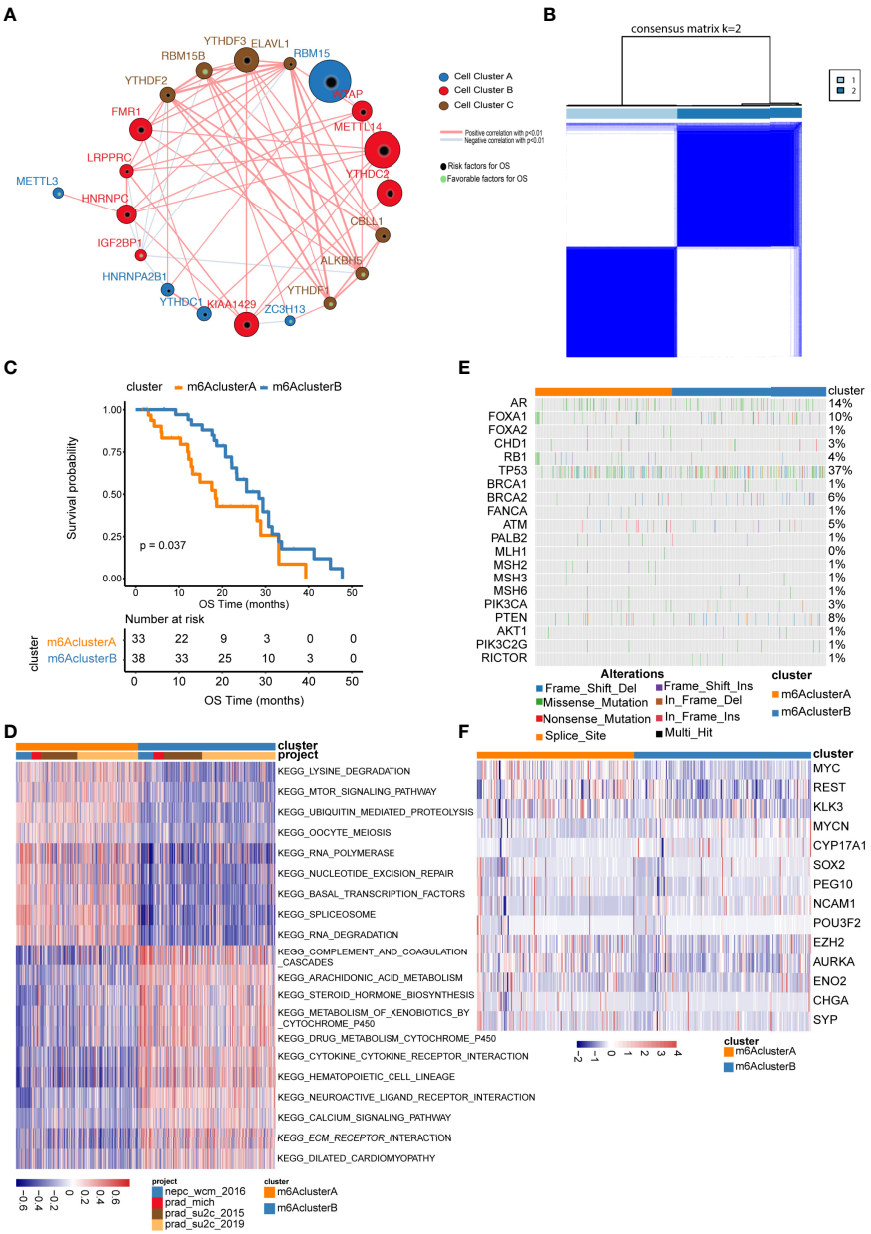

FIGURE 2 | Unsupervised clustering of m6A regulator genes in metastatic prostate cancer. **(A)** The interaction among m6A regulator genes. The size of circle indicates the effect of each gene on survival, the larger the size, the greater the effect is; green spots inside the circle indicate risk prognostic factors, black spots inside the circle indicate factors; lines that connect genes exhibit genetic interactions, red and blue represent positive and negative associations, respectively; gene Cluster A, B and C are shown as blue, red and brown, respectively; **(B)** Consensus clustering m6A regulator genes in metastatic samples; **(C)** Kaplan–Meier curves indicate that there is a strong relationship between the m6Acluster types and the overall survival rate; **(D)** GSVA enrichment analysis. Heatmaps show the activation status of biological pathways, which is displayed with different m6A clusters; red denotes activation, blue denotes inhibition; **(E, F)** show the distribution of the mutation and expression of partial genes in two m6A clusters, respectively.

m6A Regulators Promote PCa Cell Metastasis and Proliferation

To further investigate the function of m6A regulators during the metastasis of PCa, METTL14-overexpressing or METTL14 knockdown PC3 cell lines were established by transfecting a stable overexpressing lentivirus and shRNA, respectively. The efficiency of METTL14 knockdown and overexpression was validated by western blotting. The results revealed that the protein levels of METTL14 were significantly increased or decreased in PC3 cell lines (**Figure 4A**). Subsequently, cell migration, invasion, wound healing, and CCK-8 assays were performed to explore the role of METTL14 in PCa cell metastasis

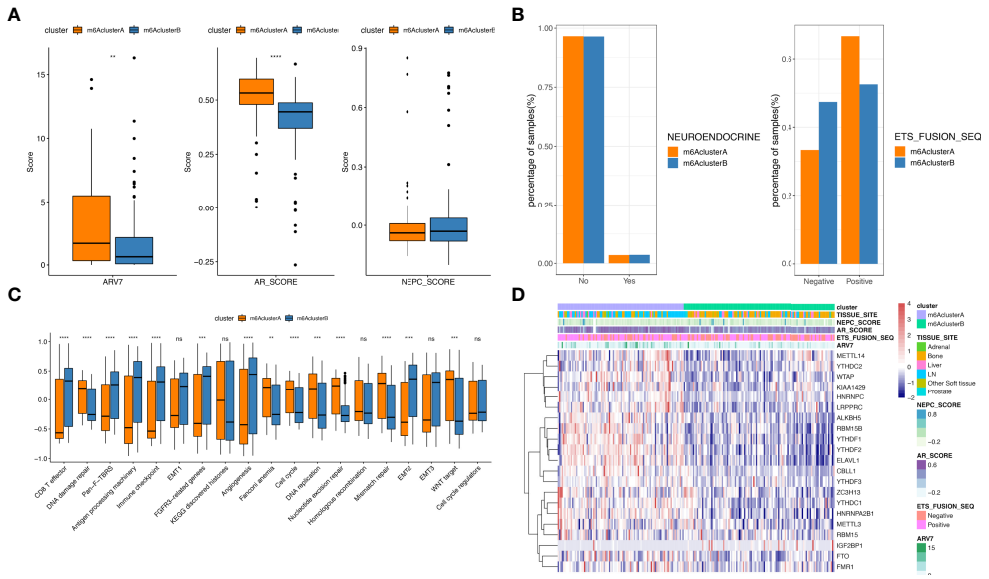

FIGURE 3 | Comparison analysis among m6A clusters. **(A)** The distribution of ARV7 (left), ARscore (middle) and NEPCscore (right) between the two m6A clusters; **(B)** The prognostic differences between the two m6A clusters; **(C)** Results for GSVA analysis of prad_su2c_2019 cohorts; **(D)** The expression of m6A regulator genes in two m6A clusters extracted from prad_su2c_2019 cohorts. ns represents P > 0.05, **P ≤ 0.01, ***P ≤ 0.001, ****P ≤ 0.0001.

and proliferation, respectively. Cell migration and invasion assays showed that downregulation of METTL14 decreased the migration and invasion cell numbers, while overexpressing METTL14 reversed the outcomes (**Figure 4B**). Wound healing assays revealed that silencing METTL14 reduced, whereas overexpressing METTL14 increased, the wound healing of PC3 cells (**Figure 4C**). Moreover, the proliferation of PC3 cells was detected by CCK-8 assay, which elucidated that METTL14 ablation inhibited, while upregulating METTL14 enhanced the proliferation capability of PCa cells (**Figure 4D**). Additionally, olaparib administration obviously reversed the cell proliferation promoted by METTL14 overexpression. Overall, our results implied that METTL14 played an essential role in PCa migration, invasion and proliferation.

Generation of m6A Phenotype Genes and Function

To further investigate each m6A cluster's potential biological behaviours, we characterized 2330 metastatic prostate cancer-related differentially expressed genes (DEGs) using the limma package (**Supplementary Table 12**). The clusterProfilter package was utilized to perform KEGG analysis for DEGs, which indicated the enrichment of shearing and RNA transportation (**Supplementary Table 13**). Then, basing on the 2330 m6A phenotype-related DEGs, unsupervised clustering analysis was performed to classify patients with metastatic prostate cancer, which could be similarly divided into two subtypes termed the m6AGenecluster.A and m6AGenecluster.B (**Supplementary Table 14**). We observed that the expression levels of most m6A regulators were higher in m6AGenecluster.A than in m6AGenecluster.B and the prognosis of m6AGenecluster.A type tumours was poorer than of those of m6AGenecluster.B (**Figure S1C**).

Establishment of the Prognostic Model

The above DEGs were made de-redundant by the random forest algorithm to select the most category-related genes (**Supplementary Table 15_sig.txt**). The Cox regression model was used to uncover the relationship between these genes and patient's survival. Next, we divided the above genes into two categories based on their coefficient values and scored for all the samples using the m6Ascore formula (**Supplementary Table 15_nGenes.txt; Supplementary Table 15_pGenes.txt**). Referring to the median m6Ascore, samples were further grouped into two categories: m6Ascore high and m6Ascore low samples (**Figure 5A**; **Supplementary Tables 16, 17**). As shown in **Figure 5B**, the prognosis of the m6Ascore high sample group was poorer than that the m6Ascore low group. This means that the prognosis of samples could be characterized by our m6Ascore model. Finally, the correlation analysis of m6Ascore and feature genes selected from gene sets constructed by Mariathasan et al. revealed that the m6Ascore was significantly associated with biological functions such as DNA repair and mismatch repair which imply the potetainal response to poly (ADP-ribose) polymerase (PARP) inhibitors (PARPis) (**Figure 5C, D**; **Supplementary Table 18**). The Wilcoxon test indicated that there was a notable difference between m6A cluster and m6AGene cluster in m6Ascore (**Figures 5E, F**). m6A risk scores of samples with enrichment of m6A cluster.A genes or m6AGene cluster.A genes were markedly higher than those of samples with highly expression of m6Acluster.B genes or m6AGenecluster.B genes.

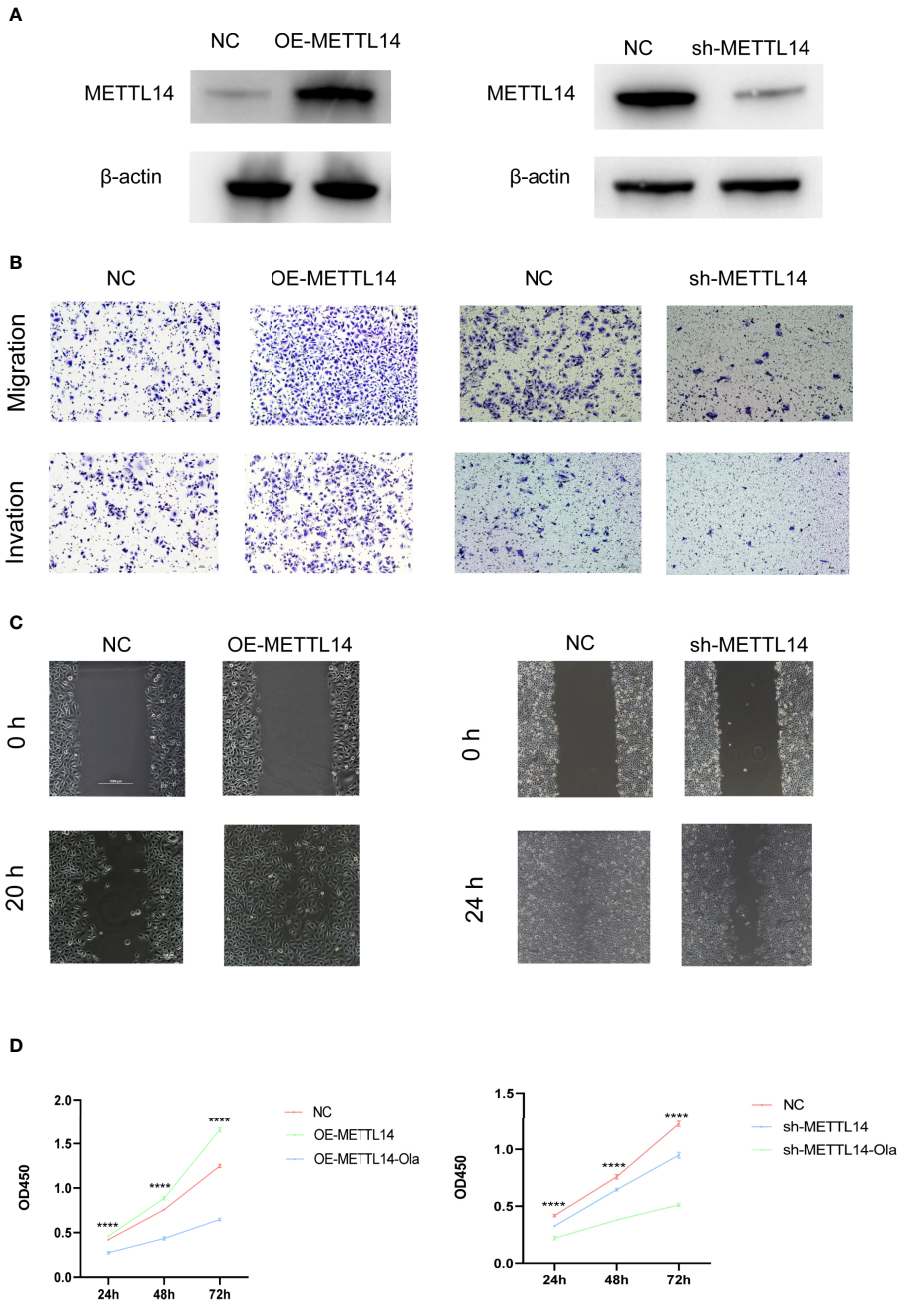

FIGURE 4 | METTL14 promotes PC3 cell metastasis and proliferation *in vitro*. **(A)** Western blot analysis of METTL14 expression levels in METTL14-downregulated, METTL14-knockdown, and vehicle control cells. **(B)** Representative images of migration (upper panels) and invasion (lower panels) assays using PC3 cells, presenting cell migration and invasion after overexpression or knockdown of METTL14. **(C)** Wound healing assays using PC3 cells presenting cell motility after overexpression or knockdown of METTL14. **(D)** Cell proliferation was evaluated in METTL14-overexpressing (left) or METTL14-knockdown (right) PC3 cells with or without olaparib administration. ****P ≤ 0.0001.

Similarly, we investigated the function of category-related genes during the metastasis of PCa. PC3 cell lines were stably transfected with lentiviruses expressing control shRNA, CSNK1D shRNA and SLC35E1 shRNA. The efficiency of CSNK1D or SLC35E1 knockdown was verified by western blotting (**Figure 6A**). Then, cell migration, invasion, wound healing, and CCK-8 assays were performed to explore the role of CSNK1D and SLC35E1 in PCa cell metastasis and proliferation, respectively. Cell migration and invasion assays showed that downregulation of CSNK1D and SLC35E1 decreased the migration and invasion cell numbers (**Figure 6B**). Wound healing assays also revealed that silencing CSNK1D or SLC35E1 reduced the wound healing

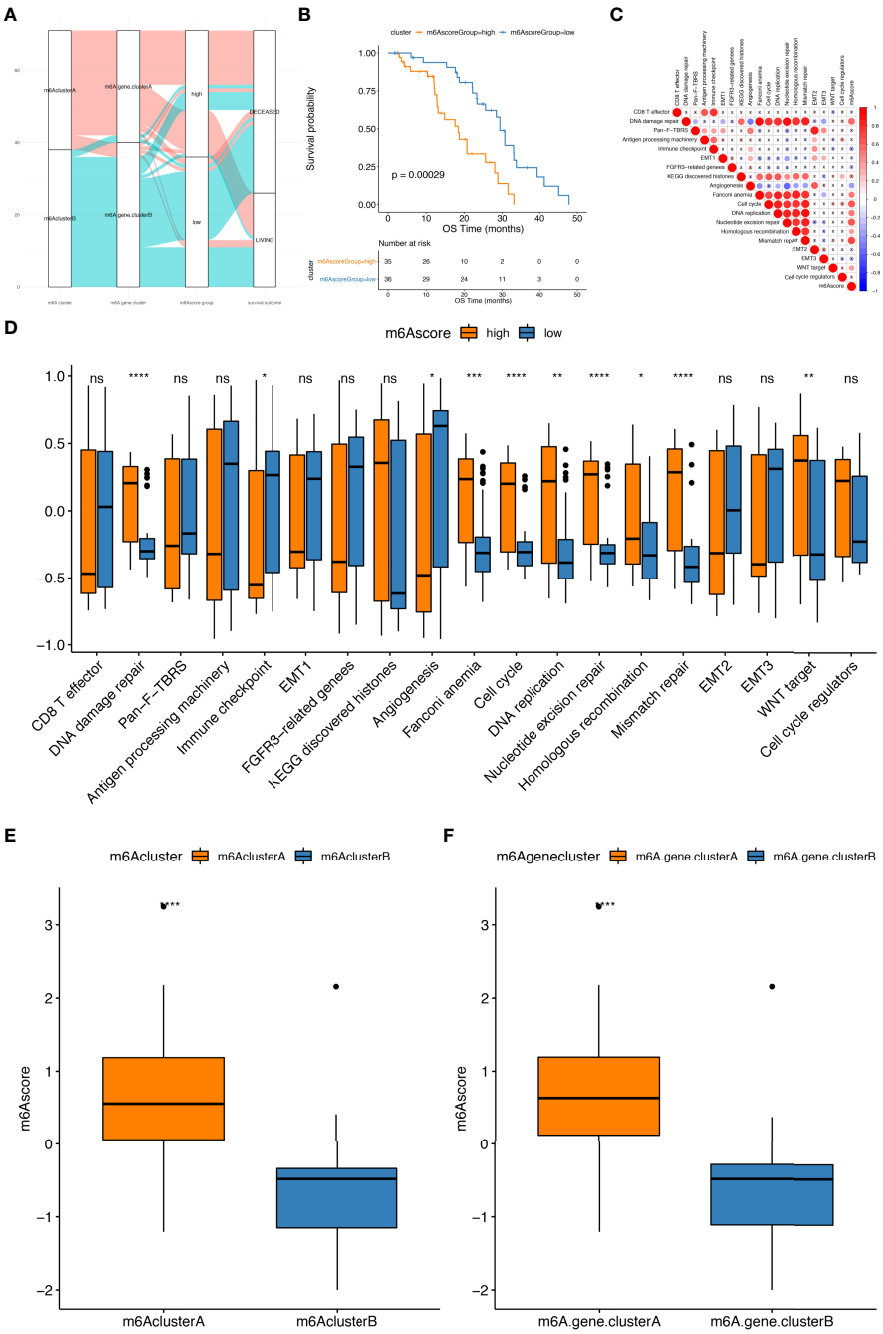

FIGURE 5 | Construction of m6A risk score model. **(A)** The alluvial plot shows the changes of m6A clusters, gene clusters and m6Ascore; **(B)** Kaplan–Meier curves indicate that there is a strong relationship between the m6Ascore and the overall survival rate; **(C)** Pearson's correlation analysis highlighting the correlations between m6Ascore and the known gene ontologies in prad_su2c_2019 cohorts. Red, blue and X symbols represent positive, negative and nonsignificant, respectively; the larger the circle, the more significant there is; **(D)** The distribution of enrichment scores of known gene ontologies prad_su2c_2019 cohorts between high and low m6Ascore samples; **(E, F)** show the distribution of m6Ascore among m6Aclusters and m6Ageneclusters, respectively. ns represents P > 0.05, *P ≤ 0.05, **P ≤ 0.01, ***P ≤ 0.001, ****P ≤ 0.0001.

abilities of PC3 cells (**Figure 6C**). Moreover, proliferation of PC3 cells was evaluated by CCK8 assay, which showed that CSNK1D or SLC35E1 ablation inhibited the proliferative capability, and administration of olaparib further inhibited the proliferative of PCa cells in the CSNK1D or SLC35E1 ablation groups (**Figure 6D**). In summary, our results revealed that both CSNK1D and SLC35E1 were of great significance in PCa migration, invasion, and proliferation.

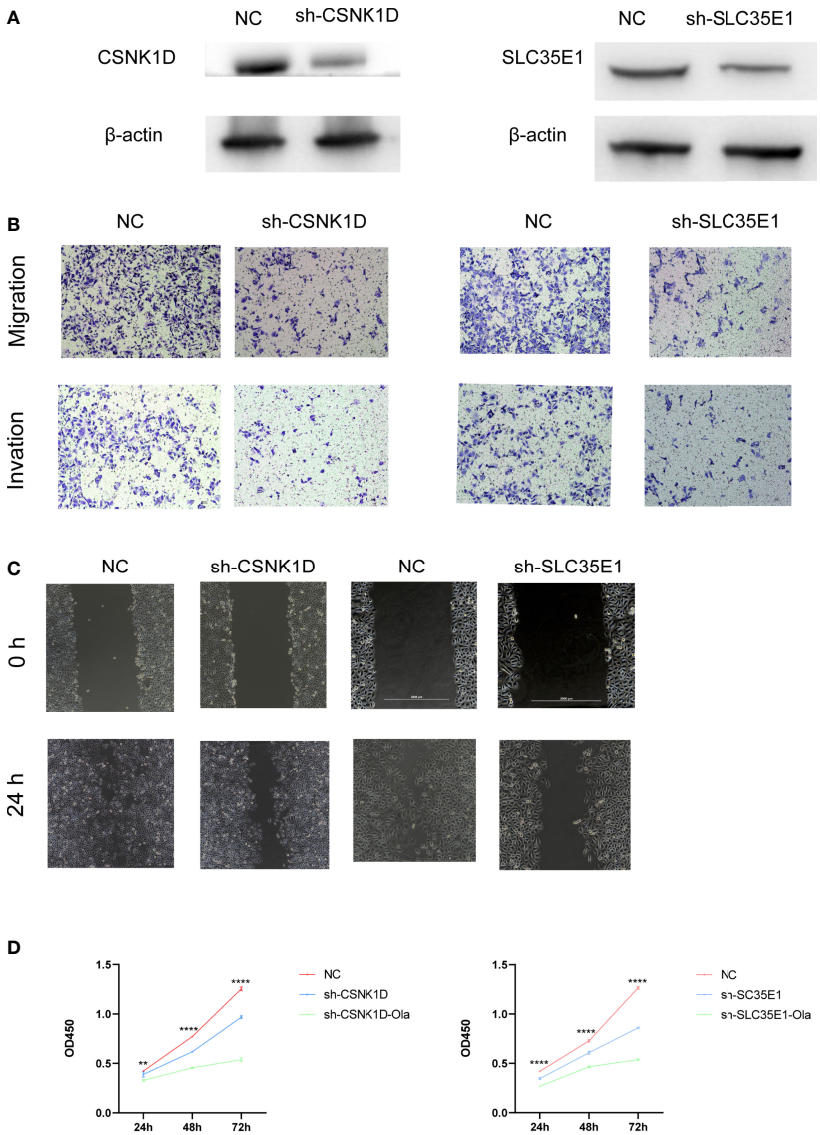

FIGURE 6 | CSNK1D or SLC35E1 ablation promotes PC3 cell metastasis and proliferation *in vitro*. **(A)** Western blot analysis of CSNK1D or SLC35E1 expression levels in CSNK1D or SLC35E1 knockdown cells and vehicle control cells. **(B)** Representative images of migration (upper panels) and invasion (lower panels) assays using PC3 cells, presenting cell migration and invasion after knockdown of CSNK1D or SLC35E1. **(C)** Wound healing assays using PC3 cells presenting cell motility after knockdown of CSNK1D or SLC35E1 ablation. **(D)** Cell proliferation was evaluated in CSNK1D (left) or SLC35E1 (right) ablated PC3 cells with or without olaparib administration. **P ≤ 0.01, ****P ≤ 0.0001.

Molecular Characteristics Between High and Low m6Ascore

Additional investigations of differences between high and low m6Ascore groups in prad_su2c_2019 datasets revealed that the ARscore in different groups were distinct; in the high m6Ascore group, the ARscore was also high (**Figure 7A**). Then, we analysed the difference in somatic mutations between groups with high and low m6Ascore. As depicted in **Figures 7B, C**, the mutation numbers in the high m6Ascore groups were higher than those in the low m6Ascore group. Similarly, CNV numbers were also higher in the high m6Ascore groups than in the low m6Ascore groups (**Supplementary Table 19**). In the m6Ascore high groups, 18 copy number amplifications and 31 copy number deletions were detected, while in the low m6Ascore groups, 16 copy number amplifications and 30 copy number deletions were detected (**Figures 7D, E**).

Verification of m6Ascore

To further validate the predictive performance of our prognostic model, the m6A risk scores of TCGA samples were calculated.

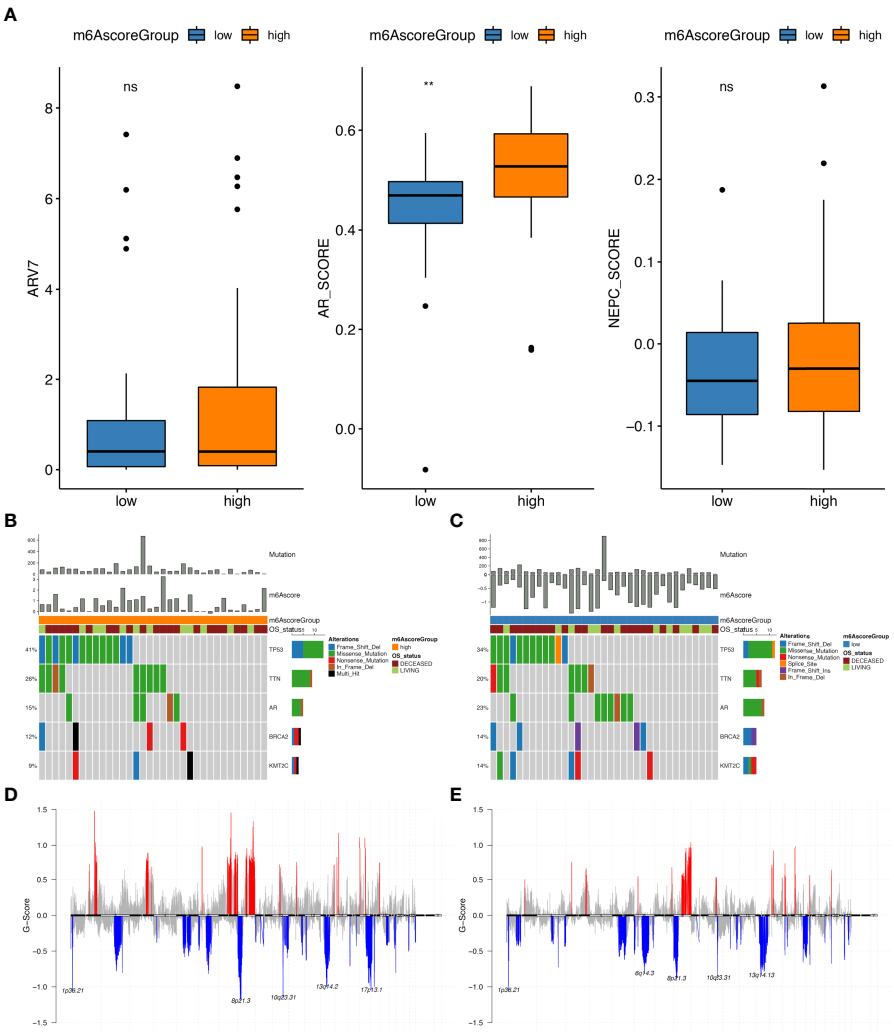

FIGURE 7 | Molecular profiling of sample groups with high and low m6Ascore. **(A)** The distribution of ARV7 (middle), ARscore (middle) and NEPCscore (right) between samples with high and low m6Ascore; Gene mutation distribution of high **(B)** and low **(C)** m6Ascore samples; The distribution of copy number amplifications and deletions in high **(D)** and low **(E)** m6Ascore samples. ns, no significance; **P ≤ 0.01.

The threshold of classification was determined by the R function surv_cutpoint. Consistently, survival analysis indicated that the prognosis of the m6Ascore-high group was poorer than the m6Ascore-low group (**Figure 8A**; **Supplementary Table 20**). Furthermore, the m6Ascore also showed a significant difference in parts of the GLEASON_SCORE groups (**Figures 8B, C**).

In particular, we trained our prostate cancer metastasis prediction model in the prad_su2c_2019 and TCGA cohorts, which achieved an ROC AUC of 70% (**Figure 8D**). This indicated that our m6A risk score is efficient for the prognosis of metastatic prostate cancer.

DISCUSSION

PCa is a major malignancy affecting the male population worldwide, and effective therapeutic options for advanced-stage PCa, especially metastatic PCa, are still scarce (23). As the most wide-ranging posttranscriptional modification, m6A is strongly correlated with cancer cell proliferation, progression and metastasis (6). In PCa, however, relevant studies are still lacking, and there are no effective prediction models based on m6A regulators to evaluate the prognosis of metastatic PCa.

In our study, we found that the mRNA expression of most genes did not exhibit prominent differences between primary and metastatic samples, except for a few genes such as FMR1 and FTO. We also performed integrative analysis on primary, metastatic and NEPC prostate cancer samples basing on the CNVs and mutation alterations and mRNA expression of m6A regulators. Although few mutations were observed, their biological significance had been verified to be vital during tumour progression. A mutation in METTL14 could facilitate tumour proliferation *via* the AKT signalling pathway (24). There

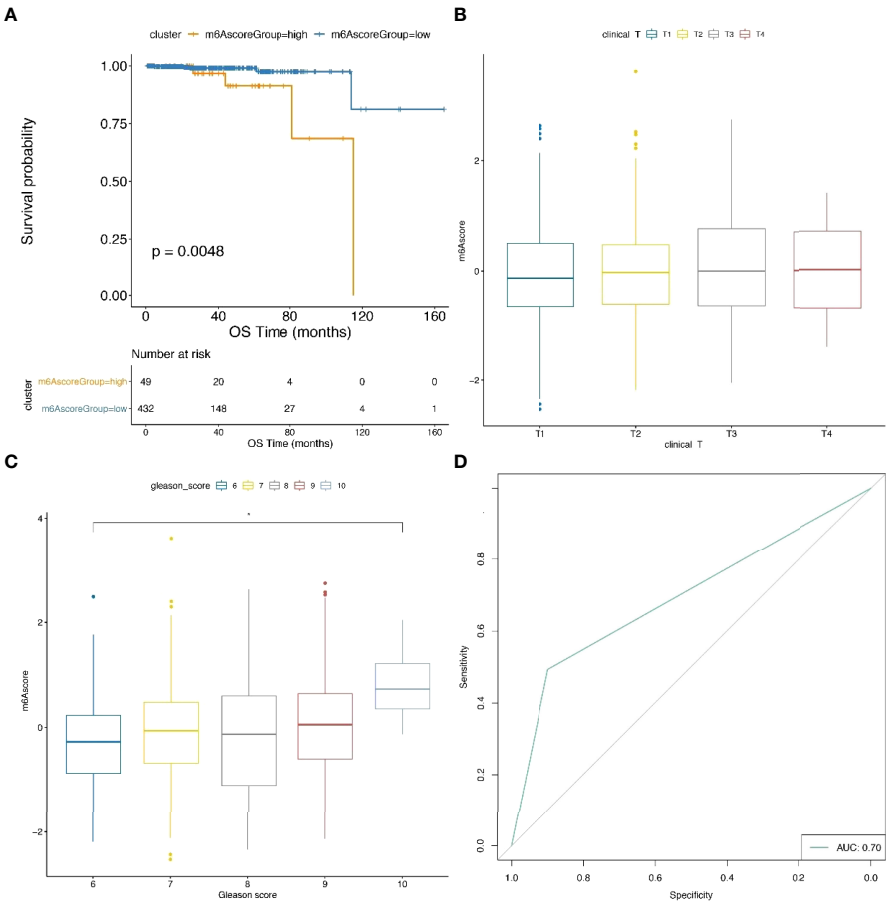

FIGURE 8 | Comparison analysis and validation of m6Ascore model. **(A)** Survival analysis plot indicates a significant difference between TCGA samples with high and low m6A score. **(B, C)** The distribution of m6A score within distinct T stages and GLEASON_SCORE subgroups using TCGA data. **(D)** ROC curves for the prediction of metastatic and nonmetastatic prostate cancer between groups with high and low m6A score.

is a paucity of studies focusing on mutations of m6A regulators in PCa, but in acute myeloid leukaemia, mutations of m6A regulators were predictive of unfavourable prognosis (25). CNVs are strongly related to mRNA expression. Specifically, copy number gain could foster amplification of genes, and copy number reduction inhibits the expression of genes. Except for a few regulators, such as YTHDF2, FTO and RBM15B, most of them experienced CNV amplification. Amplification of FTO was reported to significantly improve the prognosis of prostate cancer (26).

However, the same m6A regulator may exert different roles in distinct tumours through diverse mechanisms. Herein, two distinct molecular subgroups of metastatic prostate cancer with obviously distinct characteristics were shown based on 21 m6A regulators related to prognosis. m6Acluster.A regulators were significantly enriched in lysine degradation and the mTOR signalling pathway. While the m6Acluster.B regulators were mainly enriched in arachidonic acid metabolism and steroid hormone biosynthesis. It's well known that activating mTOR signalling can enhance tumour proliferation and progression *via* distinct mechanisms, including the enhancement of angiogenesis, glyolytic and lipid metabolism, and inhibition of autophagy (27). Additionally, the expression level of m6A regulator was higher in m6A clusters. A than in m6Acluster.B. To further investigate the relationship between the expression of m6A regulators and PCa prognosis, METTL14-overexpressing or METTL14 knockdown PC3 and DU145 cell lines were constructed. Similar to previous studies, METTL14 ablation inhibited the proliferation and metastasis capability, while upregulating METTL14 enhanced the proliferation and metastasis of PCa cells (28).

Furthermore, in our study, the transcriptomic heterogeneity among distinct subgroups of metastatic prostate cancer was found to be markedly related to shearing and RNA transportation. A total of 2330 DEGs were presented as m6A phenotype-related genes. Similar to m6A regulator clustering results, two distinct genomic subtypes were identified based on m6A phenotype-related genes (2330). Prognosis in m6AGenecluster.A type tumour was dismal, and the expression level of most regulators in the m6A cluster. A were higher than m6AGenecluster.B. Next,

we selected the most category-related genes based on the above DEGs and then constructed a prognostic model to provide a reference for treating patients with metastatic prostate cancer. We observed that the m6Ascore was significantly correlated with some biological functions such as DNA repair and mismatch repair. Similarly, the m6A risk scores of samples with upregulated m6Acluster.A regulators or m6Agenecluster.A genes were distinctively higher than samples overexpressing m6Acluster.B regulators or m6Agenecluster.B genes. This work implied that m6A regulators play an essential role in the prognosis of metastatic PCa, and patients with high m6A risk scores may be more appropriate for targeted therapy against DNA repair mechanisms such as PARPi.

Androgen receptor (AR) plays an important role in the occurrence and development of prostate cancer, and when it is activated by androgen, it can regulate the expression of downstream target genes, thus promoting the progression and metastasis of prostate cancer. As our results showed, in the high m6Ascore groups, the ARscore, mutation and CNV numbers, which were unfavourable factors for prognosis, were correspondingly elevated. In this model, CSNK1D is located on chromosome 17. Gene expression and activity changes of CSNK1D have been observed in distinct cancers (29). In metastatic HCC, the expression level of CSNK1D was higher than that in nonmetastatic HCC (30). SLC35E1 (solute carrier family 35, member E1) is a nucleotide sugar transporter carrier. It has been reported that during colorectal liver metastasis, SLC35E1 could be a predictive factor for the therapeutic effect of 5-fluorouracil–based chemotherapy (31). In our validation experiment, silencing CSNK1D or SLC35E1 reduced the proliferation and metastasis of DU145 and PC3 cells, which showed similar effects to the vehicle groups that were administered olaparib. Furthermore, KDM1A, the first identified demethylase, also termed LSD1 or KIAA0601, can regulate the initiation of tumours (32). CCCTC-binding factor (CTCF) is a well-known regulator facilitating chromatin into topologically associated domains by enhancing cohesin-mediated loop formation (33), which is strongly associated with cancer initiation (34). RBBP4 could promote the malignant progression of colon cancer through the Wnt/β-catenin pathway (35). CDC23 regulates the tumour cell phenotype and is upregulated in papillary thyroid cancer (36). Cell division cycle 5-like (CDC5L) protein, a cell phase regulator of the G2/M transition, has been demonstrated to improve bladder cancer cell proliferation, migration and invasion (37). As an RNA-binding protein, hnRNPA1 can regulate the expression and translation of several mediators involved in tumour initiation and progression (38).

In this model, m6A risk score was positively correlated with Gleason score, an index widely used for the prognosis of prostate cancer, and negatively correlated with the survival time of patients with metastatic prostate cancer. These signified that our prognostic model is effective for the prognosis of metastatic prostate cancer. However, there was no significant association between the m6A risk score and T stages. In short, the prognostic model could be applied to guide more effective judgement of prognosis as well as treatment effects of metastatic prostate cancer in clinical practice. For metastatic PCa patients, a high m6A risk score indicates a dismal prognosis. Since the m6Ascore was significantly correlated with biological functions such as DNA repair and mismatch repair, patients with high m6Ascores may be appropriate candidates for pharmacy therapy targeted for DNA repair, such as PARPi. However, there are some pitfalls in this study. Although an independent dataset was used to validate the prognostic model and cell studies were performed to uncover the vital role of m6A-associated genes in metastatic PCa, other animal and clinical studies should be performed. Moreover, the present study is largely a bioinformatic analysis, and potential underlying mechanisms need to be further studied.

DATA AVAILABILITY STATEMENT

The original contributions presented in the study are included in the article/**Supplementary Material**. Further inquiries can be directed to the corresponding authors.

AUTHOR CONTRIBUTIONS

QL and JW designed the experiment. ZL performed some experiments. QL performed some experiments and finished the manuscript. LH performed some experiments. JW and HX participated in the experimental design and supervised the manuscript. The final version of the manuscript was read and approved by all authors.

FUNDING

This work was funded by the National Natural Science Foundation of China (81771573).

SUPPLEMENTARY MATERIAL

The Supplementary Material for this article can be found online at: https://www.frontiersin.org/articles/10.3389/fonc.2022.914692/full#supplementary-material

Supplementary Figure 1 | Comparison analysis of distinct m6Agenecluster. **(A)** Unsupervised clustering of m6A phenotype-related genes in metastatic prostate cancer samples. Samples were separated into two different groups, termed m6Agenecluster.A and m6Agenecluster.B; **(B)** Kaplan–Meier curves show that there is a significant correlation between m6A-modified genomes and the overall survival rate; **(C)** The expression of 21 m6A regulator genes in two gene sets. The upper end, line and lower end of the box denote 1/4 quartiles, median and 3/4 quartiles, respectively; the black dots represent abnormal values; significant differences were determined by t test.

Supplementary Table S1 | Sample information.

Supplementary Table S2 | Copy number variations of 21 m6A regulators in primary, metastatic, adenocarcinoma and NEPC samples.

Supplementary Table S3 | Cellular interactions.

Supplementary Table S4 | m6A clusters.

Supplementary Table S5, 6 | Gene Set Variant Analysis between m6A. Cluster A and m6A. Cluster B.

Supplementary Table S7, 8 | The expression and mutation of specific genes between m6A. Cluster A and m6A. Cluster B.

Supplementary Table S9 | The ARV7 score and ARscore between m6A.Cluster A and m6A.Cluster B.

Supplementary Table S10 | Gene Set Variant Analysis between m6A. Cluster A and m6A. Cluster B based on the gene sets constructed by Mariathasan et al.

Supplementary Table S11 | The expression levels of m6A regulators between m6A.Cluster A and m6A.Cluster B.

Supplementary Table S12 | Metastatic prostate cancer-related differentially expressed genes (DEGs).

Supplementary Table S13 | KEGG analysis for DEGs.

Supplementary Table S14 | m6AGene clusters.

Supplementary Table S15 | Category-related DEGs.

Supplementary Table S16, 17 | m6Ascore.

Supplementary Table S18 | Correlation analysis of m6Ascore and feature genes.

Supplementary Table S19 | CNV numbers between m6Ascore high groups and low groups.

Supplementary Table S20 | Survival analysis between m6Ascore high groups and low groups.

REFERENCES

1. Gundem G, Van Loo P, Kremeyer B, Alexandrov LB, Tubio JMC, Papaemmanuil E, et al. The Evolutionary History of Lethal Metastatic Prostate Cancer. *Nature* (2015) 520:353–7. doi: 10.1038/nature14347
2. Litwin MS, Tan HJ. The Diagnosis and Treatment of Prostate Cancer A Review. *Jama-J Am Med Assoc* (2017) 317:2532–42. doi: 10.1001/jama.2017.7248
3. Boccaletto P, Machnicka MA, Purta E, Piatkowski P, Baginski B, Wirecki TK, et al. MODOMICS: A Database of RNA Modification Pathways. 2017 Update. *Nucleic Acids Res* (2018) 46:D303–7. doi: 10.1093/nar/gkx1030
4. Yue Y, Liu J, He C. RNA N6-Methyladenosine Methylation in Post-Transcriptional Gene Expression Regulation. *Genes Dev* (2015) 29:1343–55. doi: 10.1101/gad.262766.115
5. Jiang XL, Liu BY, Nie Z, Duan LC, Xiong QX, Jin ZX, et al. The Role of M6a Modification in the Biological Functions and Diseases. *Signal Transd Targeted Ther* (2021) 6:74. doi: 10.1038/s41392-020-00450-x
6. Sun T, Wu R, Ming L. The Role of M6a RNA Methylation in Cancer. *BioMed Pharmacother* (2019) 112:108613. doi: 10.1016/j.biopha.2019.108613
7. Cui Q, Shi H, Ye P, Li L, Qu Q, Sun G, et al. M(6)A RNA Methylation Regulates the Self-Renewal and Tumorigenesis of Glioblastoma Stem Cells. *Cell Rep* (2017) 18:2622–34. doi: 10.1016/j.celrep.2017.02.059
8. Weng H, Huang H, Wu H, Qin X, Zhao BS, Dong L, et al. : METTL14 Inhibits Hematopoietic Stem/Progenitor Differentiation and Promotes Leukemogenesis *via* mRNA M(6)A Modification. *Cell Stem Cell* (2018) 22:191–205.e199. doi: 10.1016/j.stem.2017.11.016
9. Chen M, Wei L, Law CT, Tsang FH, Shen J, Cheng CL, et al. RNA N6-Methyladenosine Methyltransferase-Like 3 Promotes Liver Cancer Progression Through YTHDF2-Dependent Posttranscriptional Silencing of SOCS2. *Hepatology* (2018) 67:2254–70. doi: 10.1002/hep.29683
10. Ma JZ, Yang F, Zhou CC, Liu F, Yuan JH, Wang F, et al. METTL14 Suppresses the Metastatic Potential of Hepatocellular Carcinoma by Modulating N(6) -Methyladenosine-Dependent Primary MicroRNA Processing. *Hepatology* (2017) 65:529–43. doi: 10.1002/hep.28885
11. Chen J, Sun Y, Xu X, Wang D, He J, Zhou H , et al. YTH Domain Family 2 Orchestrates Epithelial-Mesenchymal Transition/Proliferation Dichotomy in Pancreatic Cancer Cells. *Cell Cycle* (2017) 16:2259–71. doi: 10.1080/15384101.2017.1380125
12. Huang LT, Zhu J, Kong WKX, Li PF, Zhu SJ. Expression and Prognostic Characteristics of M6a RNA Methylation Regulators in Colon Cancer. *Int J Mol Sci* (2021) 22:2134. doi: 10.3390/ijms22042134
13. Zhang B, Wu Q, Li B, Wang D, Wang L, Zhou YL. M(6)A Regulator-Mediated Methylation Modification Patterns and Tumor Microenvironment Infiltration Characterization in Gastric Cancer. *Mol Cancer* (2020) 19:53. doi: 10.1186/s12943-020-01170-0
14. Wang JM, Lin H, Zhou MD, Xiang Q, Deng YH, Luo LM, et al. The M6a Methylation Regulator-Based Signature for Predicting the Prognosis of Prostate Cancer. *Future Oncol* (2020) 16:2421–32. doi: 10.2217/fon-2020-0330
15. Mounir M, Lucchetta M, Silva TC, Olsen C, Bontempi G, Chen X, et al. New Functionalities in the TCGAbiolinks Package for the Study and Integration of Cancer Data From GDC and GTEx. *PloS Comput Biol* (2019) 15:e1006701. doi: 10.1371/journal.pcbi.1006701
16. Wilkerson MD, Hayes DN. ConsensusClusterPlus: A Class Discovery Tool With Confidence Assessments and Item Tracking. *Bioinformatics* (2010) 26:1572–3. doi: 10.1093/bioinformatics/btq170
17. Hänzelmann S, Castelo R, Guinney J. GSVA: Gene Set Variation Analysis for Microarray and RNA-Seq Data. *BMC Bioinform* (2013) 14:7. doi: 10.1186/1471-2105-14-7
18. Ritchie ME, Phipson B, Wu D, Hu Y, Law CW, Shi W, et al. Limma Powers Differential Expression Analyses for RNA-Sequencing and Microarray Studies. *Nucleic Acids Res* (2015) 43:e47. doi: 10.1093/nar/gkv007
19. Scornet E. Random Forests and Kernel Methods. *IEEE Trans Inf Theory* (2016) 62:1485–500. doi: 10.1109/TIT.2016.2514489
20. Zeng D, Li M, Zhou R, Zhang J, Sun H, Shi M, et al. Tumor Microenvironment Characterization in Gastric Cancer Identifies Prognostic and Immunotherapeutically Relevant Gene Signatures. *Cancer Immunol Res* (2019) 7:737–50. doi: 10.1158/2326-6066.CIR-18-0436
21. Mariathasan S, Turley SJ, Nickles D, Castiglioni A, Yuen K, Wang Y, et al. TGFbeta Attenuates Tumour Response to PD-L1 Blockade by Contributing to Exclusion of T Cells. *Nature* (2018) 554:544–8. doi: 10.1038/nature25501
22. Liu Q, Cui Y, Lin H, Hu D, Qi T, Wang B, et al. MicroRNA-145 Engineered Bone Marrow-Derived Mesenchymal Stem Cells Alleviated Erectile Dysfunction in Aged Rats. *Stem Cell Res Ther* (2019) 10:398. doi: 10.1186/s13287-019-1509-1
23. Sandhu S, Moore CM, Chiong E, Beltran H, Bristow RG, Williams SG. Prostate Cancer. *Lancet (London England)* (2021) 398:1075–90. doi: 10.1016/S0140-6736(21)00950-8
24. Liu J, Eckert MA, Harada BT, Liu SM, Lu Z, Yu K, et al. M(6)A mRNA Methylation Regulates AKT Activity to Promote the Proliferation and Tumorigenicity of Endometrial Cancer. *Nat Cell Biol* (2018) 20:1074–83. doi: 10.1038/s41556-018-0174-4
25. Kwok CT, Marshall AD, Rasko JE, Wong JJ. Genetic Alterations of M(6)A Regulators Predict Poorer Survival in Acute Myeloid Leukemia. *J Hematol Oncol* (2017) 10:39. doi: 10.1186/s13045-017-0410-6
26. Ji GJ, Huang C, He SM, Gong YQ, Song G, Li XS, et al. Comprehensive Analysis of M6a Regulators Prognostic Value in Prostate Cancer. *Aging-Us* (2020) 12:14863–84. doi: 10.18632/aging.103549
27. Saxton RA, Sabatini DM. mTOR Signaling in Growth, Metabolism, and Disease. *Cell* (2017) 169:361–71. doi: 10.1016/j.cell.2017.03.035

28. Yang X, Zhang S, He C, Xue P, Zhang L, He Z , et al. METTL14 Suppresses Proliferation and Metastasis of Colorectal Cancer by Down-Regulating Oncogenic Long non-Coding RNA XIST. *Mol Cancer* (2020) 19:46. doi: 10.1186/s12943-020-1146-4
29. Xu P, Ianes C, Gartner F, Liu C, Burster T, Bakulev V, et al. Structure, Regulation, and (Patho-)Physiological Functions of the Stress-Induced Protein Kinase CK1 Delta (CSNK1D). *Gene* (2019) 715:144005. doi: 10.1016/j.gene.2019.144005
30. Zhang H, Qiu C, Zeng H, Zhu W, Lyu W, Lao X. Upregulation of Stress-Induced Protein Kinase CK1 Delta Is Associated With a Poor Prognosis for Patients With Hepatocellular Carcinoma. *Genet Testing Mol Biomarkers* (2021) 25:504–14. doi: 10.1089/gtmb.2020.0093
31. Matsuyama R, Togo S, Shimizu D, Momiyama N, Ishikawa T, Ichikawa Y, et al. Predicting 5-Fluorouracil Chemosensitivity of Liver Metastases From Colorectal Cancer Using Primary Tumor Specimens: Three-Gene Expression Model Predicts Clinical Response. *Int J Cancer* (2006) 119:406–13. doi: 10.1002/ijc.21843
32. Ismail T, Lee HK, Kim C, Kwon T, Park TJ, Lee HS. KDM1A Microenvironment, Its Oncogenic Potential, and Therapeutic Significance. *Epigenet Chromatin* (2018) 11:33. doi: 10.1186/s13072-018-0203-3
33. Tang Z, Luo OJ, Li X, Zheng M, Zhu JJ, Szalaj P, et al. CTCF-Mediated Human 3d Genome Architecture Reveals Chromatin Topology for Transcription. *Cell* (2015) 163:1611–27. doi: 10.1016/j.cell.2015.11.024
34. Guo Y, Xu Q, Canzio D, Shou J, Li J, Gorkin DU, et al. CRISPR Inversion of CTCF Sites Alters Genome Topology and Enhancer/Promoter Function. *Cell* (2015) 162:900–10. doi: 10.1016/j.cell.2015.07.038
35. Li YD, Lv Z, Zhu WF. RBBP4 Promotes Colon Cancer Malignant Progression *via* Regulating Wnt/β-Catenin Pathway. *World J Gastroenterol* (2020) 26:5328–42. doi: 10.3748/wjg.v26.i35.5328
36. Zhang L, Rahbari R, He M, Kebebew E. CDC23 Regulates Cancer Cell Phenotype and is Overexpressed in Papillary Thyroid Cancer. *Endocrine-related Cancer* (2011) 18:731–42. doi: 10.1530/ERC-11-0181
37. Zhang Z, Mao W, Wang L, Liu M, Zhang W, Wu Y, et al. Depletion of CDC5L Inhibits Bladder Cancer Tumorigenesis. *J Cancer* (2020) 11:353–63. doi: 10.7150/jca.32850
38. Roy R, Huang Y, Seckl MJ, Pardo OE. Emerging Roles of Hnrnpa1 in Modulating Malignant Transformation. *Wiley Interdiscip Rev RNA* (2017) 8:e1431. doi: 10.1002/wrna.1431

Conflict of Interest: The authors declare that the research was conducted in the absence of any commercial or financial relationships that could be construed as a potential conflict of interest.

Publisher's Note: All claims expressed in this article are solely those of the authors and do not necessarily represent those of their affiliated organizations, or those of the publisher, the editors and the reviewers. Any product that may be evaluated in this article, or claim that may be made by its manufacturer, is not guaranteed or endorsed by the publisher.

frontiers | Frontiers in Oncology

TYPE Review
PUBLISHED 18 July 2022
DOI 10.3389/fonc.2022.955718

OPEN ACCESS

EDITED BY
Wen-Hao Xu,
Fudan University, China

REVIEWED BY
Qianzheng Zhu,
The Ohio State University, United States
Shuang Zhao,
Henan University, China
Douglas Gray,
University of Ottawa, Canada

*CORRESPONDENCE
Litao Sun
litaosun1971@sina.com
Chen Yang
yangchendldx@163.com

†These authors have contributed equally to this work and share first authorship

SPECIALTY SECTION
This article was submitted to Genitourinary Oncology, a section of the journal Frontiers in Oncology

RECEIVED 29 May 2022
ACCEPTED 28 June 2022
PUBLISHED 18 July 2022

CITATION
Guo J, Zhao J, Sun L and Yang C (2022) Role of ubiquitin specific proteases in the immune microenvironment of prostate cancer: A new direction.
Front. Oncol. 12:955718.
doi: 10.3389/fonc.2022.955718

Role of ubiquitin specific proteases in the immune microenvironment of prostate cancer: A new direction

Jinhui Guo[1,2†], Jie Zhao[3†], Litao Sun[4*] and Chen Yang[4*]

[1]Cancer Center, Institute of clinical medicine, Zhejiang Provincial People's Hospital, Affiliated People's Hospital, Hangzhou Medical College, Hangzhou, China, [2]Qingdao Medical College, Qingdao University, Qingdao, China, [3]College of Biotechnology and Bioengineering, Zhejiang University of Technology, Hangzhou, China, [4]Cancer Center, Department of Ultrasound, Zhejiang Provincial People's Hospital, Affiliated People's Hospital, Hangzhou Medical College, Hangzhou, China

Regulation of ubiquitination is associated with multiple processes of tumorigenesis and development, including regulation of the tumor immune microenvironment. Deubiquitinating enzymes (DUBs) can remove ubiquitin chains from substrates, thereby stabilizing target proteins and altering and remodeling biological processes. During tumorigenesis, deubiquitination-altered biological processes are closely related to tumor metabolism, stemness, and the immune microenvironment. Recently, tumor microenvironment (TME) modulation strategies have attracted considerable attention in cancer immunotherapy. Targeting immunosuppressive mechanisms in the TME has revolutionized cancer therapy. Prostate cancer (PC) is one of the most common cancers and the second most common cause of cancer-related death in men worldwide. While immune checkpoint inhibition has produced meaningful therapeutic effects in many cancer types, clinical trials of anti-CTLA4 or anti-PD1 have not shown a clear advantage in PC patients. TME affects PC progression and also enables tumor cell immune evasion by activating the PD-1/PD-L1 axis. Over the past few decades, an increasing number of studies have demonstrated that deubiquitination in PC immune microenvironment may modulate the host immune system's response to the tumor. As the largest and most diverse group of DUBs, ubiquitin-specific proteases (USPs) play an important role in regulating T cell development and function. According to current studies, USPs exhibit a high expression signature in PC and may promote tumorigenesis. Elevated expression of USPs often indicates poor tumor prognosis, suggesting that USPs are expected to develop as the markers of tumor prognosis and even potential drug targets for anti-tumor therapy. Herein, we first summarized recent advances of USPs in PC and focused on the relationship between USPs and immunity. Additionally, we clarified the resistance mechanisms of USPs to targeted drugs in PC. Finally, we reviewed the major achievement of targeting USPs in cancers.

KEYWORDS

ubiquitylation, deubiquitination, prostate cancer, USPs, tumor microenvironment, immune evasion

Introduction

Prostate cancer (PC) is one of the leading causes of morbidity and mortality in men worldwide (1). Radical surgical resection combined with androgen deprivation therapy (ADT) can be selected for the treatment of localized disease (2). Even though local treatment reduces mortality in PC patients, 20-40% of men experience recurrence (3). Although the initial effect of ADT is significant, this subset of patients will eventually progress to castration-resistant PC (CRPC) (4). Once PC spreads, the survival rate drops significantly to around 30% (5). Despite the success of ADT, chemotherapeutics, and radiopharmaceuticals in PC, none of these therapies cures advanced PC (6–8). As a novel treatment, immunotherapy has achieved remarkable success in solid tumors, such as melanoma, but has shown limited therapeutic benefits in PC. The insensitivity of PC to immunotherapy (such as checkpoint inhibitors) may reflect the immunosuppressive nature of the tumor microenvironment (TME) in PC. Cells within the TME express and secrete molecules, including programmed death-ligand 1 (PD-L1), transforming growth factor-beta (TGF-β), and vascular endothelial growth factor (VEGF) to mediate immunosuppression. Additionally, immune tolerance plays a key role in the occurrence and development of prostate tumors (9, 10).

Ubiquitination is involved in nearly all cellular processes, including protein activation/inactivation, DNA repair, gene regulation, and signal transduction (11, 12). In addition to these broad roles, ubiquitination was closely associated with the regulation of immune responses, as well as immune tolerance (13). Ubiquitination regulates T cell development, activation, and differentiation, thereby maintaining adaptive immune responses and immune tolerance to self-tissues (13). Many proteins in the T cell receptor (TCR) signaling pathway are regulated by the ubiquitin-proteasome system (UPS), which is critical for T-cell activation (14).

In the UPS, the substrate proteins are covalently attached to ubiquitin *via* isopeptide bonds catalyzed by an E1-E2-E3 ligase cascade, followed by proteasomal degradation (**Figure 1**) (15). It should be noted that not all ubiquitination modifications lead to protein degradation. Some ubiquitination do not degrade proteins, but alters protein activity, thereby mediating biological effects, such as gene regulation and DNA damage repair (12). Ubiquitin molecules are linked to target proteins as mono- or poly-ubiquitin. Generally, polyubiquitination marks signals for protein degradation by cellular proteasomes, while monoubiquitination marks can act as non-degradative modifications. Ubiquitins are mainly connected by lysine (K6, K11, K27, K29, K33, K48, and K63) and methionine (M1) residues. The K48 and K63 chains are the most studied ubiquitin chain linkages that guide the expression of substrate proteins. The K48 ubiquitin chain has been shown to play an important role in ATP-dependent proteasomal degradation (16), while the K63 ubiquitin chain is mainly involved in the modification of protein location and function (17).

Deubiquitinases (DUBs) regulate a variety of cellular functions by removing ubiquitin chains from substrates. Currently, more than 100 DUBs have been found in humans, and are divided into seven different families according to their structure and function (18): ubiquitin-specific proteases (USPs), ovarian tumor proteases(OTUs), ubiquitin C-terminal hydrolases (UCHs), Jab1/Mov34/MPN+ proteases (JAMMs),

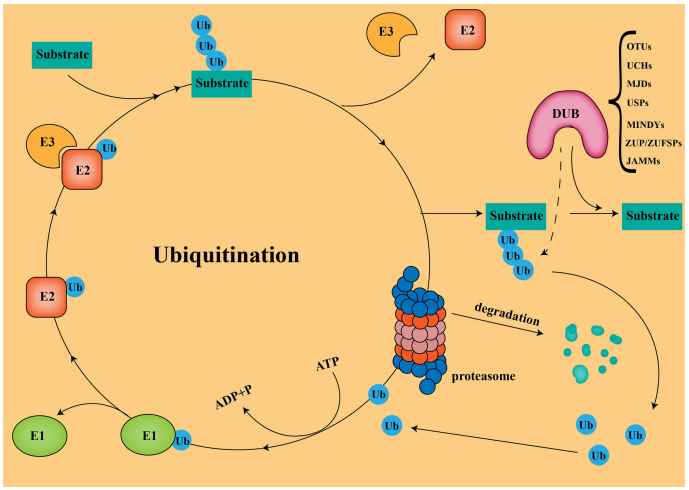

FIGURE 1
Ubiquitination and Deubiquitination The substrate proteins are covalently attached to ubiquitin *via* isopeptide bonds catalyzed by an E1-E2-E3ligase cascade, followed by proteasomal degradation.

Machado-Joseph disease protein proteases (MJDs), the motif interacting with ubiquitins(MIUs)-containing novel DUB family members (MINDYs), and Zinc Finger ubiquitin-specific proteases (ZUP/ZUFSPs). USPs is the largest and most diverse group of DUBs, accounting for about 60%, ranging between 50-300 kDa in size (19). To date, finding effective ways to enhance tumor immunotherapy in PC has been a great challenge. Turning "cold" tumors into "hot" tumors by modulating USPs to influence the immune response of the TME could effectively improve the efficacy of checkpoint inhibitors. Combining small-molecule inhibitors of USPs with checkpoint inhibitors in PC will be a promising therapeutic strategy.

USPs and PC

Introduction of USPs

USPs belong to the family of cysteine proteases whose enzymatic activity is located in the thiol group of the central cysteine (20). The catalytic sites all contain a cysteine residue with nearby histidine and asparagine/aspartate residues that facilitate nucleophilic attack by the cysteine (21). USPs promote the occurrence and development of PC by participating in multiple signaling pathways, such as androgen receptor (AR) accumulation, TGF-β pathway, and p53 pathway (22). Additionally, deubiquitination of USP can also regulate the AKT phosphorylation and fatty acid synthase pathways in PC (22, 23).

AR is the most common cause of signaling pathways in PC and may contribute to the emergence of CRPC (24). Activation of AR inhibits proteasomal degradation of MYC, leading to PC cell invasion (25). In primary PC, MYC is commonly amplified and overexpressed in 37% of metastatic focus (26, 27). MYC was regarded as the key driver of CRPC pathogenesis, and its amplification usually indicated poor outcomes (28). Stability of MYC is precisely regulated by UPS, which further regulates the growth of PC cells. Multiple USPs (USP2a, USP16, and USP22) are known to regulate MYC stability (29–31). USP22 is a functional mediator necessary for MYC to exert oncogenicity, thereby increasing the stability and tumorigenic activity of MYC in PC cells (31).

Damage to DNA triggers corresponding cellular responses, ranging from arresting the cell cycle to activating specific DNA repair mechanisms that vary, depending on the type of damage (32). Unrepaired DNA damage disrupts genome integrity and contributes to the pathogenesis of a range of human diseases, including cancer and premature aging (33). Additionally, DNA damage-induced senescence is associated with a pro-inflammatory secretory phenotype that remodels the tumor immune microenvironment (34). This study found that some USP families are also involved in the DNA damage repair pathway. Both USP26 and USP37 participate in homologous recombination by regulating rap80, and then repair DNA double-strand break (DSB) (35). Additionally, USP14 regulates DNA damage repair by targeting RNF168-dependent ubiquitination (36). During nucleotide excision repair, the nucleotide excision repair protein represented by XPC could repair the damaged DNA by ubiquitination binding (37). The USP22 could significantly protect XPC from deubiquitination; thus, promoting the survival of damaged DNA (38). Additionally, USP7 and USP11 can also regulate nucleotide excision repair through deubiquitinating XPC (39, 40).

USPs maintain AR stability

AR, a steroid receptor transcription factor for testosterone and dihydrotestosterone, is a central driver of PC development. Androgens act as ligands that bind to AR, and the activated AR binds to the DNA sequences of downstream genes, which initiates the expression of a series of genes that promote PC progression. Prostate-specific antigen is the most well-characterized AR target for monitoring PC development. Due to the central role of AR signaling in PC progression, ADT therapy has been the mainstay of treatment for patients with locally advanced PC. Reactivation of AR signaling can still be detected in CRPC cells despite multiple therapeutic options for inhibiting AR signaling (41). Amplification and mutation of the AR gene are also associated with the progression of CRPC, ultimately rendering it incurable.

Most of the previous studies have focused on the regulation of AR synthesis in PC, while the regulation of AR post-translational modification and degradation is easily overlooked. Several USPs (USP7, USP10, USP12, USP14, USP22, and USP26) have been reported to regulate AR signaling pathways, thereby affecting AR stability in the prostate. USPs (USP7, USP12, USP14, and USP22) can directly deubiquitinate AR and promote AR transcription (31, 42–44). USPs (USP12, USP14, and USP26) can also protect AR through reduced ubiquitination and degradation by indirectly reducing mouse double minute 2 (MDM2, a negative regulator of the tumor suppressor p53) protein levels (44–46). Furthermore, USP7 and USP10 can indirectly stabilize AR through histone H2A deubiquitination (42, 47).

Resistance of enzalutamide

Enzalutamide is a next-generation AR pathway inhibitor that binds to the ligand-binding domain of AR and disrupts the interaction between AR and androgen. Enzalutamide was initially effective in men with hormone-sensitive PC, but in most cases, resistance to the therapy tends to develop over time. Overexpression of some USPs in PC inhibits the enzalutamide effect and confers resistance to ADT therapy. Overexpression of

USP22 enhanced AR protein accumulation, which in turn activated downstream target genes regulated by AR and MYC. Such USP22-mediated activation can bypass androgens or AR antagonists (enzalutamide) to induce castration resistance in PC (48). Androgen receptor splice variant 7 (AR-V7), a ligand-independent activating variant of AR, is thought to be an inducer of CRPC. Targeted AR therapy is limited in CRPC due to lack of the ligand-binding domain of AR-V7. Among the AR-Vs, AR-V7 is the most abundant variant that has the highest detection frequency in PC. It should be noted that AR-V7 is the only endogenous variant detected at the protein level and can show functional activity in the absence of androgens. Protein analysis showed that USP22 depletion significantly reduced the half-life of AR-V7. Conversely, overexpression of USP22 slowed down AR-V7 degradation to some extent, partially restoring the viability of CRPC cells (48).

The kinesin family member 15 (KIF15) promotes enzalutamide resistance by enhancing AR signaling in PC cells. The KIF15 directly binds to the N-terminus of AR/AR-V7 and prevents AR/AR-V7 protein degradation by increasing USP14 binding to AR/AR-V7 (49). KDM4A demethylates the promoters or enhancers of certain AR target genes and acts as an AR co-activator. USP1 deubiquitinates and stabilizes KDM4A, thereby promoting the binding of AR to the c-MYC gene enhancer. Furthermore, inhibition of USP1 reduced PC proliferation and promoted resistance to enzalutamide in a KDM4A-dependent manner (50).

TME and USPs

Background of TME

The TME consists of tumor cells, immune cells, fibroblasts, endothelial and inflammatory cells, lymphocytes, and extracellular matrix (ECM) (51). Infiltration of immune cells (CD4+ and CD8+ T cells, dendritic cells, and natural killer cells) into tumors is associated with improved prognosis in cancer patients. Impaired cellular immunity and immunosuppressive TME may lead to PC becoming a "cold" tumor (52). In advanced PC, the function of natural killer and T cells is impaired in the TME, and myeloid suppressor cells and regulatory T cells (Tregs) are increased.

Cancer-associated fibroblasts (CAFs), a heterogeneous population of mesenchymal cells, are major players in the tumor immunosuppressive system. VEGF is a key factor secreted by CAFs to stimulate new blood vessel formation. By targeting the VEGF/VEGF receptor signaling pathway, the proliferation of tumor endothelial cells (TECs) can be inhibited, thereby controlling neovascularization in the TME. The CAFs can also build microenvironmental structures by synthesizing large amounts of ECM in the TME with important implications for maintaining stemness, regulating tumor metabolism, and therapeutic resistance. More and more researchers are paying attention to the immunosuppressive effects of CAFs through their interactions with components of the immune TME, especially immune cells (53, 54). In PC, M2 macrophages stimulate CAFs development by triggering neovascularization, both of which synergize with tumor development (55). The upregulated USP24 in M2 tumor-associated macrophages (TAMs) could promote the malignant development of cancer by increasing IL-6 expression (56). Additionally, USP22 has an important function in repairing DSBs that occur during B cell development (57).

Myeloid-derived suppressor cells

MDSCs are a heterogeneous population of immature myeloid cells that suppress T and NK cellular activity, and they can also confer resistance of tumor cells to immunotherapy. Clinical trials have found a correlation between MDSCs abundance and poor response to checkpoint inhibitor intervention (58). The recruitment of immune cells involved C-X-C motif chemokine ligand 5 (CXCR2), which promotes angiogenesis and tumor growth (59). CXCR2 plays a role in tumor progression by promoting the migration of MDSCs into the TME (60). MDSCs are enriched in prostate tumors in a CXCR2-dependent manner after surgical castration. Mast cells are innate immune cells and the number of infiltrating human prostate cancer correlates with prognosis (61). Mast cells can interact with MDSCs *via* CD40, further enhancing immunosuppression and directly impairing CD8+ T cell function (62). The extent of T-cell infiltration in prostate tumors is inversely related to the frequency of MDSCs, showing a strong synergistic response when MDSC-targeted therapy is combined with checkpoint inhibitors (63). Tyrosine kinase inhibitors can enhance the effect of immune checkpoint inhibitors by downregulating various cytokines that promote immunosuppression in MDSCs. The MDSCs may be a useful therapeutic target in the immune microenvironment of PC. Studies have found that USP22 deletion may lead to a significant reduction of MDSCs in the TME and promote the infiltration of T cells and NK cells while the expression of USP22 confers tumor resistance to immunotherapy (64).

Tregs and PD1/PDL1

Tregs are a unique class of immunosuppressive CD4+ T cells that primarily suppress the immune system by expressing the master transcription factor forkhead box protein 3 (FOXP3). Tregs penetrate the TME and suppress antitumor immune responses, and the ratio of Tregs to T cells reveals the effect of immunotherapy (65, 66). Tregs can inhibit antigen-presenting cells (APCs), thereby producing immunosuppressive factors, leading to the development of immunosuppressive TME.

FOXP3 is a hallmark transcription factor that determines and maintains the functional program of Tregs (67). It inhibits interleukin-2 (IL-2) transcription and induces CD25 expression (68). CD25 is a high-affinity receptor for IL-2, IL-2 is an essential cytokine for the survival of Tregs and effector T cells, thus, CD25 expression in Tregs can compete for more IL-2 binding in the TME than effector T cells. Therefore, Tregs accumulate more in the TME than effector T cells (**Figure 2**) (69). FOXP3 protein expression can be regulated by polyubiquitination-mediated proteasomal degradation. Expression of USP7 is up-regulated and active in Tregs cells, associated with FOXP3 in the nucleus. Ectopic expression of USP7 decreased FOXP3 polyubiquitination and increased FOXP3 expression. USP7 knockdown treatment reduced the expression of endogenous FOXP3 protein, and decreased Tregs cell-mediated inhibition *in vitro* (70).

PD-1 limits immune responses primarily by inhibiting intracellular signaling in effector T cells. Compared to CTLA4, the PD-1/PD-L1 (the ligand of PD-1) axis is more critical for the continued activation and proliferation of differentiated effector cells. The binding of PD-1 to PD-L1 can mediate T cell apoptosis or induce T cell dysfunction, commonly referred to as T cell exhaustion. Additionally, PD-L1 plays an important role in regulating immune responses (71). The PD-L1 is normally expressed on APCs and can control Tregs differentiation and inhibit their activity. Tumor cells and other TME components, such as infiltrating myeloid and dendritic cells often utilize upregulated PD-1 ligands to induce T cell exhaustion, thereby promoting tumor immune escape. Depletion of USP22 promotes T cell-mediated cell killing. Moreover, USP22 could regulate PD-L1 levels through two pathways (72). On the one hand, USP22 can directly regulate PD-L1 degradation through deubiquitination. On the other hand, USP22 regulates the expression of PD-L1 through the USP22-CSN5-PD-L1 axis.

Cancer stem cells and TME

CSCs are a subpopulation of undifferentiated cancer cells within a tumor with the ability to self-renew and differentiate into multilineages. The expression of several stem cell surface markers (CD44, CD133, OCT4, SOX2, and NANOG) has been associated with the promotion of treatment resistance and cancer progression. The TME is characterized by chronic inflammation that activates and modulates CSCs by stimulating cell proliferation (73). Recent studies have revealed a close connection between immune cells in CSCs and TME (74). TAMs provide key signals to promote CSCs survival, self-renewal, maintenance, and migration capabilities, and the CSCs provide tumor-promoting signals to TAMs in turn, further enhancing tumorigenesis. The CSCs make dendritic cells tolerant and impede the aggregation of dendritic cells in the TME. CSCs may also overcome immune surveillance by inhibiting T cell proliferation and effector function (75, 76). CSCs induce Tregs infiltration through STAT3 signaling in the TME, while Tregs regulate CSCs proliferation and expansion through IL-17 and PGE2 (77). In conclusion, CSC-targeted immunotherapy has the potential to become a new type of immunotherapy for cancer.

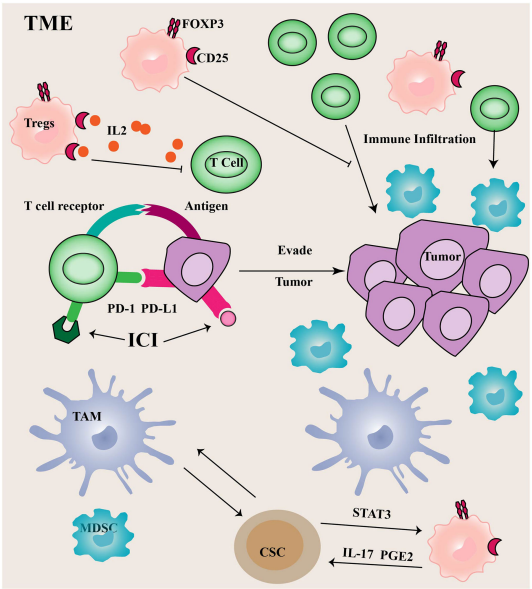

FIGURE 2
Immune cells in TME Tumor cells often utilize upregulated PD-1 ligands to induce T cell exhaustion, thereby promoting tumor immune escape.

To maintain CSC pluripotency, post-translational modifications (such as ubiquitination) are tightly regulated. USP22 is increased during progression from early-stage PC to CRPC, and it has a strong prognostic value in PC (78). In multiple tumors, USP22 has been described as a CSC marker that promotes CSC formation and stemness maintenance (79). USP22 affects the self-renewal of CSCs in cancer by regulating BMI1 protein expression (80). Additionally, USP22 promotes CSC maintenance through the Wnt/β-catenin pathway (81). Apart from USP22, USP44 has been shown to be upregulated in CSCs of breast cancer and promote tumor angiogenesis. In PC, knockdown of USP44 suppressed CSC properties and reduced the tumorigenicity of the PC. The expression of some pluripotent stem cell markers (OCT4, NANOG, and CD133) was reduced in USP44 knockdown cells. Specifically, USP44 promotes PC stemness by deubiquitinating EZH2 (a histone-modifying enzyme). The introduction of the ectopic EZH2 rescues the suppression of tumor activity after the USP44 knockout (**Figure 3**) (82).

Hypoxic microenvironment

The characteristics of vascular tortuosity and rapid tumor cell growth in TME usually induce hypoxia and recruit immunosuppressive cells, including macrophages, Tregs, and MDSCs. These immunosuppressive cells contribute to immunosuppression in the TME by secreting immunosuppressive factors, such as VEGF and TGF-β. Additionally, such a hypoxic microenvironment may lead to a polarization state transition of microphages from M1 to M2 based on their plastic properties.

Hypoxia is difficult to avoid in the process of prostate treatment. ADT therapy induces a hypoxic microenvironment in PC and triggers autocrine TGF-β signaling and differentiation of CAFs into myofibroblasts (83). Unfortunately, in a hypoxic environment, tumors can resist T cell infiltration even in the context of checkpoint inhibitors (CTLA-4 and PD-1 blocking). Studies in mouse tumor models of PC show that hypoxic regions of tumors represent centers of immunotherapy resistance, promoting the transformation of immature myeloid cells into highly suppressive myeloid-derived suppressor cells (84). Hypoxia can alter vasculature in the TME through direct (Hypoxia-inducible factor 1α-mediated upregulation of VEGF) and indirect effects (accumulation of cells leading to abnormal angiogenesis). The resulting vasculature expresses too few adhesion molecules necessary to support T cell extravasation, which can actively induce T cell apoptosis through the involvement of the Fas receptor. Those T cells capable of entering hypoxic tumors face a metabolically, highly inhibited immune environment (dense expression of PD-L and high concentrations of TGF-β). Additionally, the MDSCs are concentrated in the hypoxic regions of these tumors and they form an effective barrier to tumor immunity. Hypoxia itself inhibits T effector cell differentiation and interferon-γ production (85).

A heterodimeric transcription factor, Hypoxia-inducible factor 1(HIF-1), consist of an α subunit expressed in an oxygen-dependent manner and a constitutively expressed β subunit. Under normal toxic conditions, HIF-1α is degraded *via* the UPS. USP22 enhances the stability and transcriptional activity of HIF-1α under hypoxia through deubiquitination, and it induces upregulation of HIF-1α downstream genes (**Figure 3**) (86).

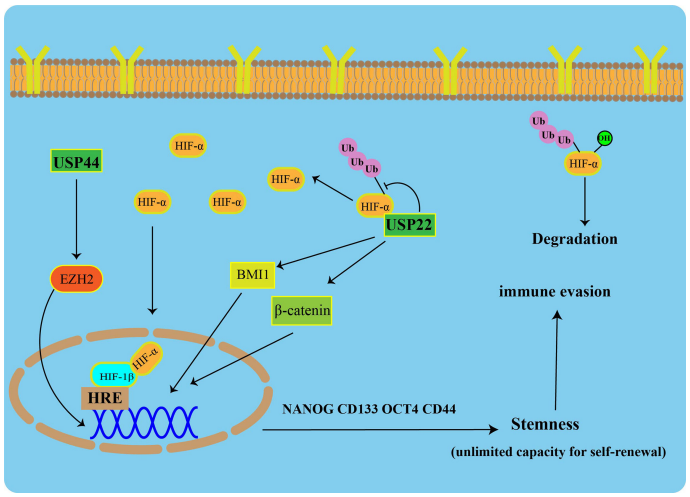

FIGURE 3
USPs-mediated tumor stemness and hypoxic microenvironment Under normoxic conditions, HIF-1α is degraded *via* the ubiquitin-proteasome pathway. USP22 enhances the stability and transcriptional activity of HIF-1α under hypoxia through deubiquitination and induces upregulation of HIF-1α downstream genes. USP22 maintains cancer stemness by regulating BMI1 and β-catenin pathways. Furthermore, USP44 promotes prostate cancer stemness by deubiquitinating EZH2.

Important signaling pathways in PC TME

P53

P53 (also known as TP53) is a tumor suppressor, and P53 degradation or gene mutation is tightly involved in cancer formation (87). P53 is a major regulatory transcription factor capable of regulating a variety of biological processes, such as cell cycle arrest, apoptosis, senescence, and repair of DNA damage (88). In addition to the known oncogenic role of P53, P53 plays an important role in immune responses and inflammation. P53 affects immunity and inflammation by regulating Toll-like receptors (TLRs) (89). TLRs are an important class of protein molecules involved in nonspecific immunity and are also a bridge between nonspecific and specific immunities. Changes in TLRs expression are associated with autoimmune diseases. There is also an important link between P53 and immune checkpoints. Cancer cells suppress immune responses and evade immune surveillance by upregulating PD-1 and its ligand PD-L1 in a P53-dependent manner. Another immune checkpoint regulator, DD1α, is also a direct transcriptional target of P53 (90). Many P53-regulated microRNAs (miRNAs) are also implicated in immunity. For example, miR34 binds directly to the 3′ untranslated region of the gene encoding PD-L1, suggesting that P53 may regulate tumor immune responses through miR-34 regulation of PD-L1 expression (91).

Mutant P53 (MTP53) protein is a tumor-specific neoantigen that is immunogenic and can mediate the immune escape of cancer cells. MTP53 makes tumors immunologically "cold" by inhibiting the STING-TBK1-IRF3 pathway, thereby allowing cancer cells expressing the "MTP53" antigen to evade immune detection (92). Importantly, disruption of the MTP53/TBK1 complex can switch the TME from "cold" to "hot" and allow the immune system to limit tumor growth. Other (TBK1-independent) mutant P53 activity may also contribute to the TME regulation. P53 also regulates the polarization of CD4+ T cells by enhancing the transcription of Foxp3, the master regulator of Tregs, and it is therefore predicted that loss of this role of p53 might enhance antitumor immunity. Targeting the P53-MDM2 interaction enhances MDM2 in T cells, thereby stabilizing STAT5 and enhancing T-cell-mediated antitumor immunity (93).

Some USPs can modulate p53 through deubiquitination or indirectly affect p53 through other signaling pathways. USP10 can interact with G3BP2 to block P53 signaling, leading to a poor prognosis in PC (94). USP12 and USP2a directly deubiquitinate and stabilize MDM2, thereby controlling the level of P53 gene in PC (45, 95). Downregulation of USP7 can increase the level of P53 *via* promoting MDM2 degradation (96). Caspase 8, a member of the cysteine protease family, is a key driver of apoptotic cell death. In cells with caspase 8 depletion, USP28 stabilizes p53 by deubiquitination to induce apoptosis of PC cells. However, in the presence of nuclear caspase 8, USP28 is cleaved and inactivated, resulting in the loss of p53 protein (97). Therefore, the dependence of caspase 8 should be considered, while developing drugs against USP28 inhibitors in the future.

TGF-β

TGF-β is a pleiotropic cytokine with a complex role in cancer progression (98). In the TME, cancer cells can exploit the pleiotropy of TGF-β signaling and its downstream mediators to create an immunosuppressive environment to evade antitumor immunity. TGF-β mediates endothelial-mesenchymal transition through SNAIL/Slug expression in TECs to support neovascularization and accumulation of myofibroblasts and CAFs in the TME (99). Moreover, TGF-β can drive immune dysfunction in the TME by inducing regulatory T cells and suppressing CD8+ and TH1 cells (100). TGF-β inhibits interferon-γ expression, restricts TH1 cell differentiation, attenuates CD8+ activation and effector T cell killing, and inhibits central memory T cell development. TGF-β induces the differentiation of CD4+ T cells in the TME into Tregs and has a major impact on the prognosis of patients with this functional tumor.

Studies have shown that USPs (USP2a, USP4, USP9X, USP15, and USP26) are involved in the regulation of TGF-β signaling pathways in various cancers (17). For example, USP9X can control the monoubiquitination of SMAD4 to regulate TGF-β-mediated cancer metastasis (101).

Small molecule inhibitors of USPs

Based on the accumulated evidence that indicated the potential of USP to promote cancer, targeting USP therapy strategy has attracted extensive attention. In the past few years, great breakthroughs have been made in the screening and development of small-molecule USPs inhibitors. USP14 is the most studied member of the USPs family. Herein, we use USP14 as a representative to describe small molecule inhibitors. USP14 contains a total of 494 amino acids with a UBL domain at its N-terminus and a catalytic USP domain at its C-terminus (102). The UBL domain is an important regulator of proteasome activity, while the C-terminal USP domain is responsible for its deubiquitinase activity (103). Structural studies show that two surface loops BL1 and BL2 on free USP14 prevent active site binding to the C-terminus of ubiquitin. The binding of USP14 to the 26S proteasome in an autoinhibited state activates its deubiquitination function.

In 2010, Finley et al. was the first to report a highly selective inhibitor of proteasome-bound USP14 named IU1 (104). As a specific inhibitor of USP14, IU1 has been used in cell-based

studies. Because DUBs are highly conserved, previous work has mainly focused on covalent inhibitors, which are compounds that form covalent bonds with active site cysteines. However, these compounds generally have poor selectivity for the DUBs family and cannot be used clinically (105). The IU1 prevents the C-terminus of ubiquitin from binding to USP14 by binding to the thumb-palm cleft region of the catalytic domain of USP14 (106). The results of this work suggest that allosteric modulation *via* steric retardation may be a viable approach for the discovery of USP inhibitors. The IU2 series is another class of USP14 inhibitors belonging to the tricyclic thiophene derivatives. The inhibitory effect of IU2 may block the entry of ubiquitinated substrates by blocking the ubiquitin-binding pocket.

However, the low inhibitory efficiency of IU1 hinders the development of drugs targeting USP14. Additionally, no selective inhibitor against phosphorylated USP14 has been found to date. The USP14 not only affects tumor progression but also plays a key role in immune and inflammatory responses. Inhibition of USP14 activity blocks IL-1β release and caspase-1 activation, showing its therapeutic potential in autoinflammatory diseases (107). Inhibition of USP14 may have broad biological effects leading to unpredictable toxicity. For example, loss of USP14 alters synaptic activity, leading to neuronal dysfunction (108). Therefore, it is important to develop a specific inhibitor that only targets the interaction of USP14 with some of its substrates.

USP22 exerts tumor-promoting effects in multiple tumor types and suppresses anti-tumor immunity by stabilizing PD-L1 in tumors (64). Increasing evidence showed that prescribing USP22 inhibitors is desirable. The USP22 has been studied in cancer for more than 15 years, but inhibitors of USP22 have not been reported until recent studies. Morgan et al. screened these cyclic peptides in a high-throughput manner based on RaPID, a combinatorial library system containing 1012 structurally unique cyclic peptides, and finally assessed their ability to inhibit DUB activity *in vitro* based on binding affinity, to develop effective and highly specific DUB inhibitor (109). The identification of ubiquitin variants targeting specific USPs by Sidhu laboratory provides new directions for designing small molecule inhibitors of USP22. Tang et al. designed a new library of combinatorial ubiquitin variants (UbVs) with high affinity and specificity for their cognate target domains found in ubiquitin specific protease (DUSPs). UbV probes can serve as potential targets for inhibition of USPs. This suppression mechanism can be extended to other USPs containing DUSPs (110).

Conclusion and future perspectives

Sipuleucel-T, an autologous cellular immunotherapy made from APCs, is the first FDA approved cancer vaccine for the treatment of metastatic CRPC (mCRPC), proving the prospect of immunotherapy in PC. Low tumor T-cell infiltration is one of the reasons for the poor efficacy of immune checkpoint inhibitors in PC. Additionally, Tregs and myeloid suppressor cells drive immunosuppression in the TME of PC. Considering the unsatisfactory results of immunotherapy in the treatment of castration-resistant PC, immunotherapy strategies for PC are beginning to turn to combination regimens to enhance antitumor immune responses.

USPs are considered important immune regulators and are involved in different aspects of immune function, from innate immunity and inflammation to activation and differentiation of immune cells. USP4 depletion impairs the suppressive function of Treg cells and upregulates gene expression levels of inflammatory cytokines, such as IL-4, 5, and 13 (111). The addition of USP inhibitors to the combination therapy regimen may help to break through the current immune dilemma of PC. Multiple USPs promote PC development through different cancer-related signaling pathways. Similar to the development of inhibitors for other targets, the specificity of small molecule inhibitors remains a great challenge. The developed small-molecule inhibitors that can be used in the clinic should ensure high specificity and do no harm normal cells.

Ideally, inhibitors of USPs should act on the deubiquitination of specific substrates without altering the overall protein levels. To develop ideal inhibitors of USPs, the next step should be a more comprehensive assessment of the cellular effects of USP inhibition. Taking USP14 as an example, substrates other than desired targets of USP14 can be identified by proteomics, which is very important to improve the selectivity of the USP14 inhibitors. At present, the specific relationship between USPs and the TME in PC is still not clear enough, and there is still a long way to go before the small molecule inhibitors of USPs are successfully applied in the clinic.

Author contributions

JG and JZ drafted the manuscript. LT and CY designed and revised the manuscript. All authors contributed to the manuscript and approved the submitted version.

Funding

This work was supported by Zhejiang Public Welfare Technology Application Research Project (Grant No. LGF22H160038).

Conflict of interest

The authors declare that the research was conducted in the absence of any commercial or financial relationships that could be construed as a potential conflict of interest.

Publisher's note

References

1. Desai K, McManus JM, Sharifi N. Hormonal therapy for prostate cancer. *Endocr Rev* (2021) 42(3):354–73. doi: 10.1210/endrev/bnab002

2. Adamaki M, Zoumpourlis V. Prostate cancer biomarkers: From diagnosis to prognosis and precision-guided therapeutics. *Pharmacol Ther* (2021) 228:107932. doi: 10.1016/j.pharmthera.2021.107932

3. Sandhu S, Moore CM, Chiong E, Beltran H, Bristow RG, Williams SG. Prostate cancer. *Lancet* (2021) 398(10305):1075–90. doi: 10.1016/S0140-6736(21)00950-8

4. Ruiz de Porras V, Font A, Aytes A. Chemotherapy in metastatic castration-resistant prostate cancer: Current scenario and future perspectives. *Cancer letters* (2021) 523:162–9. doi: 10.1016/j.canlet.2021.08.033

5. Runcie KD, Dallos MC. Prostate cancer immunotherapy-finally in from the cold? *Curr Oncol Rep*. (2021) 23(8):88. doi: 10.1007/s11912-021-01084-0

6. Chi KN, Agarwal N, Bjartell A, Chung BH, Pereira de Santana Gomes AJ, Given R, et al. Apalutamide for metastatic, castration-sensitive prostate cancer. *New Engl J Med* (2019) 381(1):13–24. doi: 10.1056/NEJMoa1903307

7. de Bono J, Mateo J, Fizazi K, Saad F, Shore N, Sandhu S, et al. Olaparib for metastatic castration-resistant prostate cancer. *N Engl J Med* (2020) 382(22):2091–102. doi: 10.1056/NEJMoa1911440

8. Parker C, Nilsson S, Heinrich D, Helle SI, O'Sullivan JM, Fosså SD, et al. Alpha emitter radium-223 and survival in metastatic prostate cancer. *New Engl J Med* (2013) 369(3):213–23. doi: 10.1056/NEJMoa1213755

9. Donkor MK, Sarkar A, Savage PA, Franklin RA, Johnson LK, Jungbluth AA, et al. T Cell surveillance of oncogene-induced prostate cancer is impeded by T cell-derived TGF-β1 cytokine. *Immunity*. (2011) 35(1):123–34. doi: 10.1016/j.immuni.2011.04.019

10. Getnet D, Maris CH, Hipkiss EL, Grosso JF, Harris TJ, Yen HR, et al. Tumor recognition and self-recognition induce distinct transcriptional profiles in antigen-specific CD4 T cells. *J Immunol (Baltimore Md 1950)* (2009) 182(8):4675–85. doi: 10.4049/jimmunol.0803400

11. Jin JO, Puranik N. The ubiquitin system: An emerging therapeutic target for lung cancer. *Int J Mol Sci* (2021) 22(17):9629. doi: 10.3390/ijms22179629

12. Sharma A, Khan H, Singh T, Grewal A, Najda A, Kawecka-Radomska M, et al. Pharmacological modulation of ubiquitin-proteasome pathways in oncogenic signaling. *Int J Mol Sci* (2021) 22(21):11971. doi: 10.3390/ijms222111971

13. Hu H, Sun SC. Ubiquitin signaling in immune responses. *Cell Res* (2016) 26(4):457–83. doi: 10.1038/cr.2016.40

14. Huang H, Jeon MS, Liao L, Yang C, Elly C, Yates JR 3rd, et al. K33-linked polyubiquitination of T cell receptor-zeta regulates proteolysis-independent T cell signaling. *Immunity* (2010) 33(1):60–70. doi: 10.1016/j.immuni.2010.07.002

15. Schauer NJ, Magin RS, Liu X, Doherty LM, Buhrlage SJ. Advances in discovering deubiquitinating enzyme (DUB) inhibitors. *J Med Chem* (2020) 63(6):2731–50. doi: 10.1021/acs.jmedchem.9b01138

16. Pinto MJ, Tomé D. The ubiquitinated axon: Local control of axon development and function by ubiquitin. *J Neurosci* (2021) 41(13):2796–813. doi: 10.1523/JNEUROSCI.2251-20.2021

17. Chen S, Liu Y, Zhou H. Advances in the development ubiquitin-specific peptidase (USP) inhibitors. *Int J Mol Sci* (2021) 22(9):4546. doi: 10.3390/ijms22094546

18. Das T, Song EJ. The multifaceted roles of USP15 in signal transduction. *Int J Mol Sci* (2021) 22(9):4728. doi: 10.3390/ijms22094728

19. Pfoh R, Lacdao IK, Saridakis V. Deubiquitinases and the new therapeutic opportunities offered to cancer. *Endocrine-Related Cancer* (2015) 22(1):T35–54. doi: 10.1530/ERC-14-0516

20. Yuan T, Yan F, Ying M, Cao J, He Q, Zhu H, et al. Inhibition of ubiquitin-specific proteases as a novel anticancer therapeutic strategy. *Front Pharmacol* (2018) 9:1080. doi: 10.3389/fphar.2018.01080

21. Komander D, Clague MJ, Urbé S. Breaking the chains: structure and function of the deubiquitinases. *Nat Rev Mol Cell Biol* (2009) 10(8):550–63. doi: 10.1038/nrm2731

22. Islam MT, Zhou X, Chen F, Khan MA, Fu J, Chen H. Targeting the signalling pathways regulated by deubiquitinases for prostate cancer therapeutics. *Cell Biochem Funct* (2019) 37(5):304–19. doi: 10.1002/cbf.3401

23. Graner E, Tang D, Rossi S, Baron A, Migita T, Weinstein LJ, et al. The isopeptidase USP2a regulates the stability of fatty acid synthase in prostate cancer. *Cancer Cell* (2004) 5(3):253–61. doi: 10.1016/S1535-6108(04)00055-8

24. Dai C, Heemers H, Sharifi N. Androgen signaling in prostate cancer. *Cold Spring Harbor Perspect Med* (2017) 7(9):a030452. doi: 10.1101/cshperspect.a030452

25. Chuan YC, Iglesias-Gato D, Fernandez-Perez L, Cedazo-Minguez A, Pang ST, Norstedt G, et al. Ezrin mediates c-myc actions in prostate cancer cell invasion. *Oncogene* (2010) 29(10):1531–42. doi: 10.1038/onc.2009.442

26. Cancer Genome Atlas Research Network. The molecular taxonomy of primary prostate cancer. *Cell* (2015) 163(4):1011–25. doi: 10.1016/j.cell.2015.10.025

27. Kumar A, Coleman I, Morrissey C, Zhang X, True LD, Gulati R. Substantial interindividual and limited intraindividual genomic diversity among tumors from men with metastatic prostate cancer. *Nat Med* (2016) 22(4):369–78. doi: 10.1038/nm.4053

28. Rebello RJ, Oing C. Prostate cancer. *Nat Rev Dis Primers* (2021) 7(1):9. doi: 10.1038/s41572-020-00243-0

29. Ge J, Yu W, Li J, Ma H, Wang P, Zhou Y, et al. USP16 regulates castration-resistant prostate cancer cell proliferation by deubiquitinating and stablizing c-myc. *J Exp Clin Cancer Res* (2021) 40(1):59. doi: 10.1186/s13046-021-01843-8

30. Benassi B, Flavin R, Marchionni L, Zanata S, Pan Y, Chowdhury D, et al. MYC is activated by USP2a-mediated modulation of microRNAs in prostate cancer. *Cancer Discovery* (2012) 2(3):236–47. doi: 10.1158/2159-8290.CD-11-0219

31. Schrecengost RS, Dean JL, Goodwin JF, Schiewer MJ, Urban MW, Stanek TJ, et al. USP22 regulates oncogenic signaling pathways to drive lethal cancer progression. *Cancer Res* (2014) 74(1):272–86. doi: 10.1158/0008-5472.CAN-13-1954

32. Ou HL, Schumacher B. DNA Damage responses and p53 in the aging process. *Blood* (2018) 131(5):488–95. doi: 10.1182/blood-2017-07-746396

33. Gewirtz DA, Alotaibi M, Yakovlev VA, Povirk LF. Tumor cell recovery from senescence induced by radiation with PARP inhibition. *Radiat Res* (2016) 186(4):327–32. doi: 10.1667/RR14437.1

34. Sharma A, Almasan A. Autophagy and PTEN in DNA damage-induced senescence. *Adv Cancer Res* (2021) 150:249–84. doi: 10.1016/bs.acr.2021.01.006

35. Typas D, Luijsterburg MS, Wiegant WW, Diakatou M, Helfricht A, Thijssen PE, et al. The de-ubiquitylating enzymes USP26 and USP37 regulate homologous recombination by counteracting RAP80. *Nucleic Acids Res* (2015) 43(14):6919–33. doi: 10.1093/nar/gkv613

36. Sharma A, Alswillah T, Singh K, Chatterjee P, Willard B, Venere M, et al. USP14 regulates DNA damage repair by targeting RNF168-dependent ubiquitination. *Autophagy* (2018) 14(11):1976–90. doi: 10.1080/15548627.2018.1496877

37. van Cuijk L, van Belle GJ, Turkyilmaz Y, Poulsen SL, Janssens RC, Theil AF, et al. SUMO and ubiquitin-dependent XPC exchange drives nucleotide excision repair. *Nat Commun* (2015) 6:7499. doi: 10.1038/ncomms8499

38. McCann JJ, Vasilevskaya IA, Poudel Neupane N. USP22 functions as an oncogenic driver in prostate cancer by regulating cell proliferation and DNA repair. *Cancer Res* (2020) 80(3):430–43. doi: 10.1158/0008-5472.CAN-19-1033

39. Shah P, Qiang L, Yang S, Soltani K, He YY. Regulation of XPC deubiquitination by USP11 in repair of UV-induced DNA damage. *Oncotarget* (2017) 8(57):96522–35. doi: 10.18632/oncotarget.22105

40. He J, Zhu Q, Wani G, Sharma N, Han C, Qian J, et al. Ubiquitin-specific protease 7 regulates nucleotide excision repair through deubiquitinating XPC protein and preventing XPC protein from undergoing ultraviolet light-induced and VCP/p97 protein-regulated proteolysis. *J Biol Chem* (2014) 289(39):27278–89. doi: 10.1074/jbc.M114.589812

41. Antonarakis ES, Lu C, Wang H, Luber B, Nakazawa M, Roeser JC, et al. AR-V7 and resistance to enzalutamide and abiraterone in prostate cancer. *New Engl J Med* (2014) 371(11):1028–38. doi: 10.1056/NEJMoa1315815

42. Chen ST, Okada M, Nakato R, Izumi K, Bando M, Shirahige K. The deubiquitinating enzyme USP7 regulates androgen receptor activity by

modulating its binding to chromatin. *J Biol Chem* (2015) 290(35):21713–23. doi: 10.1074/jbc.M114.628255

43. Burska UL, Harle VJ, Coffey K, Darby S, Ramsey H, O'Neill D, et al. Deubiquitinating enzyme Usp12 is a novel co-activator of the androgen receptor. *J Biol Chem* (2013) 288(45):32641–50. doi: 10.1074/jbc.M113.485912

44. Liao Y, Liu N, Hua X, Cai J, Xia X, Wang X, et al. Proteasome-associated deubiquitinase ubiquitin-specific protease 14 regulates prostate cancer proliferation by deubiquitinating and stabilizing androgen receptor. *Cell Death Disease* (2017) 8(2):e2585. doi: 10.1038/cddis.2016.477

45. McClurg UL, Chit N, Azizyan M, Edwards J. Molecular mechanism of the TP53-MDM2-AR-AKT signalling network regulation by USP12. *Oncogene* (2018) 37(34):4679–91. doi: 10.1038/s41388-018-0283-3

46. Dirac AM, Bernards R. The deubiquitinating enzyme USP26 is a regulator of androgen receptor signaling. *Mol Cancer Res* (2010) 8(6):844–54. doi: 10.1158/1541-7786.MCR-09-0424

47. Draker R, Sarcinella E, Cheung P. USP10 deubiquitylates the histone variant H2A.Z and both are required for androgen receptor-mediated gene activation. *Nucleic Acids Res* (2011) 39(9):3529–42. doi: 10.1093/nar/gkq1352

48. Liu Y, Yu C, Shao Z. Selective degradation of AR-V7 to overcome castration resistance of prostate cancer. *Cell Death Dis* (2021) 12(10):857. doi: 10.1038/s41419-021-04162-0

49. Gao L, Zhang W, Zhang J, Liu J, Sun F, Liu H, et al. KIF15-mediated stabilization of AR and AR-V7 contributes to enzalutamide resistance in prostate cancer. *Cancer Res* (2021) 81(4):1026–39. doi: 10.1158/0008-5472.CAN-20-1965

50. Cui SZ, Lei ZY, Guan TP, Fan LL, Li YQ, Geng XY, et al. Targeting USP1-dependent KDM4A protein stability as a potential prostate cancer therapy. *Cancer Sci* (2020) 111(5):1567–81. doi: 10.1111/cas.14375

51. Mao X, Xu J, Wang W, Liang C, Hua J, Liu J, et al. Crosstalk between cancer-associated fibroblasts and immune cells in the tumor microenvironment: new findings and future perspectives. *Mol Cancer* (2021) 20(1):131. doi: 10.1186/s12943-021-01428-1

52. Boettcher AN, Usman A, Morgans A, VanderWeele DJ, Sosman J, Wu JD. Past, current, and future of immunotherapies for prostate cancer. *Front Oncol* (2019) 9:884. doi: 10.3389/fonc.2019.00884

53. An Y, Liu F, Chen Y, Yang Q. Crosstalk between cancer-associated fibroblasts and immune cells in cancer. *J Cell Mol Med* (2020) 24(1):13–24. doi: 10.1111/jcmm.14745

54. Barrett RL, Puré E. Cancer-associated fibroblasts and their influence on tumor immunity and immunotherapy. *Elife* (2020) 9:e57243. doi: 10.7554/eLife.57243

55. Comito G, Giannoni E, Segura CP, Barcellos-de-Souza P, Raspollini MR, Baroni G, et al. Cancer-associated fibroblasts and M2-polarized macrophages synergize during prostate carcinoma progression. *Oncogene* (2014) 33(19):2423–31. doi: 10.1038/onc.2013.191

56. Wang YC, Wu YS. USP24 induces IL-6 in tumor-associated microenvironment by stabilizing p300 and β-TrCP and promotes cancer malignancy. *Nat Commun* (2018) 9(1):3996. doi: 10.1038/s41467-018-06178-1

57. Li C, Irrazabal T, So CC, Berru M, Du L, Lam E, et al. The H2B deubiquitinase Usp22 promotes antibody class switch recombination by facilitating non-homologous end joining. *Nat Commun* (2018) 9(1):1006. doi: 10.1038/s41467-018-03455-x

58. Bejarano L, Jordão MJC, Joyce JA. Therapeutic targeting of the tumor microenvironment. *Cancer Discovery* (2021) 11(4):933–59. doi: 10.1158/2159-8290.CD-20-1808

59. Zhang W, Wang H, Sun M, Deng X, Wu X, Ma Y, et al. CXCL5/CXCR2 axis in tumor microenvironment as potential diagnostic biomarker and therapeutic target. *Cancer Commun* (2020) 40(2-3):69–80. doi: 10.1002/cac2.12010

60. Yang J, Yan C. Targeted deletion of CXCR2 in myeloid cells alters the tumor immune environment to improve antitumor immunity. *Cancer Immunol Res* (2021) 9(2):200–13. doi: 10.1158/2326-6066.CIR-20-0312

61. Johansson A, Rudolfsson S, Hammarsten P, Halin S, Pietras K, Jones J, et al. Mast cells are novel independent prognostic markers in prostate cancer and represent a target for therapy. *Am J Pathol* (2010) 177(2):1031–41. doi: 10.2353/ajpath.2010.100070

62. Jachetti E, Cancila V, Rigoni A, Bongiovanni L, Cappetti B, Belmonte B, et al. Cross-talk between myeloid-derived suppressor cells and mast cells mediates tumor-specific immunosuppression in prostate cancer. *Cancer Immunol Res* (2018) 6(5):552–65. doi: 10.1158/2326-6066.CIR-17-0385

63. Lu X, Horner JW, Paul E, Shang X, Troncoso P, Deng P, et al. Effective combinatorial immunotherapy for castration-resistant prostate cancer. *Nature* (2017) 543(7647):728–32. doi: 10.1038/nature21676

64. Li J, Yuan S. Tumor cell-intrinsic USP22 suppresses antitumor immunity in pancreatic cancer. *Cancer Immunol Res* (2020) 8(3):282–91. doi: 10.1158/2326-6066.CIR-19-0661

65. Saleh R, Elkord E. FoxP3(+) T regulatory cells in cancer: Prognostic biomarkers and therapeutic targets. *Cancer letters* (2020) 490:174–85. doi: 10.1016/j.canlet.2020.07.022

66. Saito T, Nishikawa H, Wada H. Two FOXP3(+)CD4(+) T cell subpopulations distinctly control the prognosis of colorectal cancers. *Nat Med* (2016) 22(6):679–84. doi: 10.1038/nm.4086

67. Khattri R, Cox T, Yasayko SA, Ramsdell F. An essential role for scurfin in CD4+CD25+ T regulatory cells. *Nat Immunol* (2003) 4(4):337–42. doi: 10.1038/ni909

68. Wu Y, Borde M, Heissmeyer V, Feuerer M, Lapan AD, Stroud JC, et al. FOXP3 controls regulatory T cell function through cooperation with NFAT. *Cell* (2006) 126(2):375–87. doi: 10.1016/j.cell.2006.05.042

69. Nishikawa H, Koyama S. Mechanisms of regulatory T cell infiltration in tumors: implications for innovative immune precision therapies. *J immunother Cancer* (2021) 9(7):e002591. doi: 10.1136/jitc-2021-002591

70. van Loosdregt J, Fleskens V, Fu J, Brenkman AB, Bekker CP, Pals CE, et al. Stabilization of the transcription factor Foxp3 by the deubiquitinase USP7 increases treg-cell-suppressive capacity. *Immunity* (2013) 39(2):259–71. doi: 10.1016/j.immuni.2013.05.018

71. Gong J, Chehrazi-Raffle A, Reddi S, Salgia R. Development of PD-1 and PD-L1 inhibitors as a form of cancer immunotherapy: a comprehensive review of registration trials and future considerations. *J Immunother Cancer* (2018) 6(1):8. doi: 10.1186/s40425-018-0316-z

72. Wang Y, Sun Q, Mu N, Sun X, Wang Y, Fan S, et al. The deubiquitinase USP22 regulates PD-L1 degradation in human cancer cells. *Cell Commun Signaling* (2020) 18(1):112. doi: 10.1186/s12964-020-00612-y

73. Shibue T, Weinberg RA. EMT, CSCs, and drug resistance: the mechanistic link and clinical implications. *Nat Rev Clin Oncol* (2017) 14(10):611–29. doi: 10.1038/nrclinonc.2017.44

74. Seebacher NA, Krchniakova M. Tumour microenvironment stress promotes the development of drug resistance. *Antioxidants (Basel)* (2021) 10(11):1801. doi: 10.3390/antiox10111801

75. Jachetti E, Caputo S, Mazzoleni S, Brambillasca CS, Parigi SM, Grioni M, et al. Tenascin-c protects cancer stem-like cells from immune surveillance by arresting T-cell activation. *Cancer Res* (2015) 75(10):2095–108. doi: 10.1158/0008-5472.CAN-14-2346

76. Zhong M, Zhong C, Cui W, Wang G, Zheng G, Li L, et al. Induction of tolerogenic dendritic cells by activated TGF-β/Akt/Smad2 signaling in RIG-i-deficient stemness-high human liver cancer cells. *BMC Canc* (2019) 19(1):439. doi: 10.1186/s12885-019-5670-9

77. Lei MML, Lee TKW. Cancer stem cells: Emerging key players in immune evasion of cancers. *Front Cell Dev Biol* (2021) 9:692940. doi: 10.3389/fcell.2021.692940

78. Glinsky GV, Berezovska O, Glinskii AB. Microarray analysis identifies a death-from-cancer signature predicting therapy failure in patients with multiple types of cancer. *J Clin Invest* (2005) 115(6):1503–21. doi: 10.1172/JCI23412

79. Feng T, Ling S, Xu C, Ying L, Su D, Xu X. Ubiquitin-specific peptidase 22 in cancer. *Cancer letters* (2021) 514:30–7. doi: 10.1016/j.canlet.2021.05.004

80. Qiu GZ, Liu Q, Wang XG, Xu GZ, Zhao T, Lou MQ. Hypoxia-induced USP22-BMI1 axis promotes the stemness and malignancy of glioma stem cells *via* regulation of HIF-1α. *Life Sci* (2020) 247:117438. doi: 10.1016/j.lfs.2020.117438

81. Jiang S, Miao D, Wang M, Lv J, Wang Y, Tong J. MiR-30-5p suppresses cell chemoresistance and stemness in colorectal cancer through USP22/Wnt/β-catenin signaling axis. *J Cell Mol Med* (2019) 23(1):630–40. doi: 10.1111/jcmm.13968

82. Park JM, Lee JE, Park CM, Kim JH. USP44 promotes the tumorigenesis of prostate cancer cells through EZH2 protein stabilization. *Molecules Cells* (2019) 42(1):17–27. doi: 10.14348/molcells.2018.0329

83. Ammirante M, Shalapour S, Kang Y, Jamieson CA, Karin M. Tissue injury and hypoxia promote malignant progression of prostate cancer by inducing CXCL13 expression in tumor myofibroblasts. *Proc Natl Acad Sci USA* (2014) 111(41):14776–81. doi: 10.1073/pnas.1416498111

84. Jayaprakash P, Ai M, Liu A, Budhani P, Bartkowiak T, Sheng J, et al. Targeted hypoxia reduction restores T cell infiltration and sensitizes prostate cancer to immunotherapy. *J Clin Invest* (2018) 128(11):5137–49. doi: 10.1172/JCI96268

85. Cho SH, Raybuck AL, Stengel K, Wei M, Beck TC, Volanakis E, et al. Germinal centre hypoxia and regulation of antibody qualities by a hypoxia response system. *Nature* (2016) 537(7619):234–8. doi: 10.1038/nature19334

86. Ling S, Shan Q, Zhan Q, Ye Q, Liu P, Xu S, et al. USP22 promotes hypoxia-induced hepatocellular carcinoma stemness by a HIF1α/USP22 positive feedback loop upon TP53 inactivation. *Gut* (2020) 69(7):1322–34. doi: 10.1136/gutjnl-2019-319616

87. Muñoz-Fontela C, Mandinova A, Aaronson SA, Lee SW. Emerging roles of p53 and other tumour-suppressor genes in immune regulation. *Nat Rev Immunol* (2016) 16(12):741–50. doi: 10.1038/nri.2016.99

88. Liu Y, Leslie PL, Zhang Y. Life and death decision-making by p53 and implications for cancer immunotherapy. *Trends Canc* (2021) 7(3):226–39. doi: 10.1016/j.trecan.2020.10.005

89. Agupitan A, Neeson P, Williams S, Howitt J, Haupt S, Haupt Y. P53: A guardian of immunity becomes its saboteur through mutation. *Int J Mol Sci* (2020) 21(10):3452. doi: 10.3390/ijms21103452

90. Yoon KW, Byun S, Kwon E, Hwang SY, Chu K, Hiraki M, et al. Control of signaling-mediated clearance of apoptotic cells by the tumor suppressor p53. *Science* (2015) 349(6247):1261669. doi: 10.1126/science.1261669

91. Cortez MA, Ivan C, Valdecanas D, Wang X, Peltier HJ, Ye Y, et al. PDL1 regulation by p53 *via* miR-34. *J Natl Cancer Inst* (2016) 108(1):djv303. doi: 10.1093/jnci/djv303

92. Ghosh M, Saha S, Bettke J, Nagar R, Parrales A, Iwakuma T, et al. Mutant p53 suppresses innate immune signaling to promote tumorigenesis. *Cancer Cell* (2021) 39(4):494–508.e5. doi: 10.1016/j.ccell.2021.01.003

93. Zhou J, Kryczek I. The ubiquitin ligase MDM2 sustains STAT5 stability to control T cell-mediated antitumor immunity. *Nat Immunol* (2021) 22(4):460–70. doi: 10.1038/s41590-021-00888-3

94. Takayama KI, Suzuki T, Fujimura T, Takahashi S, Inoue S. Association of USP10 with G3BP2 inhibits p53 signaling and contributes to poor outcome in prostate cancer. *Mol Cancer Res* (2018) 16(5):846–56. doi: 10.1158/1541-7786.MCR-17-0471

95. Stevenson LF, Sparks A, Allende-Vega N, Xirodimas DP, Lane DP, Saville MK. The deubiquitinating enzyme USP2a regulates the p53 pathway by targeting Mdm2. *EMBO J* (2007) 26(4):976–86. doi: 10.1038/sj.emboj.7601567

96. Colland F, Formstecher E, Jacq X, Reverdy C, Planquette C, Conrath S, et al. Small-molecule inhibitor of USP7/HAUSP ubiquitin protease stabilizes and activates p53 in cells. *Mol Cancer Ther* (2009) 8(8):2286–95. doi: 10.1158/1535-7163.MCT-09-0097

97. Müller I, Strozyk E, Schindler S, Beissert S, Oo HZ, Sauter T, et al. Cancer cells employ nuclear caspase-8 to overcome the p53-dependent G2/M checkpoint through cleavage of USP28. *Mol Cell* (2020) 77(5):970–84.e7. doi: 10.1016/j.molcel.2019.12.023

98. Tauriello DVF, Sancho E. Overcoming TGFβ-mediated immune evasion in cancer. *Nat Rev Cancer* (2022) 22(1):25–44. doi: 10.1038/s41568-021-00413-6

99. Welch-Reardon KM, Ehsan SM, Wang K, Wu N, Newman AC, Romero-Lopez M, et al. Angiogenic sprouting is regulated by endothelial cell expression of slug. *J Cell Sci* (2014) 127(Pt 9):2017–28. doi: 10.1242/dev.112474

100. Ravi R, Noonan KA, Pham V, Bedi R, Zhavoronkov A, Ozerov IV, et al. Bifunctional immune checkpoint-targeted antibody-ligand traps that simultaneously disable TGFβ enhance the efficacy of cancer immunotherapy. *Nat Commun* (2018) 9(1):741. doi: 10.1038/s41467-017-02696-6

101. Dupont S, Mamidi A, Cordenonsi M, Montagner M, Zacchigna L, Adorno M, et al. FAM/USP9x, a deubiquitinating enzyme essential for TGFbeta signaling, controls Smad4 monoubiquitination. *Cell* (2009) 136(1):123–35. doi: 10.1016/j.cell.2008.10.051

102. Hu M, Li P, Song L, Jeffrey PD, Chenova TA, Wilkinson KD, et al. Structure and mechanisms of the proteasome-associated deubiquitinating enzyme USP14. *EMBO J* (2005) 24(21):3747–56. doi: 10.1038/sj.emboj.7600832

103. Kim HT, Goldberg AL. UBL domain of Usp14 and other proteins stimulates proteasome activities and protein degradation in cells. *Proc Natl Acad Sci USA* (2018) 115(50):E11642–e50. doi: 10.1073/pnas.1808731115

104. Wang F, Ning S, Yu B, Wang Y. USP14: Structure, function, and target inhibition. *Front Pharmacol* (2021) 12:801328. doi: 10.3389/fphar.2021.801328

105. D'Arcy P, Wang X, Linder S. Deubiquitinase inhibition as a cancer therapeutic strategy. *Pharmacol Ther* (2015) 147:32–54. doi: 10.1016/j.pharmthera.2014.11.002

106. Wang Y, Jiang Y, Ding S, Li J, Song N, Ren Y, et al. Small molecule inhibitors reveal allosteric regulation of USP14 *via* steric blockade. *Cell Res* (2018) 28(12):1186–94. doi: 10.1038/s41422-018-0091-x

107. Lopez-Castejon G, Luheshi NM, Compan V, High S, Whitehead RC, Flitsch S, et al. Deubiquitinases regulate the activity of caspase-1 and interleukin-1β secretion *via* assembly of the inflammasome. *J Biol Chem* (2013) 288(4):2721–33. doi: 10.1074/jbc.M112.422238

108. Wilson SM, Bhattacharyya B, Rachel RA, Coppola V, Tessarollo L, Householder DB, et al. Synaptic defects in ataxia mice result from a mutation in Usp14, encoding a ubiquitin-specific protease. *Nat Genet* (2002) 32(3):420–5. doi: 10.1038/ng1006

109. Morgan M, Ikenoue T, Suga H, Wolberger C. Potent macrocycle inhibitors of the human SAGA deubiquitinating module. *Cell Chem Biol* (2022) 29(4):544–54.e4. doi: 10.1016/j.chembiol.2021.12.004

110. Tang JQ, Veggiani G, Singer A, Teyra J, Chung J, Sidhu SS. A panel of engineered ubiquitin variants targeting the family of domains found in ubiquitin specific proteases (DUSPs). *J Mol Biol* (2021) 433(24):167300. doi: 10.1016/j.jmb.2021.167300

111. Lin R, Nie J, Ren J, Liang R, Li D, Wang P, et al. USP4 interacts and positively regulates IRF8 function *via* K48-linked deubiquitination in regulatory T cells. *FEBS letters* (2017) 591(12):1677–86. doi: 10.1002/1873-3468.12668

frontiers | Frontiers in Oncology

ORIGINAL RESEARCH
published: 19 July 2022
doi: 10.3389/fonc.2022.935093

Interplay Between Immune and Cancer-Associated Fibroblasts: A Path to Target Metalloproteinases in Penile Cancer

Sarah Santiloni Cury[1,2,3†], Hellen Kuasne[1,4,5†], Jeferson dos Santos Souza[3], Juan Jose Moyano Muñoz[5,6], Jeyson Pereira da Silva[5], Ademar Lopes[7], Cristovam Scapulatempo-Neto[8,9], Eliney Ferreira Faria[8,10], Jean-Marie Delaissé[11,12], Fabio Albuquerque Marchi[5] and Silvia Regina Rogatto[1,2]*

[1] Department of Clinical Genetics, University Hospital of Southern Denmark, Vejle, Denmark, [2] Institute of Regional Health Research, University of Southern Denmark, Odense, Denmark, [3] Department of Structural and Functional Biology, São Paulo State University (UNESP), Botucatu, Brazil, [4] Rosalind and Morris Goodman Cancer Institute, McGill University, Montreal, QC, Canada, [5] International Research Center (CIPE), A. C. Camargo Cancer Center, São Paulo, Brazil, [6] Universidad Señor de Sipán, Chiclayo, Peru, [7] Pelvic Surgery Department, A. C. Camargo Cancer Center, São Paulo, Brazil, [8] Molecular Oncology Research Center, Barretos Cancer Hospital, Barretos, Brazil, [9] Department of Pathology, Diagnósticos da América - DASA, Barueri, Brazil, [10] Uro-oncology and Robotic Surgery, Hospital Felicio Rocho, Belo Horizonte, Brazil, [11] Clinical Cell Biology, Lillebaelt Hospital, University Hospital of Southern Denmark, Vejle, Denmark, [12] Department of Clinical Research, Clinical Cell Biology, University of Southern Denmark, Odense, Denmark

OPEN ACCESS

Edited by:
Dingwei Ye,
Fudan University, China

Reviewed by:
Guru Sonpavde,
Dana–Farber Cancer Institute, United States
Bryan E. Strauss,
University of São Paulo, Brazil

***Correspondence:**
Silvia Regina Rogatto
silvia.regina.rogatto@rsyd.dk

[†]These authors have contributed equally to this work

Specialty section:
This article was submitted to Genitourinary Oncology, a section of the journal Frontiers in Oncology

Received: *03 May 2022*
Accepted: *30 May 2022*
Published: *19 July 2022*

Citation:
Cury SS, Kuasne H, Souza JdS, Muñoz JJM, da Silva JP, Lopes A, Scapulatempo-Neto C, Faria EF, Delaissé J-M, Marchi FA and Rogatto SR (2022) Interplay Between Immune and Cancer-Associated Fibroblasts: A Path to Target Metalloproteinases in Penile Cancer. Front. Oncol. 12:935093. doi: 10.3389/fonc.2022.935093

Extracellular matrix (ECM) remodeling and inflammation have been reported in penile carcinomas (PeCa). However, the cell types and cellular crosstalk involved in PeCa are unexplored. We aimed to characterize the complexity of cells and pathways involved in the tumor microenvironment (TME) in PeCa and propose target molecules associated with the TME. We first investigated the prognostic impact of cell types with a secretory profile to identify drug targets that modulate TME-enriched cells. The secretome analysis using the PeCa transcriptome revealed the enrichment of inflammation and extracellular matrix pathways. Twenty-three secreted factors were upregulated, mainly collagens and matrix metalloproteinases (MMPs). The deregulation of collagens and MMPs was confirmed by Quantitative reverse transcription - polymerase chain reaction (RT-qPCR). Further, the deconvolution method (digital cytometry) of the bulk samples revealed a high proportion of macrophages and dendritic cells (DCs) and B cells. Increased DCs and B cells were associated with better survival. A high proportion of cancer-associated fibroblasts (CAFs) was observed in low-survival patients. Patients with increased CAFs had decreased immune cell proportions. The treatment with the MMP inhibitor GM6001 in CAF cells derived from PeCa resulted in altered cell viability. We reported a crosstalk between immune cells and CAFs, and the proportion of these cell populations was associated with prognosis. We demonstrate that a drug targeting MMPs modulates CAFs, expanding the therapeutic options of PeCa.

Keywords: penile cancer, secretome, transcriptome, cancer-associated fibroblasts, response to therapy

INTRODUCTION

Penile cancer (PeCa) represents 0.2% of all cancers diagnosed worldwide (1). However, poor and developing countries have a high incidence of the disease (2–4). Partial penectomy is frequently used for localized carcinomas (5). The disease could be aggressive, metastatic, and mutilating, mainly due to the delay in seeking treatment (6). Despite all efforts to improve the therapeutic strategies, the survival rates of PeCa patients remained almost unchanged over the past years (7).

Molecular and functional studies have revealed an important role of cells composing the tumor microenvironment (TME) in PeCa. The presence and distribution of immune checkpoint molecules or immune cell components were shown to be a potential predictor of clinical outcomes [reviewed in Aydin et al. (8)]. However, the immune fraction of TME alone is insufficient to predict treatment response and survival (8). Cancer-associated fibroblasts (CAFs) are a key component of the TME, playing a critical role in the extracellular matrix (ECM) deposition and remodeling. Moreover, CAFs have been implicated in the modulation of the immune system by establishing an immunosuppressive stroma, which can promote resistance to immune-based therapies (9). Although a limited number of transcriptome analyses in PeCa has been reported (7), the enrichment of pathways associated with ECM organization was described in patients with lymph node (LN) metastasis (10).

Immunotherapeutic drugs inhibit the immune checkpoint genes such as programmed cell death 1 (PD-1) and its ligand (PD-L1) (11). Cocks et al. (2016) identified PD-L1 expression in approximately 40% of PeCa patients, who may benefit from immunotherapies (12). Immunotherapy was further supported by studies that found that most patients presented advanced cancer (12, 13). The remaining 60% of PeCa patients have limited therapeutic options, including organ amputation and standard-of-care chemotherapies. In these cases, the immunotherapy response could be enhanced using a combinatorial treatment with TME-modulating drugs (14). Targetable molecular mechanisms that modulate CAFs are suggested to increase the cytotoxic T-cell level in the tumor, contributing to an increased immunotherapy response (15). Despite efforts to characterize the immune environment in PeCa (8, 13, 16, 17), there is a lack of in-depth knowledge on how the immune cells and CAFs simultaneously affect tumor progression.

The transcriptome analysis of bulk tumor samples allows *in silico* deconvolution using computational tools to infer cell type proportions (18). Moreover, the tumor transcriptome profile of the secretome (genes encoding secreted proteins) indicates which cell is activated in the tumor and releases factors that allow communication with other cells (19–21). These strategies are valuable tools to identify enriched cell types within the TME and their contribution to the tumor progression and response to therapy.

Here, we explored the transcriptome from two perspectives: 1) identify enriched immune and stromal cells using an *in silico* deconvolution method and 2) investigate targetable secretome components for TME modulation in PeCa. These strategies allowed us to characterize the TME composition of PeCa, in which we verified an enrichment of CAFs inversely correlated with immune cell proportion and an association with poor survival. Once the TME was characterized, the next step was to evaluate genes associated with ECM remodeling to identify potential drug targets able to modulate CAFs. Among these genes, we confirmed high expression levels of matrix metalloproteinase (MMP) genes in PeCa samples. Using PeCa–derived CAFs, we inhibited MMP expression and demonstrated a low viability of the cells.

Abbreviations: PeCa, penile cancer; CAF, cancer-associated fibroblasts; TME, tumor microenvironment; ECM, extracellular matrix; MMPs, matrix metalloproteinases; HPV, human papillomavirus; DEGs, differentially expressed genes; HPA, human protein atlas; PPI, protein–protein interactions; FC, fold change; FDR, false discovery ratio.

MATERIALS AND METHODS

Patients and Samples

A cohort of 63 squamous cell penile carcinomas (PeCa) usual type, 16 adjacent normal tissues, and 13 histologically normal glands (obtained from necropsies) from patients treated at A.C.Camargo Cancer Center and Barretos Cancer Hospital, São Paulo, Brazil, from 2006 to 2015 were included in the present study (**Table S1**). The entire cohort of 63 patients was distributed as described in the flowchart (**Figure S1**). The Human Research Ethics Committee from both Institutions approved the study (Protocols 1884/14 and 1030/2015, respectively). All patients and or family members were informed regarding the protocols and provided written informed consent before sample collection. The study was conducted according to the guidelines of the Declaration of Helsinki. The human papillomavirus (HPV) genotyping was performed using the Linear Array HPV Test Genotyping (Roche Molecular Diagnostics, Branchburg, NJ, USA).

Transcriptomic Analysis

Transcriptomic analysis was performed in 16 PeCa compared to six histologically normal penile glans using the GeneChip™ Human Transcriptome Array 2.0 (HTA 2.0; Affymetrix Santa Clara, California, USA), following the manufacturer's recommendations. The HTA 2.0 platform (Affymetrix, USA) was designed to interrogate >6 million probes targeting coding and non-coding transcripts, and exon–exon splice junctions (245,349 protein coding transcripts and 40,914 non-coding transcripts). RNA was isolated from fresh-frozen samples using the RNeasy mini kit (Qiagen, Valencia Germantown, Maryland, USA). RNA integrity was verified in all samples using the Agilent 2100 Bioanalyzer RNA 6000 LabChip kit (Agilent Technologies, Santa Clara, CA, USA). The scanning was performed using Affymetrix GeneChip Scanner 7000 (Affymetrix/ThermoFisher Waltham, Massachusetts, USA). The CEL files were generated by Affymetrix® GeneChip® Command Console® (AGCC) 4.0. The Transcriptome Analysis Console (TAC, ThermoFisher, USA, v.4.0) was used for data normalization and differential

expression analysis. Microarray data are available on the Gene Expression Omnibus (GEO) database (GSE196978). We also explored the transcriptomic profile of 30 usual PeCa previously evaluated by our group (Whole Human Genome Microarray 4x44K; Agilent Palo Alto, California, USA) (GSE57955) (22). Two datasets were analyzed independently (human GRCh37/hg19 annotation). The differentially expressed genes (DEGs) from the internal dataset were selected considering |fold change (FC)|> 2 and FDR <0.01. For the Agilent microarray data, DEGs were selected when presenting a log2 Cy3/Cy5 mean ratio ≥1.0 or ≤1.0 within a 99% confidence interval (CI) (upregulated and downregulated, respectively).

Transcriptome-Based Secretome Analysis

The upregulated genes identified in PeCa samples from each platform (Affymetrix and Agilent) were selected for secretome analysis using The Human Protein Atlas (HPA) database (www.proteinatlas.org) (23) with 2,943 predicted secretome proteins. The secretome genes were visualized using the protein–protein interaction (PPI) network with the Search Tool for the Retrieval of Interacting Genes/Proteins (STRING) tool v.11.5 (24) (http://string-db.org/). We considered experiments, database, co-expression, and co-occurrence as active interaction sources. The minimum required interaction score was 0.9 (highest confidence), and the disconnected nodes in the network were hidden for display simplification. The PPI p-values <0.05 were considered significant. The visualization and data annotation of PPI networks were constructed using Cytoscape v3.8.2.

Functional enrichment analysis was performed using the Enrichr tool (https://maayanlab.cloud/Enrichr/) (25) by accessing the libraries Gene Ontology (GO) biological process, GO Cellular Component, GO Molecular Function, Kyoto Encyclopedia of Genes and Genomes (KEGG), MSigDB Hallmark, Reactome, and Wiki Pathways. The terms were enriched with adjusted p-values <0.001. Ingenuity Pathway Analysis (IPA) software was used to identify molecules that potentially target the secretome genes.

Gene Expression Analysis by Real-Time Quantitative Polymerase Chain Reaction

The gene expression levels of matrix metalloproteinase (MMP) genes (*MMP1*, *MMP3*, *MMP7*, *MMP9*, *MMP10*, *MMP12*, and *MMP13*) and collagens (*COL1A2*, *COL3A1*, *COL4A1*, *COL5A2*, *COL10A1*, *COL11A1*, and *COL24A1*) were investigated in 47 PeCa aiming to confirm the transcriptomic results. Primer sets were designed using Primer-Blast software (http://www.ncbi.nlm.nih.gov/tools/primer-blast/) (**Table S2**). Total RNA was converted into complementary DNA (cDNA), and the amplification was carried out as previously described (10). We used *GUSB* as reference transcript (26). The relative quantification of mRNA expression was evaluated using the $2^{-\Delta\Delta CT}$ method (27). Data were analyzed statistically using Graphpad Prism 5.0 (GraphPad Software Inc., La Jolla, CA, USA). The Mann–Whitney U test was used to compare normal vs. cancer groups. *P*-values < 0.05 were considered significant.

Immune Score Classification

The transcriptome deconvolution analysis was performed in the internal set of samples to evaluate the prevalence of immune infiltrating cells. The digital cytometry analysis was conducted using the CIBERSORTx tool (https://cibersortx.stanford.edu/) to impute the immune cell fractions of 22 cell types (LM22 matrix signature) from the bulk RNA-seq data (28). We applied the default settings of CIBERSORTx and batch correction to minimize the impact of cross-platform variation. The immune scores (CIBERSORTx) were used to classify the PeCa samples as "immune hot" high immune cells infiltration and "immune cold" low immune cells infiltration (29). The immune score cut-offs for macrophages, DCs, and B cells associated with survival were also determined (EasyROC v. 1.3.1, http://www.biosoft.hacettepe.edu.tr/easyROC/) (30).

Cancer-Associated Fibroblast Score

The EPIC (http://epic.gfellerlab.org/) tool was used to estimate the fraction of CAFs and explore the changes in the matrix components of PeCa and normal tissues (internal set) (31). EPIC establishes reference gene expression profiles for major tumor-invasive immune cell types (CD4+ T, CD8+ T, B, natural killer, and macrophages) and further deduces the reference spectra of CAFs and endothelial cells (32).

The digital cytometry analysis (CIBERSORTx tool) was applied to impute the CAF proportion in PeCa samples using the CAF expression signature from single-cell RNA-seq data from head and neck squamous cell carcinomas (HNSCC) (33). First, the CAF signature matrix and CAF fractions were imputed in PeCa (default settings and batch correction). We used the CAF signature derived from HNSCC due to the absence of single-cell resolution data in PeCa samples. The criteria to select HNSCC as a reference for CAFs were based on similarities shared by these tumors, including that both are derived from epithelial cells, they are classified as squamous cell carcinomas (34), and HPV is an etiological factor–associated disease (35). In addition to CAFs from HNSCC (36), a consensus list of canonical CAF markers of human cancers was obtained (9, 37–39). The expression signature of CAF markers was compared with CAF classification using digital cytometry to confirm the reliability of the CAF signature in PeCa.

Cancer-Associated Fibroblasts Derived From Penile Cancer Cells

In a previous study, we established three cells derived from PeCa (Cell4, Cell5, and Cell6) that were molecularly and morphologically characterized as CAFs (40). The morphology of CAF in PeCa was evaluated by immunofluorescence using Texas Red: actin/phalloidin (Thermo Fisher Scientific, Waltham, MA, USA), FITC (fluorescein isothiocyanate): tubulin (Thermo Fisher Scientific, Waltham, MA, USA), and DAPI (4′,6-diamidino-2-phenylindole): nucleus (Vector Laboratories, Burlingame, CA, USA) as described by Kuasne et al. (40).

We performed chemosensitivity assays using GM6001 (Merck Life Science, Hellerup, Denmark), a broad-spectrum MMP inhibitor (MMP-1, MMP-2, MMP-3, MMP-7, MMP-8, MMP-9, MMP-12, MMP-14, and MMP-26). Briefly, PeCa cells

were seeded in a 96-well plate at a density of 1×10^5 cells/ml and incubated at 37°C in a complete medium composed of 3:1 keratinocyte serum-free medium–DMEM/F12 (Dulbecco's modified Eagle medium/nutrient mixture F-12) (GIBCO, Carlsbad, CA, USA) supplemented following the previously described protocol (40). Treatment with GM6001 was administered after 24 h in concentrations of 0, 1, 3, 10, and 20 µM, and six replicates were used for each concentration. Following 24 h of treatment incubation, 100 µl of MTT (3-(4,5-dimethylthiazol-2-yl)-2,5-diphenyltetrazolium bromide) reagent solution (0.5 mg/ml) was added to each well and incubated for 3 h at 37°C. After removing the MTT solution, 180 µl of DMSO (dimethyl sulfoxide) was added to solubilize the violet formazan crystals. The plates were incubated for 15 min at 37°C, and the absorbance readings were performed at 560 nm with a reference of 690 nm using the Biotek Synergy HT microplate reader (Agilent, Santa Clara, CA, USA).

Data Representation and Statistical Analyses

Heatmaps were created using the web tool Morpheus (https://software.broadinstitute.org/morpheus). GraphPad Prism® (GraphPad Software, v5.0, 2008, USA) was used for statistical analysis. Log-rank (Mantel–Cox)–Gehan–Breslow–Wilcoxon Tests were used for survival analysis.

RESULTS

The patients included in this study showed similar clinical and histopathological characteristics, such as mean age, alcohol consumption, tobacco usage, HPV status, TNM stage, and perineural and angiolymphatic invasion (**Table S1**).

We identified 2,199 and 1,050 upregulated genes in PeCa compared with normal tissues in our internal and validation datasets, respectively, of which 161 and 189, respectively, were predicted to encode secreted proteins. The PPI analysis of the secretome genes revealed functions associated with ECM and inflammation (**Figures 1A, B**). Seventeen terms with the highest combined score were mainly associated with inflammatory response and ECM regulation in both PeCa datasets (**Table S3**; **Figure 1C**). Despite enriching similar pathways and ontologies, only 23 secretory genes (encoding inflammatory cytokines/chemokines and ECM molecules) were upregulated in internal and validation datasets (**Table 1**). These findings suggested that PeCa cells directly interact with the immune system and the stroma.

Tumor Microenvironment Immune Composition of Penile Cancer

Based on the significance of inflammation-associated pathways and the immune system–related genes in the PeCa secretome (**Figure 1**; **Table 1**), we first identified enriched immune cells within the TME using an *in silico* deconvolution by applying digital cytometry. PeCa samples presented a higher proportion of dendritic cells (DCs), macrophages, and B cells, while normal samples presented a high number of monocytes, NK cells, and mast cells (**Figure 2A**). We identified a set of PeCa patients with high scores of CD8 T cells, macrophages, and DCs and higher mean immune score (immune hot; **Figure 2B**). Although not significant, immune-cold patients had a trend to present shorter overall survival (**Figure 2C**). Since we found an increased proportion of macrophages, DCs, and B cells in PeCa compared to normal samples and differential scores among the tumor samples, we next investigated the association of these cells with overall survival. The best score cutoff for macrophage, DC, and B cells was calculated using the easyROC tool (30). The optimal immune score cutoff generated was 0.023 for macrophages, 0.059 for DCs, and 0.093 for B cells. Values above these cutoffs were considered as high. Patients with higher DC and B cell scores also had a trend toward higher overall survival (**Figures 2C, D).**

Cancer-Associated Fibroblast Profile

Since we identified enriched pathways associated with ECM organization, the next step was to assess the presence of CAFs possibly involved in the synthesis of ECM remodeling factors. We also investigated a potential interplay between immune cells and CAFs. The CAF score (EPIC tool) in tumor samples was higher and statistically significant ($p<0.0001$) compared to normal tissues (**Figure 3A**). To deconvolute the CAFs from PeCa and normal samples (CIBERSORTx), we used a gene signature of CAFs derived from the HNSCC single-cell RNA-seq study (33). We found higher scores of CAFs in PeCa compared to normal samples (**Figure 3B**). Next, we analyzed the gene expression levels of 31 canonical CAF markers (*ACTA2, S100A4, VIM, DES, FAP, PDGFRB, CAV1, MME, GPR77, TNC, GLI1, HOXB6, LRRC15, Ly6c1, ISLR, PDGFRA, PDPN, MFAP5, COL11A1, ITGA11, NG2, POSTN, COL1A1, CDH2, FN1, CD44, CD90, CD163, LOXL2, EDARADD*, and *WNT2*) (9, 36–39). Interestingly, this signature was able to cluster PeCa (**Figure 3C**). Based on the CAF scores and gene expression, we noted a heterogeneous profile, where 31% of PeCa samples (PA41T, PE27T, PA42T, PA13T, and PE17T) presented a low expression of CAF markers (**Figure 3C**). We also found that cases with higher CAF scores and an increased expression of CAF markers presented low overall survival (**Figure 3E**). The PeCa samples from the validation dataset showed a cluster composed of 18 patients presenting a higher expression of CAF markers (beige cluster), while 12 patients (40%) showed low expression (orange cluster) (**Figure 3D**). Moreover, a potential association of CAF signature expression with survival was confirmed (**Figure 3F**).

A significantly negative correlation was found between the CAF score with the mean immune score (the mean score of all immune cell types calculated for each sample) (**Figure 3G**; **Table S4**).

Genes Related to Extracellular Matrix Are Associated With Penile Cancer Development and Poor Outcome Features

The secretome of two datasets showed the enrichment of ontologies and pathways associated with ECM organization

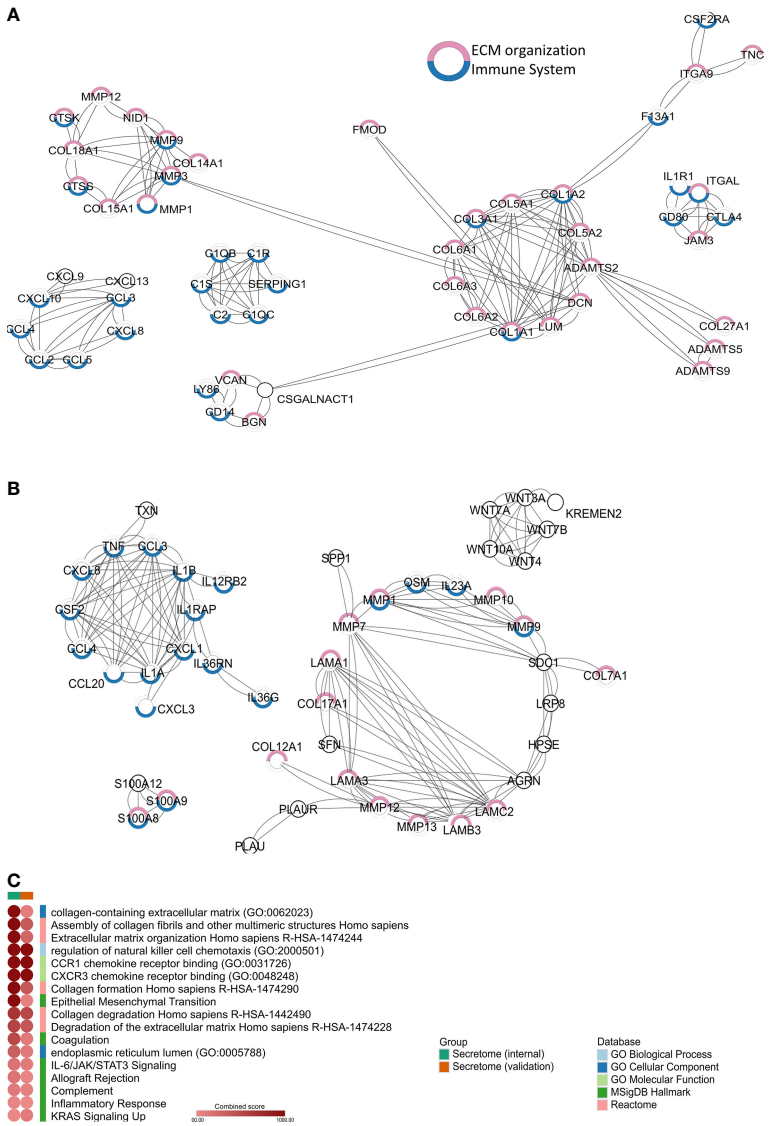

FIGURE 1 | Secretome profile of penile cancer (PeCa) **(A)** Protein–protein interactions (PPIs) of secretome genes upregulated in PeCa from the internal dataset (Affymetrix). **(B)** PPIs of secretome genes upregulated in PeCa from the validation dataset (Agilent). Network generated by STRING (Search Tool for the Retrieval of Interacting Genes/Proteins) using the highest confidence interaction score (0.9). Colored circles indicate the associated ontology; genes associated with the immune system and extracellular matrix (ECM) are highlighted in blue and pink, respectively. Edges represent interaction. **(C)** Heat-scatter plot of the combined score for the enriched pathways and ontologies. Top categories selected from enrichment analysis of secretome genes from PeCa samples. The intensity of the color in the dotplot indicates the enrichment significance by the combined score. Significant adjusted *p*-value was found in all included terms. Gene set names are colored according to the Gene Ontology (GO) biological process (light blue), GO cellular component (dark blue), GO molecular function (light green), Kyoto Encyclopedia of Genes and Genomes (KEGG, dark green), MSigDB Hallmark (pink), Reactome (red), and Wiki Pathways (orange).

and degradation. Considering the interaction between collagen and MMPs (41), we evaluated their expression pattern on PeCa according to the CAF score and compared them to normal tissues. Our interest was also confirming the altered expression of these genes, and if confirmed, we investigated whether ECM proteins are targetable for TME modulation in PeCa. *MMP1* was the only metallopeptidase with significantly increased expression levels in PeCa with a high CAF score (validation set). However, most MMPs tended to increase expression in high CAF scores in PeCa (**Figure 4A**). A high expression of *COL11A1*, *COL1A2*, *COL5A2*, and *COL10A1* was detected in PeCa samples with high CAF scores (validation set, **Figure 4C**). Using RT-qPCR in a larger set of cases, we found that all MMPs tested presented increased expression in PeCa (**Figure 4B**). In addition, *COL10A1* showed significantly increased expression, and *COL24A1* showed down expression in PeCa compared to normal samples (**Figure 4D**). A significantly increased *COL11A1* expression was found in patients with LN involvement (RT-qPCR)

TABLE 1 | Twenty-three genes encoding for secreted proteins upregulated in internal (n=16) and validation (n=30) datasets of penile cancer.

Gene Symbol	Gene Name	Function*
ADAMDEC1	ADAM Like Decysin 1	Immune response and metalloendopeptidase activity
CCL3	C-C motif chemokine 3	Inflammatory response
CCL4	C-C motif chemokine 4	Inflammatory response
CEMIP	Cell migration–inducing and hyaluronan-binding protein	Regulates epithelial–mesenchymal transition
COL7A1	Collagen alpha-1(VII) chain	Extracellular matrix structure
CXCL13	C-X-C motif chemokine 13	Inflammatory response
CXCL8	C-X-C motif chemokine 8	Inflammatory response
CXCL9	C-X-C motif chemokine 9	Inflammatory response
EGFL6	Epidermal growth factor–like protein 6	Extracellular matrix organization
ESM1	Endothelial cell–specific molecule 1	Angiogenesis
FABP5	Fatty acid–binding protein 5	Lipid metabolism
GZMA	Granzyme A	Immune response
ICOS	Inducible T-cell costimulator	Immune response
LGALS9	Galectin-9	Inflammatory response
MMP1	Interstitial collagenase	Extracellular matrix degradation
MMP12	Macrophage metalloelastase	Extracellular matrix degradation
MMP9	Matrix metalloproteinase-9	Extracellular matrix degradation
PGLYRP4	Peptidoglycan recognition protein 4	Immune response
PI3	Elafin	Immune response
PLA2G7	Platelet-activating factor acetylhydrolase	Lipid metabolism
S100A7	S100-A7	Immune response
S100A8	S100-A8	Immune response
S100A9	S100-A9	Immune response

**Information retrieved from Uniprot database – UniProtKB 2021_04 (https://www.uniprot.org/, Accessed November 2021).*

and presented a trend toward significance in microarray datasets (**Figure 4E**).

Cancer-Associated Fibroblasts Derived From Penile Cancer Cells Are Sensitive to Matrix Metalloproteinase Inhibitor

Considering the global alteration of MMPs in PeCa and their potential to promote an immunosuppressive TME by remodeling it (42), we investigated the expression of CAF markers in PeCa-derived cells previously published by our group (40). The expression profile of Cell1 (healthy individual) was distinct from cells with fibroblast-like morphology (Cell4, Cell5, and Cell6, **Figure 5B**), which presented a high expression of CAF markers (**Figure 5A**). The expression levels of MMPs and collagen genes revealed two distinct clusters (all three CAF cell lines versus Cell1). Overall, MMPs were overexpressed (especially in Cell6), while collagens were down expressed in CAFs compared to Cell1 (**Figure 5C**). Corroborating our previous results (10), MMP1 was highly overexpressed in PeCa samples (Affymetrix dataset). This gene was also overexpressed in Cell6, while MMP7 and *MMP9* presented increased expression in Cell4 (**Figure 5C**).

We evaluated a compound that potentially inhibits the enzymatic activity of secreted proteins identified in our analysis, especially the MMPs (IPA software) (**Figure 5D**). Although a modest effect was observed when CAF cells were treated with a broad MMP inhibitor (GM6001), the concentration of ~10 μM of GM6001 promoted decreased cell viability in CAFs compared to Cell1 (**Figure 5E**).

DISCUSSION

In this study, we explored the transcriptome data of PeCa samples to evaluate the interplay between cells within the TME and its relevance to disease outcomes. We identified an enrichment of immune and stromal cells and an association with survival. A second and complementary approach was based on investigating targetable MMPs for TME modulation in PeCa.

We found that immune cells and CAFs play a critical role in the TME by expressing and potentially secreting inflammatory factors and ECM remodeling proteinases. We also verified that immune cell proportions were negatively correlated with CAFs in PeCa samples. Interestingly, patients with high CAF scores presented lower survival rates and an increased expression of MMPs and collagens. These results demonstrate that our strategy to profile and deconvolute bulk tumors brings new perspectives to understand the TME of PeCa better. These findings also provided the rationale to test, *in vitro*, the MMP inhibitor GM6001 on PeCa-derived CAFs. We observed a higher effect of this inhibitor in penile CAFs than in normal fibroblasts.

Extracellular components and inflammatory factors were the main class of upregulated secreted proteins found in our internal and validation PeCa datasets. We found 23 secretome genes shared in these two datasets. This small overlap could be explained by the different microarray platforms used or simply by the intrinsic heterogeneity found in cancer samples. However, enriched pathways and gene ontologies were mainly associated with extracellular matrix and immune response in both datasets, reinforcing their relevance to the disease despite the differences in the overlapping secretome. The immune-inflammatory system and matrix metalloproteases were previously demonstrated to be overrepresented in PeCa compared to normal penile tissues (10, 43). In oral carcinomas, high levels of pro-inflammatory cytokines affect the TME by increasing ECM degradation *via* MMPs during disease progression (44). Our findings suggest that interactions

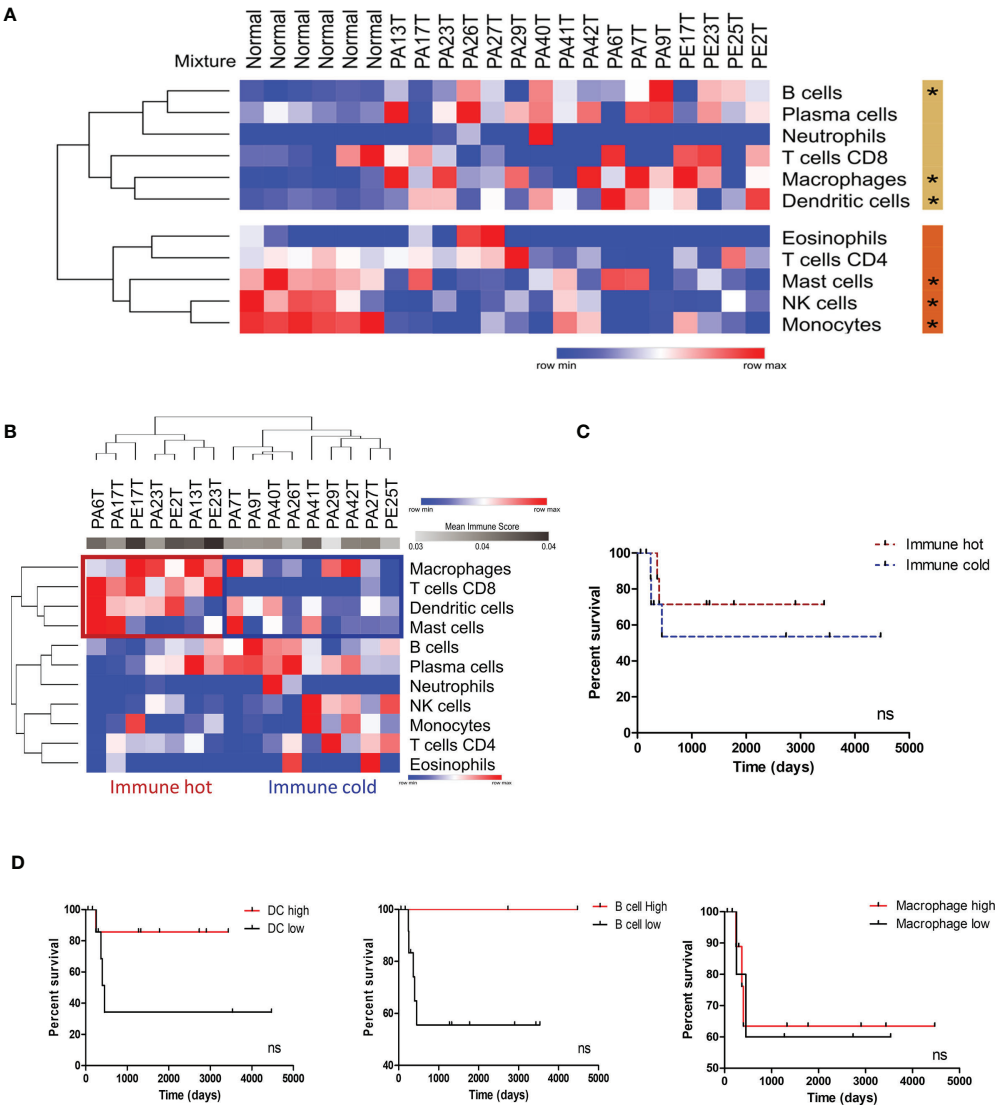

FIGURE 2 | Immune profile characterization of PeCa samples using digital cytometry. **(A)** Heatmap representative of the immune cell score in normal and PeCa samples calculated using CIBERSORTx. (*) significant p-values comparing tumor versus normal samples. Rows were clustered based on the Euclidean distance of immune score values. Two clusters were generated using K-means analysis (K-means = 2). The beige and orange bars indicate the clusters of cells enriched in PeCa samples and normal samples, respectively. **(B)** Heatmap representative of immune cell scores in PeCa samples calculated using CIBERSORTx. Rows and columns were clustered based on the one minus Pearson correlation of immune score values. **(C)** Kaplan–Meier plot of immune hot and immune cold PeCa patients based on Figure 2B. **(D)** Kaplan–Meier plot of patients presenting high and low scores of dendritic cells (DCs), B cells, and macrophages. The bets cutoffs for survival analysis were determined by the easyROC web tool. **(C, D)** The Gehan–Breslow–Wilcoxon Test determined the hazard ratio (HR) with 95% confidence intervals (CIs). ns: p-values not statistically significant.

between inflammation and matrix remodeling have a crucial role in penile carcinogenesis and progression.

We found increased scores of B cells, macrophages, and DCs in PeCa compared to normal tissues. Moreover, we described that a subset of PeCa patients presented an immune hot phenotype (higher scores of CD8 in T cells, DC, and mast cells). These features are potentially associated with a better prognosis. Although the low number of our cases precluded statistical significance, B cells and DCs improve prognosis in cancer patients due to the antitumor activity and the potential to increase immunotherapy response (45–48). The immune hot score classification predicts a better prognosis in cancer patients (29). Altogether, the immune classification of PeCa could be used as a tool to predict the outcome and immunotherapy response, mainly because we also found a negative correlation between immune and CAF scores in PeCa. These results open new scenarios to test whether immunotherapy response could be enhanced using a combinatorial treatment with TME-modulating drugs.

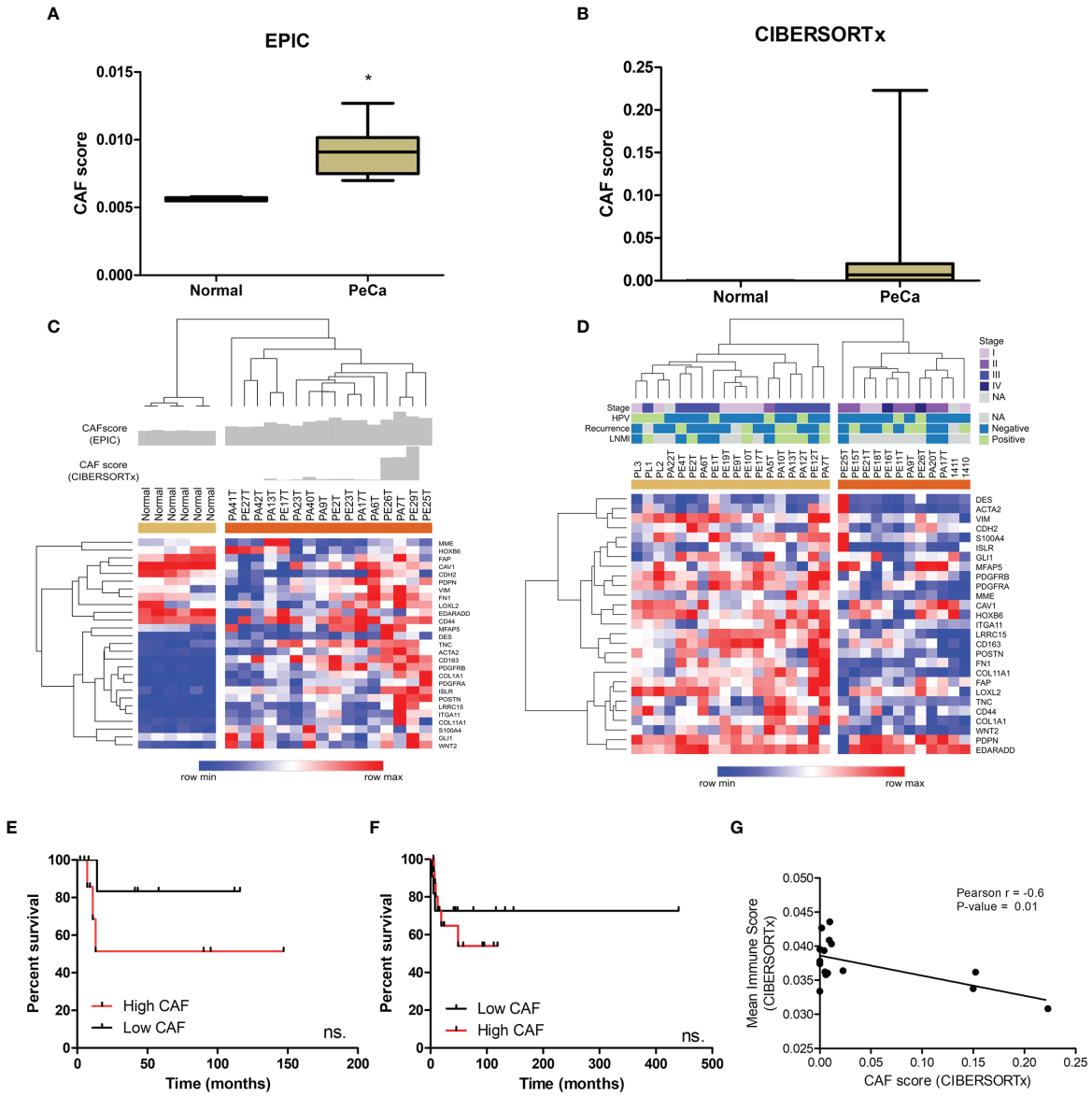

FIGURE 3 | CAF characterization of PeCa samples using digital cytometry. **(A)** Bar graph demonstrating the mean score estimated using EPIC. The statistical significance was analyzed using Student's t-test. *P < 0.001. **(B)** Bar graph demonstrating mean score estimated using CIBERSORTx. **(C)** Heatmap representing the gene expression of CAF markers in the internal set of cases (Affymetrix). The top panel indicates the CAF score in normal and PeCa samples calculated using CIBERSORTx and EPIC. Rows and columns were clustered based on the Euclidean distance of CAF marker expression. Three clusters were generated using k-means analysis (K-means = 3). **(D)** Heatmap representing the gene expression of CAF markers in the validation dataset (Agilent). Rows and columns were clustered based on Euclidean distance of CAFs marker expression. Two clusters were generated using k-means analysis (K-means = 2). **(E)** Kaplan–Meier plot of patients presenting high and low scores of CAFs (Affymetrix; internal set). **(F)** Kaplan–Meier plot of patients presenting high and low expression of CAF markers (Agilent; validation set). **(E, F)** The HR with 95% confidence intervals (CI) was determined by the Gehan–Breslow–Wilcoxon Test. ns, not statistically significant. **(G)** The partial Pearson's rank correlation (r) and p-value are given for the CAF score generated by CIBESORTx with the mean immune score also generated by CIBESORTx.

The CAF score is increased in PeCa compared to normal samples, but we also found a subset of PeCa highly expressing CAF markers with lower overall survival (internal and validation sets). It has been established that CAF gene signatures can distinguish between low and high CAF tumors and predict patient survival (49, 50). The impact of CAFs on patients' survival has been reported, and their inhibition has emerged as a promising anti-cancer therapy (51). However, the pharmaceutical inhibition of CAFs expressing the canonical marker *FAP* (fibroblast activation protein) has not been proven to be successful yet (51). CAFs contribute to an immunosuppressive TME and targeting CAFs, or their products have the potential to improve current

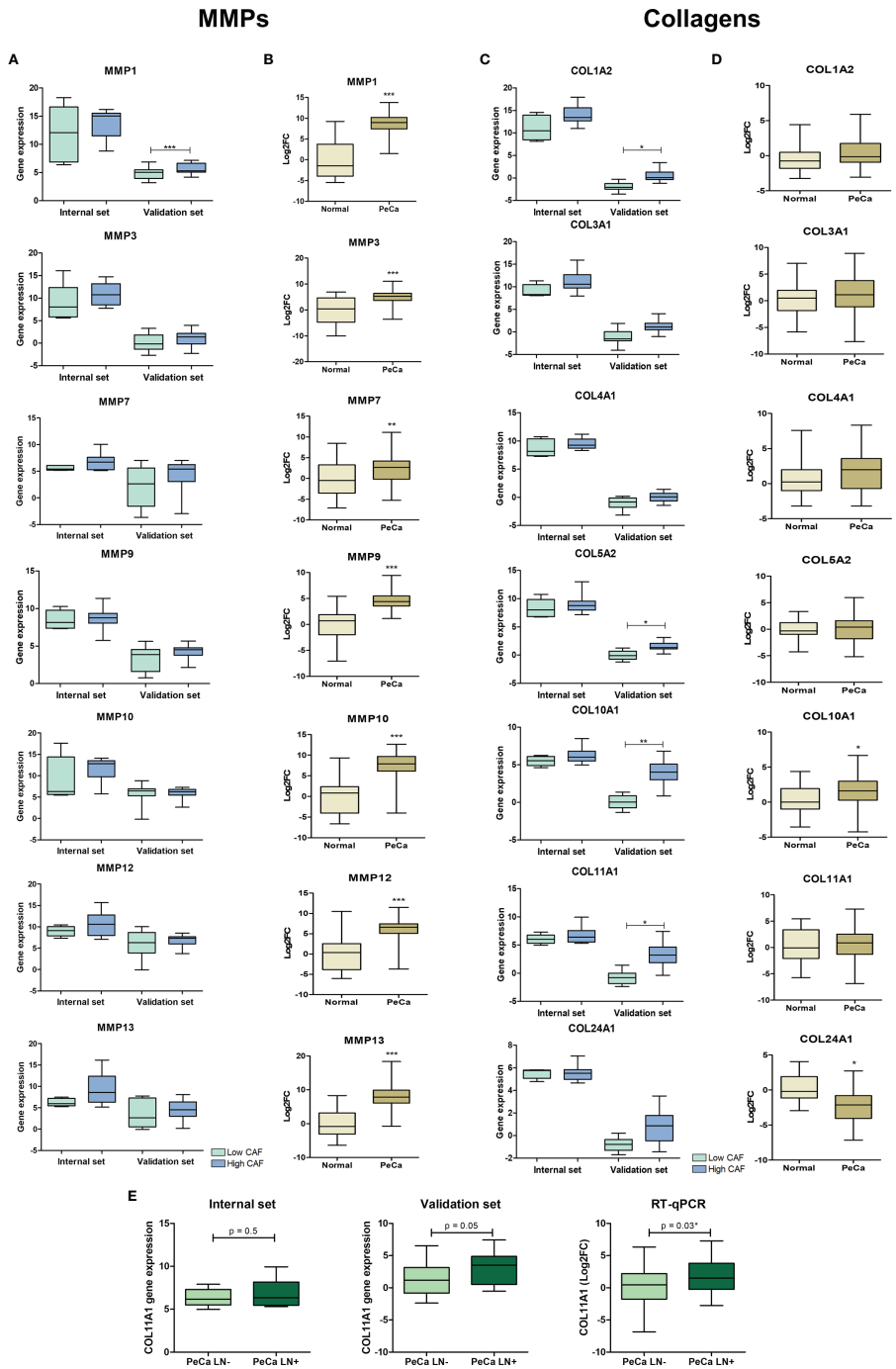

FIGURE 4 | Expression pattern of matrix metalloproteinases and collagens in PeCa samples. **(A)** Box plots representative of expression levels of *MMP1*, *MMP3*, *MMP9*, *MMP10*, *MMP12*, and *MMP13* genes in PeCa compared to normal samples from internal [normalized-expression Robust Multi-ArrayAverage (RMA)] and validation set (expression ratio) according to the CAF score. **(B)** Box plots showing the expression levels of *MMP1*, *MMP3*, *MMP9*, *MMP10*, *MMP12*, and *MMP13* in PeCa samples compared to normal tissues using RT-qPCR [$\log_2$fold change (2–DDCt) relative to *GUSB*]. The statistical difference was analyzed by the Mann–Whitney U test. **(C)** Box plot representative of the expression levels of *COL11A1, COL1A2, COL4A1, COL3A1, COL5A2, COL10A1*, and *COL24A1* genes in PeCa samples from internal (normalized-expression RMA) and validation set (expression ratio) according to the CAF score. **(D)** Box plots showing the expression levels of *COL11A1, COL1A2, COL4A1, COL3A1, COL5A2, COL10A1*, and *COL24A1* genes in PeCa compared to normal samples using RT-qPCR [$\log_2$fold change (2–DDCt) relative to *GUSB*]. Statistical difference was analyzed by the Mann–Whitney U test. **(E)** Box plot showing the expression levels of *COL11A1* in PeCa compared to normal tissues from internal (normalized-expression RMA), validation set (expression ratio), and RT-qPCR according to lymph node (LN) metastasis. LN+: patients positive for LN metastasis; LN-: patients negative for LN metastasis. Statistical difference was analyzed by Student's t-test. *p-values < 0.05, **p-values < 0.01, and ***p-values < 0.001.

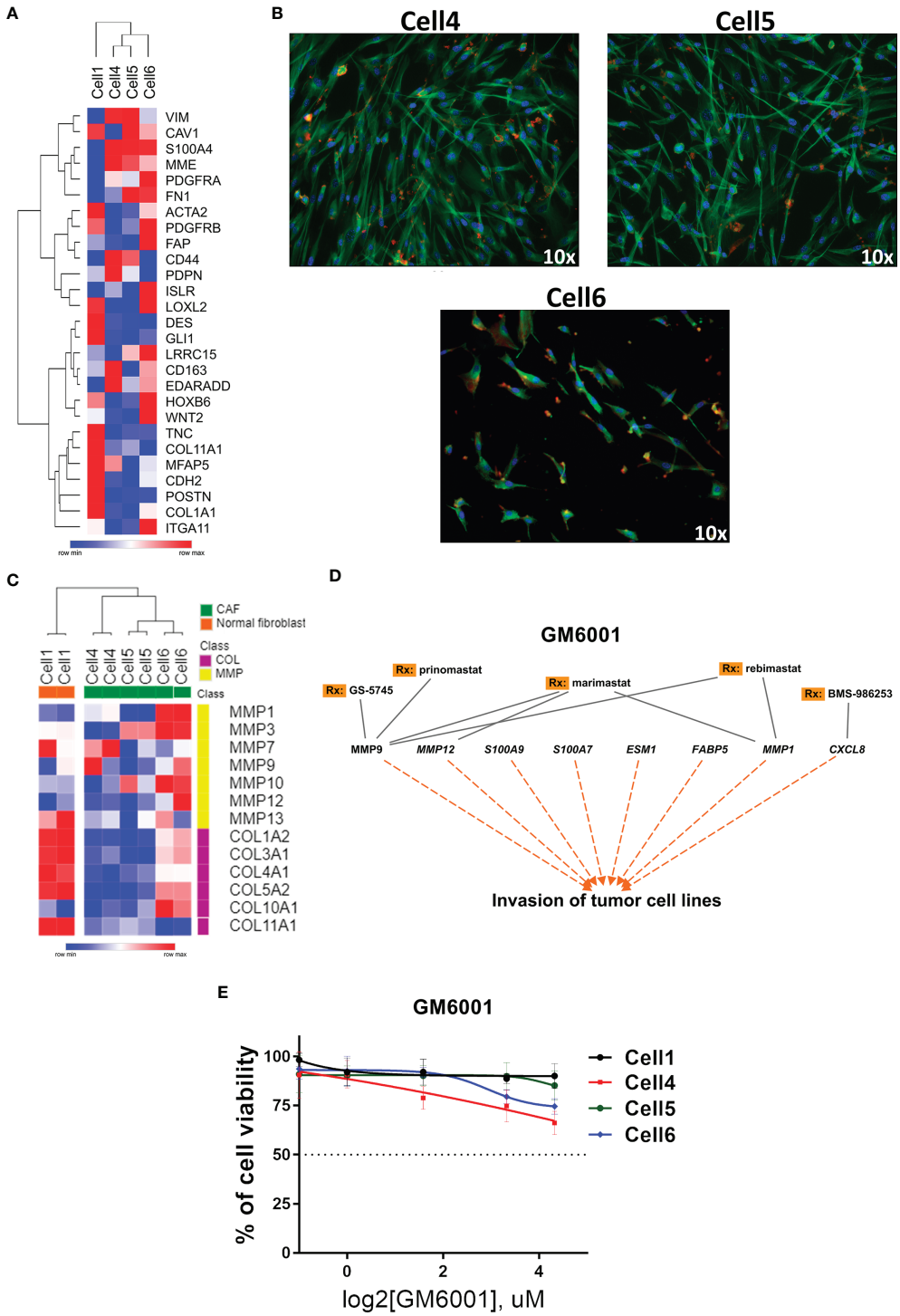

FIGURE 5 | Targeted therapy in PeCa–derived CAF cells. **(A)** Heatmap representative of gene expression of CAF markers in PeCa–derived cells (Cell4, Cell5, and Cell6) and normal foreskin cell line (Cell 1). Rows and columns were clustered based on the Euclidean distance of CAF marker expression. **(B)** Immunofluorescence images (Texas Red: actin/phalloidin; FITC: tubulin; and DAPI: nucleus, ×10 magnification, Nikon TE2000) of CAF cells (Cell4, Cell5, and Cell6). **(C)** Heatmap representative of the expression levels of MMP and collagen genes (same gene set used in the validation) in PeCa-derived cells (Cell4, Cell5, and Cell6) and Cell1. **(D)** Potential target therapy for secreted genes, especially MMPs (IPA analysis). **(E)** Cell viability assay using an MMP inhibitor (GM6001—Pan inhibitor of MMPs) at the indicated concentrations for 24 h to treat Cell1, Cell4, Cell5, and Cell6.

immunotherapy approaches for cancer patients (42). Therefore, a comprehensive understanding of CAF markers is needed, aiming to design effective therapeutic strategies for PeCa.

We showed that PeCa presented a global alteration of MMPs and collagens, in which tumors with high CAF scores have an increased expression of collagens. *COL11A1* was associated with LN metastasis, corroborating with previous findings (52, 53), and a novel prognostic biomarker of PeCa. Collagens are the most abundant ECM component, increasing tumor tissue stiffness, among other features (54). MMPs are essential to degrade collagen during ECM remodeling (41). A previous study demonstrated that *MMP1* and *MMP12* presented increased expression in usual and mixed PeCa subtypes (10). Herein, we confirmed these alterations and found an increased expression of *MMP1* in tumors with high CAF scores. Epithelial cells express MMPs (55); thus, the inhibition of MMP must modulate the microenvironment and malignant epithelial cells. We showed that MMPs are highly expressed in PeCa cells and PeCa-derived CAFs. The implication of MMPs in tumor invasion and metastasis has prompted the development of strategies that promote MMP inhibition (56). A high expression of *MMP1* has been related to poor outcomes and shorter overall survival in PeCa (10). CAFs express MMPs that assist the immunosuppression of TME, counteracting CAFs that secrete MMPs, which have the potential to enhance the efficacy of immunotherapies (42). Therefore, MMP inhibition is a potential therapeutic strategy for PeCa, especially in combination with standard-of-care therapies.

PeCa–derived cell lines were previously described as reliable models to investigate the molecular mechanisms associated with carcinogenesis and treatment resistance and to develop effective treatment strategies (57). Targeting therapies enabled personalized approaches to improve the outcome of PeCa patients (7, 58). The genomic profiling of PeCas revealed the potential of Epidermal Growth Factor Receptor (EGFR) target therapy, in which tumors with *EGFR* amplification could be more sensitive (59). However, the number of preclinical studies in PeCa is still limited. Genetically engineered mouse models of PeCa were elegantly evaluated, showing that a combined target therapy and immunotherapy could be used in the treatment of PeCa patients (17).

In the present study, to better investigate the behavior of CAFs and the therapy response, we showed that the inhibition of MMPs using a broad-spectrum MMP inhibitor presented a modest effect in PeCa-derived CAFs (2 out of 3 cells) and no effect in normal fibroblasts. The slight alteration on cell viability was not surprising; the TME remodeling does not necessarily require CAFs to die but is often associated with the modulation of CAF functions (60). Cell4 had higher MMP inhibitor sensitivity than the other cells, which could be explained by the high expression of *MMP7* and *MMP9* (targets of GM6001). High levels of *MMP7* are associated with shorter survival in cancer patients, while the prognostic role of *MMP9* is controversial (61). Cell6 presented the higher expression levels of *MMP1* and *MMP12* (direct targets of GM6001) and showed a better response to MMP inhibition. Thus, the MMP modulation in the TMEs needs to be individually evaluated in different tumor types to design suitable MMP targeting therapies (61). Several clinical trials have tested MMP inhibitors during the last decades, and most of these studies failed due to the lack of efficacy and severe side effects (56). As more selective inhibitors of MMPs are now available, MMP targeting could be reconsidered for cancer therapy (56). Clinical trials with new MMP inhibitors and combined therapies should be undertaken to improve therapy efficacy for PeCa patients. Considering that extensive degradation of ECM proteins *via* MMPs promotes tumor invasion and metastasis (62), it is crucial to remodel the ECM for the most effective treatment. Therapeutic strategies targeting aberrant ECM components for cancer treatment can act as an adjuvant for conventional chemotherapy and immunotherapy (63).

Herein, we highlighted for the first time the role of CAFs and the interplay of cells within the TME in PeCa; however, this retrospective study also has limitations, including the small sample size. We overcome this limitation by validating the gene expression findings in an independent dataset. Additional studies are necessary to validate the computational prediction of cell proportions in the TME and its prognostic impact, such as single-cell RNA sequencing studies. Translational research for PeCa is still a challenge, but recent advances in PeCa patient–derived tumor xenografts demonstrate the potential of this model to design a personalized treatment considering the genomic and TME profiling (64).

CONCLUSIONS

Our data highlight the interplay between cell types in the TME of penile carcinomas. We demonstrated the complexity of the TME and the association between immune cells and CAFs as a prognostic factor for PeCa patients. We found a global deregulation of collagens and MMPs and tested CAF cell lines using an MMP inhibitor, which proved the ability to modulate these cells. These findings pave the way for future studies to understand the impact of TME-modulating therapies in PeCa patients.

DATA AVAILABILITY STATEMENT

The datasets presented in this study can be found in online repositories. The names of the repository/repositories and accession number(s) can be found in the article/**Supplementary Material**.

ETHICS STATEMENT

The studies involving human participants were reviewed and approved by the Human Research Ethics Committee from A.C.Camargo Cancer Center and Barretos Cancer Hospital, São Paulo, Brazil (Protocols 1884/14 and 1030/2015, respectively). The patients/participants provided their written informed consent to participate in this study.

AUTHOR CONTRIBUTIONS

SR: Concept, design, and supervision. HK, JJM, and JPS: Conduction of the experiments. SC, JSS, and FM: Bioinformatic analysis. SC, HK, and SR: Writing and editing the manuscript. AL, CS-N, and EF: Assistance with sample collection and clinical data. J-MD: Design and supervision of the drug assays. All authors: Data analysis and interpretation, reading, and approval of the final manuscript.

FUNDING

This work was supported by the National Institute of Science and Technology in Oncogenomics (São Paulo Research Foundation – FAPESP: #2008/57887-9 and the National Council for Scientific and Technological Development – CNPq: #573589/08-9), and the Research Council of Lillebaelt Hospital, Denmark.

ACKNOWLEDGMENTS

The authors would like to acknowledge Barretos Cancer Hospital and A.C.Camargo Cancer Center, SP, Brazil, for providing human specimens.

SUPPLEMENTARY MATERIAL

The Supplementary Material for this article can be found online at: https://www.frontiersin.org/articles/10.3389/fonc.2022.935093/full#supplementary-material

REFERENCES

1. Sung H, Ferlay J, Siegel RL, Laversanne M, Soerjomataram I, Jemal A, et al. Global Cancer Statistics 2020: GLOBOCAN Estimates of Incidence and Mortality Worldwide for 36 Cancers in 185 Countries. *CA A Cancer J Clin* (2021) 71:209–49. doi: 10.3322/caac.21660
2. Douglawi A, Masterson TA. Updates on the Epidemiology and Risk Factors for Penile Cancer. *Transl Androl Urol* (2017) 6:785–90. doi: 10.21037/tau.2017.05.19
3. Christodoulidou M, Sahdev V, Houssein S, Muneer A. Epidemiology of Penile Cancer. *Curr Problems Cancer* (2015) 39:126–36. doi: 10.1016/j.currproblcancer.2015.03.010
4. Thomas A, Necchi A, Muneer A, Tobias-Machado M, Tran ATH, Van Rompuy A-S, et al. Penile Cancer. *Nat Rev Dis Primers* (2021) 7:11. doi: 10.1038/s41572-021-00246-5
5. Peyraud F, Allenet C, Gross-Goupil M, Domblides C, Lefort F, Daste A, et al. Current Management and Future Perspectives of Penile Cancer: An Updated Review. *Cancer Treat Rev* (2020) 90:102087. doi: 10.1016/j.ctrv.2020.102087
6. Vieira CB, Feitoza L, Pinho J, Teixeira-Júnior A, Lages J, Calixto J, et al. Profile of Patients With Penile Cancer in the Region With the Highest Worldwide Incidence. *Sci Rep* (2020) 10:2965. doi: 10.1038/s41598-020-59831-5
7. Thomas A, do Canto Alvim LM, Rainho CA, Juengel E, Blaheta RA, Spiess PE, et al. Systemic Treatment of Penile Squamous Cell Carcinoma—Hurdles and Hopes of Preclinical Models and Clinical Regimens: A Narrative Review. *Transl Androl Urol* (2021) 10:4085–98. doi: 10.21037/tau-20-945
8. Aydin AM, Chahoud J, Adashek JJ, Azizi M, Magliocco A, Ross JS, et al. Understanding Genomics and the Immune Environment of Penile Cancer to Improve Therapy. *Nat Rev Urol* (2020) 17:555–70. doi: 10.1038/s41585-020-0359-z
9. Barrett RL, Puré E. Cancer-Associated Fibroblasts and Their Influence on Tumor Immunity and Immunotherapy. *eLife* (2020) 9:e57243. doi: 10.7554/eLife.57243
10. Kuasne H, Barros-Filho MC, Busso-Lopes A, Marchi FA, Pinheiro M, Muñoz JJM, et al. Integrative miRNA and mRNA Analysis in Penile Carcinomas Reveals Markers and Pathways With Potential Clinical Impact. *Oncotarget* (2017) 8:15294–306. doi: 10.18632/oncotarget.14783
11. Tang J, Yu JX, Hubbard-Lucey VM, Neftelinov ST, Hodge JP, Lin Y. The Clinical Trial Landscape for PD1/PDL1 Immune Checkpoint Inhibitors. *Nat Rev Drug Discovery* (2018) 17:854–5. doi: 10.1038/nrd.2018.210
12. Cocks M, Taheri D, Ball MW, Bezerra SM, Del Carmen Rodriguez M, Ricardo BFP, et al. Immune-Checkpoint Status in Penile Squamous Cell Carcinoma: A North American Cohort. *Hum Pathol* (2017) 59:55–61. doi: 10.1016/j.humpath.2016.09.003
13. Ahmed ME, Falasiri S, Hajiran A, Chahoud J, Spiess PE. The Immune Microenvironment in Penile Cancer and Rationale for Immunotherapy. *JCM* (2020) 9:3334. doi: 10.3390/jcm9103334
14. Economopoulou P, Kotsantis I, Psyrri A. Tumor Microenvironment and Immunotherapy Response in Head and Neck Cancer. *Cancers* (2020) 12:3377. doi: 10.3390/cancers12113377
15. Hanley CJ, Thomas GJ. T-Cell Tumour Exclusion and Immunotherapy Resistance: A Role for CAF Targeting. *Br J Cancer* (2020) 123:1353–5. doi: 10.1038/s41416-020-1020-6
16. Ottenhof SR, Djajadiningrat RS, Thygesen HH, Jakobs PJ, Jóźwiak K, Heeren AM, et al. The Prognostic Value of Immune Factors in the Tumor Microenvironment of Penile Squamous Cell Carcinoma. *Front Immunol* (2018) 9:1253. doi: 10.3389/fimmu.2018.01253
17. Huang T, Cheng X, Chahoud J, Sarhan A, Tamboli P, Rao P, et al. Effective Combinatorial Immunotherapy for Penile Squamous Cell Carcinoma. *Nat Commun* (2020) 11:2124. doi: 10.1038/s41467-020-15980-9
18. Avila Cobos F, Alquicira-Hernandez J, Powell JE, Mestdagh P, De Preter K. Benchmarking of Cell Type Deconvolution Pipelines for Transcriptomics Data. *Nat Commun* (2020) 11:5650. doi: 10.1038/s41467-020-19015-1
19. Ding M, Malhotra R, Ottosson T, Lundqvist M, Mebrahtu A, Brengdahl J, et al. Secretome Screening Reveals Immunomodulating Functions of Ifnα-7, PAP and GDF-7 on Regulatory T-Cells. *Sci Rep* (2021) 11:16767. doi: 10.1038/s41598-021-96184-z
20. da Cunha BR, Domingos C, Stefanini ACB, Henrique T, Polachini GM, Castelo-Branco P, et al. Cellular Interactions in the Tumor Microenvironment: The Role of Secretome. *J Cancer* (2019) 10:4574–87. doi: 10.7150/jca.21780
21. Armingol E, Officer A, Harismendy O, Lewis NE. Deciphering Cell–Cell Interactions and Communication From Gene Expression. *Nat Rev Genet* (2020) 22(2):71–88. doi: 10.1038/s41576-020-00292-x
22. Kuasne H, Cólus IM de S, Busso AF, Hernandez-Vargas H, Barros-Filho MC, Marchi FA, et al. Genome-Wide Methylation and Transcriptome Analysis in Penile Carcinoma: Uncovering New Molecular Markers. *Clin Epigenet* (2015) 7:46. doi: 10.1186/s13148-015-0082-4
23. Thul PJ, Åkesson L, Wiking M, Mahdessian D, Geladaki A, Ait Blal H, et al. A Subcellular Map of the Human Proteome. *Science* (2017) 356:eaal3321. doi: 10.1126/science.aal3321
24. von Mering C. STRING: Known and Predicted Protein-Protein Associations, Integrated and Transferred Across Organisms. *Nucleic Acids Res* (2004) 33:D433–7. doi: 10.1093/nar/gki005
25. Chen EY, Tan CM, Kou Y, Duan Q, Wang Z, Meirelles G, et al. Enrichr: Interactive and Collaborative HTML5 Gene List Enrichment Analysis Tool. *BMC Bioinf* (2013) 14:128. doi: 10.1186/1471-2105-14-128
26. Muñoz JJ, Drigo SA, Barros-Filho MC, Marchi FA, Scapulatempo-Neto C, Pessoa GS, et al. Down-Regulation of SLC8A1 as a Putative Apoptosis Evasion Mechanism by Modulation of Calcium Levels in Penile Carcinoma. *J Urol* (2015) 194:245–51. doi: 10.1016/j.juro.2014.11.097
27. Livak KJ, Schmittgen TD. Analysis of Relative Gene Expression Data Using Real-Time Quantitative PCR and the 2–ΔΔct Method. *Methods* (2001) 25:402–8. doi: 10.1006/meth.2001.1262
28. Chen B, Khodadoust MS, Liu CL, Newman AM, Alizadeh AA. Profiling Tumor Infiltrating Immune Cells With CIBERSORT. In: L von Stechow,

editor. *Cancer Systems Biology. Methods in Molecular Biology*. New York, NY: Springer New York (2018). p. 243–59. doi: 10.1007/978-1-4939-7493-1_12
29. Galon J, Bruni D. Approaches to Treat Immune Hot, Altered and Cold Tumours With Combination Immunotherapies. *Nat Rev Drug Discov* (2019) 18:197–218. doi: 10.1038/s41573-018-0007-y
30. Goksuluk D, Korkmaz S, Zararsiz G, Karaagaoglu AE. easyROC: An Interactive Web-Tool for ROC Curve Analysis Using R Language Environment. *R J* (2016) 8:213. doi: 10.32614/RJ-2016-042
31. Racle J, Gfeller D. EPIC: A Tool to Estimate the Proportions of Different Cell Types From Bulk Gene Expression Data. In: S Boegel, editor. *Bioinformatics for Cancer Immunotherapy. Methods in Molecular Biology*. New York, NY: Springer US (2020). p. 233–48. doi: 10.1007/978-1-0716-0327-7_17
32. Liu B, Chen X, Zhan Y, Wu B, Pan S. Identification of a Gene Signature for Renal Cell Carcinoma–Associated Fibroblasts Mediating Cancer Progression and Affecting Prognosis. *Front Cell Dev Biol* (2021) 8:604627. doi: 10.3389/fcell.2020.604627
33. Puram SV, Tirosh I, Parikh AS, Patel AP, Yizhak K, Gillespie S, et al. Single-Cell Transcriptomic Analysis of Primary and Metastatic Tumor Ecosystems in Head and Neck Cancer. *Cell* (2017) 171:1611–24.e24. doi: 10.1016/j.cell.2017.10.044
34. Pai SI, Westra WH. Molecular Pathology of Head and Neck Cancer: Implications for Diagnosis, Prognosis, and Treatment. *Annu Rev Pathol Mech Dis* (2009) 4:49–70. doi: 10.1146/annurev.pathol.4.110807.092158
35. Ragin CCR, Modugno F, Gollin SM. The Epidemiology and Risk Factors of Head and Neck Cancer: A Focus on Human Papillomavirus. *J Dent Res* (2007) 86:104–14. doi: 10.1177/154405910708600202
36. Custódio M, Biddle A, Tavassoli M. Portrait of a CAF: The Story of Cancer-Associated Fibroblasts in Head and Neck Cancer. *Oral Oncol* (2020) 110:104972. doi: 10.1016/j.oraloncology.2020.104972
37. Chen X, Song E. Turning Foes to Friends: Targeting Cancer-Associated Fibroblasts. *Nat Rev Drug Discov* (2019) 18:99–115. doi: 10.1038/s41573-018-0004-1
38. Nurmik M, Ullmann P, Rodriguez F, Haan S, Letellier E. In Search of Definitions: Cancer-Associated Fibroblasts and Their Markers. *Int J Cancer* (2020) 146:895–905. doi: 10.1002/ijc.32193
39. Baker AT, Abuwarwar MH, Poly L, Wilkins S, Fletcher AL. Cancer-Associated Fibroblasts and T Cells: From Mechanisms to Outcomes. *JI* (2021) 206:310–20. doi: 10.4049/jimmunol.2001203
40. Kuasne H, do Canto LM, Aagaard MM, Muñoz JJM, Jamblinne CD, Marchi FA, et al. Penile Cancer-Derived Cells Molecularly Characterized as Models to Guide Targeted Therapies. *Cells* (2021) 10:814. doi: 10.3390/cells10040814
41. Van Doren SR. Matrix Metalloproteinase Interactions With Collagen and Elastin. *Matrix Biol* (2015) 44–46:224–31. doi: 10.1016/j.matbio.2015.01.005
42. Kakarla S, Song X-T, Gottschalk S. Cancer-Associated Fibroblasts as Targets for Immunotherapy. *Immunotherapy* (2012) 4:1129–38. doi: 10.2217/imt.12.112
43. Marchi FA, Martins DC, Barros-Filho MC, Kuasne H, Busso Lopes AF, Brentani H, et al. Multidimensional Integrative Analysis Uncovers Driver Candidates and Biomarkers in Penile Carcinoma. *Sci Rep* (2017) 7:6707. doi: 10.1038/s41598-017-06659-1
44. Radulescu R, Totan A, Imre M, Miricescu D, Didilescu A, Greabu M. Mediators of Extracellular Matrix Degradation and Inflammation: A New Team of Possible Biomarkers for Oral Squamous Cell Carcinoma Stage. *Exp Ther Med* (2021) 22:877. doi: 10.3892/etm.2021.10309
45. Petitprez F, de Reyniès A, Keung EZ, Chen TW-W, Sun C-M, Calderaro J, et al. B Cells are Associated With Survival and Immunotherapy Response in Sarcoma. *Nature* (2020) 577:556–60. doi: 10.1038/s41586-019-1906-8
46. Kim SS, Shen S, Miyauchi S, Sanders PD, Franiak-Pietryga I, Mell L, et al. B Cells Improve Overall Survival in HPV-Associated Squamous Cell Carcinomas and Are Activated by Radiation and PD-1 Blockade. *Clin Cancer Res* (2020) 26:3345–59. doi: 10.1158/1078-0432.CCR-19-3211
47. Truxova I, Kasikova L, Hensler M, Skapa P, Laco J, Pecen L, et al. Mature Dendritic Cells Correlate With Favorable Immune Infiltrate and Improved Prognosis in Ovarian Carcinoma Patients. *J Immunother Cancer* (2018) 6:139. doi: 10.1186/s40425-018-0446-3
48. Gardner A, de Mingo Pulido Á, Ruffell B. Dendritic Cells and Their Role in Immunotherapy. *Front Immunol* (2020) 11:924. doi: 10.3389/fimmu.2020.00924
49. Ko Y-C, Lai T-Y, Hsu S-C, Wang F-H, Su S-Y, Chen Y-L, et al. Index of Cancer-Associated Fibroblasts Is Superior to the Epithelial–Mesenchymal Transition Score in Prognosis Prediction. *Cancers* (2020) 12:1718. doi: 10.3390/cancers12071718
50. Herrera M, Berral-González A, López-Cade I, Galindo-Pumariño C, Bueno-Fortes S, Martín-Merino M, et al. Cancer-Associated Fibroblast-Derived Gene Signatures Determine Prognosis in Colon Cancer Patients. *Mol Cancer* (2021) 20:73. doi: 10.1186/s12943-021-01367-x
51. Liao Z, Tan ZW, Zhu P, Tan NS. Cancer-Associated Fibroblasts in Tumor Microenvironment – Accomplices in Tumor Malignancy. *Cell Immunol* (2019) 343:103729. doi: 10.1016/j.cellimm.2017.12.003
52. Wu Y-H, Chang T-H, Huang Y-F, Huang H-D, Chou C-Y. COL11A1 Promotes Tumor Progression and Predicts Poor Clinical Outcome in Ovarian Cancer. *Oncogene* (2014) 33:3432–40. doi: 10.1038/onc.2013.307
53. Chong I-W, Chang M-Y, Chang H-C, Yu Y-P, Sheu C-C, Tsai J-R, et al. Great Potential of a Panel of Multiple Hmth1, SPD, ITGA11 and COL11A1 Markers for Diagnosis of Patients With non-Small Cell Lung Cancer. *Oncol Rep* (2006). doi: 10.3892/or.16.5.981
54. Xu S, Xu H, Wang W, Li S, Li H, Li T, et al. The Role of Collagen in Cancer: From Bench to Bedside. *J Transl Med* (2019) 17:309. doi: 10.1186/s12967-019-2058-1
55. Chen P, Parks WC. Role of Matrix Metalloproteinases in Epithelial Migration. *J Cell Biochem* (2009) 108:1233–43. doi: 10.1002/jcb.22363
56. Winer A, Adams S, Mignatti P. Matrix Metalloproteinase Inhibitors in Cancer Therapy: Turning Past Failures Into Future Successes. *Mol Cancer Ther* (2018) 17:1147–55. doi: 10.1158/1535-7163.MCT-17-0646
57. Zhou Q, Deng C, Li Z, Chen J, Yao K, Huang K, et al. Molecular Characterization and Integrative Genomic Analysis of a Panel of Newly Established Penile Cancer Cell Lines. *Cell Death Dis* (2018) 9:684. doi: 10.1038/s41419-018-0736-1
58. Azizi M, Spiess PE. Targeted Therapy in Penile Cancer: A New Treatment Paradigm. *Nat Rev Urol* (2018) 15:5–6. doi: 10.1038/nrurol.2017.183
59. McDaniel AS, Hovelson DH, Cani AK, Liu C-J, Zhai Y, Zhang Y, et al. Genomic Profiling of Penile Squamous Cell Carcinoma Reveals New Opportunities for Targeted Therapy. *Cancer Res* (2015) 75:5219–27. doi: 10.1158/0008-5472.CAN-15-1004
60. Chiu K-J, Chiou H-YC, Huang C-H, Lu P-C, Kuo H-R, Wang J-W, et al. Natural Compounds Targeting Cancer-Associated Fibroblasts Against Digestive System Tumor Progression: Therapeutic Insights. *Biomedicines* (2022) 10:713. doi: 10.3390/biomedicines10030713
61. Liu T, Zhou L, Li D, Andl T, Zhang Y. Cancer-Associated Fibroblasts Build and Secure the Tumor Microenvironment. *Front Cell Dev Biol* (2019) 7:60. doi: 10.3389/fcell.2019.00060
62. Blackburn JS, Liu I, Coon CI, Brinckerhoff CE. A Matrix Metalloproteinase-1/Protease Activated Receptor-1 Signaling Axis Promotes Melanoma Invasion and Metastasis. *Oncogene* (2009) 28:4237–48. doi: 10.1038/onc.2009.272
63. Huang J, Zhang L, Wan D, Zhou L, Zheng S, Lin S, et al. Extracellular Matrix and its Therapeutic Potential for Cancer Treatment. *Sig Transduct Target Ther* (2021) 6:153. doi: 10.1038/s41392-021-00544-0
64. Elst L, Van Rompuy A-S, Roussel E, Spans L, Vanden Bempt I, Necchi A, et al. Establishment and Characterization of Advanced Penile Cancer Patient-Derived Tumor Xenografts: Paving the Way for Personalized Treatments. *Eur Urol Focus* (2022), S2405456922001080. doi: 10.1016/j.euf.2022.04.012

Conflict of Interest: The authors declare that the research was conducted in the absence of any commercial or financial relationships that could be construed as a potential conflict of interest.

frontiers | Frontiers in Oncology

TYPE Original Research
PUBLISHED 16 September 2022
DOI 10.3389/fonc.2022.893877

OPEN ACCESS

EDITED BY
Hailiang Zhang,
Fudan University, China

REVIEWED BY
Flavio Cárcano,
Barretos Cancer Hospital, Brazil
Daniel Adrian Landero Huerta,
National Institute of Pediatrics, Mexico

*CORRESPONDENCE
Peng Du
dupeng9000@126.com

†These authors share first authorship

SPECIALTY SECTION
This article was submitted to Genitourinary Oncology, a section of the journal Frontiers in Oncology

RECEIVED 11 March 2022
ACCEPTED 01 September 2022
PUBLISHED 16 September 2022

CITATION
Wang S, Yang X, Yu Z, Du P, Cao Y, Ji Y, Ma J and Yang Y (2022) The values of systemic immune-inflammation index and neutrophil-lymphocyte ratio in predicting testicular germ cell tumors: A retrospective clinical study. *Front. Oncol.* 12:893877. doi: 10.3389/fonc.2022.893877

The values of systemic immune-inflammation index and neutrophil-lymphocyte ratio in predicting testicular germ cell tumors: A retrospective clinical study

Shuo Wang†, Xiao Yang†, Ziyi Yu†, Peng Du*, Yudong Cao, Yongpeng Ji, Jinchao Ma and Yong Yang

Key Laboratory of Carcinogenesis and Translational Research (Ministry of Education), Urological Department, Peking University Cancer Hospital and Institute, Beijing, China

Purpose: To determine whether complete blood count (CBC) based inflammatory parameters can be used as markers predicting testicular germ cell tumors (TGCT).

Material and methods: Between 2013 to 2018 the data of 58 patients with testicular TGCT undergoing radical orchiectomy and 54 malignancy-free healthy men were retrospectively analyzed as tumor group and control group. Patient baseline characteristics including age, pathological stage and pre-surgery CBC based inflammatory parameters including neutrophil/lymphocyte ratio (NLR), platelet/lymphocyte ratio (PLR), lymphocyte/monocyte ratio (LMR), systemic immune-inflammation index (SII), lymphocyte ratio (LR), neutrophil ratio (NR), mean platelet volume (MPV) and red cell distribution width (RDW) were analyzed and compared between tumor group and control group. Receiver operating characteristic (ROC) curve were used analyzing data with significantly difference to assess the discriminative ability of the markers for TGCT, area under the curve (AUC), cut-off value, sensitivity and specificity were calculated. The binary logistic regression model was used to evaluate the association between significant inflammatory markers and risk of TGCT.

Results: Mean age of the tumor and control group was 41.1 ± 15.36 and 44.89 ± 9.2 years, respectively. Mean NLR, SII and RDW were significantly higher in tumor group compared with control group with P=0.005, P=0.001 and P=0.016, respectively; there were no significantly differences of age, PLR, LMR, LR, NR, MPV and RDW between groups. The ROC curve for NLR, SII and RDW was plotted in the diagnosis of TGCT and tumor progression, the cut-off value for NLR, SII and RDW were found as 3.38 (AUC: 0.704, sensitivity=51.4%, specificity=88.6%, P=0.003), 881.24 (AUC: 0.725, sensitivity=45.7%, specificity=91.4%, P=0.001) and 0.14 (AUC: 0.63, sensitivity=28.6%, specificity=97%, P=0.063), respectively.

Patients were divided into two groups according to the threshold values, respectively. By using the multivariable logistic regression models, NLR ≥ 3.38 (OR, 5.86; 95% CI, 1.67-20.65, P=0.006) and SII ≥ 881.24 (OR, 4.89; 95% CI, 1.48-15.32, P=0.009) were independent risk factors predicting TGCT. Significantly statistical difference of pathological stage was also found between groups with respect to NLR cut-off values (P=0.034) and SII cut-off values (P=0.049). Combined the data together, NLR and SII both exhibited good differential diagnosis potential which could be used as markers predicting the TGCT.

Conclusion: As the CBC based inflammation parameters, both NLR and SII could be used as effective tumor markers predicting the TGCT, and higher NLR and SII are associated with higher pathological stage. In addition, SII is a more powerful tool among these two inflammatory markers.

KEYWORDS

germ cell tumors, neutrophil/lymphocyte ratio, systemic immune-inflammation index, red cell distribution, inflammation

Introduction

Testicular tumor is quiet a rare disease, 90-95% of testicular tumors are testicular germ cell tumors (TGCT) (1). The main methods for diagnosis of testicular tumors are physical examination, radiography, ultrasound and biochemical tumors markers including alpha-fetoprotein (AFP), human chorionic gonadotropin (HCG) and lactate dehydrogenase (LDH) (2). However, these markers are not very specific, AFP and HCG are increased in only 40-60% patients with TGCT, while HCG elevation can be detected in only 30% of seminoma (3), therefore, false positive and negative result are often observed by those examinations, so other simple, inexpensive, easily applicable and more accurate markers are needed in the clinical approach.

Inflammatory markers are with low cost and can be easily available from the routine hemorrhagic data, and the relationship between inflammation and various tumor is confirmed by several studies, it may play an essential role in regulating the progression of the cancer by stimulating or suppressing tumor cells (4, 5). When regrading to urological tumors, several studies demonstrated that inflammatory factors may be associated with progression and prognostic of renal cancer, bladder cancer and prostate cancer (6). Especially for neutrophil to lymphocyte (NLR), as one of the most important inflammatory markers, it has been reported to be closely related with recurrence and prognosis of kidney and bladder cancer (6, 7). However, few studies have detected the association of inflammation with testicular tumor, and among the published papers the conclusions are still controversial, further studies are needed to detect whether there is an association between inflammation and testicular tumors, and whether inflammatory parameters can be used as predicting markers for testicular TGCT. The aim of this study is to clarify whether complete blood count (CBC) based inflammatory markers including lymphocyte ratio (LR), platelet/lymphocyte ratio (PLR), lymphocyte/monocyte ratio (LMR), systemic immune-inflammation index (SII), lymphocyte ratio (LR), neutrophil ratio (NR), mean platelet volume (MPV) and red cell distribution width (RDW) could be used as serum markers for predicting TGCT, if so, great clinical values will be provided in predicting testis TGCT for patients with testis masses before surgery.

Materials and methods

Methods

The data of 58 patients who underwent inguinal orchiectomy as tumor group and 54 malignancy-free healthy men who underwent physical examination as control group in Beijing Cancer Hospital between 2013 and 2018 were analyzed retrospectively. The studies involving human participants were reviewed and approved by Institutional Review Board of Peking University Cancer Hospital & Institution in April 2020 (protocol code 2018KT27). Pathological confirmed testicular TGCT of stage I-III and malignancy-free healthy men were included in this study and defined as tumor and control group. Patients with acute infections, chronic inflammation disease, malignancies beside testicular GTCs, hematological disorders and blood product administration recently were excluded.

Blood samples of the patients were taken within the pre-surgery 24h. Hematological parameters including LR, NR, MPV and RDW

were evaluated with peripheral blood samples, and NLR, PLR, LMR and SII were calculated by using the numbers of blood cell counts based systemic markers of inflammation. SII (SII= platelet × neutrophil/lymphocyte) has been presented as a combination of NLR and PLR and shown to suggest oncological results for many tumors (8, 9). The age of all patients and clinicopathological data including tumor stage I-III and histopathology according to current testicular tumor guidelines (2019 TNM classification) (10) were recorded. Stage I tumors localized to the testis, stage II tumors were with positive localized lymph nodes, stage III tumors were with distant metastasis, and differences between inflammatory markers were assessed and calculated.

Statistical analysis

Measurement data conforming to normal distribution analyzed by Shapiro-Wilk test are represented as Mean ± SD, independent sample t test and Box-plot graphics are used for comparison between groups. Data on categorical variables are presented as frequency with percentages and differences among groups are analyzed with Pearson's chi-square test or Fisher exact test as appropriate. Receiver operating characteristic (ROC) curve analyses were performed to assess the discriminative ability of the inflammatory markers for TGCT. The cut-off points for markers were defined by a criterion based on Youden's index defined as YI (c)=max c [Se(c)+Sp(c)-1] and corresponding specificity-sensitivity levels were provided. The binary logistic regression model (univariable and multivariable analysis) was used to evaluate the association between significant factors and risk of TGCT, which were all compared with reference group (Ref). The software used to run the analysis was IBM-SPSS version 20. All tests were two-sided, P<0.05 was considered to be the threshold for statistically meaningful differences.

Results

Clinicopathological characteristics of patients

A total of 112 patients were included in this study after determine the inclusion and exclusion criteria with ages ranging from 20 to 73 years. The mean age was 39.9 ± 13.23 years. The cases were divided into two groups: tumor (n=58) and control (n=54). Mean age of tumor and control group was 41.1 ± 15.36 and 44.89 ± 9.2 years, respectively. Demographic, clinicopathologic and pathological stage features of patients with TGCT were summarized in Table 1. For metastatic cases, the international germ cell tumor cancer collaborative group (IGCCCG) has identified three prognostic groups: good, intermediate and poor risk (11). Among 9 patients with stage II, according to IGCCCG, 7 (77.8%) were with good prognostic (6 seminoma, 1 non-seminoma), 2 (22.2%) were with intermediate prognostic (2 non-seminoma); among 21 patients with stage III, 12 (57.1%) were with good prognostic (5 seminoma, 7 non-seminoma), 5 (23.8%) were with intermediate prognostic (2 seminoma, 3 non-seminoma), 4 (19.0%)were with poor prognostic (4 non-seminoma).

Analysis of clinical and CBC based parameters for predicting TGCT

In tumor group, the median NLR, SII and RDW levels were significantly higher than those in control group (P=0.005; P=0.001; P=0.016) as shown in Figure 1 and Table 2. There were no significantly statistical differences between groups in terms of ages, PLR, LMR, LR, NR and MPV as shown in Table 2.

The ROC curve for NLR, SII, and RDW was plotted in the diagnosis of testicular tumor as shown in Table 3 and Figure 2. AUC for NLR in tumor group was 0.704 which was significantly higher than 0.5 (P=0.003), with a threshold value of 3.38 and sensitivity 51.4% and specificity 88.6%; AUC for SII in tumor groups was 0.725 which was significantly higher than 0.5 (P=0.001), with a threshold value of 881.24 and sensitivity 45.7% and specificity 91.4%; AUC for RDW in tumor groups was 0.63 which was higher than 0.5 (P=0.063), with a threshold value of 0.14 and sensitivity 28.6% and specificity 97%, together NLR and SII exhibited good differential diagnosis potential which could be used as adjuvant tool in the prediction of testicular germ cell tumors.

Then patients were divided into 2 groups according to the threshold value of NLR and SII, univariable and multivariable logistic regression models were used to evaluate the association between factors and risk of TGCT. In univariable analysis, NLR ≥ 3.38 (OR, 4.5; 95% CI, 1.52-13.30, P=0.007) and SII ≥ 881.24 (OR, 5.33; 95% CI, 1.55-18.30, P=0.008) were risk factors predicting

TABLE 1 Demographic and clinicopathologic features of patients with testis tumor.

	Number	Seminoma	Non-seminoma		
			Immature Teratoma	Choriocarcinoma	Mix germ cell
Stage, n (%)	58	35	9	3	11
I	28 (48.3)	22 (62.9)	3 (33.3)	0 (0)	3 (27.3)
II	9 (15.5)	6 (17.1)	0 (0)	1 (33.3)	2 (18.2)
III	21 (36.2)	7 (20)	6 (66.7)	2 (66.7)	6 (54.5)

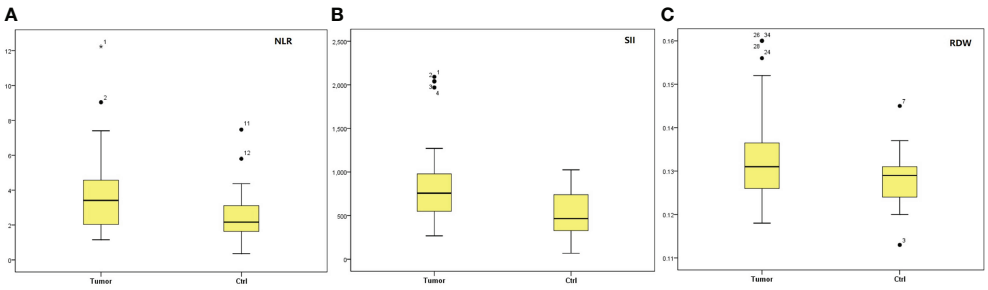

FIGURE 1
Box-blot graphics of markers of NLR, SII and RDW for testis tumors and ctrl group. **(A)** NLR, **(B)** SII, **(C)** RDW. NLR, neutrophil/lymphocyte ratio; SII, systemic immune-inflammation index; RDW, red cell distribution.

TABLE 2 Descriptive statics and comparison of CBC based parameters with respect to groups.

Variables	Tumor group (n = 58)	Control group (n = 54)	P-value
Age (years)	41.1 ± 15.36	44.89 ± 9.2	0.209
NLR (%)	3.79 ± 2.36	2.45 ± 1.4	0.005
PLR (%)	173.87 ± 62.9	157.68 ± 54.26	0.339
LMR (%)	4.11 ± 2.17	5.1 ± 2.11	0.616
SII (%)	870.39 ± 496.35	526.55 ± 263.64	0.001
LR (%)	24.35 ± 8.06	25.7 ± 9.8	0.533
NR (%)	68.04 ± 9.4	64.8 ± 10.7	0.184
MPV (10^3/μL)	9.86 ± 1.24	9.16 ± 1.82	0.062
RDW (%)	13.41 ± 1.2	12.83 ± 0.6	0.016

NLR, neutrophil/lymphocyte ratio; PLR, platelet/lymphocyte ratio; LMR, lymphocyte/monocyte ratio; SII, systemic immune-inflammation index; LR, lymphocyte ratio; NR, neutrophil ratio; MPV, mean platelet volume; RDW, red cell distribution; CBC, complete blood count.

TGCT as shown in Table 4; In multivariable analysis, NLR ≥ 3.38 (OR, 5.86; 95% CI, 1.67-20.65, P=0.006) and SII ≥ 881.24 (OR, 4.89; 95% CI, 1.48-15.32, P=0.009) were independent risk factors predicting TGCT as shown in Table 4.

We also compared the CBC based parameters between seminomatous testicular germ cell tumors (sTGCT) and non-seminomatous testicular germ cell tumors (nsTGCT), but there seemed no significantly statistical differences of NLR, PLR, LMR, SII, LR, NR, MPV and RDW between these two groups, P=0.128, 0.258, 0.413, 0.085, 0.234, 0.194, 0.192 and 0.116, respectively, as shown in Table 5.

Among TGCT patients, post-operative CBCs bases parameters including SII and NLR (1 month after inguinal orchiectomy) were also collected, when compared with pre-operative SII and NLR, the level of post-operative SII significantly reduced compared with pre-operative SII (870.39 ± 496.35 vs 721.21 ± 328.17, P=0.032), but there was no difference of NLR between groups (3.79 ± 2.36 vs 3.23 ± 1.89, P=0.089).

Distribution of pathological stage with regard to cut-off value of SII, NLR

Comparison of age and pathological stage between the patients with respect to NLR (< 3.38 and ≥3.38) or SII cut-off

TABLE 3 Cut-off, AUC, sensitivity and specificity values of NLR, SII and RDW.

Variables	AUC	Cut-off	Sensitivity	Specificity	95% CI	P-value
Preop NLR	0.704	≥ 3.38	51.4%	88.6%	0.581-0.826	0.003
Preop SII	0.725	≥ 881.24	45.7%	91.4%	0.608-0.842	0.001
Preop RDW	0.63	≥ 0.14	28.6%	97%	0.499-0.762	0.063

AUC, Area under the curve; NLR, neutrophil/lymphocyte ratio; SII, systemic immune-inflammation index; RDW, red cell distribution.

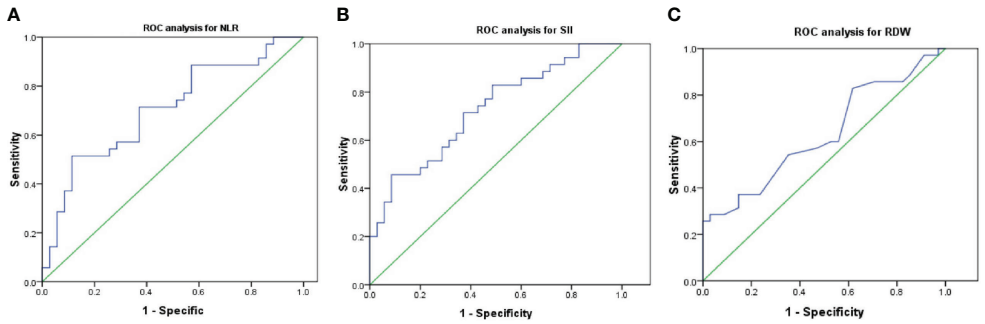

FIGURE 2
Optimal cut-off values and ROC analyses for NLR **(A)**, SII **(B)** and RDW **(C)**. NLR, neutrophil/lymphocyte ratio; SII, systemic immune-inflammation index; RDW, red cell distribution; ROC, receiver operating characteristic.

TABLE 4 Univariable and multivariable analyses for predicting testicular germ cell tumors.

	Univariable analysis Tumor vs. Control			Multivariable analysis Tumor vs. Control		
	OR	95% CI	P value	OR	95% CI	P-value
NLR						
<3.38	1 (Ref)	1 (Ref)		1 (Ref)	1 (Ref)	
≥3.38	4.5	1.52-13.30	0.007	5.86	1.67-20.65	0.006
SII						
<881.24	1 (Ref)	1 (Ref)		1 (Ref)	1 (Ref)	
≥881.24	5.33	1.55-18.30	0.008	4.89	1.48-15.32	0.009

Ref, reference; NLR, neutrophil-lymphocyte ratio; SII, systemic immune-inflammation index.

values (<881.24 and ≥881.24) are shown in Table 6. Significantly Statistical difference of pathological stage was found between groups with respect to NLR cut-off values (P=0.034) and SII cut-off values (P=0.049), when NLR ≥3.38 or SII ≥881.24 more patients are with stage II and stage III. There was no significantly difference of age between groups.

Comparison of SII, NLR in this study with traditional biomarkers and microRNA reported by other studies in TGCT.

We compared the data of SII, NLR of our study with traditional biomarkers (AFP, HCG and LDH) and 3 most

TABLE 5 Comparison of CBC based parameters between sTGCT and nsTGCT.

Variables	sTGCT (n = 35)	nsTGCT (n = 23)	P-value
NLR (%)	2.69 ± 1.36	2.95 ± 2.03	0.128
PLR (%)	165.97 ± 42.8	169.97 ± 53.16	0.258
LMR (%)	4.58 ± 1.88	4.99 ± 2.02	0.413
SII (%)	718.40 ± 289.25	629.65 ± 159.63	0.085
LR (%)	29.25 ± 7.85	24.37 ± 6.82	0.234
NR (%)	67.94 ± 8.13	65.18 ± 12.37	0.194
MPV (10^3/μL)	9.34 ± 2.14	9.56 ± 1.92	0.192
RDW (%)	14.41 ± 1.31	11.92 ± 1.26	0.116

NLR, neutrophil/lymphocyte ratio; PLR, platelet/lymphocyte ratio; LMR, lymphocyte/monocyte ratio; SII, systemic immune-inflammation index; LR, lymphocyte ratio; NR, neutrophil ratio; MPV, mean platelet volume; RDW, red cell distribution; CBC, complete blood count; sTGCT, seminomatous testicular germ cell tumors; nsTGCT, non-seminomatous testicular germ cell tumors.

important kinds of miR related with TGCT (miR-371-3p, miR-372-3p and miR-373-3p) reported by other studies. SII and NLR were with comparable or better values of sensitivity compared with AFP, HCG and LDH, and are with comparable values of specific compared with miR cluster, but the sensitivity of SII, NLR is much lower than that of miR cluster. Markers including SII, AFP, HCG, LDH and miR cluster were all decreased after orchiectomy. The levels of these 3 kinds of markers could be used for predicting the stages of the tumors (Table 7). Due to the methodological limitations of our study, some data were not available according to the recent methods, further studies were needed.

Discussion

The relationship between inflammation and cancer has long been known, a range patterns of cellular immune response to different histological tumors types are reported. In 1863, Virchow hypothesized that chronic inflammation could irritate cell proliferation along with the inflammation leading to cancer occurs (19). The immunocompetent cells that infiltrate tumors are mostly T-lymphocytes and microphages, with a few B-lymphocytes and NK-cells (20). Neutrophils mediate inflammation through various biochemical mechanisms such as platelet aggravating factors and release of arachidonic acid metabolites, and lymphopenia is associated with cortisol induced stress response (21). Other systemic inflammatory markers including C-reactive protein, leukocyte and cytokines were reported to be independent prognostic factors for patients with malignant (22). In recently, in addition to those inflammatory markers some papers reported that several CBC based parameters including NLR, PLR and SII are associated with the formation and progression of several kinds of malignant tumor (22, 23). Inflammation caused neutrophil response increasing and lymphocyte suppression led to the high NLR supported the development of malignant tumor by inhibiting the antitumor immune response (24). In preclinical experiment, data shown that increased neutrophils could stimulate tumor growth through different mechanisms (25). PLR has also been proved to be effective markers of system inflammation, and PLR combined with NLR are thought to be reliable independent prognostic factors in patients with malignancy (26). SII is a new developed joined tool combined with neutrophils, lymphocytes and platelet, recently it is used to assess the information of progression and prognostic in patients with malignant tumor (8, 27). Compared with NLR and PLR, SII is thought to be a more powerful tool combining three independent prognostic factors in cancer (28). And high SII has been demonstrated to be associated with tumor progression and poor outcomes in various kinds of cancer (29).

Meanwhile, the presence and consequences of cancer-related systemic inflammatory response have been investigated in various urologic cancers. Studies assessed that inflammation might be associated with development of urinary system malignancies such as bladder cancer, renal cancer and prostate cancer (30). A meta-analysis evaluating the relationship between NLR and prognostic found that high NLR was associated with poor prognosis in urological tumors beyond testis tumor (31). Bell et al. investigated the nature of inflammatory cell infiltrated in 10 testicular seminomas, found all of the 10 tumors contained a slight to marked inflammatory cell infiltrate at the periphery of the tumor, indicated that 2 types of immune-inflammatory reactions may play crucial role in the testicular seminomas (32), as sensitive markers reflecting inflammatory-immune status of the body NLR and SII may be affected, but the number of studies on the association of inflammation with testicular tumors is really small, most evaluations were performed using NLR and PLR, and the results are controversial. A study comparing patients with early-stage testicular tumors with healthy men confirmed that NLR above 2.7 should be considered the diagnosis of tumor (33). Another study demonstrated pre-operative CBC based parameters including NRL, RDW, MPV, LR and NR are all associated with progression and prognostic in patients with testicular tumors (34). Some other literatures demonstrated that TGCT were associated with prominent lymphocytic infiltrate (35, 36). In contrast, in some other studies, the conclusion was different. In a study assessing the association between inflammation factors and progression and prognostic in patients with TGCT, no correlation was found between NLR and stage, cancer specific survival (CSS) time and progression free survival (PFS) time (37). As a powerful tool in predicting various cancers, few studies reported the relationship between SII and testicular

TABLE 6 Distribution of descriptive properties and comparison of Clinical parameters between the patients with respect to NLR <3.38 and ≥3.38, SII<881.24 and ≥881.24.

Variables	NLR<3.38 (n = 31)	NLR≥3.38 (n = 27)	P value	SII<881.24 (n = 34)	SII≥881.24 (n = 24)	P-value
Ages (years)	33.6 ± 9.8	45.1 ± 14.8	0.011	37.16 ± 14.17	42.25 ± 13.11	0.281
Stage, n (%)			0.034			0.049
IA, B, S	19 (61.3)	9 (33.3)		20 (58.8)	8 (33.3)	
II+III	12 (38.7)	18 (66.7)		14 (41.2)	16 (66.7)	

NLR, neutrophil/lymphocyte ratio; SII, systemic immune-inflammation index.

TABLE 7 Comparison of NLR, SII in present study with traditional biomarkers and miR markers reported by other studies.

Variables	NLR	SII	AFP, HCG, LDH	miR-371-3p	miR-372-3p	miR-373-3p
Predicting role in TGCT	Yes	Yes	Yes	Yes (12–16)	Yes (12–14, 16, 17)	Yes (12–14, 17)
Sensitivity (%)	51.4%	45.7%	AFP:13.6-47.1% (14–16) bHCG:9.3-64.7% (14–16) LDH:52.9% (16) AFP+bHCG+LDH: 50.4% (18);	70.8-88.7% (14, 15, 18)	82-87.5% (16, 17)	59% (17, 18)
Specificity (%)	88.6%	91.4%	NA	93.4-99% (15, 18)	65-94% (16, 17)	91% (17)
Markers' level decreased after orchiectomy	No	Yes	Yes (14, 15) [1]	Yes (14, 15)	Yes (14, 15)	Yes (14, 15)
Consistent in fluids and tissues	NA	NA	NA	Yes [2,3]	Yes [2,3]	Yes [2,3]
Stages distinguish	Yes	Yes	Yes [1]	Yes (15, 18)	NA	Yes (17)
Histological distinguish between sTGCT and nsTGCT	No	No	Yes [1]	Yes (15)	NA	NA
Specific expressed in TGCT	No [4]	No [5,6]	No [1]	Yes (12–16)	Yes (12–14, 16, 17)	Yes (12–14, 17)

NA, not applicable; TGCT, testicular germ cell tumors; sTGCT, seminomatous testicular germ cell tumors; nsTGCT, non-seminomatous testicular germ cell tumors.

[1]Paolo Pedrazzoli, Giovanni Rosti, Elenora Soresini, et al. Serum tumour markers in germ cell tumours: from diagnosis to cure. Crit Rev Oncol Hematol. 2021, 159:103224.

[2]Almstrup K, Lobo J, Morup N, et al. Application of miRNAs in the diagnosis and monitoring of testicular germ cell tumours. Nat Rev Urol. 2020;17:201-203.

[3]Lobo J, van Zogchek MJ, Nuru MG, et al. Combining hypermethylated RASSF1A detection using ddPCR with miR-371a-3p testing: an improvement panel of liquid biomarkers for testicular germ cell tumor patients. Cancer (Basel). 2021, 13:5228.

[4]Wang S, Ji Y, Chen Y, et al. The values of systemic immune-inflammation index and neutrophil-lymphocyte ratio in the localized prostate cancer and benign prostate hyperplasia: a retrospective clinical study. Front Oncol. 2022, 11:812319.

[5]Kao SC, Pavlakis N, Harvie R, et al. High blood neutrophil-to-lymphocyte ratio is an indicator of poor prognostic in malignant mesothelioma patients undergoing systemic therapy. Clin Cancer Res. 2010, 16:5805-5813.

[6]Viers BR, Boorjian SA, Frank I, et al. Pretreatment neutrophil-to-lymphocyte ratio is associated with advanced pathologic tumor stage and increased cancer-specific mortality among patients with urothelial carcinoma of the bladder undergoing radical cystectomy. Eur Urol. 2014, 66:1157-1164.

tumors. Only in recently years, a retrospective study demonstrated that high SII (≥1003) was associated with poor outcomes in patients with TGCT (23). Therefore, it is still controversial to define whether inflammation factors are associated with occurrence and progression of testicular tumors and which parameters can be considered as the most effective predictors for diagnosis of testicular tumors and disease progression, and further studies are needed detecting the role of SII in TGCT.

The most usually used methods for diagnosis of testicular germ cell tumors included testicular ultrasound, serum AFP and HCG, but false positive and negative result are often observed by these examinations, it is difficult for ultrasound to separate germ cell tumors from other testicular tumors, and the level of AFP and HCG are easily influenced by other diseases, eg: hepatitis, hepatoma tumors, ovarian tumors, stomach tumors (38, 39), so other simple, inexpensive and easily applicable markers are needed in the clinical approach. New miR based serum biomarkers including miRNA-367-3p, 371a-3p, 372-3p and 373-3p have shown great potential with high sensitivity and specificity for predicting TGCT, compared with miR cluster, the specific of SII and NLR are comparable, but the sensitivity is much lower (12–18, 40), inflammatory markers in this study seemed have no too much advantage compared with miR cluster, but the extraction of miR from the fluid needs specific equipment and professional researchers, not all the centers could perform that, for SII and NLR, they could be calculated based on CBC, easily available and much cheaper compared with extraction of miR cluster. Therefore, SII and NLR could be considered as valuable markers, and they were more likely becoming the common clinical method for predicting TGCT compared with miR cluster. In this study, we sought to detect the potential association between pre-operative CBC based blood count parameters including NLR, PLR, LMR, SII, LR, NR, MPV and RDW with TGCT. After analyzing the data, the major findings of our study are: 1) NLR, SII and RDW are significantly higher in patients with TGCT compared to tumor-free healthy patients; 2) NLR and SII all could be used as effective bio-markers for the prediction of TGCT, while SII seemed to be a more favorable choice due it got the largest AUC area of 0.725 compared with NLR of 0.704; 3) More than half of the cases in this study are with stage II or III, due to the small sample size, we did not compare the data of tumor group with control group according to the pathological stage, separately. However, after grouping the patients by cut-off value of SII or NLR, we found that NLR above 3.38 or SII above 881.24 are associated with higher pathological stage, the volume of the disease may affect the inflammatory parameters. The outcome of NLR including its role in predicting testicular tumor and cut-off value are mostly conformal with data reported by literatures (33, 41). While few studies have detected the correlation between SII and TGCT, in our study, for the first time in the literature, the role of SII in predicting TGCT was analyzed and the results indicated that SII had diagnostic value in detection TGCT, which was really help for patients with testis mass who refused performing surgery or biopsy, and the cut-of value of SII was similar with that reported by Michal et al. (23).However, according to our study, inflammatory markers seemed not able to distinguish the pathological types of the

TGCT, for there were no significant differences of CBC based parameters between sTGCT and nsTGCT.

Meanwhile, our study has some limitations. As a retrospective study, the sample size is relatively small due to the low incidence of testicular tumor, only 58 cases with GTCs are included. And our study lacks the following-up data while most of the patients included are seminoma making it very difficult to measure the factors associated with prognostic. And one single time point was used for measuring the biomarkers leading to the inaccurate of the data collected, it can be strengthened by collecting blood samples at different pre-operative sets. Extended sample size and following-up data were needed in further research.

Conclusions

In conclusion, this study demonstrated that NLR and SII were all effective markers for urologists predicting the occurrence of TGCT, as they showed superior performance in detecting TGCT; in addition, SII is a more powerful tool among these 2 inflammatory factors for predicting TGCT. Extended sample size and prospective studies are needed.

Data availability statement

The raw data supporting the conclusions of this article will be made available by the authors, without undue reservation.

Ethics statement

The studies involving human participants were reviewed and approved by Institutional Review Board of Peking University Cancer Hospital & Institution in April 2020 (protocol code 2018KT27). Written informed consent for participation was not required for this study in accordance with the national legislation and the institutional requirements.

Author contributions

DP and WS designed the study. SW, XY, and ZY made the same contribution in this study. SW, XY, ZY, YJ, YC, JM and YY performed the study and analyzed the data. PD, SW, XY and ZY wrote the manuscript draft and revised the manuscript. All authors contributed to the article and approved the submitted version.

Funding

Beijing Municipal Science & Technology Commission. No. Z181107001718142. Science Foundation of Peking University Cancer Hospital. No.2021-7; Wu Jie Ping Medical Foundation. No. 320.6750.2020-19-2.

Conflict of interest

The authors declare that the research was conducted in the absence of any commercial or financial relationships that could be construed as a potential conflict of interest.

Publisher's note

References

1. Haas EC, Altena R, Boezen HM, Zwart N, Smit AJ, Bakker SJL, et al. Early development of the metabolic syndrome after chemotherapy for testicular cancer. *Ann Oncol* (2013) 24:749–55. doi: 10.1093/annonc/mds527

2. Smith ZL, Werntz RP, Eggener SE. Testicular cancer: Epidemiology, diagnosis and management. *Med Clin North Am* (2018) 102:251–64. doi: 10.1016/j.mcna.2017.10.003

3. Albers P, Albrecht W, Algaba F, Bokemeyer C, Cohn-Cedermark G, Fizazi K, et al. Guidelines on testicular cancer. *Eur Urol* (2015) 68:1054–68. doi: 10.1016/j.eururo.2015.07.044

4. Hu K, Lou L, Ye J, Zhang S. Prognostic role of the neutrophil-lymphocyte ratio in renal cell carcinoma: A meta-analysis. *BMJ Open* (2015) 5(4):e00604. doi: 10.1136/bmjopen-2014-006404

5. Kao SC, Pavlakis N, Harvie R, Vardy JL, Boyer MJ, van Zandwijk N, et al. High blood neutrophil-to-lymphocyte ratio is an indicator of poor prognosis in malignant mesothelioma patients undergoing systemic therapy. *Clin Cancer Res* (2010) 16(23):5805–13. doi: 10.1158/1078-0432.CCR-10-2245

6. Viers BR, Boorjian SA, Frank I, Tarrell RF, Thapa P, Karnes RJ, et al. Pretreatment neutrophil to lymphocyte ratio is associated with advanced pathologic tumor stage and increased cancer specific mortality among patients with urothelial carcinoma of the bladder undergoing radical cystectomy. *Eur Urol* (2014) 66:115764. doi: 10.1016/j.eururo.2014.02.042

7. Grimes N, Hannan C, Tyson M, Thwaini A. The role of neutrophil lymphocyte ratio as a prognostic indicator in patients undergoing nephrectomy for renal cell carcinoma. *Can Urol Assoc J* (2018) 12:345–8. doi: 10.5489/cuaj.4872

8. Hu B, Yang XR, Xu Y, Sun YF, Sun C, Guo W, et al. Systemic immune-inflammation index predicts prognosis of patients after curative resection for hepatocellular carcinoma. *Clin Cancer Res* (2014) 20:6212–22. doi: 10.1158/1078-0432.CCR-14-0442

9. Chovanec M, Cierna Z, Miskovska V, Machalekova K, Kalavska K, Rejlekova K, et al. Systemic immune-inflammation index is prognostic in testicular germ cell tumors with PD-L1 expressing tumor infiltrating lymphocytes. *J Clin Oncol* (2017) 35:e16042. doi: 10.1200/JCO.2017.35.15_suppl.e16042

10. Tourne M, Radulescu C, Allroy Y. Testicular germ cell tumors: Histopathological and molecular features. *Bull Cancer* (2019) 106:328–41. doi: 10.1016/j.bulcan.2019.02.004

11. Schmoll HJ, Souchon SL, Albers P, Beyer J, Kollmannsberger C, Fossa SD, et al. European Consensus on diagnosis and treatment of germ cell cancer: a report

of the European germ cell cancer consensus group (EGCCCG). *Ann Oncol* (2004) 15(9):1377–99.doi: 10.1093/annonc/mdh301

12. Murray MJ, Nicholson JC, Coleman N. Biology of childhood germ cell tumours, focussing on the significance of microRNAs. *Andrology* (2015) 3:129–39. doi: 10.1111/andr.277

13. Rijlaarsdam MA, van Agthoven T, Gillis AJ, Patel S, Hayashibara K, Lee KY, et al. Identification of known and novel germ cell cancer-specific (embryonic) miRs in serum by high-throughput profiling. *Andrology* (2015) 3:85–91. doi: 10.1111/andr.298

14. Dieckmann KP, Spiekermann M, Balks T, Flor I, Löning T, Bullerdiek J, et al. MicroRNAs miR-371-3 in serum as diagnostic tools in the management of testicular germ cell tumors. *BRIT J CANCER* (2012) 107:1754–60. doi: 10.1038/bjc.2012.469

15. Syring I, Bartels J, Holdernrieder S, Kristiansen G, Müller SC, Ellinger J. Circulating serum miRNA (miR-367-3p, miR-371a-3p, miR-372-3p and miR-373-3p) as biomarkers in patients with testicular germ cell tumors. *J Urol* (2015) 193 (1):331–337. doi: 10.1016/j.juro.2014.07.010

16. Ye F, Feldman DR, Valentino A, So R, Bromberg M, Khan S, et al. Analytical validation and performance characteristics of molecular serum biomarkers, miR-317a-3p and miR-372-3p, for male germ cell tumors, in a clinical laboratory setting. *J Mol Diagn* (2022) 8:867–77. doi: 10.1016/j.jmoldx.2022.04.007

17. Piao J, Lafin JT, Scarpini CG, Nuño MM, Syring I, Dieckmann KP, et al. A multi-institutional polled analysis demonstrates that circulating miR-371a-3p alone is sufficient for testicular malignant germ cell tumor diagnosis. *Clin Genitourin Cancer* (2021) 6:469–79. doi: 10.1016/j.clgc.2021.08.006

18. Dieckmann KP, Radtke A, Spiekermann M, Balks T, Matthies C, Becker P, et al. Serum levels of microRNA miR-371a-3p: A sensitive and specific new biomarker for germ cell tumours. *Eur Urol* (2017) 71:213–20. doi: 10.1016/j.eururo.2016.07.029

19. Balkwill F, Mantovani A. Inflammation and cancer: Back to virchow? *Lancet* (2001) 357:539–45. doi: 10.1016/S0140-6736(00)04046-0

20. Torres A, Casanova JF, Nistal M, Regadera J. Quantification of immunocompetent cells in testicular germ cell tumors. *Histopathology* (1997) 30:23–30. doi: 10.1046/j.1365-2559.1997.d01-560.x

21. Tamhane UU, Aneja S, Montgomery D, Rogers EK, Eagle KA, Gurm HS. Association between admission neutrophil to lymphocyte ratio and outcomes in patients with acute coronary syndrome. *Am J Cardiol* (2008) 102:653–7. doi: 10.1016/j.amjcard.2008.05.006

22. Fankhauser CD, Sander S, Roth L, Gross O, Eberli D, Sulser T, et al. Systemic inflammatory markers have independent prognostic value in patients with metastatic testicular germ cell tumors undergoing first-line chemotherapy. *Br J Cancer* (2018) 118:825–30. doi: 10.1038/bjc.2017.467

23. Chovanec M, Cierna Z, Miskovska V, Machalekova K, Kalavska K, Rejlekova K, et al. Systemic immune-inflammation index in germ-cell tumors. *Bri J Cancer* (2018) 118:831–8. doi: 10.1038/bjc.2017.460

24. Schaider H, Oka M, Bogenrieder T, Nesbit M, Satyamoorthy K, Berking C, et al. Differential response of primary and metastatic melanomas to neutrophils attracted by IL-8. *Int J Cancer* (2003) 103:33543. doi: 10.1002/ijc.10775

25. Fridlender ZG, Sun J, Kim S, Kapoor V, Cheng G, Ling L, et al. Polarization of tumor associated neutrophil phenotype by TGF-beta: "N1" versus "N2" TAN. *Cancer Cell* (2009) 16:183–94. doi: 10.1016/j.ccr.2009.06.017

26. Moore MM, Chua W, Charles KA, Clarke SJ. Inflammation and cancer: causes and consequences. *Clin Pharmacol Ther* (2010) 87:5048. doi: 10.1038/clpt.2009.254

27. Lolli C, Caffo O, Scarpi E, Aieta M, Conteduca V, Maines F, et al. Systemic immune-inflammation index predicts the clinical outcome in patients with mCRPC treated with abiraterone. *Front Pharmacol* (2016) 7:376. doi: 10.3389/fphar.2016.00376

28. Hong X, Cui B, Wang M, Yang Z, Wang L, Xu Q. Systemic immune-inflammation index, based on platelet counts and neutrophil-lymphocyte ratio, is useful for predicting prognosis in small cell lung cancer. *Tohoku J Exp Med* (2015) 236:297–304. doi: 10.1620/tjem.236.297

29. Cool LJ, Spicer J, Mcdonald B, Gowing S, Chow S, Giannias B, et al. Neutrophil extracellular traps sequester circulating tumor cells and promote metastasis. *J Clin Invest* (2013) 123(8):3446–3458. doi: 10.1172/JCI67484

30. Keizman D, Ish-Shalom M, Huang P, Eisenberger MA, Pili R, Hammers H, et al. The association of pre-treatment neutrophil to lymphocyte ratio with response rate, progression free survival and overall survival of patients treated with sunitinib for metastatic renal cell carcinoma. *Eur J Cancer* (2012) 48:202–8. doi: 10.1016/j.ejca.2011.09.001

31. Wei Y, Jiang ZY, Qian WH. Prognostic role of NLR in urinary cancers: A meta-analysis. *PloS One* (2014) 9:e92079. doi: 10.1371/journal.pone.0092079

32. Debra AB, Thomas J, Atul B. Immunohistochemical characterization of seminoma and its inflammatory cell infiltrate. *Hum Pathol* (1987) 18:511–20. doi: 10.1016/S0046-8177(87)80037-0

33. Yuksel OH, Verit A, Sahin A, Urkmez A, Uruc F. White blood cell counts and neutrophil ratio in the diagnosis of testicular cancer: A simple secondar serum tumor marker. *Int Brazl J Urol* (2016) 42:53–9. doi: 10.1590/S1677-5538.IBJU.2014.0593

34. Arda E, Arikan G, Akdere H, Akgul M, Yuksel I. Predictive and prognostic impact of preoperative complete blood count based systemic inflammatory markers in testicular cancer. *Int Braz J Urol* (2020) 46:213–6. doi: 10.1590/s1677-5538.ibju.2018.0820

35. Parker C, Milosevic M, Panzarella T, Banerjee D, Jewett M, Catton C, et al. The prognostic significance of the tumor infiltrating lymphocyte count in stage I testicular seminoma managed by surveillance. *Eur J Cancer* (2002) 38:2014–9. doi: 10.1016/S0959-8049(02)00235-6

36. Yakirevich E, Lefel O, Sova Y, Stein A, Cohen O, Izhak OB, et al. Activated status of tumor-infiltration lymphocytes and apoptosis in testicular seminoma. *J Pathol* (2002) 196:67–75. doi: 10.1002/path.996

37. Bolat D, Aydogdu O, Polat S, Yarımoğlu S, Bozkurt İH, Yonguç T, et al. Predictive value of preoperative neutrophil-to-lymphocyte ratio on the prognosis of germ cell testicular tumors. *Turk J Urol* (2017) 43:55–61. doi: 10.5152/tud.2016.38924

38. Dambadarjaa D, Mukhtar Y, Tsogzolbaatar EO, Khuyag SO, Dayan A, Oyunbileg NE, et al. Hepatitis b, c and d virus infections and AFP tumor marker prevalence among the elderly population in mongolia: a national survey. *J Prev Med Public Health* (2022) 55:263–72. doi: 10.3961/jpmph.21.573

39. Chen J, Wang J, Cao D, Yang J, Shen K, Huang H, et al. Alpha-fetoprotein (AFP) producing epithelial ovarian carcinoma (EOC): A retrospective study of 27 cases. *Arch Gynecol Obstet* (2021) 304:1043–53. doi: 10.1007/s00404-021-06017-7

40. Mørup N, Rajpert-De Meyts E, Juul A, Daugaard G, Almstrup K. Evaluation of circulating miRNA biomarkers of testicular germ cell tumors during therapy and follow up a Copenhagen experience. *Cancers* (2020) 12:759. doi: 10.3390/cancers12030759

41. Şahin A, Toprak T, Kutluhan MA, Vural Y, Ürkmez A, Verit A. Increased neutrophil/lymphocyte ratio in testicular cacner. *Archiv Italiano Di Urol Androl* (2019) 91:97–101. doi: 10.4081/aiua.2019.2.97

frontiers | Frontiers in Oncology

TYPE Original Research
PUBLISHED 04 October 2022
DOI 10.3389/fonc.2022.970576

OPEN ACCESS

EDITED BY
Hailiang Zhang,
Fudan University, China

REVIEWED BY
Junlong Wu,
Fudan University, China
Yinglong Huang,
The Second Affiliated Hospital of Kunming Medical University, China
Wen-Hao Xu,
Fudan University, China

*CORRESPONDENCE
Xiaodong Liu
xiaodongliu1988@126.com
Peng Gu
gupeng@ydyy.cn

†These authors have contributed equally to this work

SPECIALTY SECTION
This article was submitted to Genitourinary Oncology, a section of the journal Frontiers in Oncology

RECEIVED 16 June 2022
ACCEPTED 14 September 2022
PUBLISHED 04 October 2022

CITATION
Tu H, Liu H, Zhang L, Tan Z, Wang H, Jiang Y, Xia Z, Guo L, Xia X, Gu P and Liu X (2022) A novel prognostic model based on three integrin subunit genes-related signature for bladder cancer. *Front. Oncol.* 12:970576. doi: 10.3389/fonc.2022.970576

A novel prognostic model based on three integrin subunit genes-related signature for bladder cancer

Hongtao Tu[1,2†], Haolin Liu[3†], Longfei Zhang[4†], Zhiyong Tan[5†], Hai Wang[1,2], Yongming Jiang[1,2,5], Zhongyou Xia[1,2], Liwei Guo[6], Xiaodong Xia[6], Peng Gu[1,2*] and Xiaodong Liu[1,2*]

[1]Department of Urology, The First Affiliated Hospital of Kunming Medical University, Kunming, China, [2]The First Affiliated Hospital of Kunming Medical University, Yunnan Province Clinical Research Center for Chronic Kidney Disease, Kunming, China, [3]Department of Urology, Institute of Urology, West China Hospital, Sichuan University, Chengdu, China, [4]Department of Vascular Surgery, The First Affiliated Hospital of Bengbu Medical College, Bengbu, China, [5]Department of Urology, The Second Affiliated Hospital of Kunming Medical University, Kunming, China, [6]Department of Urology, The Dazhu County People's Hospital, Dazhou, China

Background: Presently, a comprehensive analysis of integrin subunit genes (ITGs) in bladder cancer (BLCA) is absent. This study endeavored to thoroughly analyze the utility of ITGs in BLCA through computer algorithm-based bioinformatics.

Methods: BLCA-related materials were sourced from reputable databases, The Cancer Genome Atlas (TCGA) and Gene Expression Omnibus (GEO). R software-based bioinformatics analyses included limma-differential expression analysis, survival-Cox analysis, glmnet-Least absolute shrinkage and selection operator (LASSO), clusterProfiler-functional annotation, and gsva-estimate-immune landscape analysis. The expression difference of key genes was verified by quantitative real-time polymerase chain reaction (qRT-PCR).

Results: Among the 11 ITGs that were abnormally expressed in BLCA, ITGA7, ITGA5, and ITGB6 were categorized as the optimal variables for structuring the risk model. The high-risk subcategories were typified by brief survival, abysmal prognosis, prominent immune and stromal markers, and depressed tumor purity. The risk model was also an isolated indicator of the impact of clinical outcomes in BLCA patients. Moreover, the risk model, specifically the high-risk subcategory with inferior prognosis, became heavily interlinked with the immune-inflammatory response and smooth muscle contraction and relaxation.

Conclusion: This study determined three ITGs with prognostic values (ITGA7, ITGA5, and ITGB6), composed a novel (ITG-associated) prognostic gene

signature, and preliminarily probed the latent molecular mechanisms of the model.

KEYWORDS

integrin subunit genes (ITGs), bladder cancer (BLCA), prognostic model, immune landscape, qRT-PCR

Introduction

Bladder cancer (BLCA) originates from the mucosal epithelium of the bladder and is one of the most common malignancies of the genitourinary system. Globally, the prevalence of BLCA ranks ninth among malignant tumors, with about 500,000 new cases and 130,000 deaths from BLCA each year, and the tendency is gradually rising annually (1). Clinically, the prognosis of patients with BLCA is closely related to the degree of infiltration, depth of invasion and metastatic potential of the lesion. BLCA is classified into non-muscle invasive bladder cancer (NMIBC) and muscle invasive bladder cancer (MIBC) according to the degree of tumor infiltration (2). About 60% of bladder cancers are NMIBC at the initial diagnosis and have a better prognosis. Approximately 50%-70% of NMIBC still recur and may develop into MIBC or even distant metastases after treatment, and the 5-year overall survival rate for metastatic MIBC is only 6% (3). Despite tremendous advances in imaging, chemotherapy and surgery, there has been no significant change in clinical survival benefits. In recent years, our understanding of the molecular pathogenesis of BLCA has improved dramatically with the rapid advances in gene sequencing technology; however, the number of known biomarkers associated with BLCA prognosis remains limited (4). Therefore, exploring and studying biomarkers that can predict and monitor the development of BLCA is crucial for the diagnosis, precise treatment and improved prognosis of BLCA patients.

Integrins are a group of heterophilic cell adhesion molecules commonly associated with vertebrate cell surfaces, mediating cell-to-cell and cell-to-extracellular matrix mutual recognition and adhesion, and having a role in linking intra and extracellular structures (5, 6). The primary function of integrins is to provide position control of the actions of cytokine and growth factor receptors to coordinate development, regeneration and various repair processes, and also act as signaling receptors that can control intracellular pathways that regulate cell survival, proliferation and cell fate (7, 8). For example, integrins and receptor tyrosine kinases (RTKs) are jointly involved to ensure optimal activation of pro-native and pro-survival signals *via* the Ras-extracellular signal-regulated kinase (ERK) and phosphatidylinositol 3-kinase (PI3K)-AKT signaling pathways. Integrins and growth factor receptors co-activate critical downstream signaling components such as Shc, PI3K, Rac and MEK in a summated, co-dependent or synergistic manner, and optimal activation of many downstream targets such as AP-1 (cJun/c-Fos) and target of rapamycin (TOR) requires the simultaneous linkage of integrins and RTK (9). Integrin signaling drives a variety of stem cell functions including tumor inception, epithelial plasticity, metastatic reactivation and resistance to oncogenes and immune-targeted therapies (10). A few integrin subunit genes (ITGs) have also been reported to be associated with epigenetic alterations in BLCA, but the underlying mechanisms of ITGs remain unclear. Based on the above, integrin-related pathways could be potential targets for bladder cancer treatment and may be of targeted therapeutic value in the future. However, few studies have been reported on the clinical prognosis and biological course of ITG in BLCA. To date, there are no relevant reports in the literature on comprehensive analysis of ITGs in BLCA. Therefore, this study aimed to explore the expression of ITGs in BLCA based on publicly available high-throughput sequencing data, and to reveal their biological processes and signaling through bioinformatics approaches, and to elucidate the potential prognostic value of ITGs in BLCA.

In this study, we aimed to thoroughly investigate the role of ITGs in BLCA and develop a novel survival risk stratification model based on ITGs signature. First, BLCA transcriptome data were downloaded from TCGA to comprehensively analyze the expression profile of ITGs and their prognostic value in BLCA prognosis. Subsequently, ITGs signature was created in the TCGA cohort and then validated in the GEO cohort. Finally, we also analyzed the association of the ITGs signature with the immune microenvironment of BLCA. We hope that our findings will provide a more comprehensive understanding of the role of ITGs in BLCA.

Materials and methods

Data capture

The 19 normal and 414 tumor samples selected for inclusion in this study were from the TCGA-BLCA cohort, of which, 383

BLCA samples contained complete survival time records. Both the GSE32894 and GSE7476 sets were extracted from the GEO database. The GSE32894 dataset (https://www.ncbi.nlm.nih.gov/geo/query/acc.cgi?acc=GSE32894) (11), which was focused on the risk model validation, contained 224 available BLCA samples (which could be queried for complete survival information and matched expression profiles). The GSE7476 dataset (https://www.ncbi.nlm.nih.gov/geo/query/acc.cgi?acc=GSE7476) (12), which embraced 3 healthy bladder tissues (controls) and 7 BLCA tumor tissues, was mainly responsible for the authentication of the prognostic genes' expression patterns.

Variance expression analysis

Gene expression abnormality analysis was implemented in the R software using the limma package. The database for the analysis was the mRNA expression profiles of normal and BLCA samples from the TCGA database. Saliency thresholds: $|\log_2$ fold change (FC)$|$ > 0.5 and adjusted (adj.) P< 0.05.

Differentially expressed ITGs (DE-ITGs)

Thirty ITGs were retrieved from the reviewed published literature (13) (Table 1). ITGs belonging to differentially expressed genes (DEGs), designated as DE-ITGs, were recognized in Jvenn online tool (14) using intersection analysis.

Connectivity networks for DE-ITGs

The physical and functional linkages of DE-ITGs were evaluated using the Search Tool for the Retrieval of Interacting Genes (STRING) database (URL: http://string-db.org) (15). Cytoscape software (16) was in turn deployed to imagine the PPI network of DE-ITGs.

Regression analysis and risk scoring system

The 383 TCGA-BLCA samples were sorted by randomization (ratio 7:3) into a training set (n = 269) and a test set (n = 114). The optimal DE-ITGs were appraised by a combination of Cox (univariate) and LASSO (glmnet package in the R) analyses (in the training set). Variables with Cox P< 0.05 were incorporated into the LASSO procedure, and the corresponding variables were retrieved subject to the minimum value of Lambda (λ). Risk scores for the BLCA samples in each dataset were captured by the regression coefficients (coef; Table 2) and expressions of the selected ITGs based on the following formula:

$$risk\ \ score = coef_1 \times expression\ \ of\ \ gene_1 + coef_2 \times expression\ \ of\ \ gene_2 + \cdots coef_n \times expression\ \ of\ \ gene_n$$

The optimal threshold for separating patients into high-risk and low-risk subgroups (based on risk scores in the corresponding dataset) was calculated using the surv_cutpoint function, which is affiliated with the R package survminer. The competence of the risk model to distinguish and forecast patient clinical endpoints was scrutinized using the R package survival and survivalROC.

The independence of the model affecting the overall survival of BLCA patients was furthermore inferred by Cox analysis (R package), univariate and multivariate regression, and other considered parameters including baseline (age and sex) and

TABLE 1 Thirty ITGs.

ITG names

NO.	Name	NO.	Name	NO.	Name
1	ITGA1	11	ITGA8	21	ITGB1BP2
2	ITGA10	12	ITGA9	22	ITGB2
3	ITGA11	13	ITGAD	23	ITGB3
4	ITGA2	14	ITGAE	24	ITGB3BP
5	ITGA2B	15	ITGAL	25	ITGB4
6	ITGA3	16	ITGAM	26	ITGB5
7	ITGA4	17	ITGAV	27	ITGB6
8	ITGA5	18	ITGAX	28	ITGB7
9	ITGA6	19	ITGB1	29	ITGB8
10	ITGA7	20	ITGB1BP1	30	ITGBL1

TABLE 2 The regression coefficients of three gene characterastics calculated by LASSO regression algorithm.

Gene	Coefficent
ITGA7	0.08440408
ITGA5	0.0920655
ITGB6	-0.10878208

clinical characteristics (grade, stage, and TNM stage) of the sample.

Enrichment analysis of pre-defined gene sets based on the risk model

The Gene Set Enrichment Analysis (GSEA) was implemented using the GSEA subfunction from the R software clusterProfiler package (17). Specifically, we first calculated $\log_2$ FC values for all genes between each risk subsection by the R package limma, and then set the Gene Ontology (GO) and Kyoto Encyclopedia of Genes and Genomes (KEGG) gene sets in the clusterProfiler package as the indicator gene sets, and the gene sets that satisfied the |normalized enrichment scores (NES)| > 1, $P< 0.05$, and q< 0.05 as significantly enriched.

Inference of immune cell abundance based on the risk model

The level and activity of 28 immune gene sets in BLCA patients were appraised by the single-sample gene set enrichment analysis (ssGSEA) (18) function of R package GSVA (19). The extent of immune cell infiltration (immune score), stromal cell content (stromal score), ESTIMATE score (combined immune and stromal markers), and tumor purity were also measured for apiece BLCA sample utilizing ESTIMATE (20) (R package estimate).

Patient preparation

Six pairs of BLCA tissues and adjacent normal specimens were collected from the First Affiliated Hospital of Kunming Medical University. All participants provided written informed consent prior to the study. The experiment was approved by the Institutional Ethics Committee of the First Affiliated Hospital of Kunming Medical University. All BLCA patients did not receive any treatment prior to surgery. Finally, the tissues were frozen in liquid nitrogen and then stored in a -80°C refrigerator pending further experiments.

RNA isolation and quantitative real-time polymerase chain reaction (qRT-PCR)

A total of six pairs of BLCA and paracancerous tissue samples were lysed with TRIzol reagent (Life Technologies-Invitrogen, Carlsbad, CA, USA), and total RNA was isolated following the manufacturer's instructions. Then the concentration and purity of the RNA solution were quantified using a NanoDrop 2000FC-3100 nucleic acid protein quantifier (Thermo Fisher Scientific, Waltham, MA, USALife Real). The extracted RNA was reverse-transcribed to cDNA using the sweScript RT I First strand cDNA SynthesisAll-in-OneTM First-Strand cDNA Synthesis Kit (Servicebio, Wuhan, China) prior to qRT-PCR. The qRT-PCR reaction consisted of 3 μl of reverse transcription product, 5 μl of 5×BlazeTaq qPCR Mix (Genecopoeia, Guangzhou, China), and 1 μl each of forward and reverse primer. PCR was performed in a BIO-RAD CFX96 Touch TM PCR detection system (Bio-Rad Laboratories, Inc., USA) under the following conditions: initial denaturation at 95° C for 1 min, followed by 40 cycles that each involved incubation at 95°C for 20 s, 55°C for 20 s, and 72°C for 30 s. The forward primer of ITGA5 was "CAGAAGCAGAAGGGAGGGGTA". The reverse primer of ITGA5 was "CGATGTGAATCGGCGA GAGTT". The forward primer of ITGA7 was "CTCTTCGCT TGCCCGTTG". The reverse primer of ITGA7 was "CTCGCT GCCTTGCCTCAT". The forward primer of ITGB6 was "TGG TTCTGTTTCCTGCTCTCTG". The reverse primer of ITGB6 was "CCACTTGGCTTTTGATCGTTCT". The forward primer of GAPDH was "GGAAGGTGAAGGTCGGAGT". The reverse primer of GAPDH was "TGAGGTCAATGAAGGGGTC". All primers were synthesized by Servicebio (Servicebio, Wuhan, China). The GAPDH gene served as an internal control, and the relative expression of 3 key mRNAs was determined using the $2^{-\Delta\Delta Ct}$ method (21). The experiment was repeated in triplicate on independent occasions. Statistical differences of 3 key mRNAs between normal and BLCA samples were detected by unpaired t-tests, using GraphPad Prism V6 (GraphPad Software, La Jolla, CA, USA), and the level of statistical significance was tested and represented as *** for $P< 0.001$ and **** for $P< 0.0001$.

Statistical analysis

All statistical analyses were executed in the corresponding R software (Version 4.0.3) as described. If not otherwise stated,$P< 0.05$ represents the optimal screening threshold.

Results

Analysis of BLCA-related DE-ITGs

According to the TCGA cohort, a total of 6732 DEGs were recognized between BLCA and normal groups after differential expression analysis. There were 3555 genes that met $\log_2$ FC > 0.5 and adj. P< 0.05, and their expression was significantly upregulated in BLCA samples; 3177 genes that were downregulated and fulfilled $\log_2$ FC< -0.5 and adj. P< 0.05 (Figure 1A). Among these DEGs, 11 genes were identified as ITGs as illustrated in Figure 1B. Among them, ITGB3BP, ITGB4, and ITGB6 were up-regulated in BLCA; while ITGA1, ITGA10, ITGA5, ITGA7, ITGA8, ITGA9, ITGB1BP2, and ITGB3 were down-regulated genes; they were defined as DE-ITGs. Figure 1C showed the reciprocal relationship of these DE-ITGs.

Risk characteristics associated with ITGs

In the training set, Cox analysis (univariate) indicated that ITGA7 (P = 0.0037), ITGA5 (P = 0.023), and ITGB6 (P = 0.032) with P< 0.05 were the candidate model genes (Figure 2A). After further feature dimensionality reduction analysis, the LASSO algorithm identified ITGA7, ITGA5, and ITGB6 as the optimal ITGs for the construction of prognostic signature based on λ_{min} = 0.003 (Figure 2B).

Risk scores for the training set-BLCA patients were calculated as previously described and the specimens were classified into high- and low-risk subgroups according to the cutoff value = 1.0532 (Figure 2C). The position of the red curve representing the high-risk score was appreciably below than the curve for the low-risk subtype (blue) (P = 0.00053; Figure 2D). Predictive sensitivity analysis indicated that the risk model had tolerable prognostic validity in the training set (Figure 2E). Moreover, ITGA5 and ITGA7 were found to be more inclined to be expressed in the high-risk group; ITGB6, on the contrary (Figure 2F).

Subsequently, we implemented equal analysis in the testing set and the GSE32894 cohort. The rendering of the risk scoring system behaved exactly as in the training set (Figure 3A). The height of the blue-low risk scoring curve outweighed the red curve (high-risk subcategory) (Figure 3B). The predictive strength of the ITGs model was more impressive in the GSE32894 cohort (Figure 3C). Additionally, the relationships across the three prognostic ITGs with risk score subcategories (in both validation cohorts) were illustrated in Figure 3D.

ITGs-based risk model as an individual predictor of outcome in BLCA patients

In the training set (Supplementary Table 1), the testing set (Supplementary Table 2), and the GSE32894 cohort (Supplementary Table 3), ANOVAs suggested that the distribution of clinical characteristics of patients in distinct risk subcategories was strikingly diverse. The Cox analyses (univariate and multivariate) pointed to the risk score as the only stand-alone prognostic predictor for patients with BLCA (both P< 0.05; Figure 4).

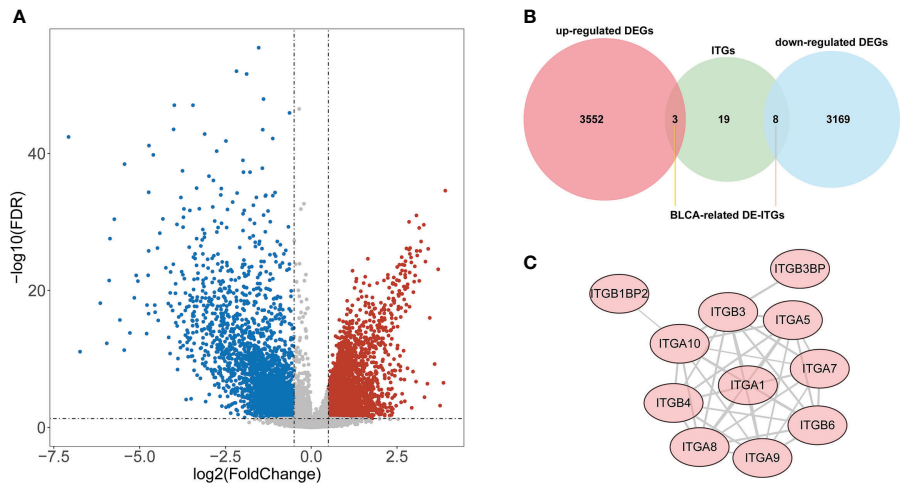

FIGURE 1
Identification of BLCA-related DE-ITGs. **(A)** 6732 DEGs were identified between BLCA and normal groups from the TCGA cohort . **(B)** 11 ITGs were illustrated from DEGs by the Venn diagram. **(C)** PPI network of DE-ITGs.

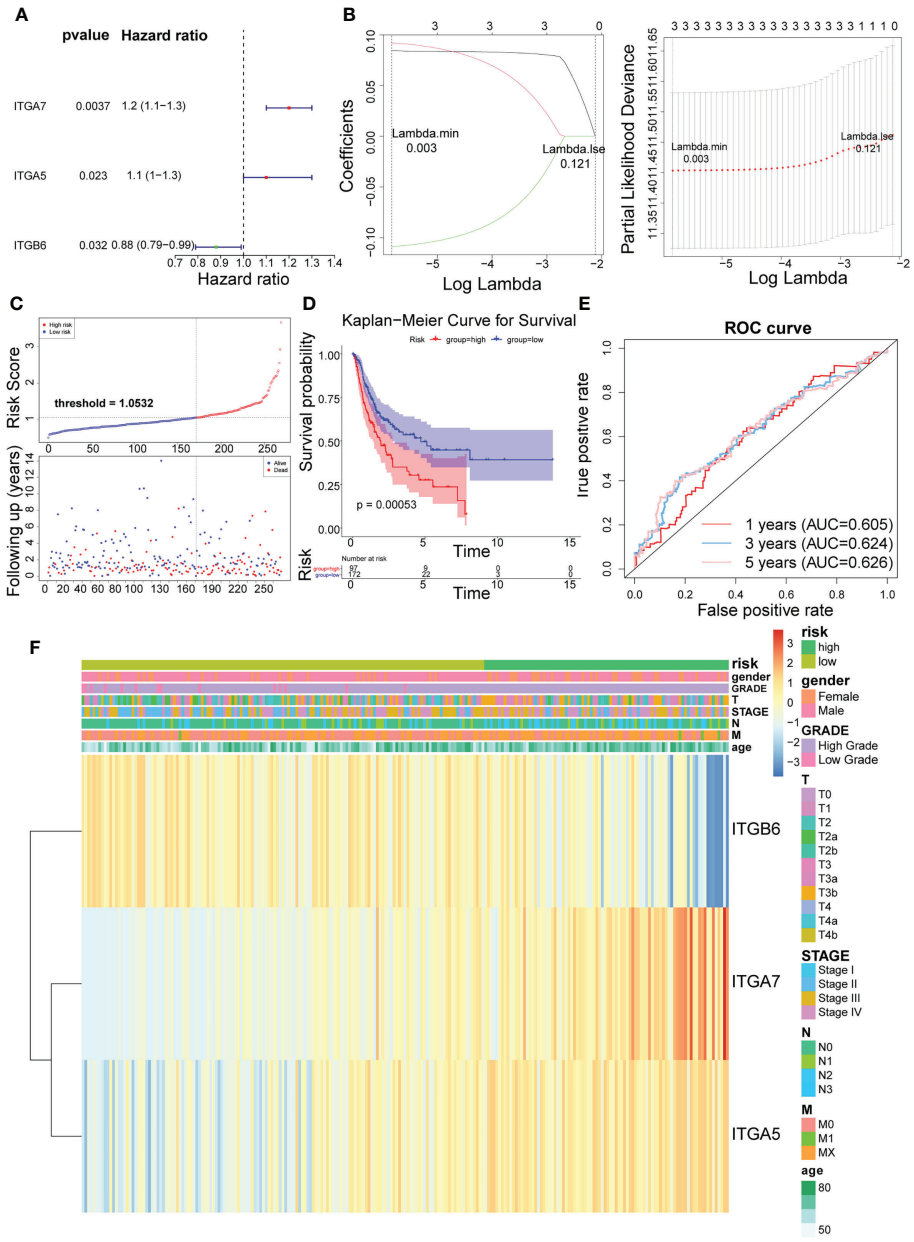

FIGURE 2
Identification of 3 risk characteristics associated with ITGs in the training set from TCGA cohort. **(A)** Three condidate model genes were screened by univariate Cox analysis. **(B)** Three risk characteristics associated with ITGs were identified by LASSO algorithm. **(C)** Risk score of the three risk characteristics. **(D)** Kaplan-Meier curve of the three risk characteristics. **(E)** ROC curve of the three risk characteristics. **(F)** The heatmap of the three risk characterastics in high- and low-risk groups, the distribution of clinicopathological features was compared between the low- and high-risk groups.

Uncovering the molecular mechanisms involved in the risk score

GSEA was conducted to analyze the enrichment differences in the terms of GO and KEGG between different risk groups. A total of 41 pathways were activated in the high-risk group, mainly related to immune-inflammatory responses ('chemokine signaling pathway', 'primary immunodeficiency', 'antigen processing and presentation', *etc.*) and multiple cancer ('systemic lupus erythematosus', 'dilated cardiomyopathy', 'pathways in cancer', *etc.*) (Figure 5A; Supplementary Table 4). In the GO annotation system, a total of 1776 terms were harvested (Supplementary Table 5), where the

10.3389/fonc.2022.970576

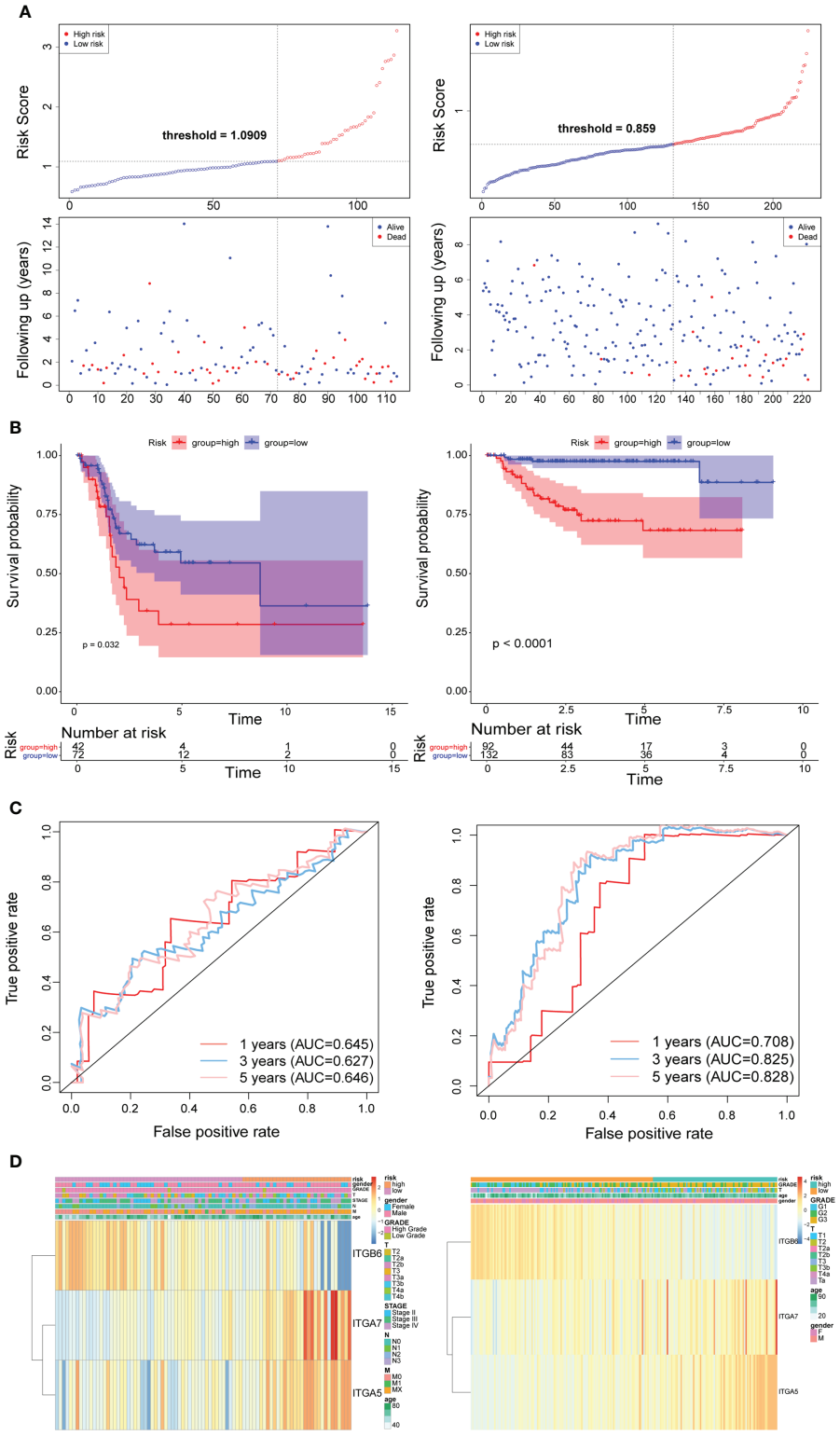

FIGURE 3
Time-dependent ROC analysis, risk score analysis, and Kaplan-Meier analysis for the three characteristics in testing set from TCGA (left) and the validation set from GSE32894 cohort (right). **(A)** Risk score of three gene signature. **(B)** Kaplan-Meier curve of the three risk characteratics. **(C)** ROC curve of the three-gene signature. **(D)** The heatmap of the three gene characterastics in high- and low-risk groups, the distribution of clinicopathological features was compared between the low- and high-risk groups.

10.3389/fonc.2022.970576

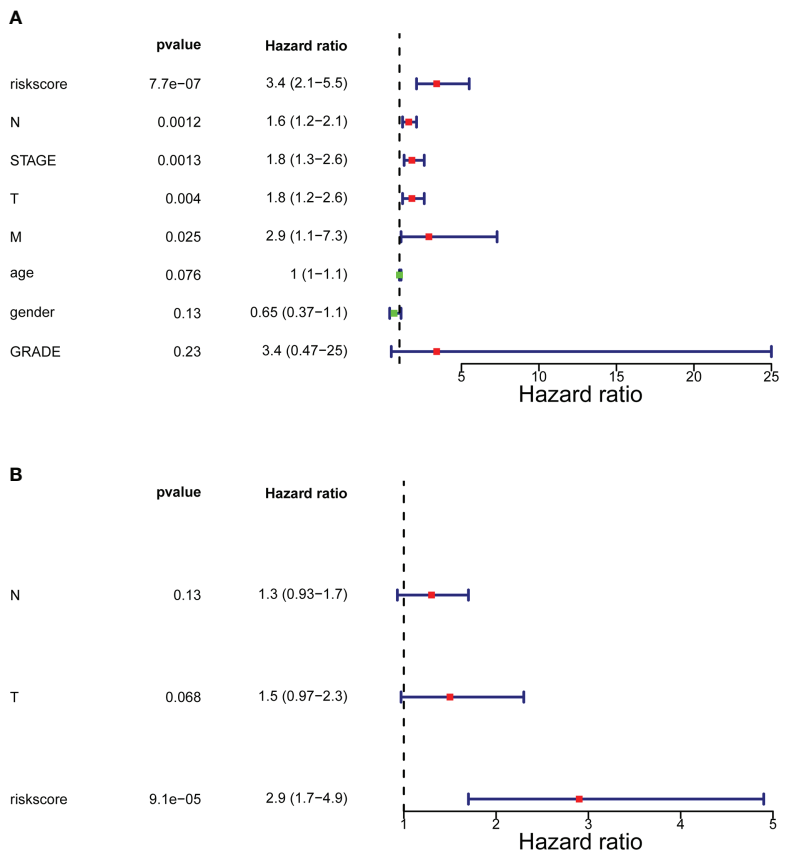

FIGURE 4
Forrest plot of the univariate and multivariate Cox regression analysis. **(A)** Engaged clinical characteristics into univariate Cox regressive. **(B)** Multivariate Cox regressive. The green square indicates that the HR value is less than 1, the red square indicates that the HR alue is larger than 1, and the line segments on both sides of the square are the 95% confidence interval of the HR Value.

high-risk subset was tightly matched to immune response ('activation of immune response', 'adaptive immune response', 'regulation of immune effector process', *etc.*), immune cell physiological processes ('granulocytes migration', 'leukocyte proliferation', 'mononuclear cell differentiation', *etc.*), tissue and organ development ('muscle organ development', 'regulation of vasculature development', 'bone development', *etc.*), and multiple diseases ('aortic aneurysm', 'meningitis', 'vasculitis', *etc.*); notably, smooth muscle (regulation of contraction and relaxation) and smooth muscle cell proliferation, migration, and differentiation terms were prominently enrolled in the high-risk subtype. Figure 5B exhibited the top 10 terms in the GO system. This evidence suggested that the risk score may influence disease progression and clinical outcomes in BLCA patients by modulating cancer trigger pathways, smooth muscle pathways, and immune response pathways.

ITGs-based high scoring group with robust immune cell infiltration characteristics

Inspired by the above results, we extrapolated the content of 28 immune cells in diverse risk subclasses *via* the ssGSEA algorithm. Except for Activated CD4 T cell, CD56dim natural killer cell, Monocyte, and Type 17 T helper cell, which were comparable in both risk subcategories (all rank-sum test $P > 0.05$), all the other 24 immune cells were strikingly divergent across the above two categories of samples (all rank-sum test $P< 0.05$); only CD56bright natural killer cell was detected to be more infiltrative in the low-risk subgroup (rank-sum test $P< 0.05$) (Figure 6A). Meanwhile, the ESTIMATE algorithm demonstrated that high-risk subgroup patients had more immune and stromal cells and reduced tumor purity (Figure 6B).

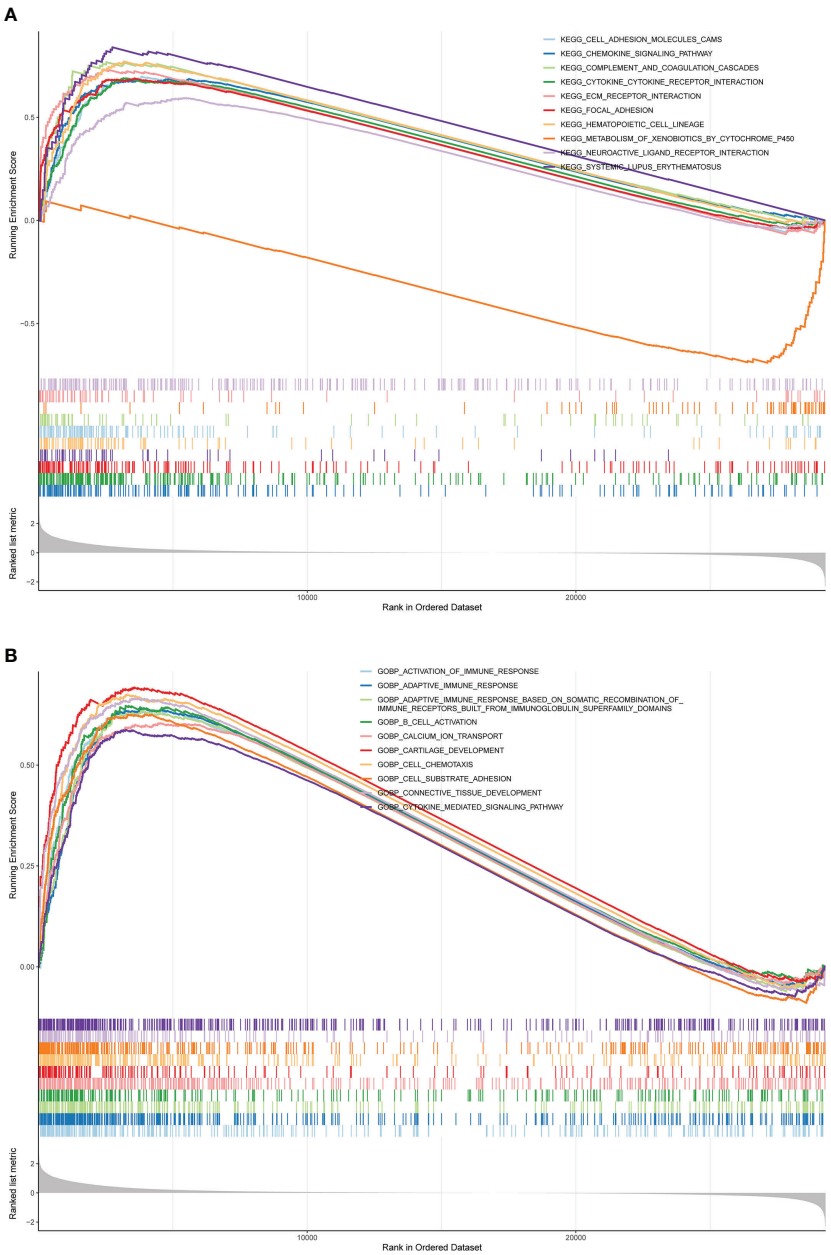

FIGURE 5
GSEA is adopted to annotate the genes with different expression in the terms of GO and KEGG between different risk groups. **(A)** Top 10 KEGG pathways. **(B)** Top 10 GO pathways.

Detection of mRNA expression levels of prognostic genes in BLCA clinical samples

We matched the expression profiles of three prognostic genes in the TCGA-BLCA (Supplementary Figure 1A) and GSE7476 (Supplementary Figure 1B) datasets and found that both ITGA5 and ITGA7 were significantly reduced in tumor samples; while ITGB6 was notably overexpressed in the BLCA group (all $P< 0.05$). Furthermore, a total of 6 samples were collected from newly diagnosed BLCA patients in The First Affiliated Hospital of Kunming Medical University from March 2022 to May 2022. ITGA5 ($P< 0.0001$) and ITGA7 ($P = 0.0002$) were significantly reduced in the BLCA population; whereas ITGB6 ($P< 0.0001$) was markedly overexpressed in the BLCA group (Figure 7), which in accordance with bioinformatics results.

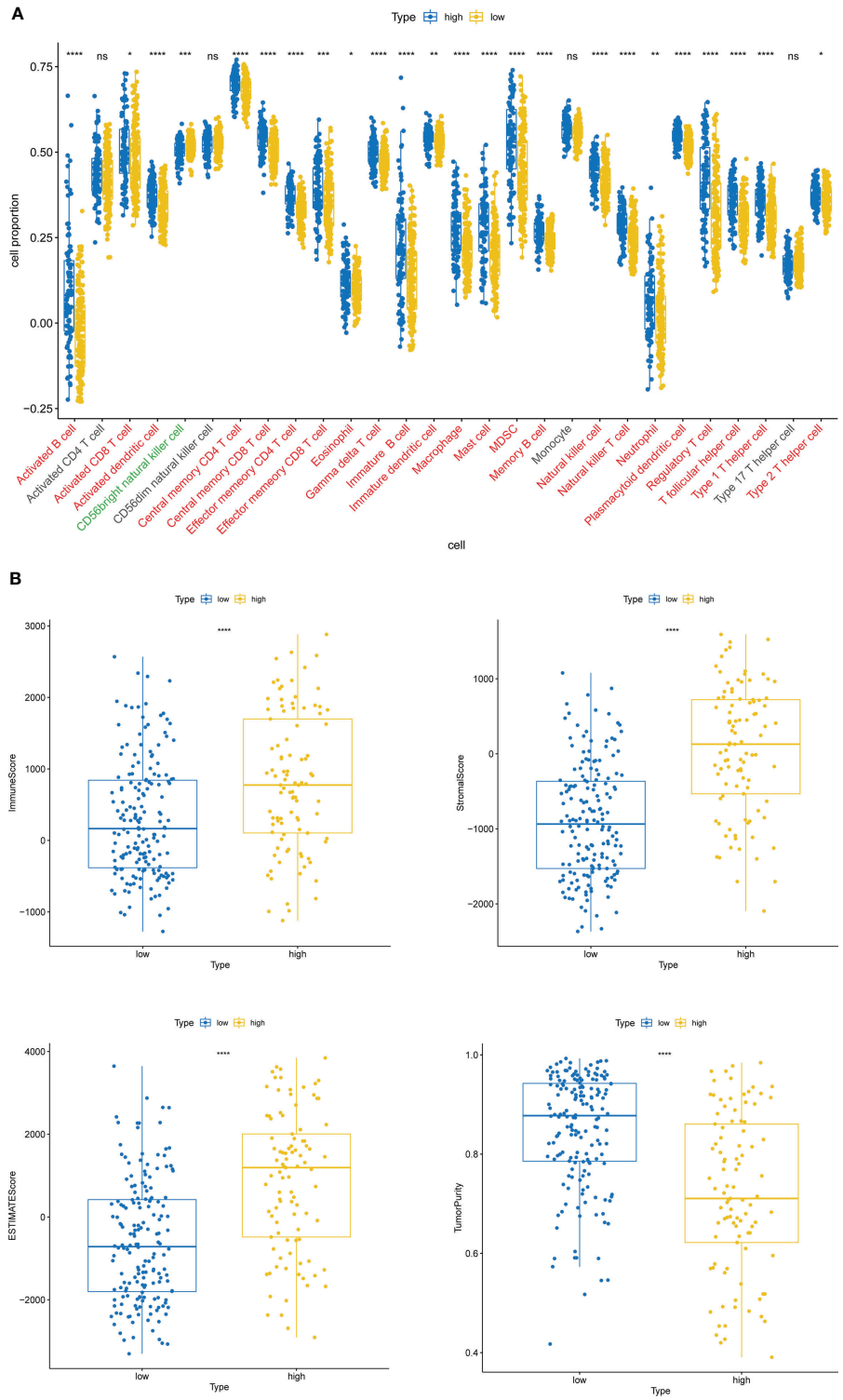

FIGURE 6
Immune cell infiltration characteristics of high- and low-risk groups. **(A)** The content of 28 immune cells in diverse risk subclasses assessed by the ssGSEA algorithm. ns, non-significant. **(B)** The immune score, stromal score, ESTIMATE score, and tumor purity in diverse risk subgroups assessed by the ESTIMATE algorithm. *P < 0.05, **P < 0.01, ***P < 0.001,****P < 0.0001.

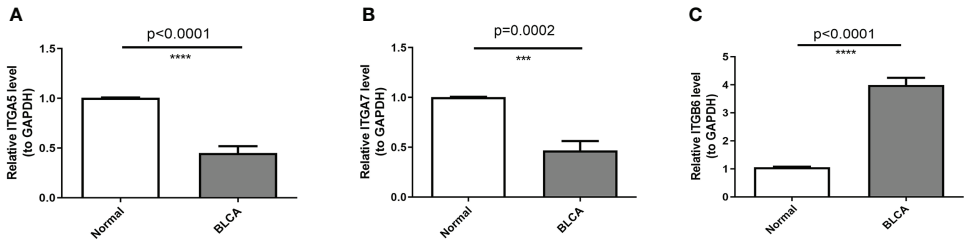

FIGURE 7
Exprerimental validation of ITGA5, ITGA7, and ITGB6. **(A)** Relative mRNA expression of ITGA5 in BLAC tissue and paracancerous tissues. **(B)** The mRNA expression level of ITGA7 in mRNA expression levels of prognostic genes in BLCA clinical samples. **(C)** The mRNA expression level of ITGB6 in mRNA expression levels of prognostic genes in BLCA clinical samples ***P < 0.001,****P < 0.0001.

Discussion

BLCA is a multi-step, multifactorial and heterogeneous disease with a high disease burden and a poor prognosis in the event of metastasis and recurrence (1, 2). ITGs are a widely known class of cell adhesion molecule receptors that have been proven to be involved in cancer progression including pancreatic, colorectal, gastric and breast cancers (13, 22). Up until now, there has been no study to explore the role of ITGs in BLCA and their predictive value for clinical prognosis. In this study, machine learning algorithms (univariate Cox and LASSO) were used to identify the prognostic signatures associated with ITGs consisting of ITGA5, ITGB6 and ITGA7.

In our risk stratification model, high expression of ITGA5 and ITGA7 was associated with poorer survival, and in contrast to ITGB6. It has been shown that overexpression of ITGA5 is closely associated with enhanced O-GlcNAcylation, accelerating the progression of colorectal cancer. ITGA5 promotes proliferation, migration and invasion of oral squamous cell carcinoma cell lines through EMT (epithelial-mesenchymal transition) (23). ITGA5 plays an important role in Ta- T2 and T1-T2 transitions (24), suggesting a correlation between increased ITGA5 expression and histological staging, and a negative correlation between ITGA5 upregulation and prognostic overall survival in BLCA. Silencing ITGB6 inhibits the proliferation, migration and invasion of cervical cancer cells and promotes apoptosis by inhibiting the JAK/STAT signaling pathway (25). Low expression of ITGB6 in cholangiocarcinoma is associated with poorer prognosis and increased invasiveness (26). In the model we studied, ITGB6 was highly expressed in a low-risk population, possibly early in tumourigenesis, enhancing tumor cell adhesion and the ECM barrier, and may act as a protective factor in the risk stratification of BLCA mortality. ITGA7 acts as a pro-oncogene, promoting the stemness of oral squamous cell carcinoma cells and subsequently inducing tumourigenicity and metastasis (27). ITGA7 is highly expressed in hepatocellular carcinoma cells and knockdown of ITGA7 inhibits proliferation, migration, invasion and EMT of hepatocellular carcinoma cells (28). Due to the complexity of malignant pathological processes, different malignancies may be different in their pathological features and the effect of ITGA7 on cellular function and its potential mechanisms in different cancers may differ. We found that high expression of ITGA7 in high-risk groups may confer a worse survival benefit to patients, and there are few studies on ITGA7 associated with BLCA, and more research is needed.

Interestingly, we found that the expression levels of both ITGA5 and ITGA7 were down-regulated in BLCA compared to normal samples, while high expression was associated with poor OS (Figures 7, 2). Conversely, ITGB6 was upregulated in BLCA, while low expression of ITGB6 was associated with poor OS (Figures 7, 2). Previous studies have shown that CXCL11 expression is significantly upregulated in colon adenocarcinoma and that upregulation of CXCL11 expression is associated with better prognosis, and it has been speculated that the contradiction between CXCL11 expression and prognosis may be due to the complexity of regulation (29). Herewith, we hypothesize that ITGA5, ITGB6 and ITGA7 are changing dynamically in influencing the onset and development.

In addition, GSEA analysis revealed that immune inflammatory responses and multiple cancers (Figure 5), among other KEGG pathways, differ significantly between high- and low-risk groups. It has been shown that the presence of a large number of immune/inflammatory cells and cytokines in the tumor microenvironment leads to a chronic inflammatory state and immune suppression, regulating tumor cell migration, invasion, metastasis and anticancer drug sensitivity (30). Studies have confirmed that SLE is associated with an overall increased risk of cancer compared to the normal population and is a risk factor for cancer (31). This suggests that patients with BLCA in the high-risk group may have an impact on survival time due to dysregulation of immune inflammatory

response pathways and multiple cancer pathways, among others. In the GO annotation system, the high-risk group is closely matched to immune responses, immune cell physiological processes, tissue and organ development and multiple diseases (32). Notably, smooth muscle (regulation of contraction and relaxation) and smooth muscle cell proliferation, migration and differentiation conditions are significantly involved in the high-risk subtype. Idiopathic urinary incontinence is a common complication of BLCA. Studies have shown that BLCA is associated with dramatic changes in the contractility of the smooth muscle of the detrusor (33, 34). One of the features of cancers that occur in the bladder is that the tumor invades and crosses the biophysical barrier of the smooth muscle (35). Based on the above literature, we hypothesise that modulation of cancer trigger pathways, smooth muscle pathways and immune response pathways contribute to the differences in prognosis between high and low risk patients and influence disease progression and clinical outcomes in patients with BLCA.

The high-risk group based on ITGs had a stronger immune cell infiltration profile with significantly higher immune scores, stromal scores and ESTIMATE scores than the low-risk group, while the opposite was true for tumor purity (Figure 6). The microenvironment of bladder tumor tissue contains not only tumor cells, but also stromal cells and immune cells, and others. Immune cells are an important component of the tumor stroma and cross-talk between cancer cells and proximal immune cells ultimately results in an environment that promotes tumor growth and metastasis (36). The predictive value of immune cells has been extensively studied. Stromal cell scores were positively correlated with cancer staging, indicating that the stromal component of TME may play an important role in BLCA progression (37). According to our findings, only CD56bright natural killer cells were detected to be more infiltrative in the low-risk subgroup (Figure 6B). It has been shown that CD56bright NK cells produce a large number of immunomodulatory cytokines and chemokines, exerting more immunomodulatory effects, and CD56bright NK cells have also recently been shown to be specifically responsive and protective against Epstein-Barr virus (EBV) infection in secondary lymphoid tissue (38). Thus, high levels of CD56bright natural killer cells may be identified as a protective factor against BLCA and are associated with good survival outcomes. The high-risk group was enriched with a high number of immune and stromal cells, diluting the purity of tumor cells and resulting in lower tumor purity in the high risk group, while the opposite was true in the low risk group. Patients with low tumor cell purity rarely show a good prognostic impact, but are more likely to be classified as malignant entities and to have a shorter survival time. On the one hand, tumor cells with limited proliferation and invasiveness tend to grow slowly, forming solid masses with less infiltration of non-tumor cells. On the other hand, the presence of tumor cells, capable of dominating the microenvironment, recruits a large number of surrounding cells and causes them to succumb, constituting a protective shield (39). Thus, high ESTIMATE scores, low tumor purity and associated cellular heterogeneity may account for the poor prognosis of invasive tumors.

Although some prognostic models for predicting BLCA have been developed in previous studies, our study has several advantages over them. Firstly, we used the new algorithm LASSO regression analysis as a screening variable to build a prognostic model, which was able to adjust for overfitting of the model, thereby avoiding extreme predictions and significantly improving prediction accuracy. Secondly, the model was able to demonstrate good performance in discrimination and calibration through internal and external validation. Clinicians may benefit from combining our model with other models. Relatively speaking, this study also has drawbacks. Firstly this is a retrospective analysis and selection bias may occur. Secondly, the endpoint of this study was OS and we did not assess the applicability of the model for predicting disease-free survival (DFS), distant metastasis-free survival (DMFS) and locoregional recurrence-free survival (LRFS) in patients with BLCA. It may be better to combine OS with DFS and DMFS. Finally, although we performed a multi-faceted, multi-database validation, the amount of data in this study was relatively small and the analysis may be biased. Therefore, future large-scale and multi-center validation of the model is needed.

In conclusion, we identified three ITGs (ITGA7, ITGA5 and ITGB6) with prognostic value, constituting a new (ITGs-related) prognostic marker for BLCA prognostic model, and preliminarily explored the potential molecular mechanisms of this model, providing potential targets for BLCA prognosis. We will continue to follow the progress of research on these genes in the coming work.

Data availability statement

The original contributions presented in the study are included in the article/Supplementary Material. Further inquiries can be directed to the corresponding authors.

Ethics statement

The studies involving human participants were reviewed and approved by Institutional Ethics Committee for Clinical Research and Animal Trials of the First Affiliated Hospital of Kunming Medical University [(2022)L36]. The patients/participants provided their written informed consent to participate in this study.

Author contributions

HT, HL, and LZ: conception and design. ZT, HW, and ZX: acquisition, analysis and interpretation of data. YJ, LG, and XX: figures drawing. HT and LZ: writing and revision of the manuscript. XL and PG: study supervision. All authors read and approved the final manuscript.

Funding

This study was supported by the National Natural Science Foundation of China (Grant No. 81802548, 81860451), Yunnan Natural Science Foundation (Grant No. 202001AW070001, 202201AY070001-045, 202101AY070001-014, 2019FE001 (-136), 2019FE001(-005)), Yunnan Health Training Project of High-Level Talents (Grant No. H2018070), Funding for Yunnan Province Clinical Research Center for Chronic Kidney Disease (Grant No. 202102AA10060), the post-graduate project of Natural Science research in Universities of Anhui Province (grant number: YJS2021A0538).

Acknowledgments

We would like to thank everyone who took part in this study.

Conflict of interest

The authors declare that the research was conducted in the absence of any commercial or financial relationships that could be construed as a potential conflict of interest.

The reviewer YH declared a shared parent affiliation with the authors HT, ZT, HW, YJ, ZX, PG, and XL to the handling editor at the time of review.

Publisher's note

Supplementary material

The Supplementary Material for this article can be found online at: https://www.frontiersin.org/articles/10.3389/fonc.2022.970576/full#supplementary-material

References

1. Siegel RL, Miller KD, Fuchs HE, Jemal A. Cancer statistics, 2021. *CA: Cancer J Clin* (2021) 71(1):7–33. doi: 10.3322/caac.21654

2. Lenis AT, Lec PM, Chamie K, Mshs MD. Bladder cancer: A review. *Jama.* (2020) 324(19):1980–91. doi: 10.1001/jama.2020.17598

3. Feng RM, Zong YN, Cao SM, Xu RH. Current cancer situation in China: good or bad news from the 2018 global cancer statistics? *Cancer Commun (Lond)* (2019) 39(1):22. doi: 10.1186/s40880-019-0368-6

4. Kim HS, Seo HK. Immune checkpoint inhibitors for urothelial carcinoma. *Invest Clin Urol* (2018) 59(5):285–96. doi: 10.4111/icu.2018.59.5.285

5. Hamidi H, Ivaska J. Every step of the way: integrins in cancer progression and metastasis. *Nat Rev Cancer* (2018) 18(9):533–48. doi: 10.1038/s41568-018-0038-z

6. Giancotti FG, Ruoslahti E. Integrin signaling. *Science* (1999) 285(5430):1028–32. doi: 10.1126/science.285.5430.1028

7. Danen EH, Yamada KM. Fibronectin, integrins, and growth control. *J Cell Physiol* (2001) 189(1):1–13. doi: 10.1002/jcp.1137

8. Giancotti FG, Tarone G. Positional control of cell fate through joint integrin/receptor protein kinase signaling. *Annu Rev Cell Dev Biol* (2003) 19:173–206. doi: 10.1146/annurev.cellbio.19.031103.133334

9. Deb M, Sengupta D, Patra SK. Integrin-epigenetics: a system with imperative impact on cancer. *Cancer Metastasis Rev* (2012) 31(1-2):221–34. doi: 10.1007/s10555-011-9341-9

10. Cooper J, Giancotti FG. Integrin signaling in cancer: Mechanotransduction, stemness, epithelial plasticity, and therapeutic resistance. *Cancer Cell* (2019) 35 (3):347–67. doi: 10.1016/j.ccell.2019.01.007

11. Sjödahl G, Lauss M, Lövgren K, Chebil G, Gudjonsson S, Veerla S, et al. A molecular taxonomy for urothelial carcinoma. *Clin Cancer Res* (2012) 18(12):3377–86. doi: 10.1158/1078-0432.CCR-12-0077-T

12. Mengual L, Burset M, Ars E, Lozano JJ, Villavicencio H, Ribal MJ, et al. DNA Microarray expression profiling of bladder cancer allows identification of noninvasive diagnostic markers. *J Urol* (2009) 182(2):741–8. doi: 10.1016/j.juro.2009.03.084

13. Cui K, Wu X, Gong L, Yao S, Sun S, Liu B, et al. Comprehensive characterization of integrin subunit genes in human cancers. *Front Oncol* (2021) 11:704067. doi: 10.3389/fonc.2021.704067

14. Bardou P, Mariette J, Escudié F, Djemiel C, Klopp C. Jvenn: An interactive Venn diagram viewer. *BMC Bioinf* (2014) 15(1):293. doi: 10.1186/1471-2105-15-293

15. Szklarczyk D, Franceschini A, Wyder S, Forslund K, Heller D, Huerta-Cepas J, et al. STRING v10: Protein-protein interaction networks, integrated over the tree of life. *Nucleic Acids Res* (2015) 43(Database issue):D447–52. doi: 10.1093/nar/gku1003

16. Shannon P, Markiel A, Ozier O, Baliga NS, Wang JT, Ramage D, et al. Cytoscape: A software environment for integrated models of biomolecular interaction networks. *Genome Res* (2003) 13(11):2498–504. doi: 10.1101/gr.1239303

17. Yu G, Wang LG, Han Y, He QY. clusterProfiler: an r package for comparing biological themes among gene clusters. *Omics J Integr Biol* (2012) 16(5):284–7. doi: 10.1089/omi.2011.0118

18. Bindea G, Mlecnik B, Tosolini M, Kirilovsky A, Waldner M, Obenauf AC, et al. Spatiotemporal dynamics of intratumoral immune cells reveal the immune landscape in human cancer. *Immunity* (2013) 39(4):782–95. doi: 10.1016/j.immuni.2013.10.003

19. Hänzelmann S, Castelo R, Guinney J. GSVA: gene set variation analysis for microarray and RNA-seq data. *BMC Bioinf* (2013) 14:7. doi: 10.1186/1471-2105-14-7

20. Yoshihara K, Shahmoradgoli M, Martínez E, Vegesna R, Kim H, Torres-Garcia W, et al. Inferring tumour purity and stromal and immune cell admixture from expression data. *Nat Commun* (2013) 4:2612. doi: 10.1038/ncomms3612

21. Livak KJ, Schmittgen TD. Analysis of relative gene expression data using real-time quantitative PCR and the 2(-delta delta C(T)) method. *Methods* (2001) 25 (4):402–8. doi: 10.1006/meth.2001.1262

22. Li Z-H, Zhou Y, Ding Y-X, Guo Q-L, Zhao L. Roles of integrin in tumor development and the target inhibitors. *Chin J Natural Medicines.* (2019) 17(4):241–51. doi: 10.1016/S1875-5364(19)30028-7

23. Deng Y, Wan Q, Yan W. Integrin α5/ITGA5 promotes the proliferation, migration, invasion and progression of oral squamous carcinoma by epithelial-mesenchymal transition. *Cancer Manage Res* (2019) 11:9609–20. doi: 10.2147/CMAR.S223201

24. Fang ZQ, Zang WD, Chen R, Ye BW, Wang XW, Yi SH, et al. Gene expression profile and enrichment pathways in different stages of bladder cancer. *Genet Mol Res* (2013) 12(2):1479–89. doi: 10.4238/2013.May.6.1

25. Zheng X, Zhu Y, Wang X, Hou Y, Fang Y. Silencing of ITGB6 inhibits the progression of cervical carcinoma *via* regulating JAK/STAT3 signaling pathway. *Ann Trans Med* (2021) 9(9):803. doi: 10.21037/atm-21-1669

26. Soejima Y, Takeuchi M, Miyamoto N, Sawabe M, Fukusato T. ITGB6-knockout suppresses cholangiocarcinoma cell migration and invasion with declining PODXL2 expression. *Int J Mol Sci* (2021) 22(12):6303. doi: 10.3390/ijms22126303

27. Lv Z, Yang Y, Yang C. Integrin α7 correlates with worse clinical features and prognosis, and its knockdown inhibits cell proliferation and stemness in tongue squamous cell carcinoma. *Int J Oncol* (2020) 56(1):69–84. doi: 10.3892/ijo.2019.4927

28. Wu Z, Kong X, Wang Z. Integrin α7 knockdown suppresses cell proliferation, migration, invasion and EMT in hepatocellular carcinoma. *Exp Ther Med* (2021) 21(4):309. doi: 10.3892/etm.2021.9740

29. Cao Y, Jiao N, Sun T, Ma Y, Zhang X , Chen H, et al. CXCL11 correlates with antitumor immunity and an improved prognosis in colon cancer. *Front Cell Dev Biol* (2021) 9:646252. doi: 10.3389/fcell.2021.646252

30. Fornarini G, Rebuzzi SE, Banna GL, Calabrò F, Scandurra G, De Giorgi U, et al. Immune-inflammatory biomarkers as prognostic factors for immunotherapy in pretreated advanced urinary tract cancer patients: an analysis of the Italian SAUL cohort. *ESMO Open* (2021) 6(3):100118. doi: 10.1016/j.esmoop.2021.100118

31. Zhao X, Zhang L, Wang J, Zhang M, Song Z, Ni B, et al. Identification of key biomarkers and immune infiltration in systemic lupus erythematosus by integrated bioinformatics analysis. *J Transl Med* (2021) 19(1):35. doi: 10.1186/s12967-020-02698-x

32. Patel VG, Oh WK, Galsky MD. Treatment of muscle-invasive and advanced bladder cancer in 2020. *CA: Cancer J Clin* (2020) 70(5):404–23. doi: 10.3322/caac.21631

33. Philyppov IB, Sotkis GV, Rock A, Roudbaraki M, Bonnal JL, Mauroy B, et al. Alterations in detrusor contractility in rat model of bladder cancer. *Sci Rep* (2020) 10(1):19651. doi: 10.1038/s41598-020-76653-7

34. Zeltz C, Primac I, Erusappan P, Alam J, Noel A, Gullberg D. Cancer-associated fibroblasts in desmoplastic tumors: Emerging role of integrins. *Semin Cancer Biol* (2020) 62:166–81. doi: 10.1016/j.semcancer.2019.08.004

35. Harryman WL, Marr KD, Hernandez-Cortes D, Nagle RB, Garcia JGN, Cress AE. Cohesive cancer invasion of the biophysical barrier of smooth muscle. *Cancer metastasis Rev* (2021) 40(1):205–19. doi: 10.1007/s10555-020-09950-2

36. Cox TR. The matrix in cancer. *Nat Rev Cancer* (2021) 21(4):217–38. doi: 10.1038/s41568-020-00329-7

37. Hinshaw DC, Shevde LA. The tumor microenvironment innately modulates cancer progression. *Cancer Res* (2019) 79(18):4557–66. doi: 10.1158/0008-5472.CAN-18-3962

38. Michel T, Poli A, Cuapio A, Briquemont B, Iserentant G, Ollert M, et al. Human CD56bright NK cells: An update. *J Immunol* (2016) 196(7):2923–31. doi: 10.4049/jimmunol.1502570

39. Zhang C, Cheng W, Ren X, Wang Z, Liu X, Li G, et al. Tumor purity as an underlying key factor in glioma. *Clin Cancer Res an Off J Am Assoc Cancer Res* (2017) 23(20):6279–91. doi: 10.1158/1078-0432.CCR-16-2598

frontiers | Frontiers in Oncology

TYPE Original Research
PUBLISHED 14 October 2022
DOI 10.3389/fonc.2022.1025195

OPEN ACCESS

EDITED BY
Hailiang Zhang,
Fudan University, China

REVIEWED BY
Jun Wang,
Sun Yat-sen University Cancer Center (SYSUCC), China
Anwaier Aihetaimujiang,
Fudan University, China

*CORRESPONDENCE
Xiqiu Zhou
zhouxiqiu1970@aliyun.com
Yuanbiao Chen
2318421260@qq.com
Yunhua Qiu
18917982481@189.cn

†These authors have contributed equally to this work

SPECIALTY SECTION
This article was submitted to Genitourinary Oncology, a section of the journal Frontiers in Oncology

RECEIVED 22 August 2022
ACCEPTED 20 September 2022
PUBLISHED 14 October 2022

CITATION
Yang J, Xu J, Gao Q, Wu F, Han W, Yu C, Shi Y, Qiu Y, Chen Y and Zhou X (2022) Identification of adenylate cyclase 2 methylation in bladder cancer with implications for prognosis and immunosuppressive microenvironment.
Front. Oncol. 12:1025195.
doi: 10.3389/fonc.2022.1025195

Identification of adenylate cyclase 2 methylation in bladder cancer with implications for prognosis and immunosuppressive microenvironment

Jianfeng Yang[1†], Jin Xu[2†], Qian Gao[3†], Fan Wu[4†], Wei Han[2], Chao Yu[5], Youyang Shi[5], Yunhua Qiu[1*], Yuanbiao Chen[6*] and Xiqiu Zhou[1*]

[1]Department of Surgery, Shangnan Branch of Longhua Hospital Affiliated to Shanghai University of Traditional Chinese Medicine, Shanghai, China, [2]Institute of Regenerative Biology and Medicine, Helmholtz Zentrum München, Munich, Germany, [3]Wound Treatment Center Affiliated Xinhua Hospital of Medicine College of Shanghai Jiaotong University, Shanghai, China, [4]Department of Urology, Renji Hospital, School of Medicine, Shanghai Jiao Tong University, Shanghai, China, [5]Longhua Hospital Affiliated to Shanghai University of Traditional Chinese Medicine, Shanghai, China, [6]Affiliated Hospital of Youjiang Medical University for Nationalities, Baise, China

Background: The incidence and mortality of bladder cancer (BCa) are increasing, while the existing diagnostic methods have limitations. Therefore, for early detection and response prediction, it is crucial to improve the prognosis and treatment strategies. However, with existing diagnostic methods, detecting BCa in the early stage is challenging. Hence, novel biomarkers are urgently needed to improve early diagnosis and treatment efficiency.

Methods: The gene expression profile and gene methylation profile dataset were downloaded from the Gene Expression Omnibus (GEO) database. Differentially expressed genes (DEGs), differentially methylated genes (DMGs), and methylation-regulated differentially expressed genes (MeDEGs) were gradually identified. A cancer genome map was obtained using online gene expression profile interaction analysis, and survival implications were produced using Kaplan-Meier survival analysis. GSEA was employed to predict the marker pathways where DEGs were significantly involved. The study used bisulfite PCR amplification combined with bisulfite amplicon sequencing (BSAS) to screen for methylation analysis of multiple candidate regions of the adenylate cyclase 2 (ADCY2) based on the sequence design of specific gene regions and CpG islands.

Results: In this study, DEGs and DMGs with significantly up- or down-regulated expression were selected. The intersection method was used to screen the MeDEGs. The interaction network group in STRING was then visualized using

Cytoscape, and the PPI network was constructed to identify the key genes. The key genes were then analyzed using functional enrichment. To compare the relationship between key genes and the prognosis of BCa patients, we further investigated ADCY2 and found that ADCY2 can be a potential clinical biomarker in BCa prognosis and immunotherapy response prediction. In human BCa 5637 and MGH1 cells, we developed and verified the effectiveness of ADCY2 primers using BSAS technology. The findings revealed that the expression of ADCY2 is highly regulated by the methylation of the promoter regions.

Conclusion: This study revealed that increased expression of ADCY2 was significantly correlated with increased tumor heterogeneity, predicting worse survival and immunotherapy response in BCa patients.

KEYWORDS

ADCY2, bladder cancer, tumor microenvironment, DNA methylation, prognosis

Introduction

Bladder cancer (BCa) is the most common malignant tumor of the urinary system, and BCa ranks 13th in the incidence spectrum of malignant tumors in China (1), and holds first place in the incidence of urogenital tumors. BCa ranks 9th in incidence and 13th in mortality among all malignant tumors worldwide (2). The etiology of BCa is complex and can occur at any age, and its incidence increases with age. It is a type of malignant tumor that is affected by internal and external influences, with smoking and occupational exposure being the two most obvious pathogenic factors. Current treatments for aggressive BCa include surgery, radiotherapy, and chemotherapy. Chemotherapy is still the primary treatment option in the late stage which includes gemcitabine, cisplatin, carboplatin, paclitaxel, and others (3). However, immunotherapy, targeted therapy, and antibody-coupled drugs are gradually used for the treatment (4, 5), which helps improve the survival rate of patients (6). The most recent clinical studies comprehensively cover all stages of BCa, including the use of new generations of antibody-coupled drugs, targeted drugs, oncolytic viruses, immunomab, dual antibodies, and others (7, 8). The diagnosis and treatment model of early diagnosis, refined surgery, comprehensive multidisciplinary process, and internationalization of clinical translational research were proposed, which significantly improved the diagnosis and treatment of BCa in China (4).

Epigenetics refers to changes in the expression of genes; though environmental factors can cause an organism's genes to be expressed differently, the genes will not be changed (9). Epigenetics processes include DNA methylation (10), genomic imprinting, maternal effects, gene silencing, dormant transposon activation, and RNA editing. Among these, DNA methylation refers to the covalent binding of a methyl group to the 5'carbon site of the CpG dinucleotide in the genome under the action of DNA methylating transferase (11, 12). It can control gene expression by causing changes in chromatin structure, DNA conformation, DNA stability, and interaction of DNA with proteins (13). DNA methylation is not a permanent change; it is reversible. Therefore, DNA methylation and demethylation modification have a wide range of applications and is associated with genetic imprinting and cancer (14, 15). Aberrant methylation can even turn normal stem cells into cancer stem cells, a sign of cancer development and progression. The researchers found that cancer cell genomes are characterized by methylation or alternative splicing events by examining methylation patterns on DNA in healthy human organs and malignant tissues (16, 17). For example, the obesity-associated protein (FTO) has been found to be overexpressed in BCa, which stimulates cancer cell metabolism and subsequently causes tumorigenesis and progression (18).

Currently, a machine learning model for predicting immunotherapy response based on tumor DNA methylation characteristics has been developed exploratively (19, 20). Methylation and genomic features are anticipated to develop into a potential research direction for tumor immune microenvironment and tumor immunotherapy marker screening using the selected methylation feature set to predict the response of pan-cancer species to immunotherapy (21–23). However, the limitation of tumor immunotherapy is that some cancer patients may not respond to such drugs and are prone to severe immune-related adverse events (irAEs), which can lead to various local and systemic autoimmunity. DNA methylation is another biomarker that is expected to be used as a predictor of immunotherapy efficacy (24, 25). In addition to its role in

tumorigenesis by regulating gene expression and promoting somatic and structural mutations, DNA methylation can assess the status of the tumor immune microenvironment. Previous studies have shown that DNA methylation characteristics can effectively predict the proportion of different types of immune cells in the tumor microenvironment, and the methylation level is related to the efficacy of immunotherapy (26). Many clinical trials of BCa immunotherapy are underway, but no efficacy has been positive to date. Studies have shown that CDH7 and LUZP1 are associated with the clinical characteristics of BCa, but more biomarkers for predictive immunotherapy and new effective therapeutic targets are still needed (27).

The current diagnosis and treatment technology has not kept up with the level of research due to the high incidence and relapse of BCa, and there are currently no reliable biomarkers for immunotherapy. Therefore, we are searching for reliable markers for early diagnosis and treatment of BCa patients to improve the survival rate and quality of life.

Methods

Acquisition and standardization of raw microarray dataset

We downloaded the gene expression profiling dataset created by high-throughput sequencing (GSE37815) and the microarray-based gene methylation profiling dataset (GSE37817) from the Gene Expression Omnibus database (GEO, https://www.ncbi.nlm.nih.gov/geo/). In total, five normal bladder mucosae and 18 primary BCa samples were included in GSE37815 (platform: GPL6102 Illumina human-6 v2.0 expression beadchip). As for the DNA methylation datasets, GSE37817 included six normal bladder mucosae and 18 primary BCa samples based on the GPL8490 platform (Illumina HumanMethylation27 BeadChip).

Identification of methylation-regulated differentially expressed genes

To identify the potential prognostic hub genes of the MeDEGs, we performed GEO2R (http://www.ncbi.nlm.nih.gov/geo/geo2r/) to compare two or more groups of samples in a GEO Series to screen genes that are differentially expressed across specific experimental conditions. In the present study, GEO2R was used to identify the differentially expressed genes (DEGs) and differentially methylated genes (DMGs). $|t| > 2$ and $P < 0.05$ were considered statistically significant. Furthermore, hypomethylation-high expression genes were obtained after the overlap of upregulated and hypomethylated genes, and hypermethylation-low expression genes were obtained after the overlap of downregulated and hypermethylated genes. The hypomethylation-high expression genes and hypermethylation-low expression genes were then identified as methylation-regulated differentially expressed genes (MeDEGs).

Functional enrichment analysis

To obtain the functional annotations of hub gens, we utilized the Database for Annotation, Visualization, and Integrated Discovery (DAVID, https://david.ncifcrf.gov/) is a straightforward web tool that can provide integrative and systematic annotation for users to unravel the biological interactions of multiple genes. It was utilized to perform functional and pathway enrichment analyses. Gene ontology (GO) analysis, including the biological process (BP), cellular component (CC), molecular function (MF), and Kyoto Encyclopedia of Genes and Genomes (KEGG) pathway enrichment analysis, were conducted for the selected MeDEGs by DAVID (28, 29). $P < 0.05$ was considered statistically significant.

PPI network construction and identification of hub genes

In this study, STRING (http://string-db.org; version 11.0) was adopted to describe protein co-regulation of hypomethylation-high expression genes and hypermethylation-low expression genes, respectively, and measure functional interactions among nodes (30). The interaction specificity score above 0.4 (the default threshold in the STRING database) was considered statistically significant. Cytoscape (version 3.6.0) was used to visualize interaction networks obtained from STRING (31). MCODE (version 1.4.2) of Cytoscape is a plug-in to cluster a given network to identify densely connected regions based on topology (32). It was utilized to find the most related module network with selection threshold as follows: MCODE scores >5, degree cutoff = 2, node score cut-off = 0.2, Max depth = 100 and k-score = 2.

Survival and hierarchical analysis

Gene Expression Profiling Interactive Analysis (GEPIA, http://gepia.cancer-pku.cn/) is an online tool that can provide customizable functionalities based on data from The Cancer Genome Atlas (TCGA; https://tcga-data.nci.nih.gov/tcga/) and the Genotype-Tissue Expression project (GTEx; https://www.gtexportal.org/home/index.html) (33). GEPIA performs survival analysis based on gene expression levels, using a log-rank test for the hypothesis evaluation. The horizontal axis (x-axis) represented the time in days, and the vertical axis (y-axis) showed the probability of surviving or the proportion of people surviving. The cut-off value was defined *via* median value or using "survminer" R package. The lines presented the survival curves of the two groups.

Data processing of gene set enrichment analysis

Based on data from the TCGA database, the GSEA tool (version 2.10.1 package) was used to predict associated up- and down-regulated genes and their significantly involved hallmarks pathways (34). The student's t-test statistical score was implemented in consistent pathways, and the mean of the DEGs was calculated for each analysis. A permutation test 1000 times was utilized to recognize the significantly involved pathways. The adjusted P using Benjamini and Hochberg (BH) and false discovery rate (FDR) method by default were used to correct for the occurrence of false positive results. Significantly related genes were defined with an adjusted P <0.01 and FDR <0.25.

Bisulfite PCR amplification and bisulfite amplicon sequencing technology

BSAS methylation next-generation sequencing of BCa cell lines was conducted by GeneChem Biotechnology Co., Ltd., Shanghai (GSGC0257632). Microsoft Office Excel software and Methylation Plotter software were used to examine the results. The Kruskal-Wallis test is a nonparametric test of three or more groups of data and was used when the ANOVA test could not be utilized. Bisulfite PCR amplification was performed using the High Pure PCR Template Preparation Kit (Roche) with forward and reverse primers provided. DNA methylation libraries were developed using the VAHTS Turbo DNA Library Prep Kit for Illumina® (ND102-0102).

Results

We selected DEGs and DMGs based on the transcriptome dataset and methylation dataset. The up-or down-regulated genes were selected to find the intersection, and the methylation-related differential genes were eliminated. We identified the key gene ADCY2 through a series of mRNA and protein level analyses of these genes, including functional enrichment analysis and protein interaction network. Further, the survival, immune infiltration, and CpG island location analyses were carried out around ADCY2 in the schematic diagram (Figure 1).

Identification of MeDEGs in BLCA

GEO2R was adopted to identify the DEGs and DMGs, respectively. For DEGs of gene expression microarray, 2425 overlapping up-regulated genes and 2563 overlapping down-

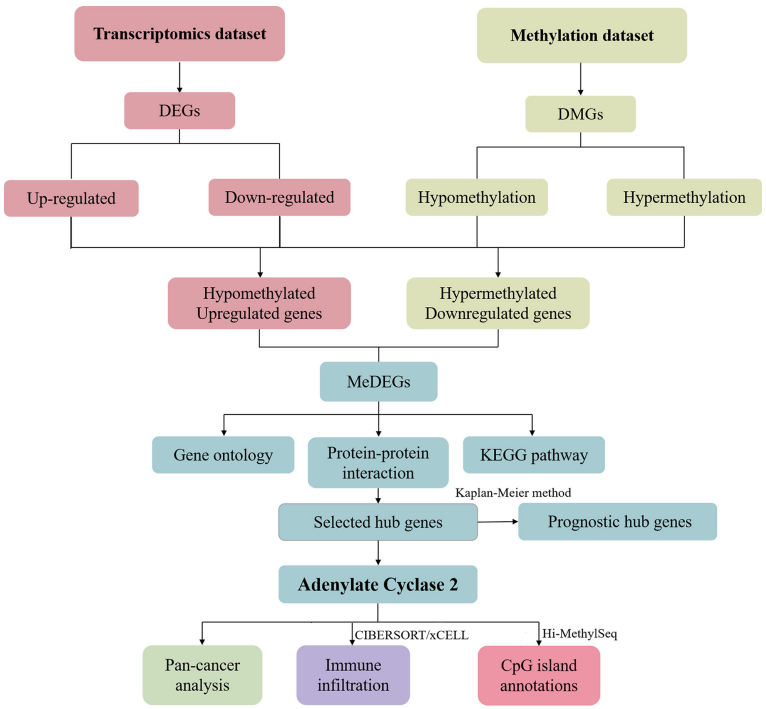

FIGURE 1
Schematic diagram of the study.

regulated genes were screened (Figures 2A, B). A total of 1114 overlapping hypermethylation genes and 10,024 overlapping hypomethylation genes were discovered for DMGs of gene methylation microarray. The study identified 1162 hypomethylated, upregulated genes and 203 hypermethylated, downregulated genes after integrating the DEGs and DMGs (Figures 2C, D).

PPI network establishment and hub genes

The PPI network of hypomethylation-upregulated genes and hypermethylation-downregulated genes was visualized using Cytoscape (version 3.6.0) [28]. A Cytoscape plug-in called MCODE (version 1.4.2) clusters a given network to select densely

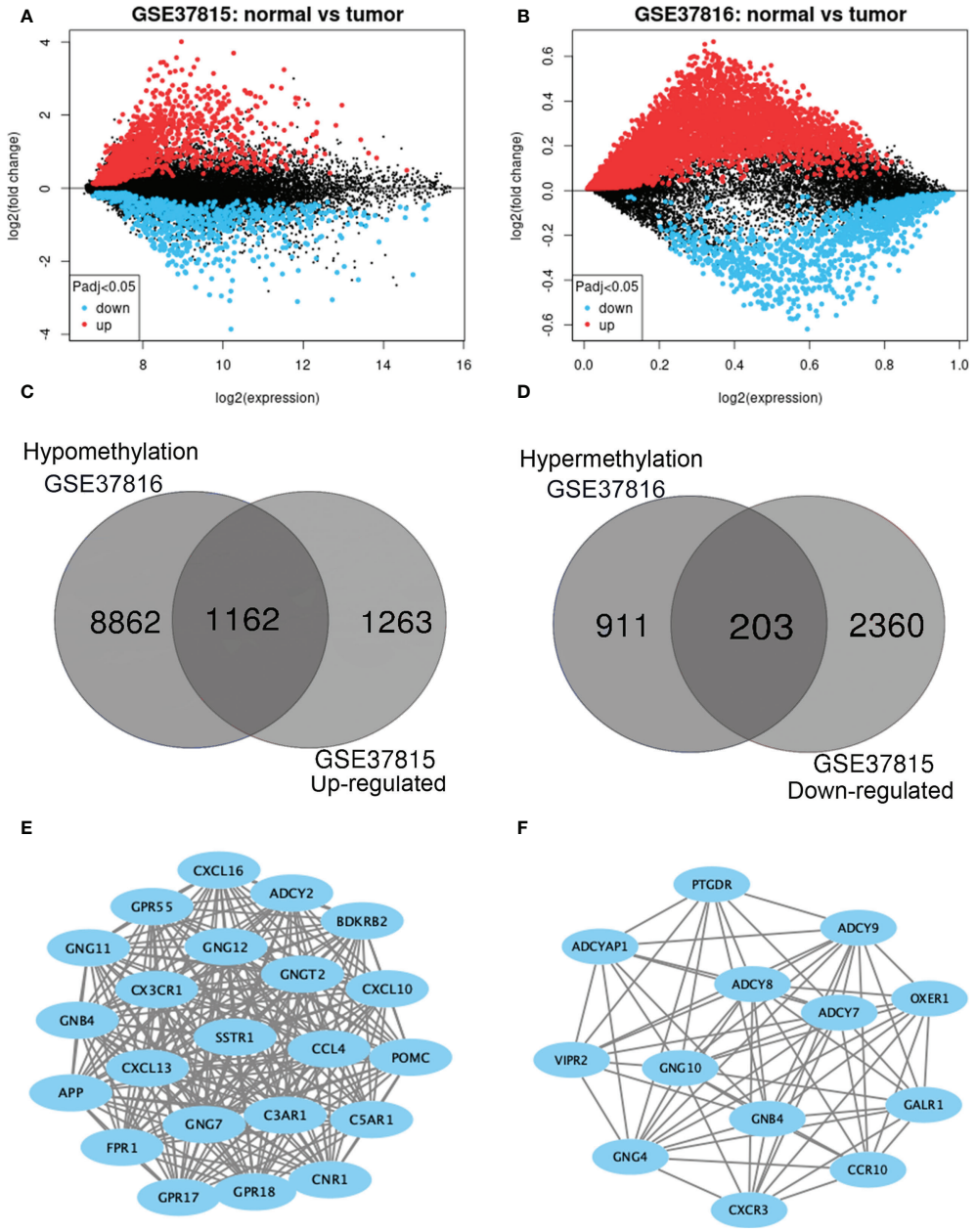

FIGURE 2
Identification of methylation-regulated differentially expressed genes (MeDEGs). **(A, B)** Mean difference plot of significantly differentially expressed genes (DEGs) in two independent validation sets. Red represents up-regulated genes, and blue represent down-regulated genes. **(C, D)** The up-regulated and down-regulated genes in the two validation sets were selected as intersections, respectively. **(E, F)** Constructed protein-protein interaction networks based on common genes.

connected regions based on topology [29]. The results are presented in Figures 2E, F. As a result, in the hypomethylation-upregulated genes module, CXCL10, CXCL16, CX3CR1, SSTR1, C3AR1, CNR1, ADCY2, BDKRB2, POMC, GPR55, GNG12, GNG11, GNGT2, CCL4, C5AR1, GNB4, CXCL13, GNG7, GPR18, APP, FPR1, GPR17, and GPR18 were confirmed as hub genes. While in the hypermethylation-downregulated genes module, PTGDR, ADCY9, OXER1, GALR1, ADCYAP1, ADCY8, ADCY7, VIPR2, GNG10, GNB4, CCR10, GNG4, and CXCR3 were confirmed as hub genes.

Functional enrichment analysis of MeDEGs

For hypomethylation-upregulated genes, changes in biological processes were mostly enriched in angiogenesis, signal transduction, aging, and immune response. The hypermethylation-downregulated genes were primarily enriched in extracellular matrix organization, signal transduction, cell adhesion, cAMP-mediated signaling, and cellular response to glucagon stimulus. Moreover, the study found that the hypomethylated, upregulated genes were associated with extracellular exosome, plasma membrane, and extracellular region. Whereas the hypermethylated, downregulated genes were associated with the proteinaceous extracellular matrix, plasma membrane, and extracellular matrix in the cellular component group. For hypomethylated, upregulated genes, changes in molecular function were primarily enriched in protein binding, heparin-binding, actin filament binding, and extracellular matrix structural constituent. On the other hand, for hypermethylated, downregulated genes, changes were significantly enriched in collagen binding, phosphorus-oxygen lyase activity, and extracellular matrix binding. Furthermore, pathway enrichment was performed using KEGG. The study revealed that hypomethylated genes predominantly participated in morphine addiction, retrograde endocannabinoid signaling, and cholinergic synapse. For hypermethylated genes, the most significantly enriched pathways involved focal adhesion, pathways in cancer, and the PI3K-Akt signaling pathway.

Survival analysis

Significant survival outcomes of hub genes in the PPI network are displayed in Figure 3. According to the expression

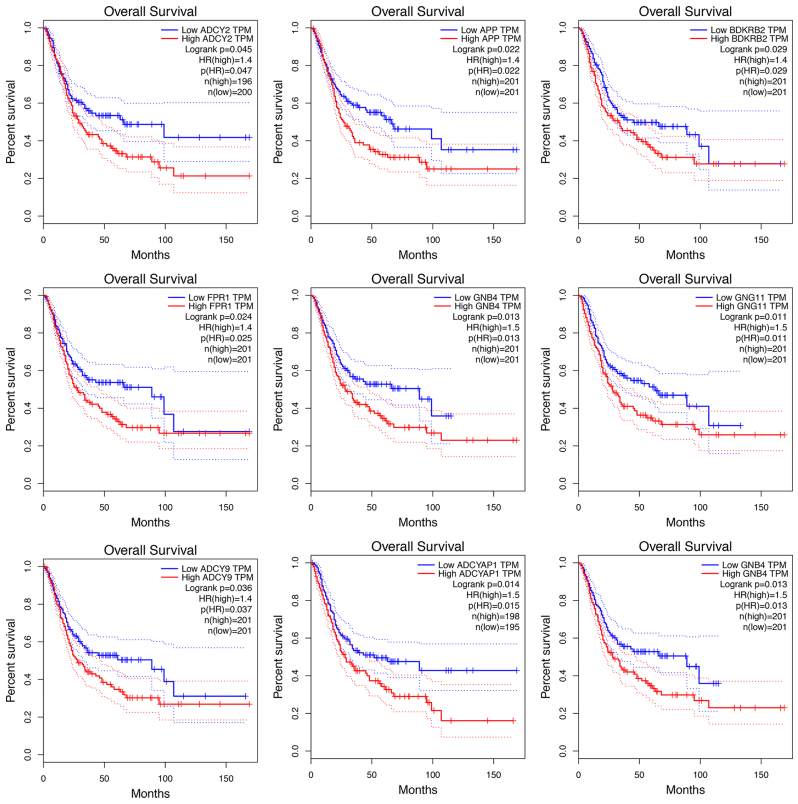

FIGURE 3
The KM curve indicates the overall survival of the selected differential genes.

of each gene, overall survival for SKCM patients was acquired. The study found that high mRNA expression of ADCY2 (P = 0.047) was significantly associated with worse prognosis for SKCM as well as APP (P = 0.022), BDKRB2 (P = 0.029), FPR1 (P = 0.025), GNB4 (P = 0.013), GNG11 (P = 0.011), ADCY9 (P = 0.036), and ADCYAP1 (P = 0.014). Significant genes and pathways were obtained using GSEA.

Differential expressed genes

After screening and analysis, this study found that ADCY2 was significantly associated with prognosis. A total of 34 cancers were then selected to observe the difference in ADCY2 expression between tumor and normal tissues. In BCa, the expression level in tumor tissues was significantly lower than that in normal tissues (n = 435, Figure 4A). Hence, a separate survival analysis of BCa patients and male and female subgroups was performed. The findings revealed that the high expression of ADCY2 predicted a worse prognosis, and it was significant in female patients, which might be due to a higher incidence of BCa in males than in females (Figures 4B, C).

Simultaneously, the significantly down-regulated genes were listed, including MFAP4, LMOD1, CNN1, COMP, SFRP4, and so on (Figure 5A). The correlation trend of these genes in populations with high and low ADCY2 expression was observed (Figure 5B).

Functional enrichment analysis

In the KEGG pathways, ADCY2 was found to be primarily enriched with protein absorption, PI3K-Akt signaling pathway, and focal adhesion pathway. An enrichment of ADCY2 was also observed in the BCa pathway, which showed that ADCY2 is involved in the development of BCa. Meanwhile, in GO term, ADCY2 was mainly enriched in extracellular structure organization and extracellular matrix organization pathways (Figure 5C).

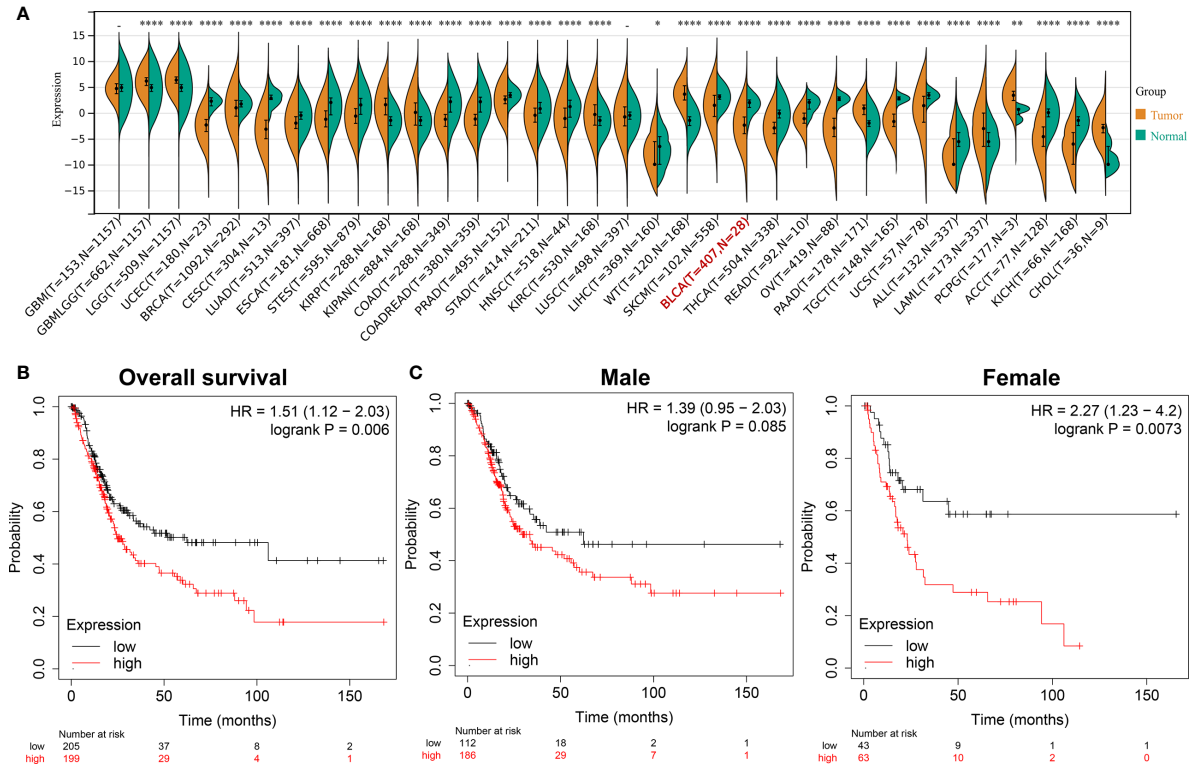

FIGURE 4
Survival outcomes of ADCY2 expression in cancers and novel role in BCa. **(A)** Differential expression of ADCY2 in tumor and normal tissues in pan-cancer. **(B)** Overall survival curve of BCa patients. **(C)** Survival curves of male and female in high and low expression groups. *p<0.05; **p<0.01; ****p<0.0001.

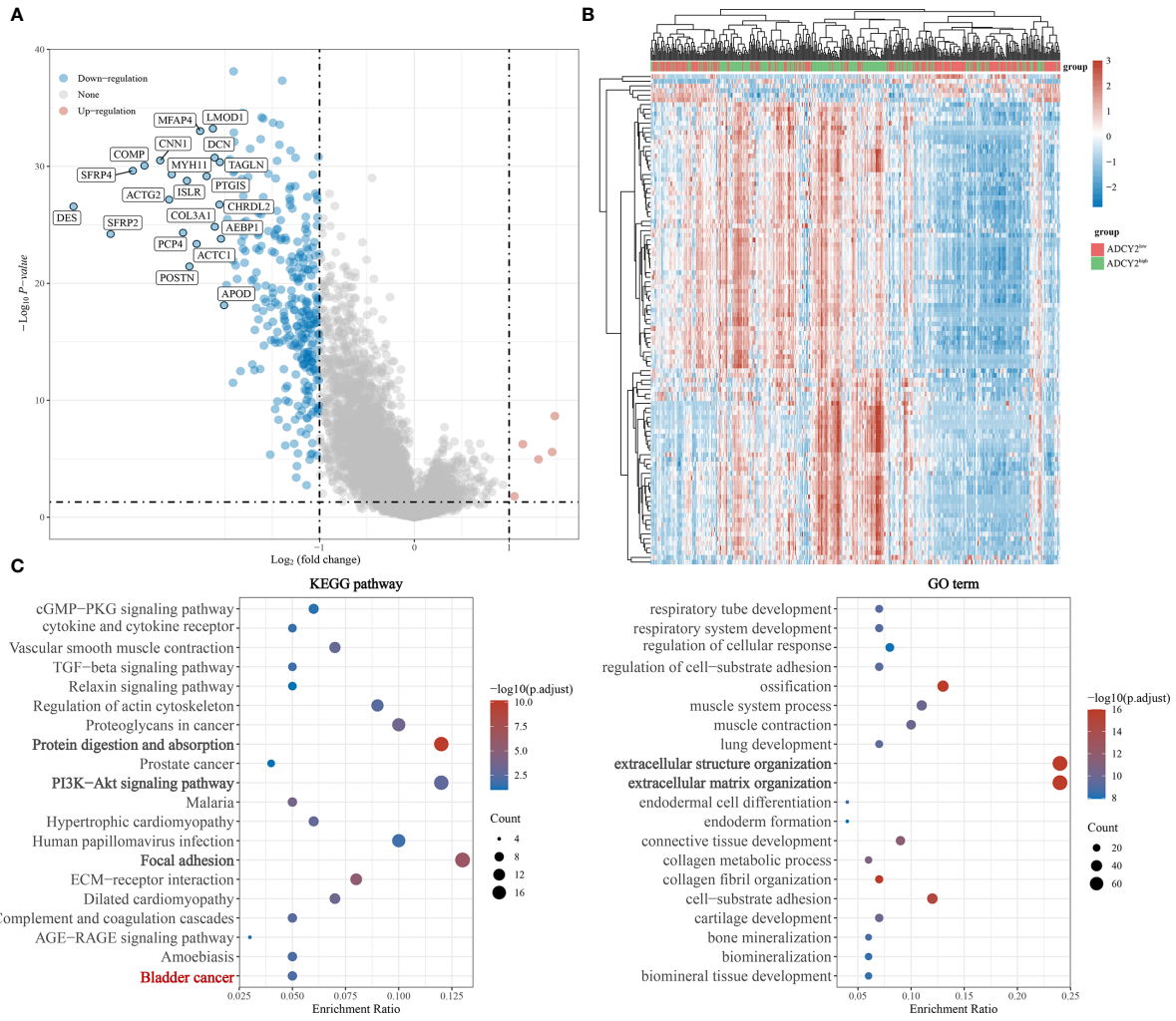

FIGURE 5
Functional enrichment annotations of ADCY2 expression in BCa. **(A)** A volcano plot of differentially expressed genes (DEGs), with down-regulated genes in blue and up-regulated genes in red. **(B)** Heat map of ADCY2 and DEGs. The low ADCY2 expression groups in red (at the top) and the high ADCY2 expression groups in green. Red and blue represent expression trends corresponding to up-regulated and down-regulated genes. **(C)** KEGG pathway and GO term functional enrichment analysis.

Immune correlation analysis of ADYC2 expression in BCa

Several immune-related cytokines were screened, mainly from five families, for correlation analysis with ADCY2 in pan-cancer. ADCY2 was found to be associated with most cytokines and presented a tumor immune microenvironment dominated by MHC and chemokine in most cancer types (Figure 6A). Notably, an immune infiltration analysis was performed in BCa using EPIC and CIBERSORT algorithms. T cell CD4+ memory resting, B cell naive, B cell memory, and macrophage M2 were significantly clustered in the ADCY2^{high} group, while uncharacterized cells were significantly increased in the ADCY2^{low} group (Figures 6B, C).

Next, the study screened for immune checkpoint molecules. The association between ADCY2 and some immune checkpoints in pan-cancer was first explored, including those that promote immunotherapy and inhibit the efficacy of immunotherapy (Figure 7A). The immune molecules, such as HAVCR2, PDCD1LG2, and TIGIT, which were significantly clustered in the high and low ADCY2 groups of BCa, were then studied independently (Figure 7B). However, the difference between the two groups was not significant. Finally, TIDE analysis was performed in the two BCa sample groups. The high score of the ADCY2^{high} group suggested a high expression of ADCY2 associated with tumor heterogeneity, indicating a worse immunotherapy effect and prognosis for BCa patients (Figure 7C).

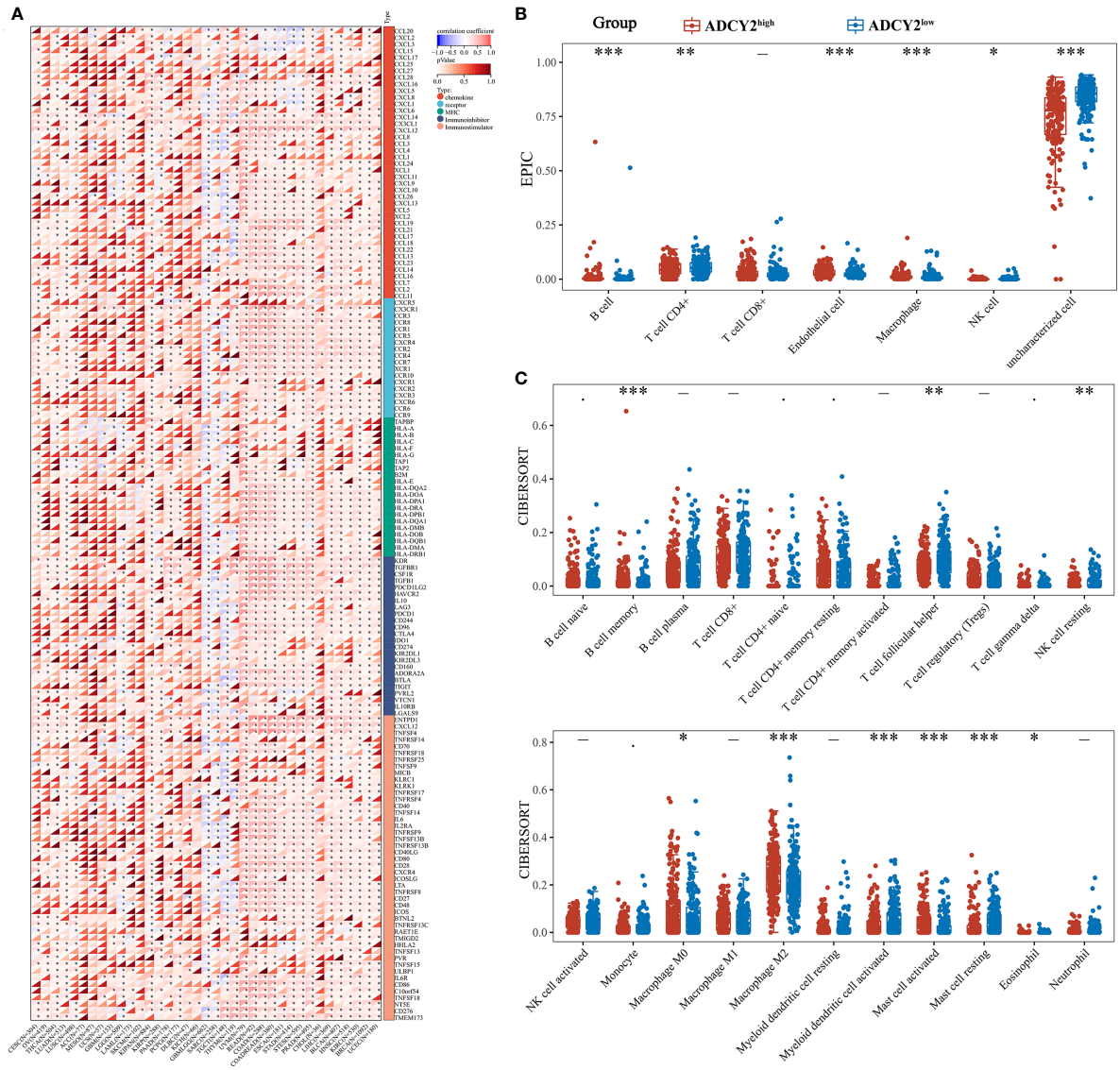

FIGURE 6
Implications of ADCY2 expression in immune regulators and tumor-infiltrated lymphocytes of cancers. **(A)** Correlation between ADCY2 and several immune-related cytokines in pan-cancer. **(B, C)** Immune infiltration difference analysis between high and low ADCY2 groups with EPIC and CIBERSORT algorithms. *p<0.05; **p<0.01; ***p<0.001.

Identification of promoter regions of ADCY2 methylation in BCa cells

In human BCa 5637 and MGH1 cells, the study developed and verified the effectiveness of ADCY2 primers using BSAS technology. Figure 8A displays the three pairs of primers for ADCY2 methylation, where the CG site of the amplified fragment is indicated in bold and red. The schematic diagram of the average methylation information of all sites in the 5637 and MGH1 cells was developed using the Methylation plotter (Figure 8B). Besides, the methylation levels of all sites in the grouped samples are shown in boxplots and dendrograms (Figures 8C–E). The findings revealed that the expression of ADCY2 is highly regulated by the methylation of the promoter regions.

Discussion

BCa is a common malignant tumor of the urinary system. The incidence of BCa ranks 9th among all malignant tumors and

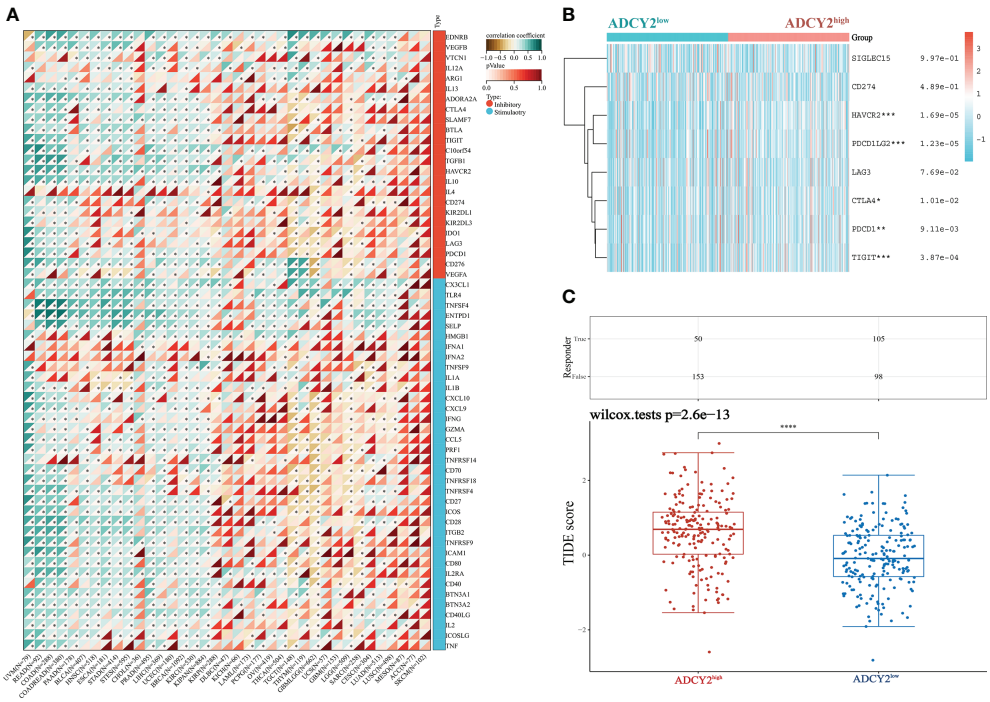

FIGURE 7
Relationship between ADCY2 expression and immune checkpoints in cancers and its implications in immunogenicity and tumor heterogeneity of BCa. **(A)** Molecular correlation analysis of ADCY2 and immune checkpoint in pan-cancer. **(B)** Heat map association between ADCY2 high and low groups and critical immune checkpoints in BCa. **(C)** TIDE scores in two groups of BCa samples. *p<0.05; **p<0.01; ***p<0.001; ****p<0.0001.

7th among male malignant tumors worldwide (6). Currently, surgery is the primary treatment method, assisted by chemotherapy and radiotherapy (5). However, many patients disqualify for radical cystectomy or refuse the therapy. Cancer immunotherapy, which harnesses the immune system of individuals to fight cancer, has revolutionized cancer treatment strategies. However, the majority of patients show no clinical response, and the mechanisms of resistance remain unclear (35–37). Therefore, there is an urgent need for novel immunotherapies and therapeutic targets.

In this study, the DEGs and DMGs from the transcriptomics dataset and methylation dataset were respectively studied. The up-regulated or down-regulated DEGs and DMGs were selected. The methylation-related differential gene sets were screened by the method of intersection using the GEO2R website to identify the DEGs as well as the DMGs. Then Cytoscape (version 3.6.0) was used to visualize the interaction networks group from STRING, based on which a PPI network was created, and the key genes were obtained. The functional enrichment analysis of key genes was carried out. For hypomethylation-upregulated genes, changes in biological processes were mainly enriched in angiogenesis, signal transduction, aging, and immune response. The hypermethylation-downregulated genes were primarily enriched in extracellular matrix organization, signal transduction, cell adhesion, cAMP-mediated signaling, and cellular response to glucagon stimulus. To compare the relationship between key genes and the prognosis of BCa patients, we further studied ADCY2, which can significantly predict the prognosis.

After a pan-cancer comparative study, immunoinfiltration analysis, real-world cohort validation, and CpG island annotations, we found that patients with high ADCY2 expression had significantly shorter overall survival and less effective immunotherapy. However, in the pan-cancer analysis, we found that the expression level of ADCY2 in tumor tissues was lower than that in normal tissues, which may be due to hypermethylation. Due to the significant immune escape of BCa cells, many immunotherapies are ineffective for all patients and are accompanied by immune rejection and side effects (38). Currently, atezolizumab (Tecentriq), pembrolizumab (Keytruda), nivolumab (Opdivo) (39), and others are approved for the treatment of locally progressive and metastatic BCa that has failed platinum-based chemotherapy (40). Both atezolizumab and pembrolizumab are also approved by the

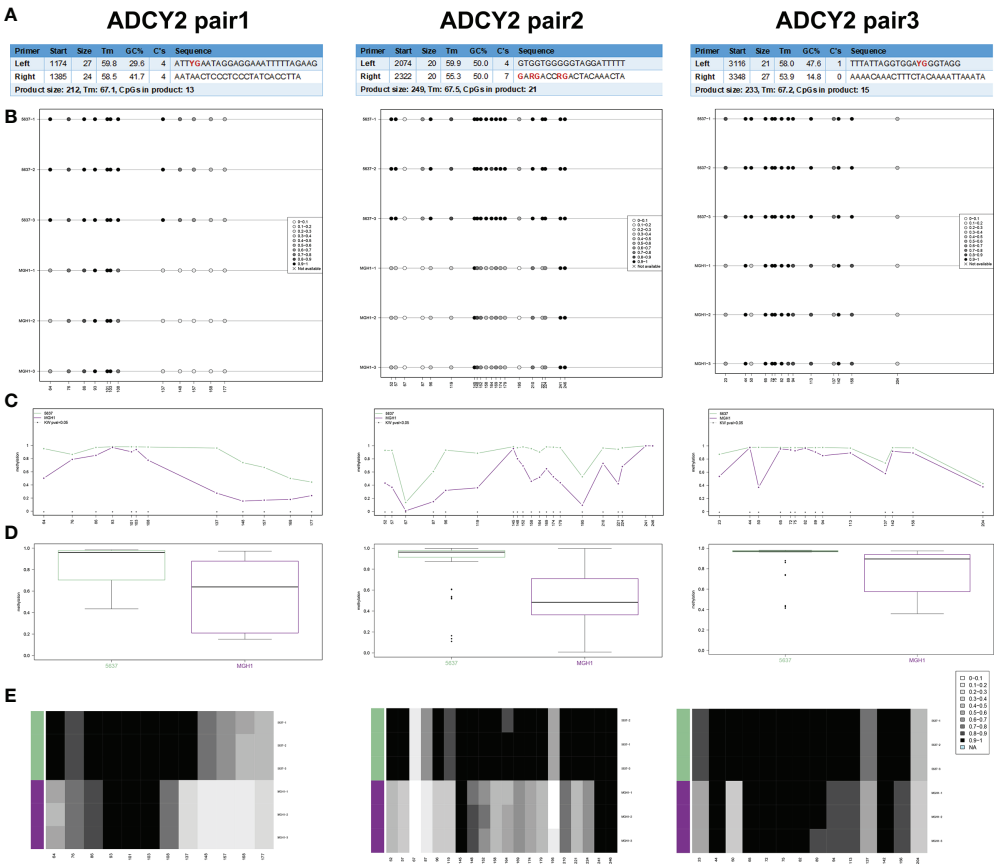

FIGURE 8
Identification of promoter regions of ADCY2 methylation in BCa cells using BSAS technology. **(A)** The effectiveness of ADCY2 primers was developed and verified in human BCa 5637 and MGH1 cells using BSAS technology. The three pairs of primers for ADCY2 methylation were shown, and the CG site of the amplified fragment was indicated in bold and red. **(B)** The schematic diagram of the average methylation information of all sites in the 5637 and MGH1 cells. **(C–E)** The methylation levels of all sites in the grouped samples were shown in boxplots and dendrograms.

FDA for first-line treatment of patients who are not eligible for platinum-based chemotherapy (41). However, some patients do not respond to these drugs, and only 20 percent benefit from them (42).

This study found that the ADCY2 gene can be used as a biological indicator for the diagnosis and immunotherapy of BCa patients. Moreover, increased ADCY2 expression is associated with worse prognosis, higher tumor heterogeneity, and worse immunotherapy effect. Though ADCY2 has been found to be a novel lipid prognostic feature in head and neck squamous cell carcinoma (43), it has not been studied in BCa. The relevant conclusions of this study innovatively discovered the differential expression of ADCY2 in BCa and proved that the expression of ADCY2 is highly regulated by the methylation of the promoter regions and could be used as a reliable biomarker in the diagnosis and treatment of BCa patients.

Data availability statement

The original contributions presented in the study are included in the article/Supplementary Material. Further inquiries can be directed to the corresponding author.

Author contributions

Conceptualization: JY, JX, YS, YQ and FW. Data curation and formal analysis: JY, WH, CY, XZ, and FW. Investigation and methodology: JY, JX, QG, WH and FW. Resources and software: JY, JX, QG, CY, XZ and YC. Supervision: XZ, YQ and YC. Validation and visualization: QG, FW and YC. Original draft: JY. Editing: QG, XZ, YQ and YC. All authors contributed to the article and approved the submitted version.

Acknowledgments

We are grateful to all patients for their dedicated participation in the current study. We thank Bullet Edits Limited for the linguistic editing and proofreading of the manuscript.

Conflict of interest

The authors declare that the research was conducted in the absence of any commercial or financial relationships that could be construed as a potential conflict of interest.

Publisher's note

Supplementary material

The Supplementary Material for this article can be found online at: https://www.frontiersin.org/articles/10.3389/fonc.2022.1025195/full#supplementary-material

References

1. Zheng R, Zhang S, Zeng H, Wang S, Sun K, Chen R, et al. Cancer incidence and mortality in China, 2016. *J Natl Cancer Center* (2016) 2(1):1–8. doi: 10.1016/j.jncc.2022.02.002

2. Lenis AT, Lec PM, Chamie K, Mshs MD. Bladder cancer: A review. *JAMA*. (2020) 324(19):1980–91. doi: 10.1001/jama.2020.17598

3. Patel VG, Oh WK, Galsky MD. Treatment of muscle-invasive and advanced bladder cancer in 2020. *CA Cancer J Clin* (2020) 70(5):404–23. doi: 10.3322/caac.21631

4. Xu W, Tang HJ, Anwaier A, Liu W, Tian X, Su J, et al. Immunogenomic characteristics of cell-Death-Associated genes with prognostic implications in bladder cancer. *Front Immunol* (2022) 13:909324. doi: 10.3389/fimmu.2022.909324

5. Miyamoto DT, Mouw KW, Feng FY, Shipley WU, Efstathiou JA. Molecular biomarkers in bladder preservation therapy for muscle-invasive bladder cancer. *Lancet Oncol* (2018) 19(12):e683–95. doi: 10.1016/S1470-2045(18)30693-4

6. Tran L, Xiao JF, Agarwal N, Duex JE, Theodorescu D. Advances in bladder cancer biology and therapy. *Nat Rev Cancer* (2021) 21(2):104–21. doi: 10.1038/s41568-020-00313-1

7. Bednova O, Leyton JV. Targeted molecular therapeutics for bladder cancer-a new option beyond the mixed fortunes of immune checkpoint inhibitors? *Int J Mol Sci* (2020) 21(19):7268–92. doi: 10.3390/ijms21197268

8. Li R, Zhang J, Gilbert SM, Conejo-Garcia J, Mule JJ. Using oncolytic viruses to ignite the tumour immune microenvironment in bladder cancer. *Nat Rev Urol* (2021) 18(9):543–55. doi: 10.1038/s41585-021-00483-z

9. Harb-de la Rosa A, Acker M, Kumar RA, Manoharan M. Epigenetics application in the diagnosis and treatment of bladder cancer. *Can J Urol* (2015) 22(5):7947–51.

10. El Azzouzi M, El Ahanidi H, Hafidi Alaoui C, Chaoui I, Benbacer L, Tetou M, et al. Evaluation of DNA methylation in promoter regions of hTERT, TWIST1, VIM and NID2 genes in Moroccan bladder cancer patients. *Cancer Genet* (2022) 260-261:41–5. doi: 10.1016/j.cancergen.2021.12.001

11. Nasrullah, Hussain A, Ahmed S, Rasool M, Shah AJ. DNA Methylation across the tree of life, from micro to macro-organism. *Bioengineered*. (2022) 13(1):1666–85. doi: 10.1080/21655979.2021.2014387

12. Yousefi PD, Suderman M, Langdon R, Whitehurst O, Davey Smith G, Relton CL. DNA Methylation-based predictors of health: applications and statistical considerations. *Nat Rev Genet Jun* (2022) 23(6):369–83. doi: 10.1038/s41576-022-00465-w

13. Nunes SP, Henrique R, Jeronimo C, Paramio JM. DNA Methylation as a therapeutic target for bladder cancer. *Cells*. (2020) 9(8):1850–78. doi: 10.3390/cells9081850

14. Liu H, Gu J, Jin Y, Yuan Q, Ma G, Du M, et al. Genetic variants in N6-methyladenosine are associated with bladder cancer risk in the Chinese population. *Arch Toxicol* (2021) 95(1):299–309. doi: 10.1007/s00204-020-02911-2

15. Greenberg MVC, Bourc'his D. The diverse roles of DNA methylation in mammalian development and disease. *Nat Rev Mol Cell Biol* (2019) 20(10):590–607. doi: 10.1038/s41580-019-0159-6

16. Patil H, Saxena SG, Barrow CJ, Kanwar JR, Kapat A, Kanwar RK. Chasing the personalized medicine dream through biomarker validation in colorectal cancer. *Drug Discovery Today* (2017) 22(1):111–9. doi: 10.1016/j.drudis.2016.09.022

17. Xu W, Anwaier A, Liu W, Tian X, Zhu W, Wang J, et al. Systematic genome-wide profiles reveal alternative splicing landscape and implications of splicing regulator DExD-box helicase 21 in aggressive progression of adrenocortical carcinoma. *Phenomics*. (2021) 1(6):243–56. doi: 10.1007/s43657-021-00026-x

18. Tao L, Mu X, Chen H, Jin D, Zhang R, Zhao Y, et al. FTO modifies the m6A level of MALAT and promotes bladder cancer progression. *Clin Transl Med* (2021) 11(2):e310. doi: 10.1002/ctm2.310

19. Chen Y, He J, Chen R, Wang Z, Dai Z, Liang X, et al. A pan-cancer analysis of predictive methylation signatures of response to cancer immunotherapy. *Front Immunol* (2021) 12:796647. doi: 10.3389/fimmu.2021.796647

20. Du Y, Zhang P, Liu W, Tian J. Optical imaging of epigenetic modifications in cancer: A systematic review. *Phenomics*. (2022) 2(2):88–101. doi: 10.1007/s43657-021-00041-y

21. Li D, Zhao W, Zhang X, Lv H, Li C, Sun L. NEFM DNA methylation correlates with immune infiltration and survival in breast cancer. *Clin Epigen* (2021) 13(1):112. doi: 10.1186/s13148-021-01096-4

22. Xu W, Zhu W, Tian X, Liu W, Wu Y, Anwaier A, et al. Integrative 5-methylcytosine modification immunologically reprograms tumor microenvironment characterizations and phenotypes of clear cell renal cell carcinoma. *Front Cell Dev Biol* (2021) 9:772436. doi: 10.3389/fcell.2021.772436

23. Fu F, Tao X, Jiang Z, Gao Z, Zhao Y, Li Y, et al. Identification of germline mutations in East-Asian young never-smokers with lung adenocarcinoma by whole-exome sequencing. *Phenomics*. (2022) [ahead of print]. doi: 10.1007/s43657-022-00062-1

24. Jung H, Kim HS, Kim JY, Sun JM, Ahn JS, Ahn MJ, et al. DNA Methylation loss promotes immune evasion of tumours with high mutation and copy number load. *Nat Commun* (2019) 10(1):4278. doi: 10.1038/s41467-019-12159-9

25. Xu W, Anwaier A, Liu W, Tian X, Su J, Shi G, et al. The unique genomic landscape and prognostic mutational signature of Chinese clear cell renal cell carcinoma. *J Natl Cancer Center* (2022) 2(3):162–70. doi: 10.1016/j.jncc.2022.07.001

26. Zhao J, Xu H, Su Y, Pan J, Xie S, Xu J, et al. Emerging regulatory mechanisms of N6-methyladenosine modification in cancer metastasis. *Phenomics*. (2022) [ahead of print]. doi: 10.1007/s43657-021-00043-w

27. Cao J, Yang X, Li J, Wu H, Li P, Yao Z, et al. Screening and identifying immune-related cells and genes in the tumor microenvironment of bladder urothelial carcinoma: Based on TCGA database and bioinformatics. *Front Oncol* (2019) 9:1533. doi: 10.3389/fonc.2019.01533

28. Huang DW, Sherman BT, Tan Q, Collins JR, Alvord WG, Roayaei J, et al. The DAVID gene functional classification tool: a novel biological module-centric algorithm to functionally analyze large gene lists. *Genome Biol* (2007) 8(9):R183. doi: 10.1186/gb-2007-8-9-r183

29. Ashburner M, Ball CA, Blake JA, Botstein D, Butler H, Cherry JM, et al. Gene ontology: tool for the unification of biology. the gene ontology consortium. *Nat Genet* (2000) 25(1):25–9. doi: 10.1038/75556

30. Franceschini A, Szklarczyk D, Frankild S, Kuhn M, Simonovic M, Roth A, et al. STRING v9.1: protein-protein interaction networks, with increased coverage and integration. *Nucleic Acids Res* (2013) 41(Database issue):D808–15. doi: 10.1093/nar/gks1094

31. Smoot ME, Ono K, Ruscheinski J, Wang PL, Ideker T. Cytoscape 2.8: new features for data integration and network visualization. *Bioinformatics.* (2011) 27 (3):431–2. doi: 10.1093/bioinformatics/btq675

32. Bandettini WP, Kellman P, Mancini C, Booker OJ, Vasu S, Leung SW, et al. MultiContrast delayed enhancement (MCODE) improves detection of subendocardial myocardial infarction by late gadolinium enhancement cardiovascular magnetic resonance: a clinical validation study. *J Cardiovasc Magn Reson* (2012) 14:83. doi: 10.1186/1532-429X-14-83

33. Tang Z, Li C, Kang B, Gao G, Li C, Zhang Z. GEPIA: a web server for cancer and normal gene expression profiling and interactive analyses. *Nucleic Acids Res* (2017) 45(W1):W98–W102. doi: 10.1093/nar/gkx247

34. Subramanian A, Tamayo P, Mootha VK, Mukherjee S, Ebert BL, Gillette MA, et al. Gene set enrichment analysis: a knowledge-based approach for interpreting genome-wide expression profiles. *Proc Natl Acad Sci U S A* (2005) 102(43):15545–50. doi: 10.1073/pnas.0506580102

35. Xu W, Wu Y, Liu W, Anwaier A, Tian X, Su J, et al. Tumor-associated macrophage-derived chemokine CCL5 facilitates the progression and immunosuppressive tumor microenvironment of clear cell renal cell carcinoma. *Int J Biol Sci* (2022) 18(13):4884–900. doi: 10.7150/ijbs.74647

36. Lu X, Li C, Xu W, Wu Y, Wang J, Chen S, et al. Malignant tumor purity reveals the driven and prognostic role of CD3E in low-grade glioma microenvironment. *Front Oncol* (2021) 11:676124. doi: 10.3389/fonc.2021.676124

37. Xu W, Ma C, Liu W, Anwaier A, Tian X, Shi G, et al. Prognostic value, DNA variation and immunologic features of a tertiary lymphoid structure-related chemokine signature in clear cell renal cell carcinoma. *Cancer Immunol Immunother* (2022) 71(8):1923–35. doi: 10.1007/s00262-021-03123-y

38. Chaudhuri S, Thomas S, Munster P. Immunotherapy in breast cancer: A clinician's perspective. *J Natl Cancer Center* (2021) 1(2):47–57. doi: 10.1016/j.jncc.2021.01.001

39. Zhang T. Immune checkpoint inhibitors in extensive-stage small cell lung cancer. *J Natl Cancer Center* (2022) 2(3):130–1. doi: 10.1016/j.jncc.2022.07.003

40. Konala VM, Adapa S, Aronow WS. Immunotherapy in bladder cancer. *Am J Ther* (2022) 29(3):e334–7. doi: 10.1097/MJT.0000000000000934

41. Lee SH, Hu W, Matulay JT, Silva MV, Owczarek TB, Kim K, et al. Tumor evolution and drug response in patient-derived organoid models of bladder cancer. *Cell.* (2018) 173(2):515–528.e17. doi: 10.1016/j.cell.2018.03.017

42. Dunn BK, Woloshin S, Kramer BS, Xie H. Cancer overdiagnosis: A challenge in the era of screening. *J Natl Cancer Center* (2022) in press. doi: 10.1016/j.jncc.2022.08.005

43. Gao X, Zhao N, Dong L, Zheng X, Zhang Y, Ding C, et al. A novel lipid prognostic signature of ADCY2, LIPE, and OLR1 in head and neck squamous cell carcinoma. *Front Oncol* (2021) 11:735993. doi: 10.3389/fonc.2021.735993

frontiers | Frontiers in Immunology

TYPE Original Research
PUBLISHED 21 November 2022
DOI 10.3389/fimmu.2022.1020729

OPEN ACCESS

EDITED BY
Wen-Hao Xu,
Fudan University, China

REVIEWED BY
Shi Jian,
Huazhong University of Science and Technology, China
Wangrui Liu,
Shanghai Jiao Tong University, China
Ning Zhang,
Beijing Cancer Hospital, Peking University, China
Wen Xiao,
Huazhong University of Science and Technology, China

*CORRESPONDENCE
Yanqing Gong
yqgongbjmu@163.com

SPECIALTY SECTION
This article was submitted to Cancer Immunity and Immunotherapy, a section of the journal Frontiers in Immunology

RECEIVED 16 August 2022
ACCEPTED 01 November 2022
PUBLISHED 21 November 2022

CITATION
Zhang C, Li Y, Qian J, Zhu Z, Huang C, He Z, Zhou L and Gong Y (2022) Identification of a claudin-low subtype in clear cell renal cell carcinoma with implications for the evaluation of clinical outcomes and treatment efficacy. *Front. Immunol.* 13:1020729. doi: 10.3389/fimmu.2022.1020729

Identification of a claudin-low subtype in clear cell renal cell carcinoma with implications for the evaluation of clinical outcomes and treatment efficacy

Cuijian Zhang[1,2,3], Yifan Li[1,2,3], Jinqin Qian[1,2,3], Zhenpeng Zhu[1,2,3], Cong Huang[1,2,3], Zhisong He[1,2,3], Liqun Zhou[1,2,3] and Yanqing Gong[1,2,3]*

[1]Department of Urology, Peking University First Hospital, Beijing, China, [2]Institute of Urology, Peking University, Beijing, China, [3]National Urological Cancer Center, Peking University First Hospital, Beijing, China

Background: In bladder and breast cancer, the claudin-low subtype is widely identified, revealing a distinct tumor microenvironment (TME) and immunological feature. Although we have previously identified individual claudin members as prognostic biomarkers in clear cell renal cell carcinoma (ccRCC), the existence of an intrinsic claudin-low subtype and its interplay with TME and clinical outcomes remains unclear.

Methods: Transcriptomic and clinical data from The Cancer Genome Atlas (TCGA)- kidney clear cell carcinoma (KIRC) cohort and E-MTAB-1980 were derived as the training and validation cohorts, respectively. In addition, GSE40435, GSE53757, International Cancer Genome Consortium (ICGC) datasets, and RNA-sequencing data from local ccRCC patients were utilized as validation cohorts for claudin clustering based on silhouette scores. Using weighted correlation network analysis (WGCNA) and multiple machine learning algorithms, including least absolute shrinkage and selection operator (LASSO), CoxBoost, and random forest, we constructed a claudin-TME related (CTR) risk signature. Furthermore, the CTR associated genomic characteristics, immunity, and treatment sensitivity were evaluated.

Results: A claudin-low phenotype was identified and associated with an inferior survival and distinct TME and cancer immunity characteristics. Based on its interaction with TME, a risk signature was developed with robust prognostic prediction accuracy. Moreover, we found its association with a claudin-low, stem-like phenotype and advanced clinicopathological features. Intriguingly, it was also effective in kidney chromophobe and renal papillary cell carcinoma. The high CTR group exhibited genomic characteristics similar to those of claudin-low phenotype, including increased chromosomal instability (such as

10.3389/fimmu.2022.1020729

deletions at 9p) and risk genomic alterations (especially *BAP1* and *SETD2*). In addition, a higher abundance of CD8 T cells and overexpression of immune checkpoints, such as LAG3, CTLA4 and PDCD1, were identified in the high CTR group. Notably, ccRCC patients with high CTR were potentially more sensitive to immune checkpoint inhibitors; their counterparts could have more clinical benefits when treated with antiangiogenic drugs, mTOR, or HIF inhibitors.

Conclusion: We comprehensively evaluated the expression features of claudin genes and identified a claudin-low phenotype in ccRCC. In addition, its related signature could robustly predict the prognosis and provide guide for personalizing management strategies.

KEYWORDS

clear cell renal cell carcinoma (ccRCC), claudin, tumor microenvironment, immunity, prognosis, immune checkpoint inhibitor (ICI)

1 Introduction

Renal cell carcinoma (RCC) is the third most prevalent genitourinary cancer worldwide, with an estimated 431,288 new cases diagnosed in 2020 (1). More than 70% of RCC cases are histologically classified as clear cell RCC (ccRCC), and approximately 65% of them are localized and can be treated with surgical resection in the form of partial or radical nephrectomy (2). However, nearly 20–40% of ccRCC patients may experience disease recurrence or develop metastases (3). Multiple prognostic models have been established and clinically verified to improve patient management, such as the UCLA Integrated Staging System (UISS), Leibovich score 2003/2018, VENUSS score, and GRANT score (4). However, these models are mainly based on traditional clinical and pathological variables and present with heterogeneous predictive accuracy according to the pathological characteristics (5). In the meantime, significant breakthroughs have been made in the past two decades, such as introducing vascular endothelial growth factor tyrosine kinase inhibitors (VEGFR TKIs), mammalian target of rapamycin (mTOR) inhibitors, and particularly immune checkpoint inhibitors (ICIs) to better manage patients with ccRCC. However, even when applying the most effective immune combination therapy, clinical benefits are limited to a certain section of patients (6). Thus, there is an urgent need to develop novel and powerful prognostic prediction biomarkers for both risk and treatment stratification.

Claudins are the backbone of the tight junction complex, which includes a group of proteins 20–34 kDa in size and a structure similar to that of a short cytoplasmic N-terminal region, two extracellular loops formed by four transmembrane domains, and a cytoplasmic C-terminal tail (7). To date, 24 claudin family members, which are commonly downregulated in tumor tissues, have been identified; however, their roles in the regulation of the development of different types of cancer are heterogeneous (8). In a previous study, we found that claudin 7 is a tumor suppressor in ccRCC, and hypermethylation of its promoter or its downregulation facilitates epithelial-mesenchymal transition (EMT) and tumor progression (9). Other claudin members, including claudin-2 (10), claudin-4 (11), claudin-5 (12), and claudin-8 (13), have been investigated in ccRCC as an individual prognostic biomarker, respectively. It is noteworthy that all previous studies were focused on a single member of claudin; thus, little is known about the comprehensive expression profile of claudin family members in ccRCC.

Meanwhile, claudin-low subtype has been widely recognized as a novel intrinsic subtype in both breast and bladder cancer, exhibiting aggressive, distinct biological and clinical behaviors (14). Previous studies have depicted its correlation with EMT and stemness in the tumor, revealing its origin and evolution (15). More importantly, increasing evidence supports the interaction between claudin phenotype and the immune profile of tumors. For instance, bladder or breast tumors with subtype classification based on claudin expression showed distinct immune features, characterized by different levels of tumor-infiltrating immune cells and expression of immune checkpoints such as programmed death-ligand 1 (PD-L1) (16, 17). These features may further contribute to a better response to immune checkpoint inhibitors (ICIs) (18). However, to the best of our knowledge, there was no study on the claudin-low phenotype in ccRCC and whether there is a correlation between claudin, cancer immunity and prognosis in patients with ccRCC remains elusive.

In this study, we sought to analyze the comprehensive landscape of the expression of claudin family members in ccRCC and mainly focused on the interaction between claudin expression features and immunity. Subsequently, a prognostic prediction signature was developed based on candidate claudin-immune genes, and its correlation with precision medicine including targeted therapy and ICIs was explored.

2 Materials and methods

2.1 Study design

The schematic workflow is shown in Figure 1.

2.2 Data retrieval and preprocessing

The RNA-sequencing (RNA-seq) and clinical data of 530 ccRCC samples (and 72 adjacent nontumor tissues) were downloaded from The Cancer Genome Atlas (TCGA)-kidney clear cell carcinoma (KIRC) cohort *via* the cbioportal website (https://www.cbioportal.org). The mRNA expression profile and clinical data of E-MTAB-1980 with 101 samples were downloaded from the ArrayExpress database (https://www.ebi.ac.uk/arrayexpress/) and used as the validation cohort for survival analysis. GSE40435 (tumor vs. normal tissue: 101 vs. 101), GSE53757 (72 vs. 72), and the International Cancer Genome Consortium (ICGC) (91 vs. 45) datasets were used as validation cohorts for claudin clustering and identify the differences in differentially expressed genes between tumor and normal kidney tissues.

2.3 RNA sequencing in the local ccRCC patients

Tumor and matched normal tissues were collected from 20 ccRCC patients in our local cohort to perform RNA-seq. This study was approved by the Biomedical Research Ethics Committee of Peking University First Hospital (approval no. 2015-977) and written informed consent was obtained from all the patients. Clinicopathological data of the 20 enrolled patients are presented in Supplementary Table 1. Before RNA extraction, the tissue was evaluated for tumor cell content and percentage, and only those with a tumor purity of at least 20% based on histopathological analysis were eligible for RNA extraction and sequencing. Total RNA from each sample was collected using a FastPure® Cell/Tissue Total RNA Isolation Kit V2 (Vazyme, Jiangsu, China), and the RNA concentration and RNA integrity number (RIN) were measured using a Qubit (Thermo Fisher Scientific, MA, United States) and an Agilent 2100 bioanalyzer (Agilent Technologies, CA, United States), respectively. Library construction was performed using the NEBNext® Ultra™ RNA Library Prep Kit for Illumina® Kit (NEB, MA, United States) and sequenced on the Illumina Novaseq-6000 system (Illumina, MA, United States).

2.4 Cluster of claudin expression profile in ccRCC

We calculated the similarity of claudin family gene expression in ccRCC samples in the TCGA-KIRC database using R package "factoextra" and the silhouette scores were obtained based on the assigned clusters. The optimal number of

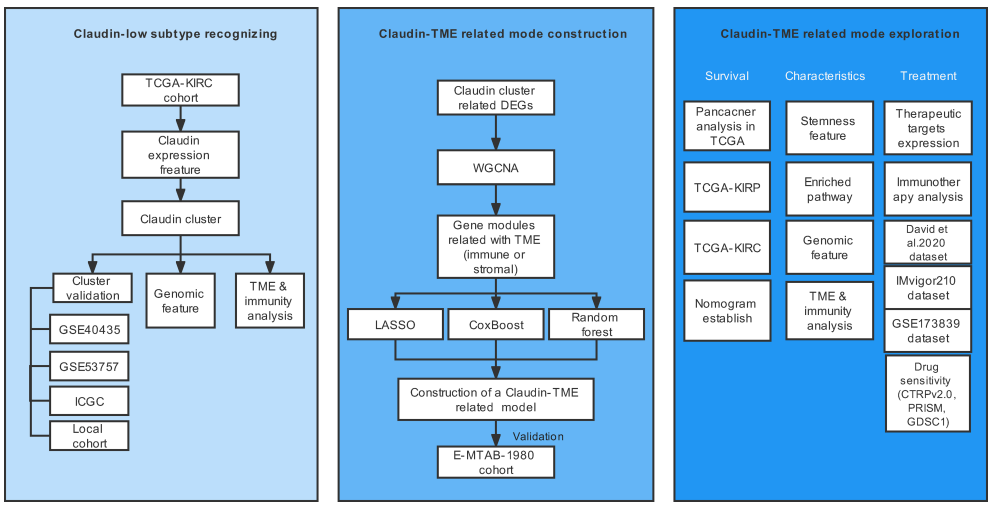

FIGURE 1
Overview of the study design. TME: tumor microenvironment.

clusters in each cohort was determined using the silhouette width.

2.5 Differentially expressed genes and weighted gene co-expression network analysis

DEGs with a threshold of $\log_2$(FoldChange) > 0.585 and adjusted $p < 0.05$ were identified using the R package "limma". DEGs between claudin clusters were collected for WGCNA using the R package "WGCNA". The appropriate power value was determined when the scale independence was > 0.85 with a relatively higher connectivity degree. When the scale independence was > 0.85 and the connectivity degree was relatively higher, the appropriate power value was determined. Genes were then sorted into several gene modules based on topological overlap matrix (TOM)-based dissimilarities. Finally, the dynamic modules were merged according to a cut-off value of 0.25 and five modules were obtained. Gene modules with correlation coefficient > 0.5 with immune and/or stromal scores, were recognized as tumor microenvironment (TME)-related gene modules.

2.6 Stromal and immune score analysis

Estimation of stromal and immune cells in malignant tumor tissues using expression data (ESTIMATE) algorithm depicts the level of tumor-infiltrating immune cells, stromal cells, and tumor purity in the form of immune score, stromal score, and ESTIMATE score, respectively (19). The stromal and immune scores of each sample were calculated using the R package "ESTIMATE".

2.7 Construction of a novel claudin-TME related prognostic prediction signature

Hub genes screened out in the TME gene module determined by WGCNA were then inputted into three machine learning algorithms, including least absolute shrinkage and selection operator (LASSO) regression analysis (R package "glmnet," version 4.1-4), CoxBoost (R package "CoxBoost," version 1.5) and random forest (R package "randomForestSRC," version 3.1.0). We chose to use three algorithms as opposed to only one to reduce the risk of bias, and the overlapping hub genes shared by all of them were selected to construct a risk signature. The CTR prognostic prediction was developed using the following formula:

$$CTR\ \ score = \sum_i \text{Coefficient of (Gene } i\text{)} \times \text{Expression of (Gene } i\text{)}$$

The patients in each cohort were dichotomized into high- and low-risk groups based on the median CTR score. A time-dependent receiver operating characteristic (ROC) curve was applied to analyze the predictive accuracy of CTR signature in the training and validation cohorts.

2.8 TME and immune profile analysis

Tumor-infiltrating immune cell profiles were comprehensively analyzed using seven different algorithms, including CIBERSOFTX (20), Microenvironment Cell Populations (MCP)-counter (21), tumor immune estimation resource (TIMER2.0) (22), and xCell (23). The seven steps involved in the cancer-immune cycle in each sample, starting from the release of cancer cell antigens to the killing of cancer cells, was evaluated using single-sample gene set enrichment analysis (ssGSEA) (24).

2.9 Stemness feature analysis

Tumor stem cell-like features (stemness) were indicated as the mRNA expression-based stemness index (mRNAsi), which was calculated using the method described by Malta et al. (25)

2.10 Genomic profile analysis

Genetic alterations were analyzed using the "maftools" package in the TCGA-KIRC database. Comparison of the prevalence of genomic alterations in certain genes was conducted between high and low CTR groups using Fisher's exact test, and only those genes with a prevalence of over 3% in at least one group were included.

2.11 Comparison with other risk models of ccRCC

Thirteen previously defined risk models for ccRCC were identified through the PubMed database (26–38), and the risk score for each model was determined based on the algorithm provided in the corresponding published study. The details are listed in Supplementary Table 2. Differences in area under the ROC curve (AUC) for survival at 1–5 years and the concordance index (C-index) were compared between the CTR score and these 13 risk models in the TCGA-KIRC dataset based on a bootstrap resampling method.

2.12 Nomogram construction

Univariate and multivariate Cox regression analyses were performed on clinicopathological variables, including age, sex, neoplasm histologic grade, neoplasm disease stage, tumor,

nodes, and metastases (TNM) stage, and risk score in the TCGA-KIRC database. Variables were integrated to establish a nomogram using the "rms" R package.

2.13 Treatment sensitivity analysis

2.13.1 Evaluation of the expression of therapeutic targets in ccRCC

A comprehensive evaluation of the difference in the expression level of the target of Food and Drug Administration (FDA)-approved drugs, including ICIs (anti-CTLA4 and anti-PD-1/PD-L1), antiangiogenic therapy (bevacizumab, and targeted therapies including sunitinib, pazopanib, axitinib, cabozantinib, lenvatinib, tivozanib, and sorafenib), mTOR inhibitors (everolimus and temsirolimus), and hypoxia-inducible factor 2α (HIF2A) inhibitor (belzutifan) between the high- and low-risk groups was performed. Matched drug-target information was retrieved from the DrugBank website (https://go.drugbank.com/). The Cancer Dependency Map (DepMap) portal (https://depmap.org/portal/) was used to evaluate the drug sensitivity of therapeutic targets from three databases (CTRPv2.0, PRISM, and GDSC1). Lower AUC values for the agents indicated a higher drug sensitivity.

2.13.2 ICI

The clinical and gene expression profiles of ccRCC patients treated with nivolumab in the CheckMate 025, 010, and 009 trials were derived from the dataset published by David et al. (39) The clinical response and genomic data from the IMvigor210 cohort (28) and GSE173839 dataset (40) were analyzed for differences in clinical benefits from ICI based on stratification using the CTR score. The criteria for treatment responses were defined as follows: CR: complete response, PR: partial response, SD: stable disease, and PD: progressive disease.

2.14 Statistical analysis

All statistical analyses were performed using the R software (version 4.1.2). Kaplan-Meier curves and log-rank tests were used to analyze the survival differences between categorical variables in each cohort. Spearman correlation coefficients were analyzed to explore the correlations between different variables. Chi-squared test or Fisher's exact test were used to compare the differences in categorical variables. Statistical significance was defined as a two-sided p value< 0.05.

3 Results

3.1 Claudin expression pattern in ccRCC

An overview of the expression features of all the claudin family genes in three kinds of kidney cancer revealed that nearly all the genes were downregulated in ccRCC tumors (Supplementary Figure 1A), with the exception of claudin 18 in ccRCC. However, the predictive function of each claudin member was inconsistent (Supplementary Figure 1B), highlighting the need for integrative research. As more claudin genes influenced patient survival in ccRCC, we focused our investigational study on this histological type. Based on the comprehensive expression profiles of claudin family genes, we identified two distinct claudin expression clusters in the TCGA-KIRC dataset (Figure 2A). To validate whether the clustering numbers were comprehensively optimal, we utilized the GSE40435, GSE53757, and ICGC datasets, and local ccRCC samples to evaluate the similarity of the expression of claudin family members and confirmed that clustering by two had the highest average silhouette width in all three datasets (Supplementary Figure 2A). Interestingly, a comparison of the difference in each claudin gene between these two clusters showed that cluster 1 also exhibited a notable claudin-low feature, characterized by an overall lower expression level of claudin genes (Figure 2B). Twenty-two percent (121/530) of ccRCC patients belonged to cluster 1, which had significantly inferior overall survival (Figure 2C), and more patients with advanced neoplasm histologic grades and/or stages were present in this cluster (Supplementary Table 3). This claudin-low feature in cluster 1 was also validated in other datasets and samples from local ccRCC patients (Supplementary Figure 2B). Altogether, 2806 DEGs were identified between these two clusters (Supplementary Table 4), which were mainly enriched in multiple cell signaling, transduction, metabolism, and particularly the immune regulation pathways, including leukocyte transendothelial migration and T cell receptor signaling pathways (Figures 2D, E). Two clusters revealed distinct genomic features (Figures 2F, G): *VHL* and *PBRM1* were significantly more prevalent in cluster 2; whereas genes including *MUC17*, *TP53*, *MEGF10* were more mutated in cluster 1. In addition, cluster 1 showed significantly increased chromosomal instability, as evidenced by growing deletions at 9p23, 9p21, 8p23, and 8p21, as well as amplifications at 3q26.33 and 3q36.2 (Figure 2H).

3.2 Claudin expression cluster and tumor microenvironment in ccRCC

As previous studies have suggested a correlation between the claudin-low phenotype and increasing levels of immune and stromal cell infiltration in breast cancer (41), we then evaluated the interaction between claudin expression features and TME profiles in ccRCC. The claudin-low related cluster (cluster 1) was associated with changes in multiple immunomodulators (Figures 3A, B), with significant downregulation of major histocompatibility complex (MHC) molecules, which revealed the association between claudin-low feature and blockade of the

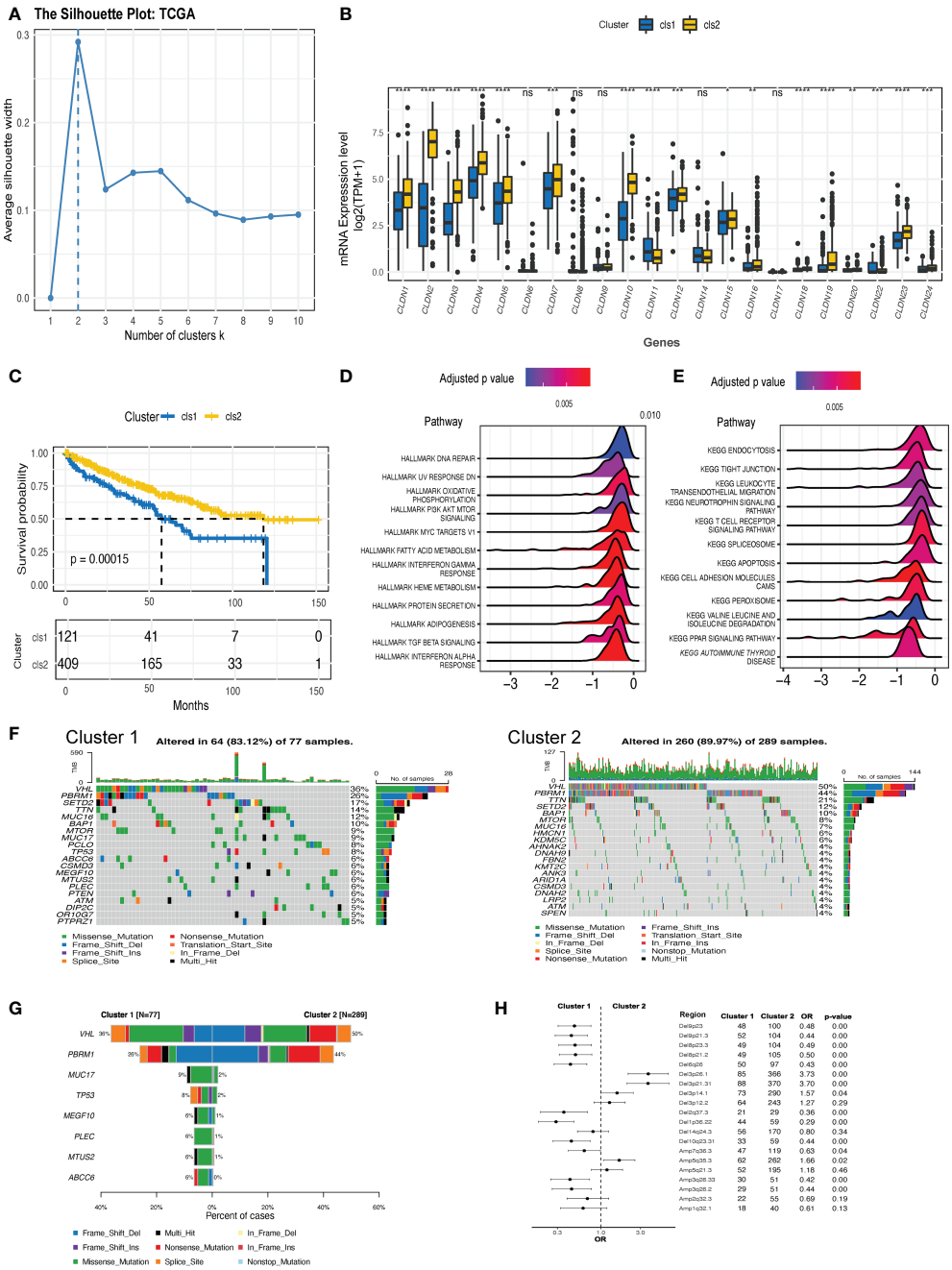

FIGURE 2
The expression clusters of claudin genes in ccRCC. **(A)** Silhouette clustering analysis in The Cancer Genome Atlas-kidney clear cell carcinoma (TCGA-KIRC) cohort. **(B)** The difference in the expression level of each claudin gene between clusters 1 and 2. **(C)** Kaplan–Meier estimates of the difference in the overall survival between cluster 1 and cluster 2. Hallmark **(D)** and Kyoto Encyclopedia of Genes and Genomes (KEGG) **(E)** pathways analysis revealed the pathways significantly enriched in the differentially expressed genes (DEGs) between the two clusters. **(F)** Oncoprints of the top 20 prevalent genes in cluster 1 (left) and cluster 2 (right). **(G)** Genes with significantly differed prevalence in cluster 1 or cluster 2. Only genes with a prevalence of over 3% in at least one cluster were analyzed. **(H)** Difference in the prevalence of copy number variants (CNV) between clusters 1 and 2. OR value below 1 is indicated as more prevalent in cluster 1. Del, deletion; Amp, amplification; OR, odds ratio; TPM, transcript per million. *p<0.05, **p<0.01, ***p<0.001, ****p<0.0001. ns, not significant.

10.3389/fimmu.2022.1020729

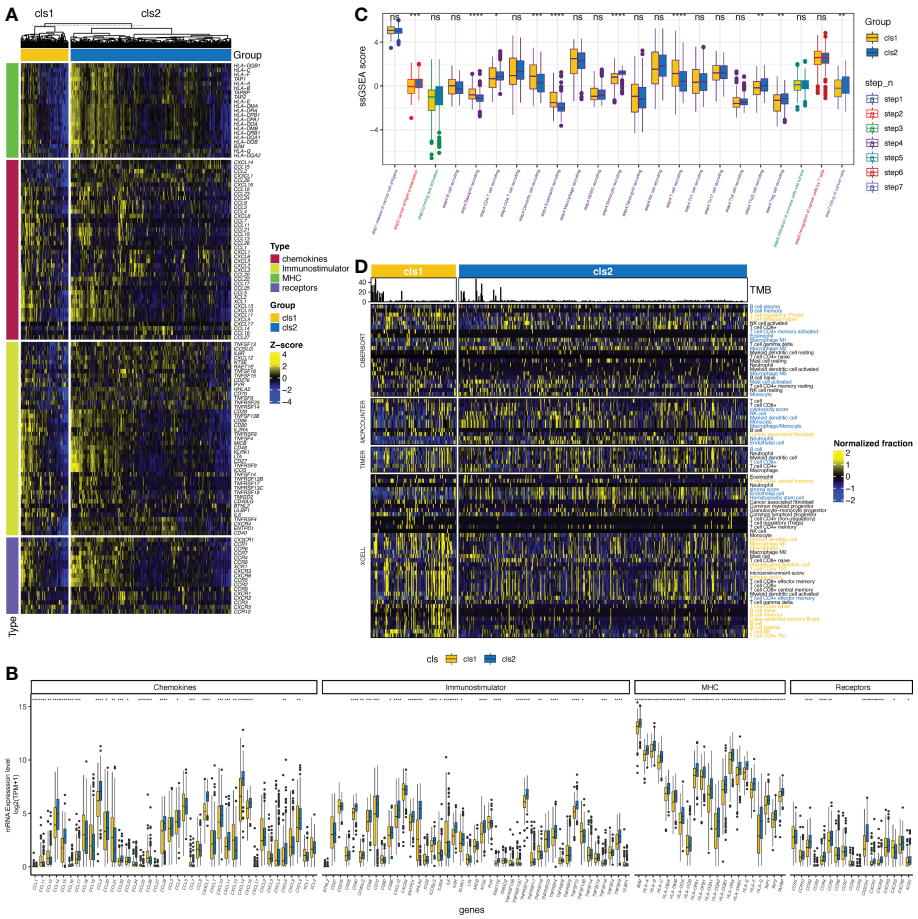

FIGURE 3
Claudin expression cluster and tumor microenvironment in ccRCC. **(A)** Difference in the expression of regulators of tumor immunology, including chemokines and their receptors, major histocompatibility complex (MHC), and immunostimulators between the two clusters in The Cancer Genome Atlas (TCGA)- kidney clear cell carcinoma (TCGA-KIRC) cohort. **(B)** Bar plot shows the difference of the expression of regulators of tumor immunology between two clusters. **(C)** Differences in the activity of seven steps of the cancer-immunity cycle between clusters. **(D)** Analysis of the difference in the tumor-infiltrated immune cells (TIICs) between the two clusters using multiple computational algorithms, including CIBERSOFT, MPCOUNTER, TIMER, and XCELL. TIICs with yellow color were significantly more enriched in cluster 1, whereas those with blue color were more enriched in cluster 2 (p< 0.05). *p< 0.05, **p< 0.01, ***p< 0.001, ****p< 0.0001, ns, not significant; TPM, transcript per million; ssGSEA, single-sample gene set enrichment analysis.

antigen presentation process (Figures 3A, B). Chemokines and their receptors, as well as immune stimulators, were also heterogeneous between these two clusters, and most of them were downregulated in cluster 1. As shown in Figure 3C, there was no significant difference in the release of cancer cell antigens (step 1), but after the cancer antigen presentation process (step 2), the two clusters began to differ in the activity of cancer immunity. Cancer antigen presentation was downregulated in cluster 1, as well as in CD4 T cells, Th22 cells, monocytes, and Treg cells (step 3). However, cluster 1 showed significantly upregulated levels of T cells, dendritic cells, eosinophils, and basophils. Finally, all these differences contributed to a reduced killing of the cancer cells (step 7) in cluster 1. Furthermore, by applying multiple algorithms, we found a distinct feature in tumor-infiltrating immune cells (TIICs) between these two clusters (Figure 3D), including an increase in Treg cells but a decrease in B cells. Even though different algorithms gave discordant results, there was a concordant difference in the levels of B cells, macrophages, and CD4 T cells between the two clusters.

3.3 Construction of a claudin-TME related risk signature

Next, we applied WGCNA to distinguish co-expressed gene modules within cluster-related genes. After 10 was determined as the optimal soft threshold (Figure 4A), five co-expressed gene

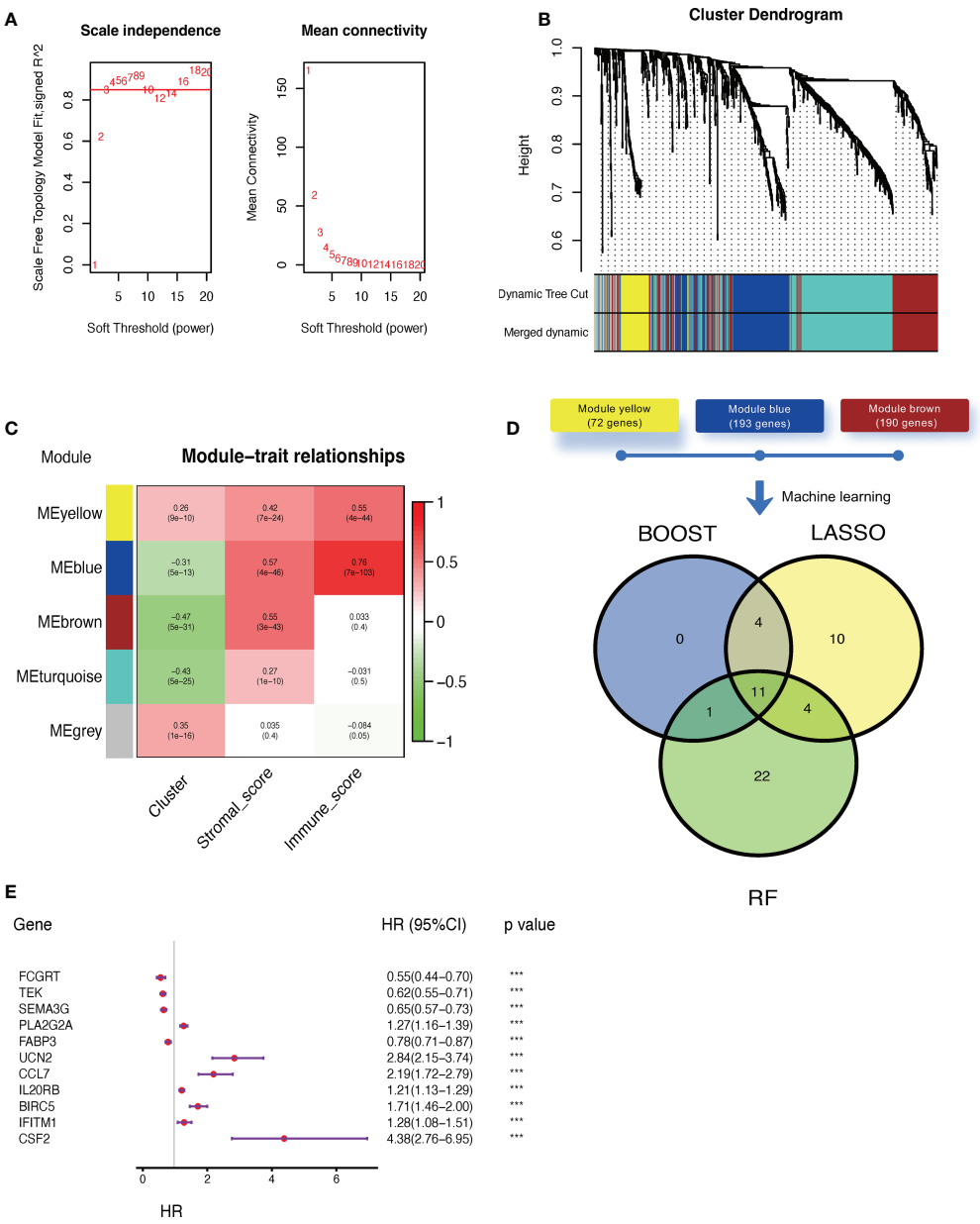

FIGURE 4
Construction of a claudin-TME related (CTR) risk signature. **(A)** Analysis of the scale-free fit index (left) and mean connectivity (right) for different soft-thresholding (power) values (numbers colored with red). **(B)** Gene clustered dendrogram based on dissimilarity measure (1-topological overlap matrix (TOM)) with defined module colors. **(C)** Heatmap of the correlations between module genes and cluster, stromal, or immune scores. **(D)** Venn plot showing the overlapping genes selected by three machine learning algorithms: CoxBoost, least absolute shrinkage and selection operator (LASSO), and random forest (RF). **(E)** Forest plot of hazard ratios for selected key genes in the Cancer Genome Atlas -kidney clear cell carcinoma (TCGA-KIRC) dataset. ***p< 0.001. HR: hazard ratio. 95% CI: 95% confidence interval.

modules were identified (Figure 4B). As depicted in Figure 4C, module yellow (containing 72 genes), module blue (193 genes), and module brown (190 genes) were strongly correlated with stromal and/or immune scores. Genes within these three modules were then selected to be used in constructing the model (Supplementary Table 5). Then, three algorithms, including CoxBoost, LASSO, and random forest (RF) were applied and the c-index was 0.77, 0.72 and 0.82, respectively. Even though they all had satisfied prediction capacity, we integrated them to eliminate the any potential bias in a single machine learning algorithm. Finally, 11 key genes were screened out by all three algorithms (Figure 4D;, Supplementary Table 6),

of which only four were suggested as tumor suppressor genes while the rest were associated with worse outcomes in ccRCC (Figure 4E). The final claudin-TME risk signature was as follows: $\text{CTR score} = 0.3518\times EXP_{CSF2} - 0.3948\times EXP_{FCGRT} - 0.3519\times EXP_{TEK} - 0.0502\times EXP_{SEMA3G} + 0.0775\times EXP_{PLA2G2A} - 0.0513\times EXP_{FABP3} + 0.2117\times EXP_{UCN2} + 0.2910\times EXP_{CCL7} + 0.0608\times EXP_{IL20RB} + 0.0977\times EXP_{BIRC5} + 0.3381\times EXP_{IFITM1}$.

3.4 Evaluation and validation of the prognostic predictive accuracy of CTR signature

Based on the median CTR score, ccRCC patients in the training cohort were dichotomized into high- or low-risk groups, and patients with high-risk scores had significantly inferior clinical outcomes (Figure 5A). The AUC of the CTR score for predicting survival at 1-, 2-, 3-, 4-, and 5- year was 0.81, 0.78, 0.78, 0.77, and 0.77, respectively (Figure 5B). The prognostic predictive accuracy of the CTR signature was also verified in the validation cohort (Figure 5C), which showed a robust predictive capacity (AUC values were all above 0.80) for survival at 1–5 year (Figure 5D). Moreover, when compared to previously published ccRCC prognostic models, we discovered that the CTR signature outperformed them in prognostic prediction of the TCGA-KIRC cohort with a significantly greater C-index (Figure 5E). Meanwhile, combined univariate and multivariate Cox regression analyses showed that the CTR score was the only significant independent risk factor for prediction survival in the TCGA-KIRC dataset (Figure 5F). Interestingly, male patients, those with advanced disease stages, and those > 60 years of age had significantly higher CTR scores (Figure 5G). In stratification by a variety of clinicopathological variables, the CTR score consistently distinguished ccRCC patients with a poor prognosis (Figure 5H). Notably, even among patients with early stage disease, the CTR score was still able to identify those with worse outcomes.

3.5 Exploration of CTR score in pan-cancer

We then investigated the prognostic value of the CTR score in pan-cancer datasets from TCGA. Higher CTR scores also indicated inferior outcomes in seven cancer types other than ccRCC, including kidney chromophobe (KICH), kidney renal papillary cell carcinoma (KIRP), uveal melanoma (UVM), thymoma (THYM), pancreatic adenocarcinoma (PAAD), brain low-grade glioma (LGG), and glioblastoma (GBM) (Figure 6A). In addition, kidney cancers, regardless of the histological type, had the lowest CTR scores when compared to other cancer types in the pan-cancer dataset (Figure 6B). We also evaluated the prediction accuracy of the CTR score for KIRP and KIRC to provide a deeper understanding of the prognostic prediction capacity of these two histological types (Figure 6C). The results revealed that the CTR score had a robust prediction accuracy in patients with kidney cancer, regardless of the histologic subtype. The claudin-low phenotype has been primarily explored in breast cancer; hence, we compared the distribution of CTR scores between claudin-low and other phenotypes in breast cancer (The Molecular Taxonomy of Breast Cancer International Consortium (METABRIC) dataset, Figure 6D). The lowest CTR score was found in the claudin-low subtype, especially when compared to the basal-like, human epidermal growth factor receptor 2 (HER2)-positive, and luminal B subtypes. Furthermore, the high CTR group had significantly higher mRNA expression-based stemness index (mRNAsi) scores, which indicated a stem cell-like feature in this group (Figure 6E).

3.6 Enrichment analysis of CTR score

Four CTR score-related genes that associated with improved survival were downregulated in kidney tumor tissues relative to normal tissues in both public datasets (Figure 7A) and local ccRCC samples (Figure 7B), with Fc gamma receptor and transporter (FCGRT) being the sole exception. In contrast, risk genes, except urocortin-2 (UCN2), were significantly upregulated in tumor tissues (Figures 7A, B). Moreover, 338 upregulated and 1716 downregulated DEGs were identified between the high and low CTR groups, and these DEGs were significantly enriched in cell metabolism (such as fatty acid metabolism), immune-related pathways (cytokine and transforming growth factor-β (TGF-β)), and cell-cell adhesion and tight junction pathways (tight junction, Figures 7C, D). The "claudin-low" characteristic of the high-risk groups was identical to the aforementioned cluster 1, with a generally lower expression level of claudin family genes (Figure 7E). Intriguingly, the expression of the four tumor suppressor genes (FCGRT, TEK, semaphorin 3G (SEMA3G), and fatty acid binding protein 3 (FABP3)) was significantly positively correlated with that of claudin genes, whereas the risk genes were shown to be negatively correlated with claudin genes, particularly claudins 2, 3, 4, 5, and 10 (Figure 7F). The majority of genes involved in increasing oxygen delivery and reducing oxygen consumption were downregulated in the high CTR group. Contrarily, the high CTR group had significantly higher enrichment scores in nearly all the immunotherapy-positive pathways (Figure 7H).

3.7 Genomic characteristics related to the CTR score

ccRCC tumors are characterized by distinct genomic features, especially the high prevalence of genomic alterations (GAs) in chromosome 3p (42). Hence, we investigated the differences in genomic profiling between the high- and low-risk groups. As depicted in the oncoprint plots in Figure 8A, the high and low CTR groups shared genomic features in highly

10.3389/fimmu.2022.1020729

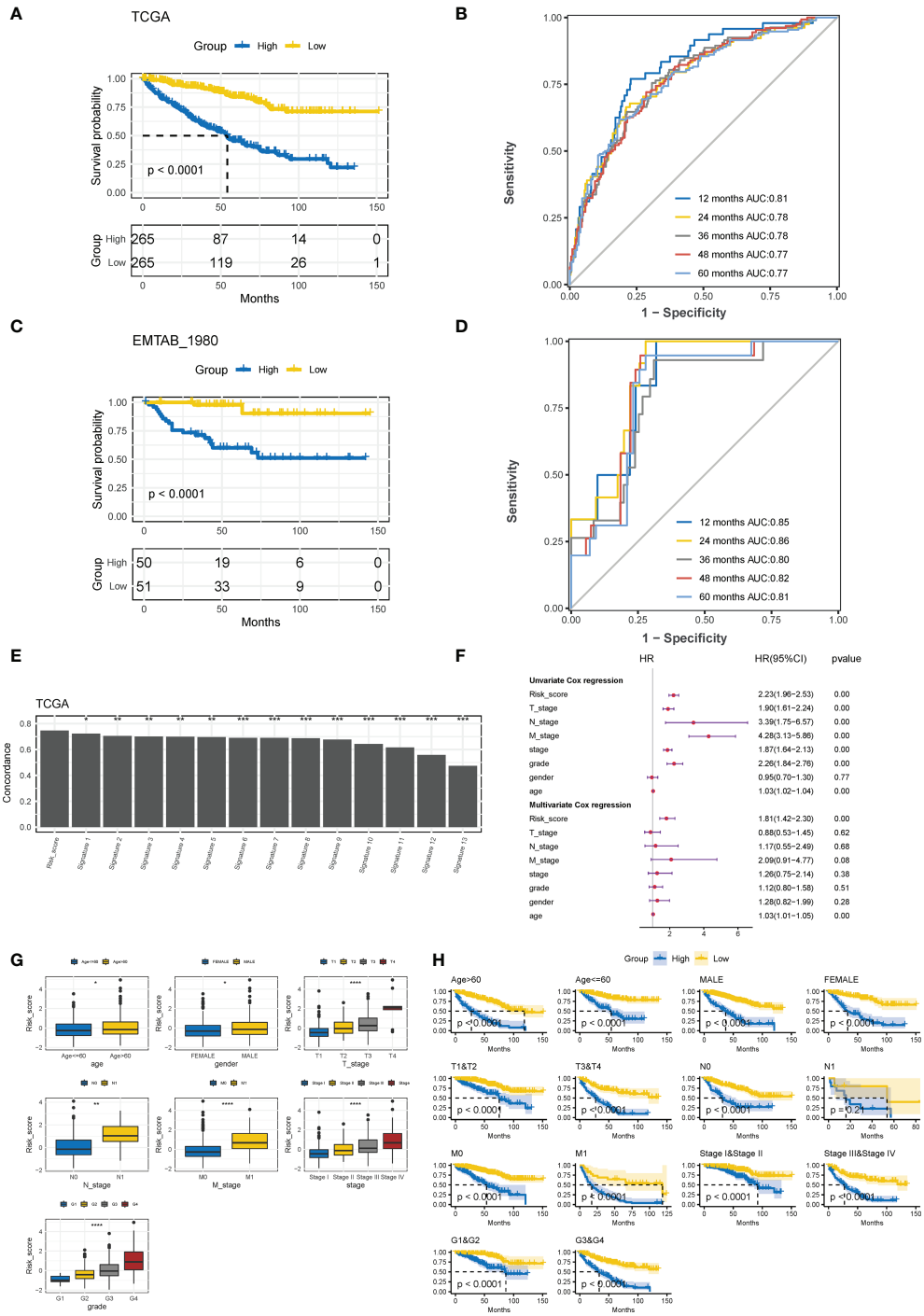

FIGURE 5
Evaluation and validation of prognostic predictive accuracy of CTR signature. **(A)** Kaplan–Meier survival analysis of the difference in the overall survival (OS) between ccRCC patients with high and low claudin-TME related (CTR) score in The Cancer Genome Atlas-kidney clear cell carcinoma (TCGA-KIRC) training cohort. Patients were dichotomized into high or low CTR groups based on the median CTR score. **(B)** Time-dependent receiver operating characteristic (ROC) curves at 1–5 years in the training cohort. **(C)** Kaplan–Meier estimates of the difference in the OS between ccRCC patients with high and low CTR scores in the validation cohort (E-MATAB-1980). Patients were also dichotomized into high or low CTR groups based on the median CTR score. **(D)** Time-dependent area under the ROC curve (AUC) value in the validation cohort. **(E)** Difference in the concordance index (C-index) between the Clinical Risk Groups (CTR) score and other previously reported prognostic models in TCGA-KIRC. **(F)** Forest plot of hazard ratios for CTR score and clinicopathologic variables in the TCGA-KIRC dataset. **(G)** Difference in the distribution of CTR scores between patients with different clinicopathologic variables. **(H)** Kaplan–Meier survival analysis of the CTR score stratified by different clinicopathologic feature. *p< 0.05, **p< 0.01, ***p< 0.001, ****p< 0.0001. CTR score, claudin-TME related risk score; AUC, area under curve; T, Tumor stage; N node stage; M, metastasis stage; Grade, Neoplasm Histologic Grade; Stage, Neoplasm Disease Stage.

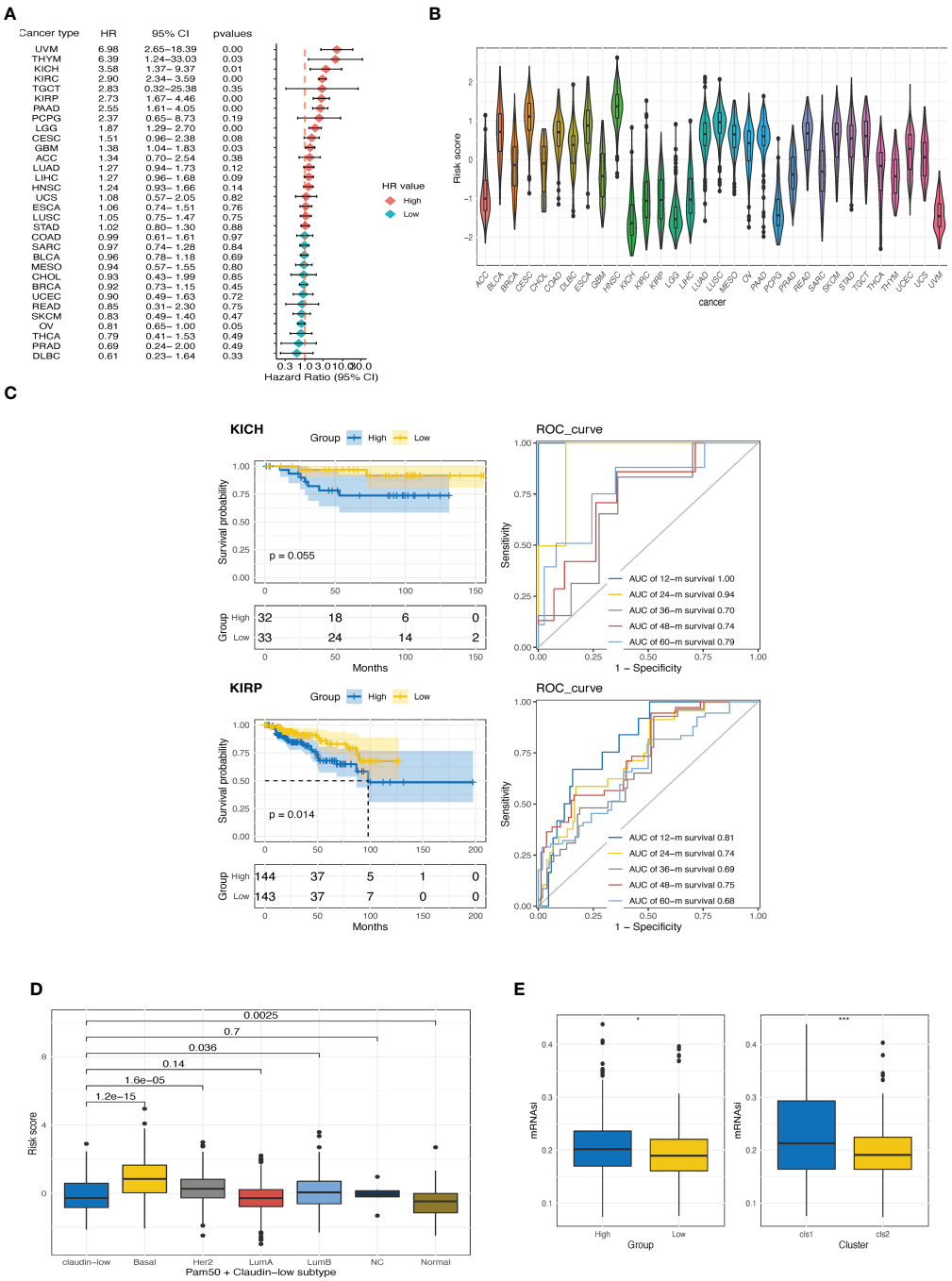

FIGURE 6
Exploration of CTR score in pan-cancer. **(A)** Forest plot of hazard ratios (HR) for the claudin-TME related (CTR) score in pan-cancers datasets from The Cancer Genome Atlas (TCGA) cohort. **(B)** Distribution of CTR scores among pan-cancers. **(C)** Kaplan–Meier curves and time-dependent area under the curve (AUC) value in the TCGA-kidney chromophobe (KICH) (upper) and TCGA-kidney renal papillary cell carcinoma (KIRP) (bottom) cohorts. **(D)** Difference in CTR scores between claudin-low and other subtypes of breast cancer in the METABRIC cohort. **(E)** Difference in the mRNA expression-based stemness index (mRNAsi) score between high and low CTR groups or between two clusters in the TCGA-kidney renal clear cell carcinoma (KIRC) cohorts. *p<0.05, ***p<0.001. KIRC, kidney renal clear cell carcinoma; KIRP, Kidney renal papillary cell carcinoma; KICH, kidney chromophobe.

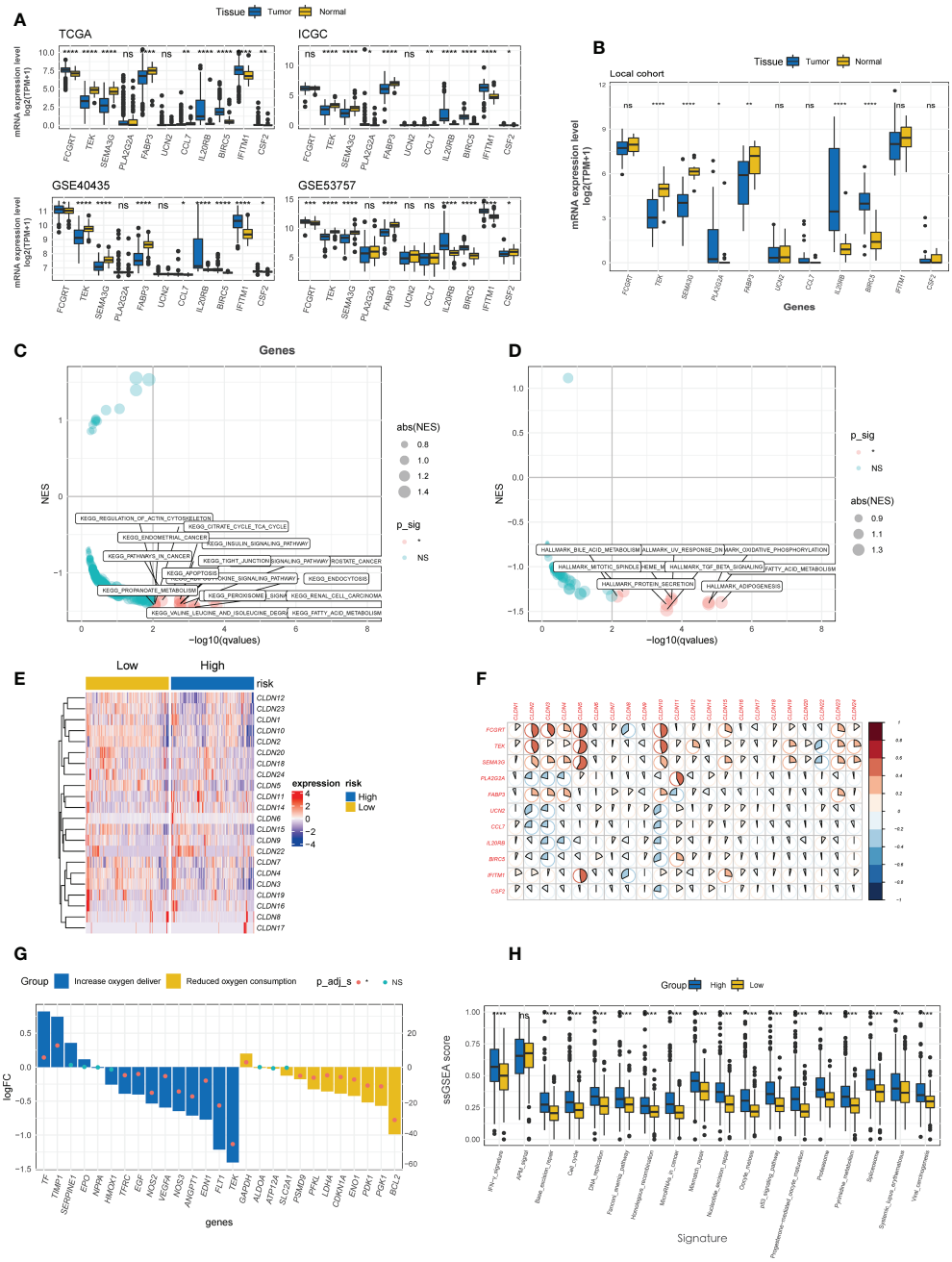

FIGURE 7
Enrichment analysis of CTR score. **(A)** Comparison of the expression difference of eleven claudin-TME related (CTR) score-related genes between tumor and normal tissues in TCGA, GSE40435, GSE53757 and International Cancer Genome Consortium (ICGC) datasets. **(B)** Difference in the expression level of 11 CTR score-related genes between tumor and normal tissues in local ccRCC patients. Kyoto Encyclopedia of Genes and Genomes (KEGG) **(C)** and Hallmark **(D)** pathways analysis revealed that the pathways were significantly enriched in the differentially expressed genes (DEGs) between high and low CTR groups in the TCGA-KIRC cohort. Only the significantly enriched pathways are shown in the figure. **(E)** Heatmap of the expression of claudin genes in high and low CTR groups in the Cancer Genome Atlas-kidney clear cell carcinoma (TCGA-KIRC) cohort. **(F)** Correlation between CTR score related genes and claudin family genes. **(G)** Expression changes (high vs. low CTR groups) of target genes involved in the hypoxia-inducible factor-1 (HIF-1) KEGG pathway. **(H)** Difference in the enrichment scores of immunotherapy-predicted pathways between high and low CTR groups. *p< 0.05, **p< 0.01, ***p< 0.001, ****p< 0.0001, ns, not significant; TPM, transcript per million; ssGSEA, single-sample gene set enrichment analysis; NES, normalized enrichment score.

prevalent genes, specifically *VHL*, *PBRM1*, and *TTN* (Figures 8A, B). However, distinct differences in the prevalence of altered genes were identified between these two groups, and genes with a significantly higher prevalence were discovered in the high CTR group, including *SETD2*, *BAP1*, *PTEN* and *SPEN* (Figure 8C). We did not observe a significant difference in tumor mutational burden (TMB) levels between the two groups (Figure 8D). More interestingly, significantly more copy number variations (CNV) were identified in the high CTR group, including a distinguishing prevalence of deletions at 9p23, 9p21.3, 8p23.3, 8p21.2, 6q26, 10q23.31, and amplifications at 3q26.33, 3q26.2 and 1q31.1 (Figure 8E).

3.8 Immune phenotypes and tumor microenvironment related to the CTR score

The CTR score was positively and negatively correlated with the expression of 21 and 11 immune checkpoints, respectively; significant associations were found with tumor necrosis factor receptor superfamily member 18 (TNFRSF18), lymphocyte activation gene 3 (LAG3), cytotoxic T-lymphocyte associated protein 4 (CTLA4), TNF superfamily member 14 (TNFSF14), programmed cell death protein 1 (PDCD1, PD-1), and T cell immunoreceptor with Ig and ITIM domains (TIGIT) (Figures 9A, C). Similar to the difference between cluster 1 and cluster 2 in MHC, the high-risk group had significantly lower expression levels of human leukocyte antigens (HLA) family genes (especially HLA-E), which may hinder the antigen presentation process (Figures 9B, C). Meanwhile, notable heterogeneity in the TIICs level was observed between the high and low CTR groups (Figure 9D). Using various algorithms, a concordant difference was identified in CD8 T cells, which was enriched in the high CTR group. A significantly higher immune score in the high CTR group was revealed by XCELL, which was also validated by the ESTIMATE algorithm ($R = 0.29$, $p < 0.0001$, Figure 9E). An immunohistochemistry (IHC) test of the ccRCC samples from the CheckMate studies showed a significantly higher level of CD8 + tumor cell (TC) ratio and CD8 + tumor margin (TM) density, which were found in the high CTR group, supporting the positive correlation between CTR score and CD8 T cells found using the algorithms (Figure 9F). Furthermore, the CTR score was associated with increased activity in all the steps of the cancer-immunity cycle, with the exception of step 2 (cancer antigen presentation, Figure 9G).

3.9 Construction of a nomogram by integrating the CTR score and clinicopathologic variables

By incorporating the clinicopathologic variables (including T, N, M, neoplasm histologic grade, neoplasm disease stage, sex, and age) with the CTR score, a novel nomogram was established (Figure 10A). The ROC curve showed that the AUC values for predicting survival at 1, 2, 3, 4 and 5 years of this nomogram were 0.88, 0.84, 0.85, 0.85, and 0.84, respectively (Figure 10B). In addition, the 1–5 year calibration curves showed outstanding agreement between the actual observations and nomogram prediction (Figure 10C).

3.10 Estimation of treatment response correlated with CTR score

We then explored whether the established CTR score could stratify ccRCC patients into different systemic treatments with differed efficacies. First, we evaluated the difference in the expression of ccRCC-related therapeutic target genes between the high and low CTR groups. Intriguingly, the majority of targeted genes of these selected drugs, most of which were antiangiogenic and kinase inhibitors, were overexpressed in the low CTR group (Figure 11A). The low-risk group showed significant overexpression of both the markers of pan-antiangiogenic drug, such as vascular endothelial growth factor receptor 1 (VEGFR1) (Fms related receptor tyrosine kinase 1 (FLT1)), VEGFR2 (kinase insert domain receptor (KDR)), and VEGFR3 (FLT4), and specific markers, including VEGFA, colony stimulating factor 1 (CSF1), SH2B adaptor protein (SH2B3), fibroblast growth factor receptor (FGFR1/2/3/4), B-Raf proto-oncogene (BRAF), Raf-1 proto-oncogene (RAF1), and tyrosine kinase with immunoglobulin-like and EGF-like domains 1 (TIE1). The expression of endothelial PAS domain protein 1 (EPAS1), the main target of belzutifan, which was a novel breakthrough HIF inhibitor, was also significantly upregulated in the low-risk group. However, the targets of ICIs, including CD274, PDCD1, and CTLA4, were upregulated in the high CTR group. Hence, we investigated whether the CTR score could distinguish patients who had improved clinical benefits with ICIs. In nivolumab-treated ccRCC patients, there was no significant difference in the objective response rate (complete response (CR) + partial response (PR)) or clinical benefit rate between the high and low CTR groups (Figure 11B). Even though the group with a low CTR had a longer overall survival (OS), this may be attributed more to the model's prognostic prediction function than to the increased sensitivity to nivolumab. In the IMVigor210 cohort, we found that CTR may not function as an effective ICI biomarker compared to TMB; however, in the TMB-low subgroups, there was a higher ratio of responders in the high CTR group (Figure 11C). In the GSE173839 cohort, patients who responded to ICI combination therapy had significantly higher CTR scores, and more responders were present in the high CTR group (Figure 11D). Furthermore, we utilized three drug response databases, GDSC1, PRISM, and CTRP-v2, to further identify CTR score-related therapeutic agents in ccRCC (Figure 11E). Among these agents, more immunity-related drugs (such as TGF β-related and janus kinase (JAK) inhibitors) were identified in the high CTR group, while more tyrosine kinase inhibitors (EGFR-related) were identified in the low CTR group.

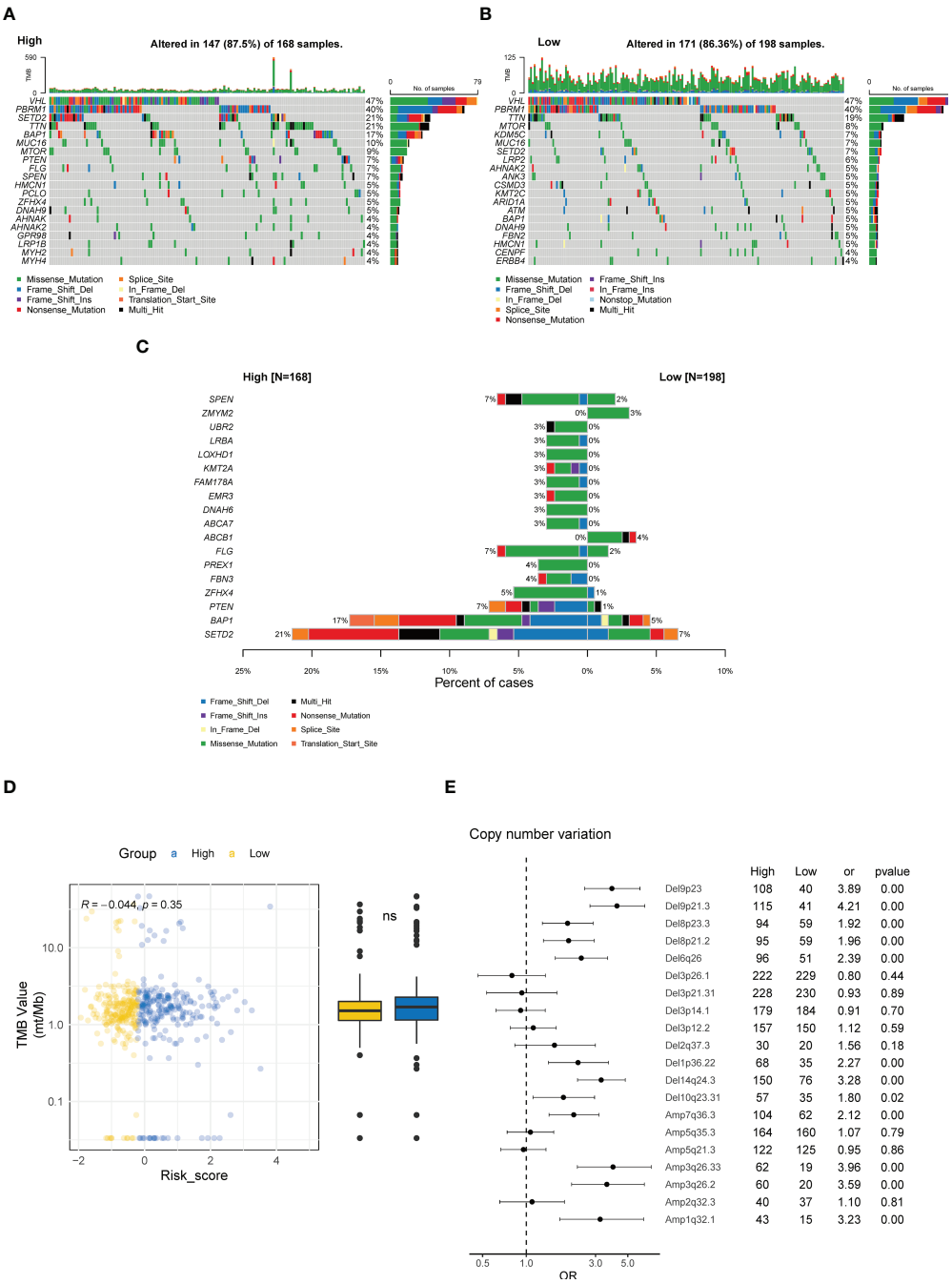

FIGURE 8
Genomic characteristics related to CTR score. Oncoplots of the top 20 altered genes in the high **(A)** and low CTR groups **(B)**. **(C)** Genes with significantly differed prevalence between the high and low CTR groups. **(D)** Difference in the tumor mutational burden (TMB) level between the high and low CTR groups. **(E)** Difference in the prevalence of copy number variations (CNV) between the high and low CTR groups. Odds ratio (OR) > 1.0 indicated a higher prevalence in the high CTR group; conversely, OR< 1.0 indicated that the event was more prevalent in the low CTR group. TMB, tumor mutation burden; CNV, copy number variant; Del, deletion; Amp, amplification; ns, not significant.

4 Discussion

Interestingly, in our study, both the cluster 1 and high CTR groups, which were associated with worse outcomes, were characterized by claudin-low features. The specific genomic, TME, and clinicopathological characteristics of claudin-low ccRCC phenotype remain unclear. It is a novel molecular subtype of breast and bladder cancer, with a prominent role in

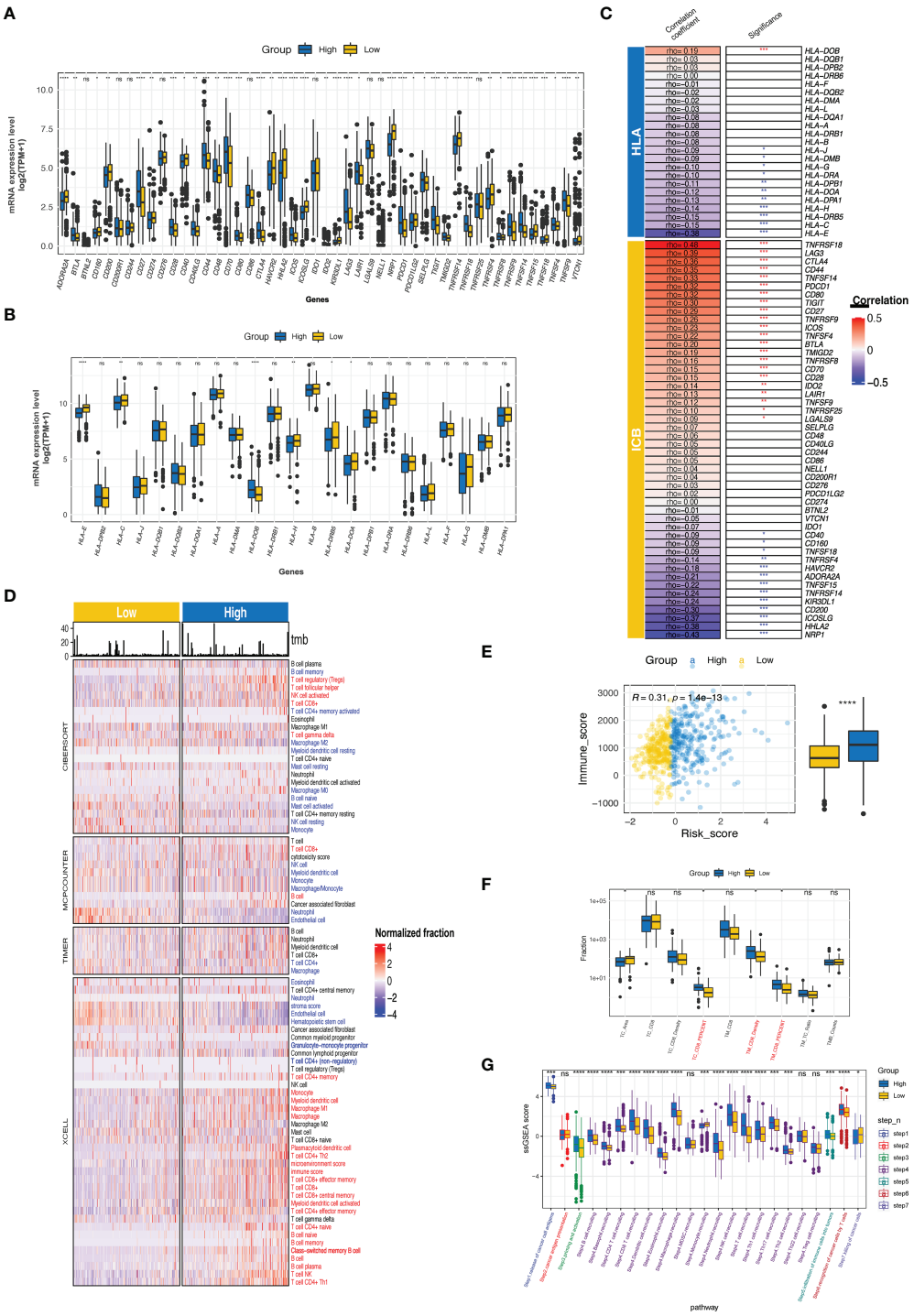

FIGURE 9
Immune phenotypes and tumor microenvironment related to CTR score. **(A)** Comparison of the expression level of immune checkpoints between high and low claudin-TME related (CTR) groups. **(B)** Analysis of the difference in the expression level of human leukocyte antigen (HLA) family genes between high and low CTR groups. **(C)** Correlation between CTR score and the expression level of immune checkpoints or HLA family genes. The asterisks indicate a significant statistical p value, and those colored with red and blue indicate positive and negative correlation with CTR score, respectively. **(D)** Comprehensive analysis of the difference in the tumor-infiltrated immune cells (TIICs) between high and low CTR groups using multiple algorithms (CIBERSOFT, MCPCOUNTER, TIMER, and XCELL). TIICs with blue color were significantly more enriched in the low CTR group; whereas, those with red color were more enriched in the high CTR group ($p < 0.05$). **(E)** Correlation between CTR score and immune score. **(F)** Difference in the CD8 + T cells between high and low CTR groups in an integration cohort with CheckMate-009, 010 and 025 cohorts. **(G)** Differences in the activity of seven steps of cancer-immunity cycle between two CTR groups. *$p < 0.05$, **$p < 0.01$, ***$p < 0.001$, ****$p < 0.0001$, ns, not significant; HLA, human leukocyte antigen; TC, tumor center; TM, tumor margin; TPM, transcript per million; ssGSEA, single-sample gene set enrichment analysis.

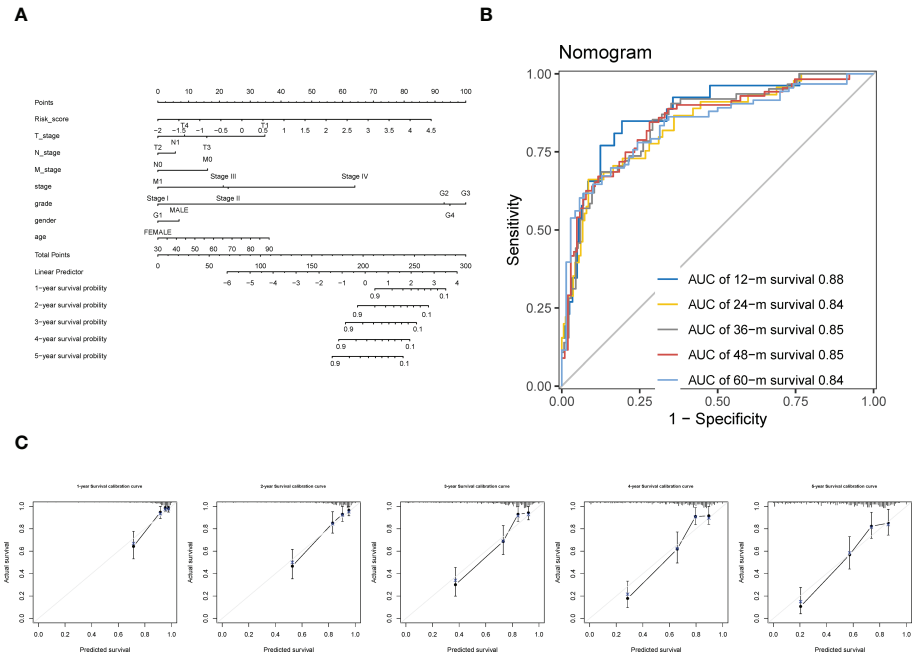

FIGURE 10
Construction of a Nomogram using integration CTR score and clinicopathologic variables. **(A)** claudin-TME related (CTR) score integrated with T (tumor stage), N (node stage), M (metastasis stage), neoplasm histologic grade, neoplasm disease stage, sex, and age to develop a Nomogram in ccRCC. **(B)** Time-dependent receiver operating characteristic (ROC) curves of the Nomogram. **(C)** Calibration curve for the prediction of overall survival (OS) at 1–5 year.

the downregulation of cell-cell adhesion genes and overexpression of epithelial–mesenchymal transition (EMT) genes and stem cell-related genes (14). In our study, we also found that cluster 1 and high CTR groups displayed notable stem cell-like features (increased mRNAsi score), but no substantial upregulation of EMT-related genes. Furthermore, in concordance with our results, other studies have shown that claudin-low tumors were enriched in immune and stromal cell infiltration (16, 41), especially a high abundance of regulatory T cells, revealing an active immunosuppression patten (43). These findings confirm our hypothesis regarding the existence of the claudin-low subtype in ccRCC, which shares similar TME and stemness characteristics with breast and bladder cancer.

However, while comprehensively discovering the separation of two claudin clusters in five public datasets and local ccRCC patients, we cannot directly apply its prognostic stratification function without first developing a predictor or risk model. Subsequently, by employing a series of algorithms and integrating the 12 identified CTR-related genes, we created a prognostic prediction signature with both stable and robust accuracy that surpassed a number of previously defined ccRCC risk models. Moreover, it can be applied to various other types of cancers, especially pan-kidney cancers (KIRC, KICH, and KIRP). The CTR score also outperformed the traditional clinicopathological factors, including clinical and histological stages, and both the clinicopathological and genomic features supported the prognostic prediction value of the signature. More known poor prognosis-related GAs, especially *BAP1* (44) and *SETD2* (45), were identified in the high CTR group. Although we found more GAs with different prevalence in the high CTR group, there was no significant correlation between CTR score and TMB, which may be attributed to the fact that ccRCC has a comprehensively modest TMB level among solid tumors (46). Meanwhile, higher chromosomal instability (CIN), characterized by the enrichment of CNV alterations, was identified in the high CTR group. Due to the increasing frequency of CNV during cancer cell proliferation, CIN-positive tumors exhibit greater intratumor heterogeneity and are more prone to develop therapeutic resistance due to their enhanced capacity to adapt to selection pressures (47). We previously found that increasing CIN drives invasion and metastasis in ccRCC (48), and in this study, some of these differed CNVs were found to be related to the progression of ccRCC. The TRACERx Renal project identified that deletion of 9p21, including the loss of tumor suppressor cyclin-dependent kinase inhibitor 2A (CDKN2A) is a pivotal event driving the metastasis of ccRCC and related death (49). Contrarily, CIN may also function as an enhancer of cancer immunology; induction of CIN promotes the upregulation of pro-inflammation genes, natural killer (NK) cell-activating

10.3389/fimmu.2022.1020729

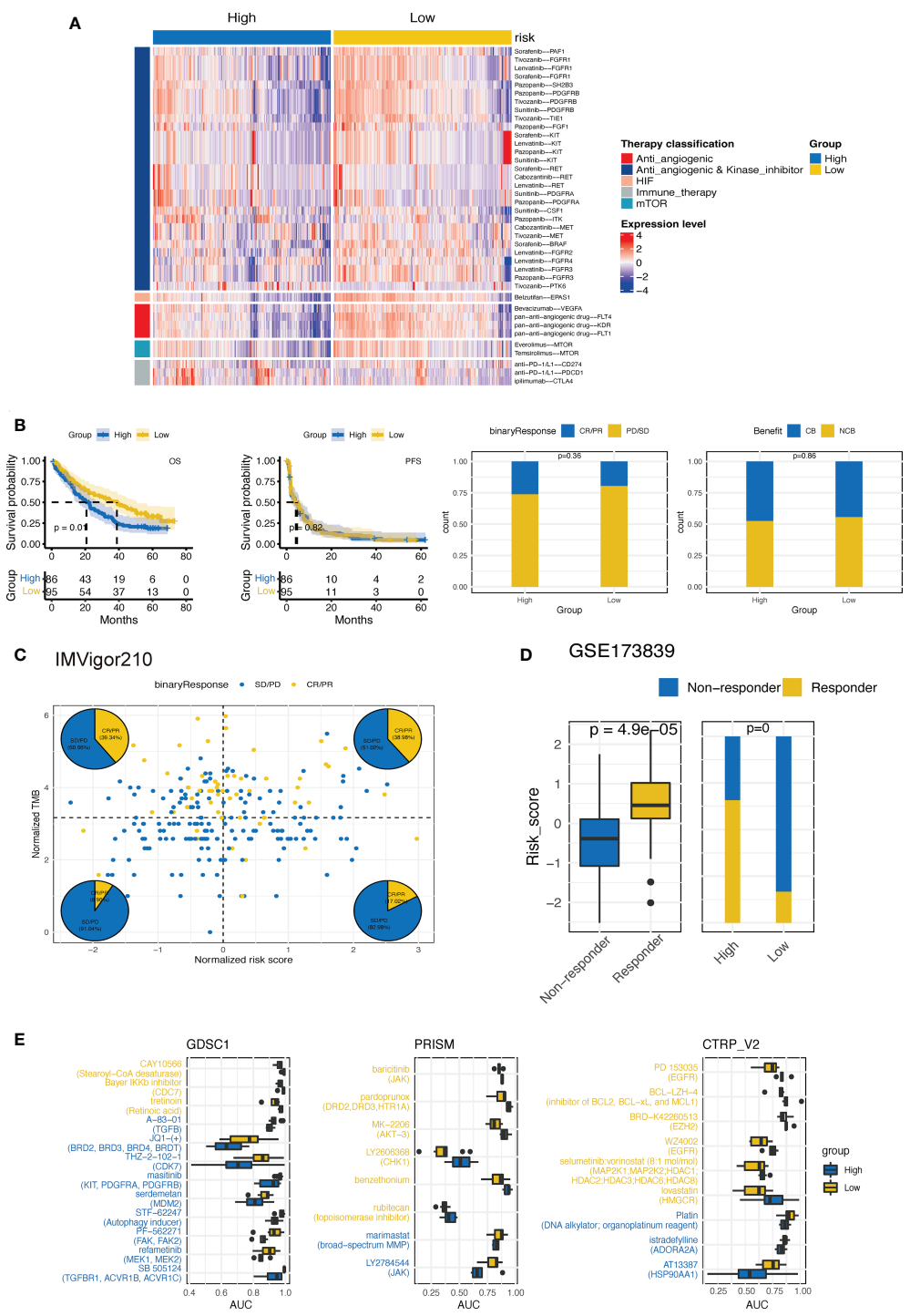

FIGURE 11
Estimation of treatment response correlated with CTR score. **(A)** Heatmap of the expression of ccRCC-related drug-target genes screened from the Drugbank database in high and low claudin-TME related (CTR) groups. **(B)** Kaplan–Meier curves and the difference in response rate between high and low CTR scores in nivolumab-treated ccRCC patients from CheckMate-009, 010 and 025 cohorts. **(C)** Response analysis with tumor mutational burden (TMB) and CTR score stratification in IMvigor210 cohort. **(D)** Comparison of the CTR score between responders and nonresponders and the response rate between high and low CTR score groups from the GSE173839 cohort. **(E)** Three drug sensitivity databases (CTRP-V2, PRISM, and GDSC1) were used to identify the sensitivity of high and low CTR group cell line subsets to specific agents. Agents with lower area under the curve (AUC) values on the x-axis of boxplots had a greater drug sensitivity, and those colored with blue had a higher sensitivity in the high CTR group.

ligands, and cytokine secretion (50); moreover, a combination of agents that promote CIN and ICI could inhibit tumor growth (51). David et al. also revealed that CD8+ T cell-infiltrated ccRCC tumors are more enriched with deletions at 9p21 than those with noninfiltrated ones. This was consistent with our findings that the high CTR group with notable CIN may have higher tumor immunity and an associated elevated sensitivity to ICIs.

Although there was a strong correlation between the number of CD8 T cells and the CTR score, this did not translate to a phenotype with greater therapeutic benefits to nivolumab monotherapy. This was consistent with a previous finding, which showed that there was no significant correlation between baseline CD8 T cells and response to ICI in ccRCC (39). However, in TMB-low patients from the IMVigor210 cohort or the combination therapy cohort (GSE173839), the high CTR group presented with more responders to ICIs. This may be ascribed to the differences in tumor immunology and genomic characteristics between ccRCC and other malignancies such as bladder or lung cancer for which conventional immunotherapy knowledge is available (52). Furthermore, significant overexpression of VEGFR1, VEGFR2, PDGFRB, and VEGFR3 was found in the low-risk group. Benoit et al. found that the expression level of these markers was associated with survival benefit in ccRCC patients treated with sunitinib, which is the standard first-line treatment (53). In addition to antiangiogenic and multiple kinase inhibitors, the low CTR group was also more sensitive to mTOR or HIF-2α inhibitors. Belzutifan is a selective inhibitor targeting HIF-2α, which has been approved by the US FDA to treat RCC with VHL disease and has a promising objective response rate (ORR) of 49% (54). In phase I trial with heavily pretreated ccRCC patients (NCT02974738), it also showed an effective antitumor efficacy with ORR of 25% and progression-free survival (PFS) of 14.5 months (55). The differential expression of TEK, which is a hub gene in this signature, may account for this disparity in hypoxia and sensitivity to associated therapeutic agents between the CTR groups.

In conclusion, the current study provided comprehensive insights into understanding the claudin-low phenotype in ccRCC and highlighted its association with the TME feature. To enhance its clinical utility, we further developed a prognostic prediction signature based on the interaction between claudin-low phenotype and TME, which could accurately predict the outcomes of patients with ccRCC and other histological forms of kidney cancer. Moreover, it was also an effective biomarker in treatment stratification, including targeted therapy and ICIs. These features may contribute to better personalizing management of patients with ccRCC.

Data availability statement

The data presented in the study are deposited in the China National Center for Bioinformation/National Genomics Data Center of China (https://ngdc.cncb.ac.cn/gsahuman/) accession number HRA003416.

Ethics statement

The studies involving human participants were reviewed and approved by Biomedical Research Ethics Committee of Peking University First Hospital. The patients/participants provided their written informed consent to participate in this study.

Author contributions

CZ: conception and design, literature research, clinical studies, experimental studies, data analysis, manuscript editing, manuscript preparation. YL and JQ: data acquisition and analysis. ZZ: literature research, experimental studies, data analysis, statistical analysis. CH: literature research and data acquisition. YG: conception and design, manuscript preparation and editing; ZH and LZ: definition of intellectual content, manuscript review. All authors contributed to the article and approved the submitted version.

Funding

The present study was funded by The National Key R&D Program of China (grant no. 2019YFA0906001) and National Natural Science Foundation of China (No. 82273347).

Conflict of interest

The authors declare that the research was conducted in the absence of any commercial or financial relationships that could be construed as a potential conflict of interest.

The reviewer NZ declared a shared affiliation with the authors to the handling editor at time of review.

Publisher's note

Supplementary material

The Supplementary Material for this article can be found online at: https://www.frontiersin.org/articles/10.3389/fimmu.2022.1020729/full#supplementary-material

SUPPLEMENTARY FIGURE 1
The expression feature and prognostic function of claudin family genes in kidney cancer. **(A)** The difference in the expression level of each claudin gene between tumor and normal tissues in kidney renal clear cell carcinoma (KIRC) (sample size, cancer vs normal: 530 vs 72), kidney renal papillary cell carcinoma (KIRP) (288 vs 32) and kidney chromophobe (KICH) (66 vs 25). **(B)** Forest plots illustrating univariate analyses for overall survival stratification with each claudin gene. CLDN13 and CLDN21 are not included because no valid expression data is available; *p< 0.05, **p< 0.01, ***p< 0.001, ****p< 0.0001, ns: not significant. KIRC: kidney renal clear cell carcinoma; KIRP: Kidney renal papillary cell carcinoma; KICH: kidney chromophobe.

SUPPLEMENTARY FIGURE 2
Validation of the expression feature of claudin genes in other dataset and local ccRCC samples. **(A)** Silhouette clustering analysis in GSE40435, GSE53757, International Cancer Genome Consortium (ICGC) datasets, and local ccRCC samples; **(B)**.

References

1. Sung H, Ferlay J, Siegel R, Laversanne M, Soerjomataram I, Jemal A, et al. Global cancer statistics 2020: GLOBOCAN estimates of incidence and mortality worldwide for 36 cancers in 185 countries. *CA: Cancer J Clin* (2021) 71(3):209–49. doi: 10.3322/caac.21660

2. Jonasch E, Walker C, Rathmell W. Clear cell renal cell carcinoma ontogeny and mechanisms of lethality. *Nat Rev Nephrol* (2021) 17(4):245–61. doi: 10.1038/s41581-020-00359-2

3. Jonasch E, Gao J, Rathmell W. Renal cell carcinoma. *BMJ (Clinical Res ed)* (2014) 349:g4797. doi: 10.1136/bmj.g4797

4. Ljungberg B, Albiges L, Abu-Ghanem Y, Bedke J, Capitanio U, Dabestani S, et al. European Association of urology guidelines on renal cell carcinoma: The 2022 update. *Eur Urol* (2022) 82(4):399–410. doi: 10.1016/j.eururo.2022.03.006

5. Rosiello G, Larcher A, Fallara G, Giancristofaro C, Martini A, Re C, et al. Head-to-head comparison of all the prognostic models recommended by the European association of urology guidelines to predict oncologic outcomes in patients with renal cell carcinoma. *Urologic Oncol* (2022) 40(6):271.e19–.e27. doi: 10.1016/j.urolonc.2021.12.010

6. Ingels A, Campi R, Capitanio U, Amparore D, Bertolo R, Carbonara U, et al. Complementary roles of surgery and systemic treatment in clear cell renal cell carcinoma. *Nat Rev Urol* (2022) 19(7):391–418. doi: 10.1038/s41585-022-00592-3

7. Lal-Nag M, Morin PJ. The claudins. *Genome Biol* (2009) 10(8):235. doi: 10.1186/gb-2009-10-8-235

8. Tabariès S, Siegel PM. The role of claudins in cancer metastasis. *Oncogene* (2017) 36(9):1176–90. doi. 10.1038/onc.2016.289

9. Li Y, Gong Y, Ning X, Peng D, Liu L, He S, et al. Downregulation of CLDN7 due to promoter hypermethylation is associated with human clear cell renal cell carcinoma progression and poor prognosis. *J Exp Clin Cancer Res* (2018) 37(1):276. doi: 10.1186/s13046-018-0924-y

10. Kumar B, Ahmad R, Giannico G, Zent R, Talmon G, Harris R, et al. Claudin-2 inhibits renal clear cell carcinoma progression by inhibiting YAP-activation. *J Exp Clin Cancer Res CR* (2021) 40(1):77. doi: 10.1186/s13046-021-01870-5

11. Owari T, Sasaki T, Fujii K, Fujiwara-Tani R, Kishi S, Mori S, et al. Role of nuclear claudin-4 in renal cell carcinoma. *Int J Mol Sci* (2020) 21(21). doi: 10.3390/ijms21218340

12. Sun H, Li H, Yan J, Wang X, Xu M, Wang M, et al. Loss of CLDN5 in podocytes deregulates WIF1 to activate WNT signaling and contributes to kidney disease. *Nat Commun* (2022) 13(1):1600. doi: 10.1038/s41467-022-29277-6

13. Zhu Z, Xu C, Lin L, Lv T, Cai T, Lin J. Prognostic value and potential biological functions of CLDN8 in patients with clear cell renal cell carcinoma. *OncoTargets Ther* (2020) 13:9135–45. doi: 10.2147/OTT.S266846

14. Prat A, Parker JS, Karginova O, Fan C, Livasy C, Herschkowitz JI, et al. Phenotypic and molecular characterization of the claudin-low intrinsic subtype of breast cancer. *Breast Cancer Res* (2010) 12(5):R68. doi: 10.1186/bcr2635

15. Pommier RM, Sanlaville A, Tonon L, Kielbassa J, Thomas E, Ferrari A, et al. Comprehensive characterization of claudin-low breast tumors reflects the impact of the cell-of-origin on cancer evolution. *Nat Commun* (2020) 11(1):3431. doi: 10.1038/s41467-020-17249-7

16. Kardos J, Chai S, Mose LE, Selitsky SR, Krishnan B, Saito R, et al. Claudin-low bladder tumors are immune infiltrated and actively immune suppressed. *JCI Insight* (2016) 1(3):e85902. doi: 10.1172/jci.insight.85902

17. Taylor N, Vick S, Iglesia M, Brickey W, Midkiff B, McKinnon K, et al. Treg depletion potentiates checkpoint inhibition in claudin-low breast cancer. *J Clin Invest* (2017) 127(9):3472–83. doi: 10.1172/JCI90499

18. Bandini M, Gibb EA, Gallina A, Raggi D, Marandino L, Bianchi M, et al. Does the administration of preoperative pembrolizumab lead to sustained remission post-cystectomy? first survival outcomes from the PURE-01 study☆. *Ann Oncol* (2020) 31(12):1755–63. doi: 10.1016/j.annonc.2020.09.011

19. Yoshihara K, Shahmoradgoli M, Martínez E, Vegesna R, Kim H, Torres-Garcia W, et al. Inferring tumour purity and stromal and immune cell admixture from expression data. *Nat Commun* (2013) 4:2612. doi: 10.1038/ncomms3612

20. Newman A, Liu C, Green M, Gentles A, Feng W, Xu Y, et al. Robust enumeration of cell subsets from tissue expression profiles. *Nat Methods* (2015) 12 (5):453–7. doi: 10.1038/nmeth.3337

21. Becht E, Giraldo NA, Lacroix L, Buttard B, Elarouci N, Petitprez F, et al. Estimating the population abundance of tissue-infiltrating immune and stromal cell populations using gene expression. *Genome Biol* (2016) 17(1):218. doi: 10.1186/s13059-016-1070-5

22. Li T, Fu J, Zeng Z, Cohen D, Li J, Chen Q, et al. TIMER2.0 for analysis of tumor-infiltrating immune cells. *Nucleic Acids Res* (2020) 48(W1):W509–W14. doi. 10.1093/nar/gkaa407

23. Aran D, Hu Z, Butte AJ. xCell: digitally portraying the tissue cellular heterogeneity landscape. *Genome Biol* (2017) 18(1):220. doi: 10.1101/114165

24. Hu J, Yu A, Othmane B, Qiu D, Li H, Li C, et al. Siglec15 shapes a non-inflamed tumor microenvironment and predicts the molecular subtype in bladder cancer. *Theranostics* (2021) 11(7):3089–108. doi: 10.7150/thno.53649

25. Malta TM, Sokolov A, Gentles AJ, Burzykowski T, Poisson L, Weinstein JN, et al. Machine learning identifies stemness features associated with oncogenic dedifferentiation. *Cell* (2018) 173(2):338–54.e315. doi. 10.1016/j.cell.2018.03.034

26. Chen J, Zhan Y, Zhang R, Chen B, Huang J, Li C, et al. A new prognostic risk signature of 8 ferroptosis-related genes in the clear cell renal cell carcinoma. *Front Oncol* (2021) 11:700084. doi. 10.3389/fonc.2021.700084

27. Jiang A, Meng J, Bao Y, Wang A, Gong W, Gan X, et al. Establishment of a prognosis prediction model based on pyroptosis-related signatures associated with the immune microenvironment and molecular heterogeneity in clear cell renal cell carcinoma. *Front Oncol* (2021) 11:755212. doi. 10.3389/fonc.2021.755212

28. Li K, Li Y, Lyu Y, Tan L, Zheng X, Jiang H, et al. Development of a phagocytosis-dependent gene signature to predict prognosis and response to checkpoint inhibition in clear-cell renal cell carcinoma. *Front Immunol* (2022) 13:853088. doi. 10.3389/fimmu.2022.853088

29. Liu L, Du X, Fang J, Zhao J, Guo Y, Zhao Y, et al. Development of an interferon gamma response-related signature for prediction of survival in clear cell renal cell carcinoma. *J Inflammation Res* (2021) 14:4969–85. doi. 10.2147/jir.S334041

30. Liu Y, Huang Z, Cheng G, Shou Y, Xu J, Liu D, et al. Development of a four-gene prognostic model for clear cell renal cell carcinoma based on transcriptome analysis. *Genomics* (2021) 113(4):1816–27. doi. 10.1016/j.ygeno.2021.04.005

31. Lv Z, Qi L, Hu X, Mo M, Jiang H, Li Y. Identification of a novel glycolysis-related gene signature correlates with the prognosis and therapeutic responses in patients with clear cell renal cell carcinoma. *Front Oncol* (2021) 11:633950. doi: 10.3389/fonc.2021.633950

32. Tang G, Guan H, Du Z, Yuan W. Comprehensive analysis of the butyrate-Metabolism-Related gene signature in tumor microenvironment-infiltrating immune cells in clear cell renal cell carcinoma. *Front Cell Dev Biol* (2022) 10:816024. doi: 10.3389/fcell.2022.816024

33. Wu J, Sun Z, Bi Q, Wang W. A ferroptosis-related genes model allows for prognosis and treatment stratification of clear cell renal cell carcinoma: A bioinformatics analysis and experimental verification. *Front Oncol* (2022) 12:815223. doi: 10.3389/fonc.2022.815223

34. Wu Y, Wei X, Feng H, Hu B, Liu B, Luan Y, et al. Integrated analysis to identify a redox-related prognostic signature for clear cell renal cell carcinoma. *Oxid Med Cell Longevity* (2021) 2021:6648093. doi: 10.18632/aging.104088

35. Wu Y, Zhang X, Wei X, Feng H, Hu B, Deng Z, et al. Development of an individualized ubiquitin prognostic signature for clear cell renal cell carcinoma. *Front Cell Dev Biol* (2021) 9:684643. doi: 10.3389/fcell.2021.684643

36. Wu Y, Zhang X, Wei X, Feng H, Hu B, Deng Z, et al. A mitochondrial dysfunction and oxidative stress pathway-based prognostic signature for clear cell renal cell carcinoma. *Oxid Med Cell Longevity* (2021) 2021:9939331. doi: 10.1155/2021/9939331

37. Yin X, Wang Z, Wang J, Xu Y, Kong W, Zhang J. Development of a novel gene signature to predict prognosis and response to PD-1 blockade in clear cell renal cell carcinoma. *OncoImmunology* (2021) 10(1):1933332. doi: 10.1080/2162402X.2021.1933332

38. Zheng B, Niu Z, Si S, Zhao G, Wang J, Yao Z, et al. Comprehensive analysis of new prognostic signature based on ferroptosis-related genes in clear cell renal cell carcinoma. *Aging-US* (2021) 13(15):19789–804. doi: 10.18632/aging.203390

39. Braun D, Hou Y, Bakouny Z, Ficial M, Sant' Angelo M, Forman J, et al. Interplay of somatic alterations and immune infiltration modulates response to PD-1 blockade in advanced clear cell renal cell carcinoma. *Nat Med* (2020) 26 (6):909–18. doi: 10.1038/s41591-020-0839-y

40. Pusztai L, Yau C, Wolf DM, Han HS, Du L, Wallace AM, et al. Durvalumab with olaparib and paclitaxel for high-risk HER2-negative stage II/III breast cancer: Results from the adaptively randomized I-SPY2 trial. *Cancer Cell* (2021) 39(7):989–98.e5. doi: 10.1016/j.ccell.2021.05.009

41. Fougner C, Bergholtz H, Norum JH, Sørlie T. Re-definition of claudin-low as a breast cancer phenotype. *Nat Commun* (2020) 11(1):1787. doi: 10.1101/756411

42. Bui T, Dao V, Nguyen V, Feugeas J, Pamoukdjian F, Bousquet G. Genomics of clear-cell renal cell carcinoma: A systematic review and meta-analysis. *Eur Urol* (2022) 81(4):349–61. doi: 10.1016/j.eururo.2021.12.010

43. Vick SC, Kolupaev OV, Perou CM, Serody JS. Anti–PD-1 checkpoint therapy can promote the function and survival of regulatory T cells. *J Immunol* (2021) 207(10):2598–607. doi: 10.4049/jimmunol.2001334

44. Peña-Llopis S, Vega-Rubín-de-Celis S, Liao A, Leng N, Pavía-Jiménez A, Wang S, et al. BAP1 loss defines a new class of renal cell carcinoma. *Nat Genet* (2012) 44(7):751–9. doi: 10.1038/ng.2323

45. Sato Y, Yoshizato T, Shiraishi Y, Maekawa S, Okuno Y, Kamura T, et al. Integrated molecular analysis of clear-cell renal cell carcinoma. *Nat Genet* (2013) 45(8):860–7. doi: 10.1038/ng.2699

46. Chen YP, Zhang Y, Lv JW, Li YQ, Wang YQ, He QM, et al. Genomic analysis of tumor microenvironment immune types across 14 solid cancer types: Immunotherapeutic implications. *Theranostics* (2017) 7(14):3585–94. doi: 10.7150/thno.21471

47. Sansregret L, Vanhaesebroeck B, Swanton C. Determinants and clinical implications of chromosomal instability in cancer. *Nat Rev Clin Oncol* (2018) 15 (3):139–50. doi: 10.1038/nrclinonc.2017.198

48. Ma Q, Wang J, Qi J, Peng D, Guan B, Zhang J, et al. Increased chromosomal instability characterizes metastatic renal cell carcinoma. *Trans Oncol* (2020) 14 (1):100929. doi: 10.1016/j.tranon.2020.100929

49. Turajlic S, Xu H, Litchfield K, Rowan A, Chambers T, Lopez JI, et al. Tracking cancer evolution reveals constrained routes to metastases: TRACERx renal. *Cell* (2018) 173(3):581–94.e512. doi. 10.1016/j.cell.2018.03.057

50. Santaguida S, Richardson A, Iyer DR, M'Saad O, Zasadil L, Knouse KA, et al. Chromosome mis-segregation generates cell-Cycle-Arrested cells with complex karyotypes that are eliminated by the immune system. *Dev Cell* (2017) 41(6):638–51.e635. doi: 10.1016/j.devcel.2017.05.022

51. Mason JM, Wei X, Fletcher GC, Kiarash R, Brokx R, Hodgson R, et al. Functional characterization of CFI-402257, a potent and selective Mps1/TTK kinase inhibitor, for the treatment of cancer [Cell biology]. *Proc Natl Acad Sci USA* (2017) 114(12):3127–32. doi: 10.1073/pnas.1700234114

52. Binnewies M, Roberts EW, Kersten K, Chan V, Fearon DF, Merad M, et al. Understanding the tumor immune microenvironment (TIME) for effective therapy. *Nat Med* (2018) 24(5):541–50. doi: 10.1038/s41591-018-0014-x

53. Beuselinck B, Verbiest A, Couchy G, Job S, de Reynies A, Meiller C, et al. Pro-angiogenic gene expression is associated with better outcome on sunitinib in metastatic clear-cell renal cell carcinoma. *Acta Oncol* (2018) 57(4):498–508. doi: 10.1080/0284186X.2017.1388927

54. Fallah J, Brave MH, Weinstock C, Mehta GU, Bradford D, Gittleman H, et al. FDA Approval summary: Belzutifan for von hippel-lindau disease associated tumors. *Clin Cancer Res* (2022). doi: 10.1158/1078-0432.CCR-22-1054

55. Choueiri TK, Bauer TM, Papadopoulos KP, Plimack ER, Merchan JR, McDermott DF, et al. Inhibition of hypoxia-inducible factor-2α in renal cell carcinoma with belzutifan: a phase 1 trial and biomarker analysis. *Nat Med* (2021) 27(5):802–5. doi: 10.1038/s41591-021-01324-7

frontiers | Frontiers in Oncology

TYPE Original Research
PUBLISHED 15 December 2022
DOI 10.3389/fonc.2022.1047515

OPEN ACCESS

EDITED BY
Hailiang Zhang,
Fudan University, China

REVIEWED BY
Dattatraya Patil,
School of Medicine, Emory University, United States
Hiroshi Fukushima,
Tokyo Medical and Dental University, Japan

*CORRESPONDENCE
Yuxin Lin
linyuxin@suda.edu.cn
Jinxian Pu
pjx62@sina.com

†These authors have contributed equally to this work

SPECIALTY SECTION
This article was submitted to Genitourinary Oncology, a section of the journal Frontiers in Oncology

RECEIVED 18 September 2022
ACCEPTED 22 November 2022
PUBLISHED 15 December 2022

CITATION
Liu Q, Yang J, Chen X, Yang J, Zhao X, Huang Y, Lin Y and Pu J (2022) Prognostic significance of sarcopenia and systemic inflammation for patients with renal cell carcinoma following nephrectomy. *Front. Oncol.* 12:1047515. doi: 10.3389/fonc.2022.1047515

Prognostic significance of sarcopenia and systemic inflammation for patients with renal cell carcinoma following nephrectomy

Qiuchen Liu[1†], Jiajian Yang[1†], Xin Chen[1], Jiakang Yang[2], Xiaojun Zhao[1], Yuhua Huang[1], Yuxin Lin[1*] and Jinxian Pu[1,3*]

[1]Department of Urology, The First Affiliated Hospital of Soochow University, Suzhou, China, [2]Department of Radiology, Changhai Hospital, Second Military Medical University, Shanghai, China, [3]Department of Urology, Dushu Lake Hospital Affiliated to Soochow University, Suzhou, China

Background: To clarify the prognostic effect of preoperative sarcopenia and systemic inflammation, and to develop a nomogram for predicting overall survival (OS) of patients with renal cell carcinoma (RCC) following partial or radical nephrectomy.

Methods: Patients with RCC following nephrectomy from the First Affiliated Hospital of Soochow University during January 2018 to September 2020 were included in this study. The relationship between sarcopenia and inflammatory markers was identified by logistic regression analysis. Then univariable Cox regression analysis, LASSO regression analysis and multivariable Cox regression analysis were analyzed sequentially to select the independent prognostic factors. Kaplan-Meier survival curves were applied to ascertain the prognostic value. Finally, the identified independent predictors were incorporated in a nomogram, which was internally validated and compared with other methods.

Results: A total of 276 patients were enrolled, and 96 (34.8%) were diagnosed with sarcopenia, which was significantly associated with neutrophil-to-lymphocyte ratio (NLR). Sarcopenia and elevated inflammation markers, i.e., NLR, platelet-to-lymphocyte ratio (PLR) and the modified Glasgow Prognostic Score (mGPS), were independent factors for determining the OS. The model had good discrimination with Concordance index of 0.907 (95% CI: 0.882–0.931), and the calibration plots performed well. Both net reclassification index (NRI) and integrated discriminant improvement (IDI) exhibited better performance of the nomogram compared with clinical stage-based, sarcopenia-based and integrated "NLR+PLR+mGPS" methods. Moreover, decision curve analysis showed a net benefit of the nomogram at a threshold probability greater than 20%.

Conclusions: Preoperative sarcopenia was significantly associated with NLR. A novel nomogram with well validation was developed for risk stratification, prognosis tracking and personalized therapeutics of RCC patients.

KEYWORDS

nomogram, renal cell carcinoma, sarcopenia, systemic inflammation, prognosis

Introduction

Renal cell carcinoma (RCC) is the most common solid lesion of the kidney, accounting for approximately 85% of all kidney malignancies and 3% of systemic malignancies, with about 76% of 5-year relative survival (1). RCC comprises three main types: clear cell RCC (ccRCC), papillary RCC (pRCC) and chromophobe RCC (chRCC), among which ccRCC has the worst prognosis. Although numerous prognostic indices, e.g., the International Society of Urological Pathology (ISUP) grading system, Tumor Node Metastasis (TNM) staging system and performance status, have been developed, they are limited in applicability, singleness and subjectivity. Considering up to 20-40% postoperative tumor recurrence rate of RCC predicting reduced survival (2), how to use preoperative routine examination for early identification of patients at high risk of adverse treatment outcomes and premature mortality is still a clinical priority. Actually, the International Metastatic Renal Cell Carcinoma Database Consortium (IMDC) score, a well-established prognostic model with a combination of serum inflammatory markers and Karnofsky performance status for risk stratification of metastatic RCC (3), provides new perspectives in clinic.

Accumulating studies confirmed strong associations between sarcopenia and poor prognosis of malignancies, including RCC (4–6). Here sarcopenia is defined as age-related loss of skeletal muscle mass, as well as low muscle strength and physical performance (7). As a hallmark of localized and metastatic tumors, systemic inflammation is also hypothesized to be integral to the progression of sarcopenia and cancer cachexia (8–10). Moreover, the combination of sarcopenia and inflammation could lead to worse prognosis of malignant tumors (11–13). In RCC studies, sarcopenia with elevated inflammation, e.g., the modified Glasgow Prognostic Score (mGPS), neutrophil-to-lymphocyte ratio (NLR) and C-reactive protein (CRP), was investigated for predicting inferior overall survival (OS) (14, 15). Although systemic inflammation was proved to be associated with sarcopenia risk in RCC patients of China (16), the combined impact of these two factors on survival have not been well explored yet.

In this study, the independent and combined impacts of preoperative sarcopenia and systemic inflammatory markers on prognosis of RCC were evaluated, and a novel informatics model based on sarcopenia and inflammatory markers was developed and validated for preoperatively predicting prognosis of RCC patients following partial nephrectomy (PN) or radical nephrectomy (RN) in the era of precision medicine and intelligent healthcare.

Materials and methods

Study patients

Data of patients who received a diagnosis of stage I to IV RCC and underwent PN or RN at the First Affiliated Hospital of Soochow University from January 2018 to September 2020 were collected and reviewed retrospectively. The inclusion criteria were set as follows: (I) age of 18 years or older; (II) a confirmed histologic diagnosis of RCC; (III) complete electronic medical records including computerized tomography (CT) images within one month before surgery and clinical laboratory tests within one week before surgery. The exclusion criteria were applied: (I) patients with other malignancies besides RCC or with bilateral RCC (n=19); (II) unreadable CT images due to poor scan quality (n=14); (III) patients who were lost to follow-up by telephone or outpatient service (n=22). As shown in Figure 1, a total of 276 patients were finally selected for further statistical analysis. The TNM staging system was performed according to the corresponding eighth edition of the American Joint Committee on Cancer (AJCC) Staging Manual (17).

Abbreviations: OS, overall survival; RCC, renal cell carcinoma; NLR, neutrophil-to-lymphocyte ratio; PLR, platelet-to-lymphocyte ratio; mGPS, modified Glasgow Prognostic Score; ccRCC, clear cell RCC; pRCC, papillary RCC; chRCC, chromophobe RCC; TNM, Tumor Node Metastasis; CRP, C-reactive protein; PN, partial nephrectomy; RN, radical nephrectomy; CT, computerized tomography; SMI, skeletal muscle index; BMI, body mass index; SIR, systemic inflammatory response; LMR, lymphocyte-to-monocyte ratio; SII, systemic immune-inflammation index; PNI, prognostic nutritional index; OR, odd ratio; HR, hazard ratio; CI, confidence interval; C-index, Concordance index; NRI, net reclassification index; IDI, integrated discriminant improvement; DCA, decision curve analysis; NF-κB, nuclear factor of kappa-B.

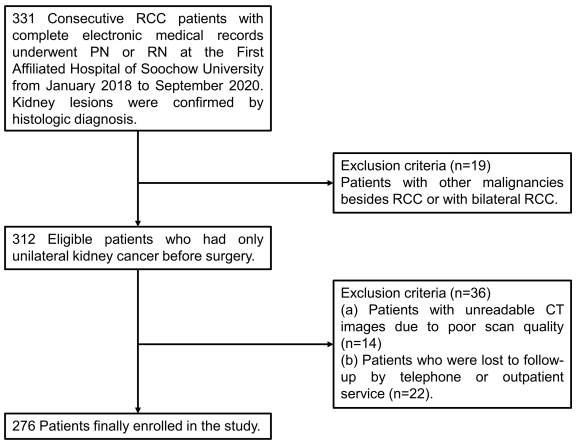

FIGURE 1
A flow chart of screening of RCC patients. RCC, renal cell carcinoma; PN, partial nephrectomy; RN, radical nephrectomy; CT, computerized tomography.

Sarcopenia and its measurement

Considering the advantages of CT examinations in body composition quantification (18), staging diagnosis and follow-up evaluation of cancer patients, we selected the skeletal muscle index (SMI, cm^2/m^2) measured by CT within 1 month before surgery to define sarcopenia (4). Concretely, the mean areas of total skeletal muscle complement (cm^2) at the third lumbar vertebra on two consecutive axial CT images was measured, based on thresholds of −29 to +150 Hounsfield units (HU), by a single trained researcher (JKY) using OsiriX software, version 12.0.4 (http://www.osirix-viewer.com) (6). SMI was ultimately derived by standardizing the skeletal muscle area with height (m^2). The cutoff values for SMI were set as 43 cm^2/m^2 for males with body mass index (BMI) <25kg/m^2, 53 cm^2/m^2 for males with BMI ≥25kg/m^2, and 41 cm^2/m^2 for females (5).

Markers of systemic inflammation

Plenty of inflammation-based prognostic scores reflecting systemic inflammatory response (SIR) were calculated by laboratory serum parameters within 1 week before surgery (19). The NLR, along with lymphocyte-to-monocyte ratio (LMR), platelet-to-lymphocyte ratio (PLR), systemic immune-inflammation index (SII), prognostic nutritional index (PNI) and mGPS, was selected in this study and reportedly associated with unfavorable prognosis of multiple tumors, including RCC (11, 19, 20). The optimal cutoff values of these indices were calculated by the X-tile software, version 3.6.1 (Yale University, New Haven, Connecticut) (21), a software to provide global assessment of all possible divisions of a population into three or two marker expression levels, to select the optimal division, and to visualize the robustness of the relationship between a biomarker and outcome. The inflammatory markers and their optimal cutoff values were listed in Supplementary Table S1, respectively.

Follow-up investigation

The study was followed until March 2021, and most routine follow-up appointments included a physical examination, clinical laboratory tests, an abdominal ultrasonography, or a chest and abdominal CT examination as required. OS was defined as the time ranging from surgery to death from any cause or the last follow-up. Clinical variables and survival outcomes of patients were collected by two independent authors (X Chen, J Yang).

Statistical analysis

Firstly, cohort characteristics and systemic inflammatory markers between preoperative sarcopenia or nonsarcopenia groups were analyzed by the Student's T test or Mann-Whitney U test for continuous variables, and the Chi-squared test or Fisher's exact test for categorical variables. Based on clinical significance and prior knowledge from previously published literatures, specific covariates associated with survival were selected. Logistic regression analysis was performed to determine the relationship between sarcopenia and inflammatory markers. Then the covariates with p-value<0.05 in univariable Cox regression analysis were chosen for LASSO regression analysis, and the identified significant factors were subsequently included in multivariable Cox regression analysis to extract independent predictors of survival. Kaplan-Meier survival curves were plotted by GraphPad Prism version 8.0.2 and their differences were examined using the log-rank test. Finally, screened independent predictors were incorporated in a nomogram for predicting the probability of 1- and 3-year OS for RCC patients undergoing nephrectomy. The nomogram was internally validated with R version 4.1.3 using 1000-sample bootstrapped validation, a statistical method in which multiple evolutionary trees are constructed to check model confidence by repeatedly sampling data sets. In particular, concordance index (C-index), calculated based on the result of Cox proportional hazards model by "survival" package in R, was used to evaluate the discrimination of the model by estimating the probability of concordance between predicted and observed value ranging from 0.5 to 1.0. Meanwhile, calibration and clinical significance of the model were assessed by 1000-sample bootstrapped calibration plots and Kaplan-Meier curves, in which patients were stratified into high-risk and low-risk group according to their nomogram scores by X-tile software.

To compare predictive ability of the nomogram with clinical stage-based, sarcopenia-based and integrated "NLR+PLR +mGPS" methods in predicting 1-, 2-, and 3-year survival in patients with RCC, net reclassification index (NRI), integrated discriminant improvement (IDI) and decision curve analysis (DCA) were utilized. Statistical analyses were carried out using SPSS 19.0 (SPSS Corporation, Armonk, NY, USA) and R version 4.1.3. All tests were two sided, and P <0.05 was considered statistically significant.

Results

Demographic features, clinicopathological characteristics, and correlations between sarcopenia and systemic inflammation

With a median follow-up of 20.00 months, the characteristics of total 276 patients classified by preoperative SMI were presented in Table 1. 96 patients (34.8%) were classified as sarcopenia, and 25 patients (9.1%) died during the follow-up. The mean age of patients was 57.8 years, and a majority were males (68.8%). Clinical stage classified 62.0%, 4.0%, 29.3% and 4.7% of the cancers as stages I, II, III and IV. Less than 5% (9 in detail) patients in stage M1 underwent cytoreductive surgery to delay disease progression in combination with interferon, sorafenib or sunitinib therapy. Patients with sarcopenia were significant in: older age, high proportion of female, lower BMI and triglyceride, bigger in tumor size, undergoing RN, having stage II or III (vs I) cancer, and shorter survival time. However, no significant differences were observed in hypertension, diabetes, pathologic category, tumor location, uric acid, serum creatinine, urea, or high-density lipoprotein cholesterol between these two groups.

The comparisons of systemic inflammatory markers between sarcopenia and nonsarcopenia groups were shown in Supplementary Table S2, where sarcopenia patients tended to have lower albumin, higher NLR and lower PNI (all P<0.05). According to Table 2, multivariable logistic regression analysis indicated that only age (P=0.029), gender (P=0.005) and NLR (P=0.004) were independent predictors of sarcopenia after adjusted for the variables of BMI, tumor location and size, clinical stage, and systemic inflammatory markers.

Survival analysis and kaplan-meier curves of sarcopenia, systemic inflammatory markers, and the combinations

3-year OS for the entire cohort was 87.0%, and 3-year cumulative survival rate was 74.9% for sarcopenia group compared with 92.7% for nonsarcopenia group (P<0.001). Table 3 illustrated variables associated with OS in univariable Cox hazards regression analysis, including age, tumor size, clinical stage, preoperative sarcopenia, NLR, LMR, PLR, SII, PNI and mGPS (all P<0.05). To check for collinearity and to avoid overfitting of the model, a LASSO regression analysis was conducted and five significant predictors (including sarcopenia, NLR, PLR, PNI and mGPS) were screened, as shown in Figure 2. In multivariable analyses, except PNI (P=0.436), sarcopenia (HR, 7.06; 95% CI, 2.77-17.97; P<0.001), NLR (HR, 3.91; 95% CI, 1.00-15.34; P=0.050), PLR (HR, 3.56; 95% CI, 1.16-10.92; P=0.026), and mGPS (HR, 2.71; 95% CI, 1.42-5.16; P=0.003) were independent prognostic variables for OS.

The Kaplan-Meier curves depicted in Figures 3A–D indicated that patients with sarcopenia, NLR ≥2.64, PLR ≥151.23 and mGPS ≥1 (no significance between mGPS of 1 and 2, P =0.112) tended to have worse survival (all log-rank P <0.001). Something interesting happened when sarcopenia was combined respectively with systemic inflammatory markers above. Figure 3E presented no significant differences between sarcopenia and nonsarcopenia groups when NLR <2.64 (P =0.720), while there were significant differences between the two groups when NLR ≥2.64 (P <0.001). Moreover, the differences between low and high NLR groups were observed in sarcopenia patients (P <0.001), as well as that in nonsarcopenia patients (P =0.014). In particularly, patients with both sarcopenia and NLR ≥2.64 were estimated with worst survival. The similar pattern could also be found when combining sarcopenia with PLR or mGPS respectively in Figures 3F, G.

Construction and internal validation of the nomogram based on sarcopenia and systemic inflammation

Based on above findings, a novel nomogram integrated four independent predictors, i.e., sarcopenia, NLR, PLR and mGPS, was developed for predicting 1- and 3-year OS of patients with RCC after nephrectomy, as shown in Figure 4A. Each variable was assigned a score on the basis of its contributions in the nomogram, and the predicted probability of patients' survival time could forecast according to the sum of points. The C-index of the model was 0.907 (95% CI, 0.882–0.931), and the calibration plots were well displayed in Figures 4B, C. After the optimal cutoff value for scores was calculated from the nomogram using X-tile software (scores <183.00 classified as low-risk group, and scores ≥183.00 classified as high-risk group), the Kaplan-Meier curve plotted in Figure 4D revealed the clinical significance of this model (P <0.001). The mean survival time was 37.89 months for low-risk group, compared with 19.05 months for high-risk group. In addition, Supplementary Figure S1 depicted the predictability of the nomogram in ccRCC subgroup (P <0.001).

TABLE 1 Baseline characteristics with comparison between sarcopenia and nonsarcopenia patients.

Characteristic	TotalNo.(%)	SMI, cm^2/m^2		P value
		SarcopeniaNo.(%)	NonsarcopeniaNo.(%)	
Total patients	276 (100)	96 (34.8)	180 (65.2)	
Age (years)	58.5 (19-87)	64.0 (26-87)	54.5 (19-83)	**<0.001**
Age categorized (years)				
≤65	193 (69.9)	57 (59.4)	136 (75.6)	**0.005**
>65	83 (30.1)	39 (40.6)	44 (24.4)	
Gender				
Male	190 (68.8)	57 (59.4)	133 (73.9)	**0.013**
Female	86 (31.2)	39 (40.6)	47 (26.1)	
BMI (kg/m^2)	24.39 ± 3.31	23.19 ± 3.11	25.03 ± 3.24	**<0.001**
BMI categorized (kg/m^2)				
<25	158 (57.2)	56 (58.3)	102 (56.7)	0.790
≥25	118 (42.8)	40 (41.7)	78 (43.3)	
Hypertension				
No	157 (56.9)	57 (59.4)	100 (55.6)	0.542
Yes	119 (43.1)	39 (40.6)	80 (44.4)	
Diabetes				
No	228 (82.6)	74 (77.1)	154 (85.6)	0.077
Yes	48 (17.4)	22 (22.9)	26 (14.4)	
Pathologic categorized				
ccRCC	233 (84.4)	86 (89.6)	147 (81.7)	0.253
pRCC	15 (5.4)	3 (3.1)	12 (6.7)	
chRCC	13 (4.7)	2 (2.1)	11 (6.1)	
Others	15 (5.4)	5 (5.2)	10 (5.6)	
Tumor location				
Upper	62 (22.5)	22 (22.9)	40 (22.2)	0.240
Middle	77 (27.9)	33 (34.4)	44 (24.4)	
Lower	80 (29.0)	26 (27.1)	54 (30.0)	
Mixed	57 (20.7)	15 (15.6)	42 (23.3)	
Tumor size (cm)				
≤4	123 (44.6)	31 (32.3)	92 (51.1)	**0.009**
>4&≤7	108 (39.1)	44 (45.8)	64 (35.6)	
>7	45 (16.3)	21 (21.9)	24 (13.3)	
Surgical options				
RN	143 (51.8)	61 (63.5)	82 (45.6)	**0.004**
PN	133 (48.2)	35 (36.5)	98 (54.4)	
Clinical stage				
I	171 (62.0)	49 (51.0)	122 (67.8)	**0.016**
II	11 (4.0)	7 (7.3)	4 (2.2)	
III	81 (29.3)	36 (37.5)	45 (25.0)	
IV	13 (4.7)	4 (4.2)	9 (5.0)	
UA (umol/L)	340.3 (166.3-776.1)	326.1 (180.8-576.8)	353.0 (166.3-776.1)	0.181
Scr (umol/L)	66.4 (38.5-211.2)	65.4 (40.9-121.0)	67.5 (38.5-211.2)	0.363
Urea (mmol/L)	5.4 (3.0-17.7)	5.7 (3.0-10.4)	5.3 (3.1-17.7)	0.771
HDL-C (mmol/L)	1.1 (0.5-2.4)	1.1 (0.6-2.4)	1.1 (0.5-2.3)	0.493
TG (mmol/L)	1.3 (0.3-8.7)	1.2 (0.5-3.2)	1.5 (0.3-8.7)	**0.001**
OS (months)	20.0 (3-39)	16.0 (3-35)	21.0 (7-39)	**<0.001**

SMI, skeletal muscle index; ccRCC, clear cell renal cell carcinoma; pRCC, papillary renal cell carcinoma; chRCC, chromophobe renal cell carcinoma; RN, radical nephrectomy; PN, partial nephrectomy; UA, uric acid; Scr, serum creatinine; HDL-C, high-density lipoprotein cholesterol; TG, triglyceride; OS, overall survival. The values in bold means $P < 0.05$.

TABLE 2 Logistic regression analysis between clinicopathologic variables and sarcopenia.

Characteristic	Univariable analysis		Multivariable analysis	
	OR (95% CI)	P value	OR (95% CI)	P value
Age categorized (years)				
≤65	Reference	**0.006**	Reference	**0.029**
>65	2.12 (1.24-3.60)		1.94 (1.07-3.53)	
Gender				
Male	Reference	**0.014**	Reference	**0.005**
Female	1.94 (1.14-3.28)		2.29 (1.28-4.10)	
BMI categorized (kg/m^2)				
<25	Reference	0.790		
≥25	0.93 (0.57-1.54)			
Tumor location				
Upper	Reference	0.377		
Middle	1.36 (0.69-2.72)	0.709		
Lower	0.88 (0.44-1.76)	0.282		
Mixed	0.65 (0.30-1.43)			
Tumor size (cm)				0.062
≤4	Reference	**0.012**		0.239
>4 & ≤7	2.04 (1.17-3.57)	**0.009**		
>7	2.60 (1.27-5.30)			
Clinical stage				
I	Reference	**0.023**		0.307
II	4.36 (1.22-15.55)	**0.014**		0.584
III	1.99 (1.15-3.45)	0.871		0.517
IV	1.11 (0.33-3.76)			
NLR				
<2.64	Reference	**<0.001**	Reference	**0.004**
≥2.64	2.64 (1.58-4.39)		2.43 (1.33-4.43)	
LMR				
<2.88	Reference	0.157		
≥2.88	0.66 (0.37-1.17)			
PLR				
<151.23	Reference	0.293		
≥151.23	1.32 (0.79-2.21)			
SII				
<482.30	Reference	0.262		
≥482.30	1.33 (0.81-2.18)			
PNI				
<43.50	Reference	**0.023**		0.914
≥43.50	0.42 (0.20-0.89)			
mGPS				
0	Reference	0.603		0.127
1	0.80 (0.34-1.89)	**0.035**		0.659
2	2.65 (1.07-6.56)			

OR; odd ratio, CI; confidence interval, NLR; neutrophil-to-lymphocyte ratio, LMR; lymphocyte-to-monocyte ratio, PLR; platelet-to-lymphocyte ratio, SII; systemic immune-inflammation index, PNI; prognostic nutritional index, mGPS; modified Glasgow Prognostic Score. The values in bold means P < 0.05.

Comparison of the nomogram based on sarcopenia and systemic inflammation with other methods

To compare the predictive ability of the nomogram with clinical stage-based, sarcopenia-based and integrated "NLR+PLR+mGPS" methods, both NRIs and IDIs shown in Table 4 were greater than 0. Figure 5 presented DCAs in predicting 1-, 2-, and 3-year survival, disclosed a net benefit of the nomogram at a threshold probability greater than 20%.

Discussion

Although clinical strategies have accumulated, there is still a lack of simple, practicable and widely accessible preoperative prognostication in management of RCC. Taking a wide range of inflammatory variables previously reported that could be linked to RCC prognosis into consideration was one of the strengths of this study. The diagnostic criteria and prevalence of sarcopenia (34.8% of total 276 patients) were similar to the reported studies in RCC (4, 16). What we found between sarcopenia and greater

TABLE 3 Univariable Cox hazards regression analysis of clinicopathologic variables in relation to OS of RCC patients following nephrectomy.

Characteristic	Univariable analysis	
	HR (95% CI)	P value
Age categorized (years)		
≤65	Reference	**0.007**
>65	2.99 (1.36-6.59)	
Gender		
Male	Reference	0.850
Female	1.09 (0.47-2.52)	
BMI categorized (kg/m^2)		0.120
<25	Reference	
≥25	0.50 (0.21-1.20)	
Tumor location		
Upper	Reference	0.321
Middle	1.72 (0.59-5.05)	0.833
Lower	0.88 (0.25-3.03)	0.831
Mixed	1.15 (0.33-3.96)	
Tumor size (cm)		
≤4	Reference	0.178
>4&≤7	2.12 (0.71-6.34)	**<0.001**
>7	7.52 (2.60-21.73)	
Clinical stage		
I	Reference	0.107
II	3.53 (0.76-16.37)	**0.032**
III	2.63 (1.09-6.34)	**0.002**
IV	8.48 (2.21-32.46)	
Sarcopenia		
No	Reference	**<0.001**
Yes	5.19 (2.23-12.06)	
NLR		**<0.001**
<2.64	Reference	
≥2.64	12.43 (3.72-41.58)	
LMR		
<2.88	Reference	**<0.001**
≥2.88	0.17 (0.08-0.37)	
PLR		
<151.23	Reference	**<0.001**
≥151.23	8.88 (3.33-23.69)	
SII		
<482.30	Reference	**0.003**
≥482.30	4.10 (1.63-10.27)	
PNI		
<43.50	Reference	**<0.001**
≥43.50	0.10 (0.04-0.22)	
mGPS		
0	Reference	**<0.001**
1	7.45 (2.87-19.35)	**<0.001**
2	18.55 (6.93-49.69)	

HR; hazard ratio, CI; confidence interval, NLR; neutrophil-to-lymphocyte ratio, LMR; lymphocyte-to-monocyte ratio, PLR; platelet-to-lymphocyte ratio, SII; systemic immune-inflammation index, SII; systemic immune-inflammation index, PNI; prognostic nutritional index, mGPS; modified Glasgow Prognostic Score. The values in bold means P < 0.05.

NLR is consistent with prior literature (16), and the effects of targeted therapy and immunotherapy on serum inflammatory indexes may help explain the differences in the correlation between PLR and sarcopenia risk between two studies. Moreover, we newly suggested that preoperative sarcopenia along with elevated systemic inflammatory markers, e.g., NLR, PLR and mGPS, was linked to inferior OS in our crowd, which agrees with previous studies. Higgins et al. (14) found the combined utility of sarcopenia and the elevated mGPS for predicting reduced survival and earlier recurrence in patients with localized RCC. Sarcopenia with elevated NLR or CRP as a negative predictor of OS after cytoreductive nephrectomy in metastatic RCC was later investigated (15). Similarly, the poor prognostic effects of sarcopenia and NLR in colorectal cancer (11), as well as sarcopenia and LMR in gastric cancer (13) have explored.

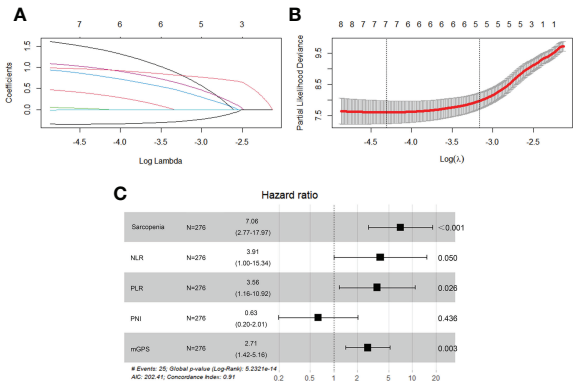

FIGURE 2
LASSO regression analysis and forest plot of multivariable Cox regression analysis. **(A)** The variation trajectory of each independent variable. The logarithm of the independent variable lambda was taken as the horizontal axis, and the coefficient of the independent variable was taken as the vertical axis. **(B)** Confidence intervals for each phase for each lambda, the vertical black dotted lines defined the optimal values of lambda, which provides the best fit. **(C)** Independent predictors screened by multivariable Cox regression analysis and presented as forest plot. NLR, neutrophil-to-lymphocyte ratio; PLR, platelet-to-lymphocyte ratio; PNI, prognostic nutritional index; mGPS, modified Glasgow Prognostic Score.

There are still some findings that differ from previous studies. BMI has previously been regarded as a prognostic indicator of tumors. In this paper, sarcopenia was found associated with a low BMI, while multivariable analysis revealed that BMI was not an independent predictor for OS, which was in agreement with prior studies examining BMI and RCC (15, 22). However, a recent research pointed out that longer survival occurred in patients with higher BMI, and it was restricted to males, but not to

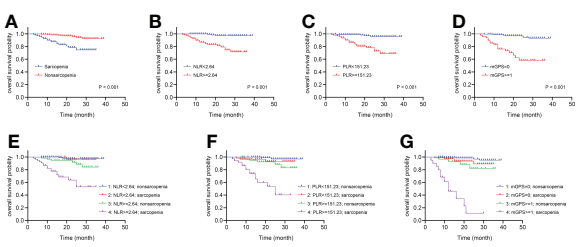

FIGURE 3
The Kaplan-Meier curves of sarcopenia, systemic inflammatory markers and the combinations for patients following nephrectomy. **(A)** OS for patients with or without sarcopenia. **(B)** OS for patients with high or low NLR. **(C)** OS for patients with high or low PLR. **(D)** OS for patients with high or low mGPS. **(E)** Four combinations of sarcopenia and NLR. **(F)** Four combinations of sarcopenia and PLR. **(G)** Four combinations of sarcopenia and mGPS. OS, overall survival; NLR, neutrophil-to-lymphocyte ratio; PLR, platelet-to-lymphocyte ratio; mGPS, modified Glasgow Prognostic Score.

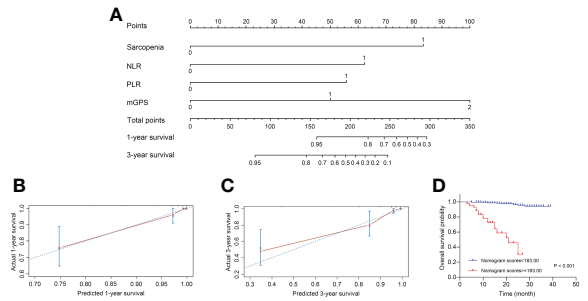

FIGURE 4
Construction and internal validation of the nomogram for predicting the 1- and 3-year OS of patients with RCC following nephrectomy. **(A)** Nomogram for predicting the 1- and 3-year OS. **(B)** Calibration plot of the nomogram for 1-year survival. **(C)** Calibration plot of the nomogram for 3-year survival. **(D)** The Kaplan-Meier curves for patients with high or low risk stratified by the nomogram scores. OS, overall survival; RCC, renal cell carcinoma; NLR, neutrophil-to-lymphocyte ratio; PLR, platelet-to-lymphocyte ratio; mGPS, modified Glasgow Prognostic Score.

females (23). Huszno et al. (24) also discovered that lower BMI was a significant predictor of worse OS in metastatic RCC. Thus, the impact of BMI on prognosis of patients with RCC needs further study, and sarcopenia seems to be a more comprehensive and accurate indicator in body composition reflection than BMI. Furthermore, a possible explanation for the irrelevance of clinical stage to OS is that the number of patients in stage II and IV is too small compared with those in stage I and III, leading to inevitable statistical bias. The staging system could have limited practical value, when almost all patients are divided into one group or subgroup (25), e.g., all patients with T2 tumors were staged in the T2a subgroup, and 92.6% of patients (75/81) with T3 tumors were staged in the T3a subgroup in the present study.

Sarcopenia, acting as an important physiological change in underlying emaciation and weakness caused by tumor progression, is the result of tumor-host interaction. Several metabolic and inflammatory factors and molecular pathways are involved in the onset and progression of sarcopenia, which is classified as primary sarcopenia (just age-related) and secondary sarcopenia (caused by disuse, neurodegenerative disease, inflammatory disease or cachexia) (26). Multiple studies have recently shown that sarcopenia is related to severe postoperative complications (27), inferior survival (4, 22), and dose limiting toxicity (28) in patients with RCC. In the current study, sarcopenia is perceived as a negative prognostic factor in patients.

Besides sarcopenia, SIR also takes a crucial part in tumor cachexia. Increased neutrophils can promote tumor growth and metastasis by remodeling the extracellular matrix, as well as inhibiting the immune system through suppressing the cytolytic activity of immune cells such as lymphocytes (29). In addition, tumor cells are deemed to overcome the damage from immune system and mechanical trauma when covered with platelets and

TABLE 4 NRI and IDI used to compare predictive ability of the nomogram with other methods in predicting 1-, 2- and 3-year survival of RCC patients.

	NRIEstimates (95% CI)	IDIEstimates (95% CI)
	1 year	
Nomogram vs. Clinical stage	0.76 (0.26-1.07)	0.29 (0.13-0.52)
Nomogram vs. Sarcopenia	0.76 (0.36-1.13)	0.28 (0.13-0.48)
Nomogram vs. NLR+PLR+mGPS	0.37 (-0.13-1.03)	0.14 (0.03-0.28)
	2 year	
Nomogram vs. Clinical stage	0.75 (0.30-1.05)	0.39 (0.21-0.60)
Nomogram vs. Sarcopenia	0.79 (0.45-1.23)	0.37 (0.26-0.51)
Nomogram vs. NLR+PLR+mGPS	0.55 (-0.04-0.86)	0.19 (0.06-0.33)
	3 year	
Nomogram vs. Clinical stage	0.70 (0.27-1.14)	0.43 (0.24-0.64)
Nomogram vs. Sarcopenia	0.83 (0.18-1.27)	0.34 (0.25-0.48)
Nomogram vs. NLR+PLR+mGPS	0.15 (-0.23-0.75)	0.19 (0.06-0.35)

CI, confidence interval; NRI, net reclassification index; IDI, integrated discrimination improvement; NLR, neutrophil-to-lymphocyte ratio; PLR, platelet-to-lymphocyte ratio; mGPS, modified Glasgow Prognostic Score. The values in bold means $P < 0.05$.

promote its growth *via* the vascular endothelial growth factor release from platelets (30). Conversely, lymphocytes and interferon (IFN)-γ could collaborate to prevent primary tumor development and shape tumor immunogenicity (31). The above may help explain the essential role of up-regulated NLR and PLR in the prognosis of our cohort (due to increased neutrophil and platelet counts, and decreased lymphocyte counts). On the other side, inflammatory cytokines such as interleukin (IL) 6 is thought to increase the synthesis of CRP and decrease the synthesis of albumin in the liver (32), the two elements contained in mGPS. This helps explain the association between higher mGPS and reduced OS in our study. It's worth noting that the mGPS, compared with NLR and PLR, is superior in differentiating favorable from poor prognostic groups in tumors (20), thus is recommended for routine assessment of patients with cancer.

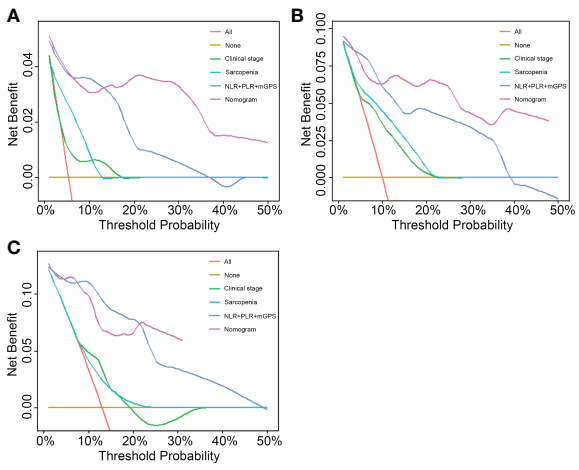

FIGURE 5
Performance comparison of the nomogram with clinical stage-based, sarcopenia-based and integrated "NLR+PLR+mGPS" methods. **(A)** 1-year decision curve analysis of the four models. **(B)** 2-year decision curve analysis of the four models. **(C)** 3-year decision curve analysis of the four models. NLR, neutrophil-to-lymphocyte ratio; PLR, platelet-to-lymphocyte ratio; mGPS, modified Glasgow Prognostic Score.

Not only are sarcopenia and inflammation respectively associated with tumor progression leading poor survival, but tumor-mediated inflammation could in turn exacerbate muscle loss and further create a tumor-pointing vicious cycle between sarcopenia and inflammation. Tumor necrosis factor (TNF)-α, as one of proinflammatory cytokines in tumor cachexia, is responsible for several metabolic derangements and stimulates catabolism of muscle mainly by activation of the ubiquitin-proteasome system (UPS) (33) and nuclear factor of kappa-B (NF-κB) (34) signaling pathway. Both elevated Smad2/3 and NF-κB seems to induce protein degradation separately by the blockade of Akt and the upregulation of muscle ring finger protein 1 (MuRF1) (35). Moreover, increased oxidative stress has significant effects on mitochondrial function, sarcolemmal integrity, and modulation of skeletal muscle during cancer (36). It is worth noting that muscle loss could in turn bring about local inflammation in muscles, leading to further muscle breakdown and inflammation status exacerbation (8). We found that only NLR, compared with other inflammatory markers, was screened as one of independent predictors of sarcopenia. It would be potentially resulted from a vicious cycle existed between muscle damage and neutrophils: muscle damage combined with immune ageing could lead to inefficient neutrophil migration, which was associated with dysregulation of constitutive phosphoinositide 3-kinase (PI3K)-Akt pathway and would in turn cause secondary damage to healthy muscles (37).

These findings should be interpreted with caution, as several limitations exist. Firstly, it is a retrospective, single-center study, leading to inevitable patient selection bias, and multi-center studies will be performed for further external validation of these results. It is also difficult to assess long-term outcomes because of the

incomplete medical records and imaging data prior to January 2018. Secondly, the prognostic value of sarcopenia measured by CT images alone at a given point in time is limited to its heterogeneous dynamic process. And the importance of diagnostic criteria of sarcopenia differs in the two European consensuses: muscle strength (38) is recommended as the most important factor in the new version, rather than low muscle mass (26) in the 2010 consensus. Finally, the nomogram is based on the result of an oriental group, and its applicability in western populations should be comprehensively validated.

Conclusions

In the present study, sarcopenia was associated with systemic inflammation, measured as NLR, in patients following nephrectomy. Four factors, i.e., sarcopenia, NLR, PLR and mGPS, were found as independent predictors of OS and integrated in a novel nomogram for risk stratification, prognosis prediction and personalized therapeutics of patients with RCC. The potential mechanisms of interactions between tumor, sarcopenia and inflammation were then uncovered. More clinical validation using multi-center data will be performed in the next-step work.

Data availability statement

The original contributions presented in the study are included in the article/Supplementary Material. Further inquiries can be directed to the corresponding authors.

Ethics statement

The studies involving human participants were reviewed and approved by the Ethics Committee of the First Affiliated Hospital of Soochow University with approval number No.(2021)332. Written informed consent for participation was not required for this study in accordance with the national legislation and the institutional requirements.

Author contributions

QL and JJY designed the study, performed data collection and analysis, and drafted the manuscript. XC, JKY and XZ collected part of the clinical data, helped with patient follow-up and manuscript draft. XZ and YH contributed to acquisition of data and critically appraised the manuscript. JP and YL designed the study, supervised and directed the project. All authors read and approved the final version, and agreed to publish the manuscript.

Funding

This study was supported by Science and Technology Planning Project of Suzhou City (SLT201905).

Conflict of interest

The authors declare that the research was conducted in the absence of any commercial or financial relationships that could be construed as a potential conflict of interest.

Publisher's note

Supplementary material

The Supplementary Material for this article can be found online at: https://www.frontiersin.org/articles/10.3389/fonc.2022.1047515/full#supplementary-material

References

1. Siegel RL, Miller KD, Fuchs HE, Jemal A. Cancer statistics, 2022. *CA Cancer J Clin* (2022) 72:7–33. doi: 10.3322/caac.21708

2. Brookman-May SD, May M, Shariat SF, Novara G, Zigeuner R, Cindolo L, et al. Time to recurrence is a significant predictor of cancer-specific survival after recurrence in patients with recurrent renal cell carcinoma–results from a comprehensive multi-centre database (CORONA/SATURN-project). *BJU Int* (2013) 112:909–16. doi: 10.1111/bju.12246

3. Heng DY, Xie W, Regan MM, Warren MA, Golshayan AR, Sahi C, et al. Prognostic factors for overall survival in patients with metastatic renal cell carcinoma treated with vascular endothelial growth factor-targeted agents:

results from a large, multicenter study. *J Clin Oncol* (2009) 27:5794–9. doi: 10.1200/JCO.2008.21.4809

4. Mao W, Wang K, Zhang H, Lu H, Sun S, Tian C, et al. Sarcopenia as a poor prognostic indicator for renal cell carcinoma patients undergoing nephrectomy in China: A multicenter study. *Clin Transl Med* (2021) 11:e270. doi: 10.1002/ctm2.270

5. Martin L, Birdsell L, Macdonald N, Reiman T, Clandinin MT, McCargar LJ, et al. Cancer cachexia in the age of obesity: Skeletal muscle depletion is a powerful prognostic factor, independent of body mass index. *J Clin Oncol* (2013) 31:1539–47. doi: 10.1200/JCO.2012.45.2722

6. Prado CM, Cushen SJ, Orsso CE, Ryan AM. Sarcopenia and cachexia in the era of obesity: Clinical and nutritional impact. *Proc Nutr Soc* (2016) 75:188–98. doi: 10.1017/S0029665115004279

7. Chen LK, Woo J, Assantachai P, Auyeung TW, Chou MY, Iijima K, et al. Asian Working group for sarcopenia: 2019 consensus update on sarcopenia diagnosis and treatment. *J Am Med Dir Assoc* (2020) 21:300–7.e2. doi: 10.1016/j.jamda.2019.12.012

8. Kalinkovich A, Livshits G. Sarcopenic obesity or obese sarcopenia: A cross talk between age-associated adipose tissue and skeletal muscle inflammation as a main mechanism of the pathogenesis. *Ageing Res Rev* (2017) 35:200–21. doi: 10.1016/j.arr.2016.09.008

9. Richards CH, Roxburgh CS, MacMillan MT, Isswiasi S, Robertson EG, Guthrie GK, et al. The relationships between body composition and the systemic inflammatory response in patients with primary operable colorectal cancer. *PLos One* (2012) 7:e41883. doi: 10.1371/journal.pone.0041883

10. Zhou ZH, Liu F, Wang WJ, Liu X, Sun LJ, Zhu Y, et al. Development and validation of a nomogram including lymphocyte-to-monocyte ratio for initial prostate biopsy: A double-center retrospective study. *Asian J Androl* (2021) 23:41–6. doi: 10.4103/aja.aja_19_20

11. Feliciano EMC, Kroenke CH, Meyerhardt JA, Prado CM, Bradshaw PT, Kwan ML, et al. Association of systemic inflammation and sarcopenia with survival in nonmetastatic colorectal cancer: Results from the c SCANS study. *JAMA Oncol* (2017) 3:e172319. doi: 10.1001/jamaoncol.2017.2319

12. Sugawara K, Yagi K, Uemura Y, Okumura Y, Nishida M, Aikou S, et al. Associations of systemic inflammation and sarcopenia with survival of esophageal carcinoma patients. *Ann Thorac Surg* (2020) 110:374–82. doi: 10.1016/j.athoracsur.2020.03.013

13. Lin JX, Lin JP, Xie JW, Wang JB, Lu J, Chen QY, et al. Prognostic value and association of sarcopenia and systemic inflammation for patients with gastric cancer following radical gastrectomy. *Oncologist* (2019) 24:e1091-e101. doi: 10.1634/theoncologist.2018-0651

14. Higgins MI, Martini DJ, Patil DH, Nabavizadeh R, Steele S, Williams M, et al. Sarcopenia and modified Glasgow prognostic score predict postsurgical outcomes in localized renal cell carcinoma. *Cancer* (2021) 127:1974–83. doi: 10.1002/cncr.33462

15. Khan AI, Psutka SP, Patil DH, Hong G, Williams MA, Bilen MA, et al. Sarcopenia and systemic inflammation are associated with decreased survival after cytoreductive nephrectomy for metastatic renal cell carcinoma. *Cancer* (2022) 128:2073–84. doi: 10.1002/cncr.34174

16. Hu Q, Mao W, Wu T, Xu Z, Yu J, Wang C, et al. High neutrophil-to-Lymphocyte ratio and platelet-to-Lymphocyte ratio are associated with sarcopenia risk in hospitalized renal cell carcinoma patients. *Front Oncol* (2021) 11:736640. doi: 10.3389/fonc.2021.736640

17. Amin MB, Edge SB, Greene FL, Byrd DR, Brookland RK, Washington MK, et al. *AJCC cancer staging manual. 8th ed*. New York: Springer (2017) p. 743–7.

18. Prado CM, Birdsell LA, Baracos VE. The emerging role of computerized tomography in assessing cancer cachexia. *Curr Opin Support Palliat Care* (2009) 3:269–75. doi: 10.1097/SPC.0b013e328331124a

19. Ozbek E, Besiroglu H, Ozer K, Horsanali MO, Gorgel SN. Systemic immune inflammation index is a promising non-invasive marker for the prognosis of the patients with localized renal cell carcinoma. *Int Urol Nephrol* (2020) 52:1455–63. doi: 10.1007/s11255-020-02440-y

20. Proctor MJ, Morrison DS, Talwar D, Balmer SM, Fletcher CD, O'Reilly DS, et al. A comparison of inflammation-based prognostic scores in patients with cancer. a Glasgow inflammation outcome study. *Eur J Cancer* (2011) 47:2633–41. doi: 10.1016/j.ejca.2011.03.028

21. Camp RL, Dolled-Filhart M, Rimm DL. X-Tile: a new bio-informatics tool for biomarker assessment and outcome-based cut-point optimization. *Clin Cancer Res* (2004) 10:7252–9. doi: 10.1158/1078-0432.CCR-04-0713

22. Sharma P, Zargar-Shoshtari K, Caracciolo JT, Fishman M, Poch MA, Pow-Sang J, et al. Sarcopenia as a predictor of overall survival after cytoreductive nephrectomy for metastatic renal cell carcinoma. *Urol Oncol* (2015) 33:339.e17–23. doi: 10.1016/j.urolonc.2015.01.011

23. Tsutsumi T, Komura K, Hashimoto T, Muraoka R, Satake N, Matsunaga T, et al. Distinct effect of body mass index by sex as a prognostic factor in localized renal cell carcinoma treated with nephrectomy ~ data from a multi-institutional study in Japan ~. *BMC Cancer* (2021) 21:201. doi: 10.1186/s12885-021-07883-9

24. Huszno J, Kolosza Z, Mrochem-Kwarciak J, Rutkowski T, Skladowski K. The role of neutrophil-lymphocyte ratio, platelet-lymphocyte ratio, and platelets in the prognosis of metastatic renal cell carcinoma. *Oncology* (2019) 97:7–17. doi: 10.1159/000498943

25. Qin C, Sun LJ, Cui L, Cao Q, Zhu J, Li P, et al. Application of the revised tumour node metastasis (TNM) staging system of clear cell renal cell carcinoma in eastern China: Advantages and limitations. *Asian J Androl* (2013) 15:550–7. doi: 10.1038/aja.2012.161

26. Cruz-Jentoft AJ, Baeyens JP, Bauer JM, Boirie Y, Cederholm T, Landi F, et al. Sarcopenia: European consensus on definition and diagnosis: Report of the European working group on sarcopenia in older people. *Age Ageing* (2010) 39:412–23. doi: 10.1093/ageing/afq034

27. Peyton CC, Heavner MG, Rague JT, Krane LS, Hemal AK. Does sarcopenia impact complications and overall survival in patients undergoing radical nephrectomy for stage III and IV kidney cancer? *J Endourol* (2016) 30:229–36. doi: 10.1089/end.2015.0492

28. Cushen SJ, Power DG, Teo MY, MacEneaney P, Maher MM, McDermott R, et al. Body composition by computed tomography as a predictor of toxicity in patients with renal cell carcinoma treated with sunitinib. *Am J Clin Oncol* (2017) 40:47–52. doi: 10.1097/COC.0000000000000061

29. el-Hag A, Clark RA. Immunosuppression by activated human neutrophils. dependence on the myeloperoxidase system. *J Immunol* (1987) 139:2406–13.

30. Bambace NM, Holmes CE. The platelet contribution to cancer progression. *J Thromb Haemost* (2011) 9:237–49. doi: 10.1111/j.1538-7836.2010.04131.x

31. Shankaran V, Ikeda H, Bruce AT, White JM, Swanson PE, Old LJ, et al. IFNgamma and lymphocytes prevent primary tumour development and shape tumour immunogenicity. *Nature* (2001) 410:1107–11. doi: 10.1038/35074122

32. Kishimoto T. The biology of interleukin-6. *Blood* (1989) 74:1–10. doi: 10.1182/blood.V74.1.1.1

33. Llovera M, García-Martínez C, Agell N, López-Soriano FJ, Argilés JM. TNF can directly induce the expression of ubiquitin-dependent proteolytic system in rat soleus muscles. *Biochem Biophys Res Commun* (1997) 230:238–41. doi: 10.1006/bbrc.1996.5827

34. Li YP, Atkins CM, Sweatt JD, Reid MB. Mitochondria mediate tumor necrosis factor-alpha/NF-kappaB signaling in skeletal muscle myotubes. *Antioxid Redox Signal* (1999) 1:97–104. doi: 10.1089/ars.1999.1.1-97

35. Sakuma K, Aoi W, Yamaguchi A. Molecular mechanism of sarcopenia and cachexia: Recent research advances. *Pflugers Arch* (2017) 469:573–91. doi: 10.1007/s00424-016-1933-3

36. Fortunati N, Manti R, Birocco N, Pugliese M, Brignardello E, Ciuffreda L, et al. Pro-inflammatory cytokines and oxidative stress/antioxidant parameters characterize the bio-humoral profile of early cachexia in lung cancer patients. *Oncol Rep* (2007) 18:1521–7. doi: 10.3892/or.18.6.1521

37. Wilson D, Jackson T, Sapey E, Lord JM. Frailty and sarcopenia: The potential role of an aged immune system. *Ageing Res Rev* (2017) 36:1–10. doi: 10.1016/j.arr.2017.01.006

38. Cruz-Jentoft AJ, Bahat G, Bauer J, Boirie Y, Bruyère O, Cederholm T, et al. Sarcopenia: Revised European consensus on definition and diagnosis. *Age Ageing* (2019) 48:16–31. doi: 10.1093/ageing/afy169

frontiers | Frontiers in Oncology

TYPE Original Research
PUBLISHED 03 February 2023
DOI 10.3389/fonc.2023.1116648

OPEN ACCESS

EDITED BY
Wen-Hao Xu,
Fudan University, China

REVIEWED BY
Ali Amin,
Rhode Island Hospital, United States
Yuanxin Yao,
People's Liberation Army General Hospital, China

*CORRESPONDENCE
Weidong Gan
gwd@nju.edu.cn

†These authors have contributed equally to this work

SPECIALTY SECTION
This article was submitted to Genitourinary Oncology, a section of the journal Frontiers in Oncology

RECEIVED 05 December 2022
ACCEPTED 16 January 2023
PUBLISHED 03 February 2023

CITATION
Guo W, Zhu Y, Pu X, Guo H and Gan W (2023) Clinical and pathological heterogeneity of four common fusion subtypes in Xp11.2 translocation renal cell carcinoma.
Front. Oncol. 13:1116648.
doi: 10.3389/fonc.2023.1116648

Clinical and pathological heterogeneity of four common fusion subtypes in Xp11.2 translocation renal cell carcinoma

Wei Guo[1,2†], Yiqi Zhu[3†], Xiaohong Pu[4], Hongqian Guo[3] and Weidong Gan[1,3*]

[1]Department of Urology, Drum Tower Clinical Medical School of Nanjing Medical University, Nanjing, Jiangsu, China, [2]Department of Urology, Taizhou People's Hospital Affiliated to Nanjing Medical University, Taizhou, Jiangsu, China, [3]Department of Urology, Nanjing Drum Tower Hospital, The Affiliated Hospital of Nanjing University Medical School, Nanjing, Jiangsu, China, [4]Department of Pathology, Nanjing Drum Tower Hospital, The Affiliated Hospital of Nanjing University Medical School, Nanjing, Jiangsu, China

Background: Xp11.2 translocation renal cell carcinoma (Xp11.2 tRCC) is a group of rare and highly heterogeneous renal cell carcinoma (RCC). The translocation involving TFE3 and different fusion partners lead to overexpression of the chimeric protein. The purpose of this study is to explore the clinicopathological features of Xp11.2 tRCC with four common fusion subtypes.

Methods: We screened out 40 Xp11.2 tRCC patients from January 2007 to August 2021 in our institution. The diagnosis was initially confirmed by TFE3 immunohistochemistry (IHC) and fluorescence *in situ* hybridization (FISH) assay and their fusion partners were verified by RNA sequencing. Then the 40 cases were divided into two groups (DBHS family and non-DBHS family group) and a clinical comparison among the four common fusion subtypes was performed.

Results: Among the 40 cases, 11 cases with SFPQ-TFE3 gene fusion and 7 cases with NONO-TFE3 gene fusion were classified in DBHS group, the remaining cases with ASPL-TFE3 (11 cases) or PRCC-TFE3 (11 cases) gene fusion were classified in non-DBHS group. Lymph node (LN) metastasis (P=0.027) and distant metastasis (P=0.009) were more common seen in non-DBHS family group than DBHS family group and cases in DBHS family group have better progressive-free survival (PFS) (P=0.02). In addition, ASPL-TFE3 fusion was associated with worse outcome (P=0.03) while NONO-TFE3 fusion (P=0.04) predicted a better prognosis.

Conclusions: Different fusion partner genes may play a functional role in various morphology, molecular and biological features of Xp11.2 tRCCs. The impact of fusion partners on clinical characteristics of Xp11.2 tRCCs deserves further exploration.

KEYWORDS

Xp11.2 translocation renal cell carcinoma, TFE3, FISH, DBHS family, prognosis

1 Background

Xp11.2 translocation renal cell carcinoma (Xp11.2 tRCC) is a rare and distinct subtype of RCC, classified in Microphthalmia (MiT) transcription factor family translocation renal cell carcinomas (RCC) in 2016 (1). The most notable feature of Xp11.2 tRCC is chromosome translocations involving TFE3 gene, resulting in fusion with various gene partners (2). Since the discovery of ASPL-TFE3 as the first gene fusion in Xp11.2 tRCC (3), the number of fusion partners has expanded with the development of next-generation sequencing (NGS) technologies. The relatively common fusion genes included ASPSCR1 (ASPL), PRCC, NONO (p54nrb), SFPQ (PSF) and other rare fusion genes such as CLTC, RBM10, MED15, SETD1B, ZC3H4, LUC7L3, KHSRP, PARP14, DVL2, GRIPAP1 were occasionally reported (3–13). The diversity of the fusion partners drastically affects biological behaviors and chromosome structures, which in turn leads to the clinical heterogeneity of Xp11.2 tRCC (14). However, due to the rarity of Xp11.2 tRCC, more cases with definite fusion types are needed to compare the clinical characteristics of Xp11.2 tRCC.

The impact of fusion genes on Xp11.2 tRCC is multifaceted. The common fusion partners of Xp11.2 tRCC, SFPQ and NONO, are both members of the drosophila behavior/human splicing (DBHS) protein family and participate in almost all steps of gene regulation (15–18). The protein products encoded by DBHS family are functionally conserved and largely considered as nuclear factors (15). Previous study has suggested SFPQ and NONO may play an important role in nuclear localization of TFE3 during tumor progression(2). In addition, the inversion of the TFE3 and NONO results in an equivocal split signal distance in fluorescence *in situ* hybridization (FISH), which makes it difficult to diagnose Xp11.2 with this special fusion type (19). On the other hand, another common fusion partner, ASPL, was proved to be associated with aggressive behavior and poor prognosis compared with other fusion genes (12, 14). PRCC can bind to MAD2B (a mitotic checkpoint protein) directly and regulate mitosis, but this interaction can be impaired by the translocation of PRCC and TFE3 (20). As most molecularly confirmed Xp11.2 tRCC cases was described in small series, so far, there are few reports about systematic clinical comparison of Xp11.2 tRCC with common fusion types.

In the present study, we identified 40 cases of Xp11.2 tRCC with four common fusion types (ASPL, PRCC, NONO and SFPQ) by RNA sequencing and described their typical morphological and molecular features. Furthermore, we divided the 40 cases into two groups (DBHS family and non-DBHS family group) and compared their clinicopathological characteristics and prognosis.

2 Methods

2.1 Patients and samples

In this study, 40 cases with suspicious morphological features of Xp11.2 tRCC were retrieved from the diagnostic files in Nanjing Drum Tower Hospital between January 2007 to August 2021. The hematoxylin & eosin (H&E) slides were reviewed independently by two specialist uropathologists and the diagnosis of these cases was based on preliminary TFE3 immunohistochemistry (IHC) or FISH assay. Some of these cases have been reported in the previous literature and their fusion partners have been confirmed by reverse transcriptase polymerase chain reaction (RT-PCR) (21, 22). The available clinicopathological features and follow-up data were recorded. The TNM stage and nuclear grade were classified by the AJCC 2017 TNM Staging System and WHO/ISUP grading system, respectively.

2.2 TFE3 IHC

The 4-μm-thick sections were prepared from 10% FFPE tissue blocks for TFE3 IHC staining. All slides were exposed to 3% H_2O_2 for 10 minutes at room temperature to block endogenous peroxidase activity. TFE3 (HPA023881, Sigma, USA), cathepsin K (ab19027, Abcam, Cambridge, UK), CD10 (ab227640, Abcam, Cambridge, UK), CA-IX (ab107257, Abcam, Cambridge, UK), Vimentin (ab8978, Abcam, Cambridge, UK), CD117(ab32363, Abcam, Cambridge, UK), CK7 (ab181598, Abcam, Cambridge, UK) antibody were incubated with tumor sections in a humidified chamber at 4°C overnight, then the anti-mouse or anti-rabbit peroxidase-conjugated secondary antibody (EnVision™ Detection Kit, DAKO, Denmark) were used with the sections at 37°C for 30 minutes.

The result was evaluated in a semiquantitative manner by multiplying the staining intensity (0 = no staining, 1 = mild staining, 2 =moderate staining, and 3 = strong staining) by the percentage of immunoreactive tumor cells (0–100). The final immunostaining result was calculated as following: negative (0), score <25; weak positive (1+), score 26–100; moderate positive (2+), score 101–200; strong positive (3+), score 201–300.

2.3 Fluorescence *in situ* hybridization

FISH assay was performed on 3-μm -thick FFPE tissue sections with TFE3 positive immunostaining. The commercial dual-color break-apart FISH probes (LBP, Guangzhou, China) were used to detect TFE3 gene arrangement. The telomere and centromeric sides were labeled with 5-ROX-dUTP (red) and fluorescein-12-dUTP (green), respectively. Briefly, the FFPE sections were deparaffinized and permeabilized after a series of treatments, then the probes were applied to the tumor region. All the slides containing the tissue DNA probes denatured at 85°C in a *in situ* thermocycler for 5 minutes and hybridized at 37°C overnight. After washing in 2×SSC for 10 minutes and in 0.1% NP-40/2×SSC for 5 minutes at room temperature, the slides were air dried and 5 μL of 4′,6-diamidino-2-phenylindole (DAPI) was used to counterstain the nuclei. The detail FISH protocol has been reported previously. Routinely, at least 100 non-overlapping nuclei were counted under Olympus BX51TRF fluorescence microscope (Olympus, Tokyo, Japan) at ×1000 magnification. The signals separated by a distance >2 signal diameter was considered to be split. For cases with suspicious NONO-TFE3 fusion (equivocal FISH pattern), RNA sequencing was performed to verify the result. When >10% of the nuclei showed evidence of split signals, the result was considered to be positive.

2.4 RNA sequencing

The 40 cases with positive FISH results were analyzed by RNA sequencing. Total RNA from FFPE samples was extracted using RNeasy kit (QIAGEN). RNase H was used to depleted ribosomal RNA and KAPA Stranded RNA-seq Kit with RiboErase (HMR) (KAPA Biosystems) was used to library preparation. Library concentration and library quality was accessed by KAPA Library Quantification Kit (KAPA Biosystems) and Agilent High Sensitivity DNA kit on Bioanalyzer 2100 (Agilent Technologies), respectively. Then the products were sequenced on Illumina HiSeq next-generation sequencing (NGS) platforms (Illumina).

2.5 Statistical methods

Statistical analyses were conducted by SPSS software version 26.0 (SPSS, Inc., Chicago, IL, USA) and figures were depicted by GraphPad Prism software version 8.0 (GraphPad Software, San Diego, CA). Student' s t test or Mann–Whitney U test or was performed to compare continuous data. Pearson chi-square test or Fisher' s exact test was performed to compare categorical data. Kaplan– Meier method was used to compare the survival data, and statistical comparisons between the two groups were evaluated with Log-rank test. A two-sided $P < 0.05$ was considered statistically significant.

3 Results

3.1 Clinicopathologic features

The detailed clinicopathologic features of the 40 Xp11.2 tRCC patients are shown in Table 1. Xp11.2 tRCC most commonly occurred in young adults, at a median age at diagnosis of 35.5 years and a mean of 37.3 years, ranging from 7 to 70 years. The incidence rate was slightly higher in female than that in male, with a male: female ratio of 1:1.4. The median tumor size was 4.5cm and the mean size was 5.5cm, respectively. Regional lymph node metastasis was found in 9 patients (22.5%) at diagnosis and distant metastasis had developed in 13 patients (32.5%) at the last follow-up. 31 patients (77.5%) were at earlier pT stage (T1-T2) while 9 patients (22.5%) were at an advanced stage (T3-T4) at the time of diagnosis. Higher nuclear grades (WHO/ISUP grade: 3-4) was observed in more than half the patients (60%). 10 (25.0%) patients died at the end of follow-up and 4 patients (10%) were alive with disease.

3.2 Pathology and molecular results

Xp11.2 tRCC showed variable morphological characteristics according to different fusion types. The typical feature of Xp11.2 tRCC was the presence of papillary, glandular, nested, or tubular architectures with clear or eosinophilic cytoplasm, psammoma bodies or calcification were occasionally seen. Papillary architecture was the most common morphology in the 40 cases. Nested architecture and pseudorosettes were seen in 4 SFPQ-TFE3 cases and 5 ASPL-TFE3 cases while none of cases with NONO-TFE3 and PRCC-TFE3 showed this architecture. The most distinctive feature of PRCC-TFE3 cases was the compact (Closely arranged tumor cells with less voluminous cytoplasm and few psammoma bodies) architecture (7/11,63.6%), which was quite different from the other subtypes. Psammoma bodies appeared the most in ASPL-TFE3 cases (8/11, 72.7%) while they were rarely observed in NONO-TFE3 (1/7, 14.3%) and PRCC-TFE3 cases (0/11, 0%). The histologic features of Xp11.2 tRCC with four main fusion types were shown in Figure 1. In term of IHC profiles, all the cases showed TFE3 nuclear positivity

TABLE 1 The clinicopathologic features of the 40 Xp11.2 tRCC patients.

Case	Gender	Laterality	Tumor size (cm)	TFE3 IHC	TNM stage	AJCC stage	Nuclear grade	Fusion partner	Metastasis or recurrence status	Follow-up	Outcome
1	F	R	3.9	3+	T1aN1M0	3	4	ASPL	Bone metastasis after 48 months	62	DOD
2	M	R	4	2+	T1aN0M0	1	3	NONO	–	152	NED
3	M	L	3	3+	T1aN0M0	1	2	ASPL	–	172	NED
4	F	R	8.6	3+	T3cN1M0	3	3	ASPL	Liver metastasis after 2 months	33	DOD
5	F	R	13	3+	T3cN1M0	3	2	ASPL	Liver and brain metastasis after 12 months	25	DOD
6	M	R	6	2+	T1bN0M0	1	3	PRCC	Lung metastasis after 11 months	75	DOD
7	F	R	6	1+	T1bN0M0	1	3	ASPL	–	121	NED
8	F	R	5.8	3+	T3bN0M0	3	3	SFPQ	Lung metastasis after 7 months	15	DOD
9	M	L	3.7	3+	T1aN0M0	1	2	NONO	–	86	NED

(Continued)

TABLE 1 Continued

Case	Gender	Laterality	Tumor size (cm)	TFE3 IHC	TNM stage	AJCC stage	Nuclear grade	Fusion partner	Metastasis or recurrence status	Follow-up	Outcome
10	F	R	7.1	3+	T2aN0M0	2	3	ASPL	–	86	NED
11	F	R	5	3+	T1bN0M0	1	2	PRCC	–	106	NED
12	F	R	3.5	2+	T1aN0M0	1	2	PRCC	Liver metastasis after 55 months	71	DOD
13	F	R	4.5	3+	T1bN0M0	1	3	PRCC	–	79	NED
14	F	L	12.4	3+	T3aN1M0	3	2	PRCC	Local recurrence after 12 months, peritoneal, LN, lung metastasis after 43 months	45	DOD
15	F	L	9.5	3+	T2aN0M0	2	2	PRCC	Local recurrence after 14 months, peritoneal metastasis after 32 months	39	DOD
16	M	L	3	2+	T1aN0M0	1	3	PRCC	–	71	NED
17	M	R	3	2+	T1aN0M0	1	2	NONO	–	54	NED
18	F	L	3.8	3+	T1aN0M0	1	2	NONO	–	47	NED
19	M	L	5.4	1+	T1bN0M0	1	2	SFPQ	–	45	NED
20	M	L	2.5	2+	T1aN0M0	1	3	NONO	–	39	NED
21	F	L	3	2+	T3aN0M0	3	3	NONO	–	40	NED
22	F	L	5	3+	T1bN0M0	1	1	SFPQ	–	38	NED
23	M	L	5.5	3+	T4N1M0	4	4	ASPL	Liver and LN metastasis at diagnosis	5	DOD
24	F	L	2.2	3+	T1aN0M0	1	2	SFPQ	–	28	NED
25	M	L	4	1+	T3aN1M0	3	4	PRCC	LN and vertebral column metastasis after 135 months	148	DOD
26	M	L	3.5	3+	T1aN0M0	1	3	NONO	–	18	NED
27	F	L	3	3+	T1aN0M0	1	3	PRCC	–	28	NED
28	M	L	2.6	2+	T1aN0M0	1	3	PRCC	–	27	NED
29	F	R	10	1+	T2aN0M0	2	2	ASPL	Vertebral column and soft tissue metastasis after 18 months	32	AWD
30	F	R	3.8	3+	T1bN1M0	3	3	ASPL	LN metastasis at diagnosis, local recurrence after 18 months	30	AWD
31	M	L	3.1	3+	T1aN0M0	1	3	SFPQ	–	20	NED
32	F	R	6	3+	T1bN0M0	1	2	SFPQ	–	16	NED
33	M	R	6.5	3+	T1bN0M0	1	3	SFPQ	–	31	NED
34	M	R	6.5	3+	T1bN1M0	3	3	SFPQ	LN metastasis at diagnosis, abdominal wall metastasis after 8 months	29	AWD
35	M	L	3	3+	T1aN0M0	1	3	ASPL	–	11	NED
36	F	L	16.5	3+	T4N1M0	4	4	ASPL	LN metastasis at diagnosis	13	AWD
37	M	R	4	2+	T1aN0M0	1	3	SFPQ	–	26	NED
38	F	R	4.4	3+	T1bN0M0	1	2	SFPQ	–	8	NED
39	F	L	6.5	3+	T1bN0M0	1	1	SFPQ	–	2	NED
40	F	R	5.5	2+	T3aN0M0	3	3	PRCC	–	1	NED

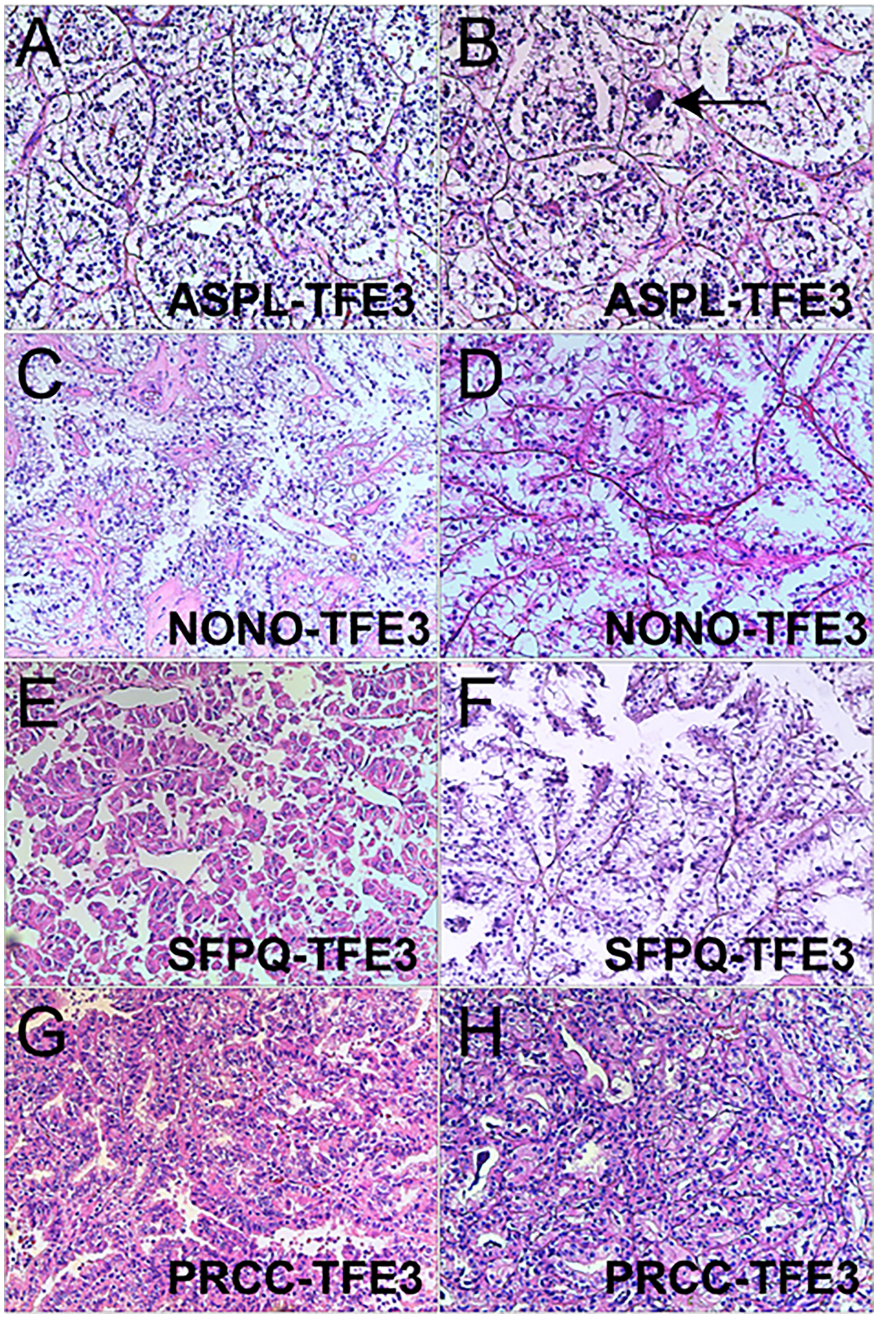

FIGURE 1
Representative images of morphologic features in Xp11.2 tRCCs with four common fusion subtypes. **(A, B)** ASPL-TFE3 cases showed nested architecture, clear to eosinophilic cells with voluminous cytoplasm and round nuclei, Psammoma bodies were frequently seen (arrowhead). **(C, D)** NONO-TFE3 cases showed papillary architecture with clear to flocculent eosinophilic cytoplasm. **(E, F)** SFPQ-TFE3 cases showed papillary architecture. **(G, H)** PRCC-TFE3 showed compact architecture with less voluminous cytoplasm. Original magnification: × 100 **(A–H)**. H&E: hematoxylin and eosin.

and the majority of Xp11.2 tRCC cases (90%) showed moderate (++) to strong (+++) positivity. Cathepsin K were seen predominantly in PRCC-TFE3 cases (7/11.63.6%), which is useful to distinguish PRCC-TFE3 cases from the other types. CD10 was positive in most of the cases (34/40, 85%) and half of the cases (22/40, 55%) showed vimentin positivity. The positivity of CA-IX, CD117 and CK7 is uncommon. The morphological and IHC profiles of 40 cases were shown in Table 2. In FISH results, 33 cases showed typical translocation signals and 7 cases with NONO-TFE3 fusion showed equivocal signals (split but adjacent signals). The representative IHC and FISH features were shown in Figures 2, 3. Gene fusions were verified by RNA sequencing, of which the gene fusions involve ASPL-TFE3 gene fusion (11 cases), PRCC-TFE3 gene fusion (11 cases), SFPQ-TFE3 gene fusion (11 case) and NONO-TFE3 gene fusion (7 cases). The representative sequencing results were shown in Table S1.

TABLE 2 Morphological and IHC features of the 40 Xp11.2 tRCC patients.

Item	SFPQ(n=11)	NONO(n=7)	ASPL(n=11)	PRCC(n=11)
Morphological features, n (%)				
Papillary architecture	6 (54.5)	5 (71.4)	3 (27.3)	3 (27.3)
Solid/nested architecture	4 (36.3)	0 (0)	5 (45.4)	0 (0)
Compact architecture	1 (9.1)	0 (0)	0 (0)	7 (63.6)
Variable morphologies	0 (0)	2 (28.6)	3 (27.3)	1 (9.1)
Psammoma bodies	5 (45.4)	1 (14.3)	8 (72.7)	0 (0)
IHC-positive results, n (%)				
TFE3	11 (100)	7 (100)	11 (100)	11 (100)
Cathepsin K	0 (0)	0 (0)	1 (9.1)	7 (63.6)
CD10	10 (90.9)	6 (63.6)	9 (81.8)	9 (81.8)
CA-IX	2 (18.2)	0 (0)	1 (9.1)	1 (9.1)
Vimentin	6 (54.5)	3 (27.3)	6 (54.5)	7 (63.6)
CD117	2 (18.2)	0 (0)	1 (9.1)	0 (0)
CK7	1 (9.1)	0 (0)	0 (0)	0 (0)

3.3 The differences between DBHS family group and non-DBHS family group

Among all the 40 cases, 11 cases with SFPQ-TFE3 gene fusion and 7 cases with NONO-TFE3 gene fusion were classified in DBHS group, the remaining cases with ASPL-TFE3 or PRCC-TFE3 gene fusion were classified in non-DBHS group (Table 3). No statistical difference was seen in the baseline clinicopathologic characteristics, including age, gender, laterality, tumor size, pT stage and AJCC stage (P >0.05) between DBHS family group and non-DBHS family group. However, there was a significant difference in pN stage (P = 0.027) at surgery and M stage at the last follow-up (P = 0.009). Furthermore, although no statistical difference was found in nuclear grade and follow-up time (all P >0.05), cases in non-DBHS family group tend to have a worse outcome (P =0.013).

3.4 Prognosis analysis for survival

The follow-up time of the 40 Xp11.2 tRCC cases with the four main fusion types was compared. The median follow-up time was 35.5 months (range, 1–172 months). Survival analysis showed that cases in DBHS family group have better progressive-free survival (PFS) (median PFS: not reached vs. 48 months, P = 0.023, Figure 4A) and overall survival (OS) (median OS: not reached vs. 75 months, P = 0.115, Figure 4B) compared with those in non-DBHS family group. In the subgroup analysis for the four different fusion types, patients with ASPL-TFE3 fusion were associated with poor PFS compared with other subtypes (median PFS: 18 months vs. 135 months, P = 0.026, Figure 4C) even though there was no significant difference in OS (median OS: 62 months vs. 148 months, P = 0.379, Figure 4D). In contrast, patients with NONO-TFE3 fusion showed better PFS (median

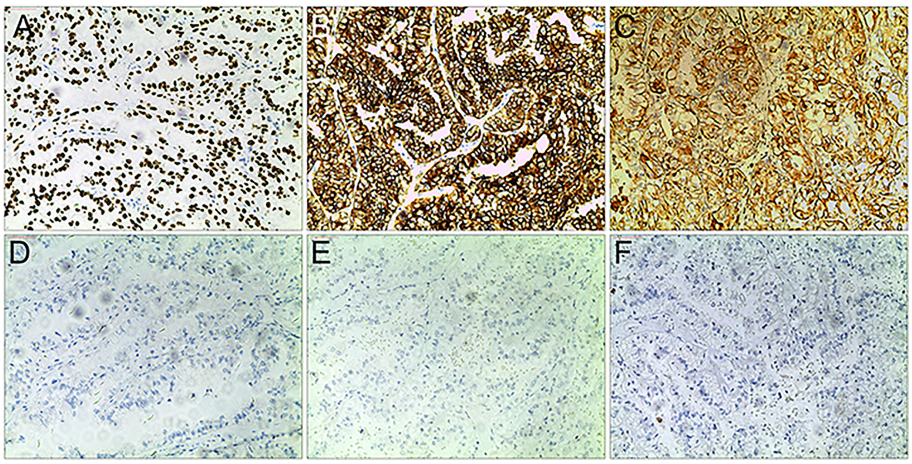

FIGURE 2
Representative IHC images of Xp11.2 tRCCs. **(A–C)** positive results of TFE3, CD10 and Vimentin. **(D–F)** Negative results of cathepsin K, CD117 and CA-IX. Original magnification: × 100 **(A–F)**.

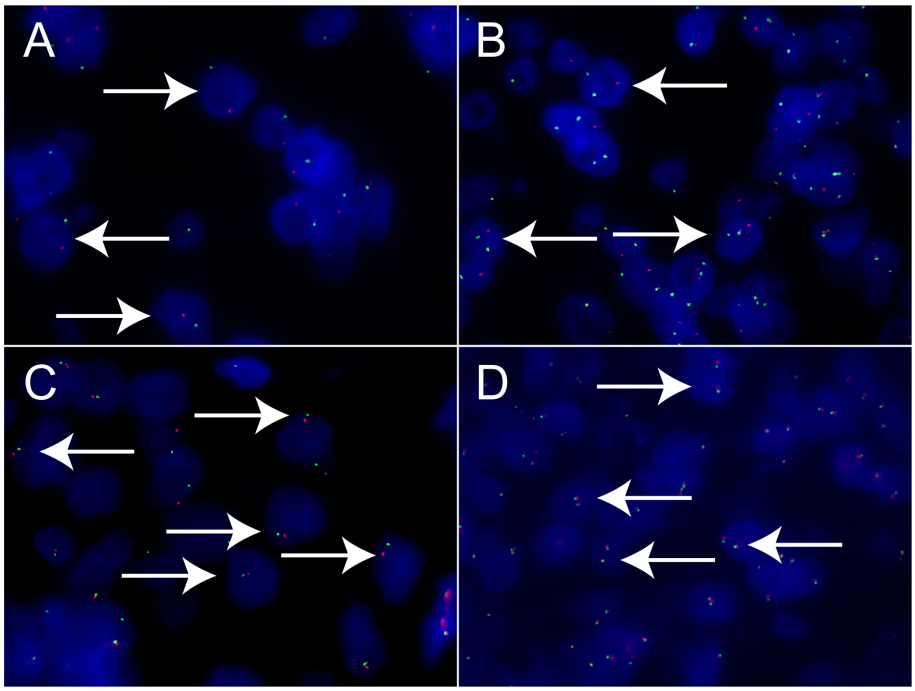

FIGURE 3
Results of TFE3 break-apart FISH in Xp11.2 tRCC. **(A, B)** Typical signal patterns in a male case (1R1G) and a female case (1R1G1F). **(C, D)** Equivocal signal patterns of NONO-TFE3 in a male case (1R1G) and a female case (1R1G1F). Original magnification: × 1000 **(A–D)**. R, red; G, green; F, fusion; FISH, fluorescence *in situ* hybridization.

PFS: not reached vs. 55 months, P = 0.040, Figure 4E) while there remained no significant difference in OS (median OS: not reached vs. 75 months, P = 0.077, Figure 4F). The difference in follow-up between TFE3-SFPQ group and the other subtypes were not compared due to the short follow-up period of TFE3-SFPQ group. Survival analysis indicated that cases with ASPL-TFE3 fusion have the worst PFS among the other three subtypes with sufficiently long follow-up (median PFS: 18 months vs. not reached vs. 135 months, P = 0.04, Figure 5A) although there was no difference in OS (P >0.05, Figure 5B). No statistically significant difference was seen in PFS and OS between PRCC and non-PRCC group (P >0.05, Figures 5C–D).

4 Discussion

In recent years, with an in-depth understanding of the genomic spectrum of RCCs, Xp11.2 tRCC has received increasing attention. Apart from morphological and molecular features different from conventional RCCs, Xp11.2 tRCC itself is a group of highly heterogeneous tumors and various fusion partners has proven to be the source of this heterogeneity (12, 14, 23, 24). ASPL, PRCC and SFPQ were regarded as relatively common fusion partners initially while the pericentric inversion of NONO and TFE3 is also not rare nowadays. Therefore, in this study, we retrospectively investigated the clinicopathological features of 40 Xp11.2 tRCC cases with the above four fusion types in our cohort by IHC, FISH and RNA sequencing. The initial diagnosis of Xp11.2 tRCC was based on IHC and FISH analysis and then the fusion types were verified by RNA sequencing.

Xp11.2 tRCCs with different fusion subtypes have respective histological characteristics. As regards morphology, cases with ASPL-TFE3 fusion could present with various features including alveolar, papillary or nested architecture, which is not much different from other subtypes, but psammoma bodies were most common seen in ASPL-TFE3 cases among the four subtypes (25, 26). Papillary architecture frequently occurred in SFPQ-TFE3 subtype while pseudorosette-like architecture was occasionally described (27). NONO-TFE3 cases could also show a papillary architecture but it was more like the appearance of secretory endometrioid(7). PRCC-TFE3 cases tended to show a compact architecture and psammoma bodies were rare (28). In addition, recent literature reported the distinctive morphology of MED15-TFE3 cases. This subtype often showed a multicystic architecture without solid composition, resembling the feature of multilocular cystic renal cell neoplasm of low malignant potential (MCRN-LMP) (29). In regard to IHC, moderate (++) to strong (+++) TFE3 nuclear positivity is the primary clue to the initial diagnosis of Xp11.2 tRCC and cathepsin K positivity seems to be relevant to PRCC-TFE3 subtype. CA-IX and CK7 were always negative in Xp11.2 tRCC, which could help to exclude clear cell RCC (ccRCC) and papillary RCC (PRCC) (30). TFE3 break-apart FISH was the most effective method to detect TFE3 rearrangement in clinical practice (31), while equivocal or false-negative split signal pattern could be observed in several special fusion subtypes such as NONO(19) and RBM10(6). Hence, suspicious Xp11.2 tRCC cases with negative FISH results should be confirmed by further sequencing.

The fusion gene partners are likely to have a functional role in the oncogenesis of Xp11.2 tRCC and the underlying mechanisms may influence clinical behavior(2). SFPQ and NONO, belonging to DBHS family, are both pre-mRNA splicing factors and associated with tumorigenesis of multiple cancers such as prostate cancer and breast cancer (16–18, 32). Due to the homology of SFPQ and NONO gene,

10.3389/fonc.2023.1116648

TABLE 3 Comparison of clinicopathological features between DBHS family group and non-DBHS family group.

Items	Total (n=40)	DBHS family group (n=18)	Non-DBHS family group (n=22)	P value
Age (years)				0.915
Median (range)	35.5 (7-70)	34.5 (24-55)	35.5 (7-70)	
Mean ± SD	37.3 ± 13.4	37.6 ± 11.2	37.1 ± 15.2	
Gender, (n, %)				0.131
Male	17 (42.5)	10 (55.6)	7 (31.8)	
Female	23 (57.5)	8 (44.4)	15 (68.2)	
Laterality, (n, %)				0.525
Left	20 (50)	10 (55.6)	10 (45.5)	
Right	20 (50)	8 (44.4)	12 (54.5)	
Tumor size (cm)				0.177
Median (range)	4.5 (2.2-16.5)	4.0 (2.2-6.5)	5.25 (2.6-16.5)	
Mean ± SD	5.5 ± 3.1	4.38 ±1.44	6.3 ± 3.8	
pT stage, (n, %)				0.149
T1-T2	31 (77.5)	16 (88.9)	15 (68.2)	
T3-T4	9 (22.5)	2 (11.1)	7 (31.8)	
pN stage (n, %)				**0.027**
N0	31 (77.5)	17 (94.4)	14 (63.6)	
N1	9 (22.5)	1 (5.6)	8 (36.4)	
M stage at the last follow-up (n, %)				**0.009**
M0	27 (67.5)	16 (88.9)	11 (50.0)	
M1	13 (32.5)	2 (11.1)	11 (50.0)	
AJCC stage (n, %)				0.096
I-II	28 (70.0)	15 (83.3)	13 (59.1)	
III-IV	12 (30.0)	3 (16.7)	9 (40.9)	
WHO/ISUP grade, (n, %)				0.243
Grade 1-2	16 (40.0)	9 (50.0)	7 (31.8)	
Grade 3-4	24 (60.0)	9 (50.0)	15 (68.2)	
TFE3 IHC (n, %)				0.683
+	4 (10.0)	1 (5.6)	3 (13.6)	
++	10 (25.0)	5 (27.8)	5 (22.7)	
+++	26 (65.0)	12 (66.7)	14 (63.6)	
Follow-up (months)				0.201
Median (range)	35.5 (1-172)	30 (2-152)	53.5 (1-172)	
Mean ± SD	49.4 ± 42.0	38.6 ± 34.3	58.2 ± 46.3	
Outcome (n, %)				**0.013**
Alive	30 (75.0)	17 (94.4)	13 (59.1)	
Dead	10 (25.0)	1 (5.6)	9 (40.9)	

Bold indicates P values less than 0.05.

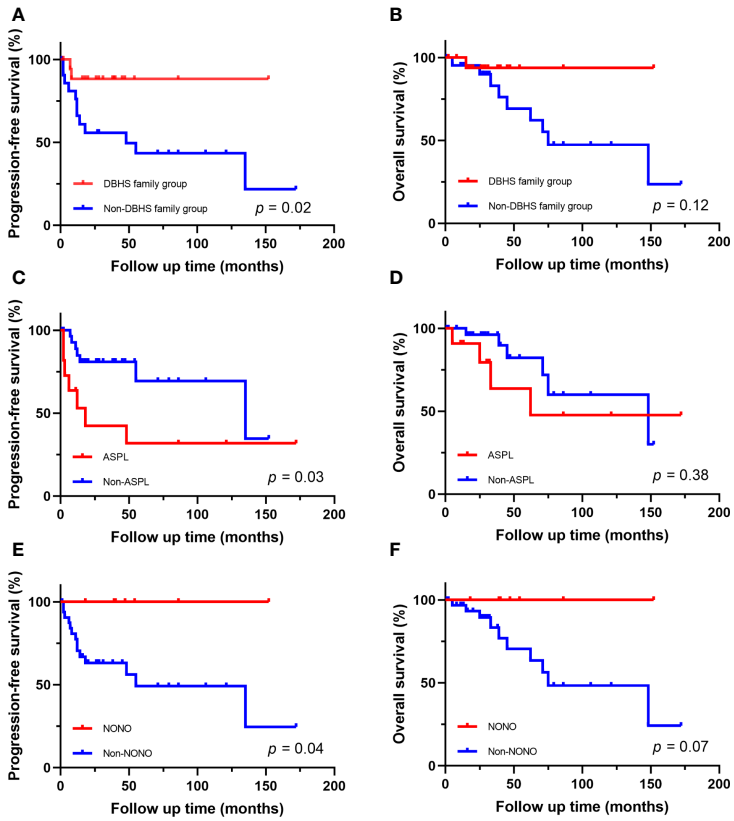

FIGURE 4
Survival analysis of different fusion partners. **(A, B)** PFS and OS for patients in DBHS famliy group and non-DBHS famliy group. **(C, D)** PFS and OS for patients with ASPL-TFE3 fusion and non-ASPL fusion. **(E, F)** PFS and OS for patients with NONO-TFE3 fusion and non-NONO fusion.

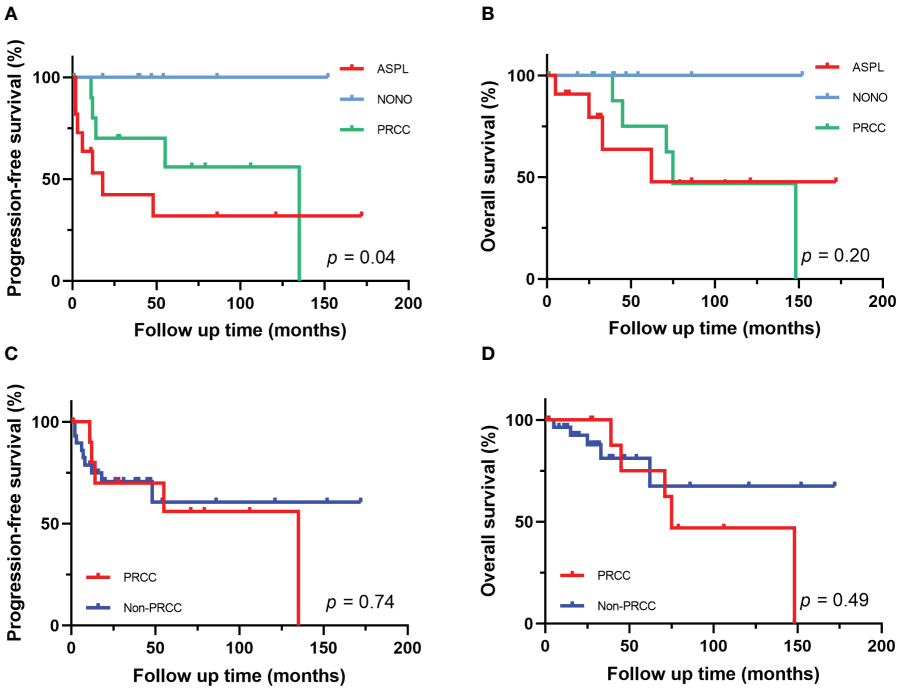

FIGURE 5
Survival analysis of different fusion partners. **(A, B)** PFS and OS for patients with different fusion subtypes. **(C, D)** PFS and OS for patients with PRCC-TFE3 fusion and non-PRCC fusion.

we classified Xp11.2 tRCC harboring SFPQ-TFE3 and NONO-TFE3 as a group and compared the characteristics of this group with non-DBHS family group (cases with PRCC-TFE3 and ASPL-TFE3 fusion). In the DBHS family group, only one patient (5.6%) was found lymph node (LN) metastasis in surgery, while 8 patients (36.4%) in non-DBHS family group had LN metastasis. This phenomenon suggested that cases in DBHS family group tend to show more lymph node metastasis in the early stages of disease. More importantly, half of the cases (50%) in non-DBHS family group showed local recurrence or distant metastasis at the last follow-up, which demonstrated that cases in non-DBHS family group were likely to display a more aggressive and invasive behavior compared with cases in DBHS family group. It is worth mentioning that previous literature reported that Xp11.2 tRCC with ASPL-TFE3 fusion are more prone to present at advanced stage than cases with PRCC-TFE3 (14), however, in our cohort, although positive lymph node status at surgery is more common in ASPL-TFE3 cases (6/11, 54.5%), there was no statistically significant difference in pM stage at the last follow-up between ASPL-TFE3 and PRCC-TFE3 cases. In addition, cases 25 presented with LN and vertebral metastasis after 10 years, which indicated follow-up period need to be long enough to estimate metastasis status and outcome.

The prognosis of Xp11.2 tRCC could be affected by a variety of factors. Above all, the impact of age on prognosis is prominent in Xp11.2 tRCC. Pediatric patients tended to show an indolent course whether the presence of lymph node metastasis (33). Case 3 in our cohort is a 7-year-old boy and showed no evidence of disease after 172-month follow-up, which seemed to support this view. Recent study has demonstrated that pediatric patients with Xp11.2 tRCC have a lower burden of genetic alteration compared with adult patients (34) and this could be a probable explanation of this phenomenon. On the contrary, Xp11.2 tRCC was more aggressive in adults, older age and distant metastasis were two predictors of poor prognosis (14, 35). Beyond that, the correlation between fusion subtypes and outcomes are currently being explored. In our study, cases with ASPL-TFE3 fusion showed a worse PFS compared with non-ASPL group, which supported that ASPL-TFE3 fusion may represent a more adverse prognosis in previous studies (12, 14, 36). Apart from fusion subtypes, copy number alterations (CNA) and chromosomal amplification could also affect the prognosis of Xp11.2 tRCC (23, 24). Patients with CNA burden had worse survival outcomes and 22q loss was an independent adverse prognostic marker (12, 37).In addition, a recent proteogenomic study revealed that deletions of 3p could lead to decreased OS *via* trans- effect or cis-effect (36). Overall, genetic alteration is an important cause of the clinical heterogeneity in Xp11.2 tRCC.

The effective treatment strategy for Xp11.2 tRCC is still unclear. Several clinical investigations have indicated that Xp11.2 tRCC patients had a poor response to immune checkpoint inhibitors (ICIs) and tyrosine kinase inhibitors (TKIs) (38, 39). However, the response to immunotherapy and vascular endothelial growth factor receptor (VEGFR)-targeted therapy seemed to vary according to the fusion subtypes. A previous case report demonstrated an 18-year-old male Xp11.2 tRCC patient with ASPL-TFE3 fusion had a favorable response to sorafenib (40). Recent transcriptomic analysis also revealed tumors with ASPL-TFE3 fusion are more likely to benefit from antiangiogenic treatments compared with the other subtypes and ICI plus TKI combination therapy may be a better choice (12). Besides, due to the activation of RPS6KB1 in Xp11.2 tRCC, Trilaciclib, an FDA-approved CDK5 inhibitor, was expected to become a potential therapeutic drug (36).

There are some limitations to our research. Firstly, although we have collected as much data of Xp11.2 tRCC cases as possible to fulfill the research goal, the sample size still needs to be further expanded. Secondly, our follow-up data only suggested there was a significant difference in PFS, therefore the patients require a longer follow-up time to validate the results.

In summary, Xp11.2 tRCC is a group of highly heterogeneous tumors. Of the four common fusion subtypes, cases in non-DBHS family group more frequently developed LN and distant metastases than cases in DBHS family group. Tumors with ASPL-TFE3 fusion tend to have a worse outcome while those with NONO-TFE3 fusion exhibit a relatively good prognosis. Novel therapeutic approaches and targets for Xp11.2 tRCC with different fusion subtypes remain to be explored.

Data availability statement

The original contributions presented in the study are included in the article and Supplementary Material. The Illumina HiSeq next generation sequencing was performed by GloriousMed. The datasets presented in this article are not readily available because patient confidentiality and participant privacy, thus requests to access the datasets should be directed to info@gloriousmed.com.

Ethics statement

The studies involving human participants were reviewed and approved by Institutional Review Board of the Nanjing Drum Tower Hospital. The patients/participants provided their written informed consent to participate in this study.

Author contributions

WGu and YZ performed study concept and design; YZ and XP performed developpment of methodology and writing, review and revision of the paper; WGu provided acquisition, analysis and interpretation of data, and statistical analysis; WGa and HG provided technical and material support. All authors read and approved the final paper.

Funding

This research was supported by the Project of Invigorating Health Care through Science, Technology and Education, Jiangsu Provincial Key Medical Discipline (Laboratory) (ZDXKB2016014) and Beijing Ronghe Medical Development Foundation. The funders had no role in study design, data collection and analysis, decision to publish, or preparation of the manuscript.

Acknowledgments

The authors thank Xiaogong Li, Gutian Zhang, Xiaozhi Zhao, Changwei Ji (Department of Urology, Nanjing Drum Tower Hospital) for providing patient information. We also thank Jun Yang and Ming Chen (Department of Pathology, Nanjing Drum Tower Hospital) for providing technical assistance.

Conflict of interest

The authors declare that the research was conducted in the absence of any commercial or financial relationships that could be construed as a potential conflict of interest.

Publisher's note

Supplementary material

The Supplementary Material for this article can be found online at: https://www.frontiersin.org/articles/10.3389/fonc.2023.1116648/full#supplementary-material

References

1. Moch H, Cubilla AL, Humphrey PA, Reuter VE, Ulbright TM. The 2016 WHO classification of tumours of the urinary system and Male genital organs-part a: Renal, penile, and testicular tumours. *Eur Urol* (2016) 70(1):93–105. doi: 10.1016/j.eururo.2016.02.029

2. Kauffman EC, Ricketts CJ, Rais-Bahrami S, Yang Y, Merino MJ, Bottaro DP, et al. Molecular genetics and cellular features of TFE3 and TFEB fusion kidney cancers. *Nat Rev Urol* (2014) 11(8):465–75. doi: 10.1038/nrurol.2014.162

3. Argani P, Antonescu CR, Illei PB, Lui MY, Timmons CF, Newbury R, et al. Primary renal neoplasms with the ASPL-TFE3 gene fusion of alveolar soft part sarcoma: a distinctive tumor entity previously included among renal cell carcinomas of children and adolescents. *Am J Pathol* (2001) 159(1):179–92. doi: 10.1016/s0002-9440(10)61684-7

4. Argani P, Antonescu CR, Couturier J, Fournet JC, Sciot R, Debiec-Rychter M, et al. PRCC-TFE3 renal carcinomas: morphologic, immunohistochemical, ultrastructural, and molecular analysis of an entity associated with the t(X;1)(p11.2;q21). *Am J Surg Pathol* (2002) 26(12):1553–66. doi: 10.1097/00000478-200212000-00003

5. Argani P, Lal P, Hutchinson B, Lui MY, Reuter VE, Ladanyi M. Aberrant nuclear immunoreactivity for TFE3 in neoplasms with TFE3 gene fusions: a sensitive and specific immunohistochemical assay. *Am J Surg Pathol* (2003) 27(6):750–61. doi: 10.1097/00000478-200306000-00005

6. Argani P, Zhang L, Reuter VE, Tickoo SK, Antonescu CR. RBM10-TFE3 renal cell carcinoma: A potential diagnostic pitfall due to cryptic intrachromosomal Xp11.2 inversion resulting in false-negative TFE3 FISH. *Am J Surg Pathol* (2017) 41(5):655–62. doi: 10.1097/pas.0000000000000835

7. Argani P, Zhong M, Reuter VE, Fallon JT, Epstein JI, Netto GJ, et al. TFE3-fusion variant analysis defines specific clinicopathologic associations among Xp11 translocation cancers. *Am J Surg Pathol* (2016) 40(6):723–37. doi: 10.1097/pas.0000000000000631

8. Clark J, Lu YJ, Sidhar SK, Parker C, Gill S, Smedley D, et al. Fusion of splicing factor genes PSF and NonO (p54nrb) to the TFE3 gene in papillary renal cell carcinoma. *Oncogene* (1997) 15(18):2233–9. doi: 10.1038/sj.onc.1201394

9. Classe M, Malouf GG, Su X, Yao H, Thompson EJ, Doss DJ, et al. Incidence, clinicopathological features and fusion transcript landscape of translocation renal cell carcinomas. *Histopathology* (2017) 70(7):1089–97. doi: 10.1111/his.13167

10. Huang W, Goldfischer M, Babayeva S, Mao Y, Volyanskyy K, Dimitrova N, et al. Identification of a novel PARP14-TFE3 gene fusion from 10-year-old FFPE tissue by RNA-seq. *Genes Chromosomes Cancer* (2015) 54(8):500–5. doi: 10.1002/gcc.22261

11. Malouf GG, Su X, Yao H, Gao J, Xiong L, He Q, et al. Next-generation sequencing of translocation renal cell carcinoma reveals novel RNA splicing partners and frequent mutations of chromatin-remodeling genes. *Clin Cancer Res* (2014) 20(15):4129–40. doi: 10.1158/1078-0432.CCR-13-3036

12. Sun G, Chen J, Liang J, Yin X, Zhang M, Yao J, et al. Integrated exome and RNA sequencing of TFE3-translocation renal cell carcinoma. *Nat Commun* (2021) 12(1):5262. doi: 10.1038/s41467-021-25618-z

13. . (!!! INVALID CITATION !!!).

14. Ellis CL, Eble JN, Subhawong AP, Martignoni G, Zhong M, Ladanyi M, et al. Clinical heterogeneity of Xp11 translocation renal cell carcinoma: impact of fusion subtype, age, and stage. *Mod Pathol* (2014) 27(6):875–86. doi: 10.1038/modpathol.2013.208

15. Knott GJ, Bond CS, Fox AH, The DBHS proteins SFPQ. NONO and PSPC1: a multipurpose molecular scaffold. *Nucleic Acids Res* (2016) 44(9):3989–4004. doi: 10.1093/nar/gkw271

16. de Silva HC, Lin MZ, Phillips L, Martin JL, Baxter RC. IGFBP-3 interacts with NONO and SFPQ in PARP-dependent DNA damage repair in triple-negative breast cancer. *Cell Mol Life Sci* (2019) 76(10):2015–30. doi: 10.1007/s00018-019-03033-4

17. Feng P, Li L, Deng T, Liu Y, Ling N, Qiu S, et al. NONO and tumorigenesis: More than splicing. *J Cell Mol Med* (2020) 24(8):4368–76. doi: 10.1111/jcmm.15141

18. Petti E, Buemi V, Zappone A, Schillaci O, Broccia PV, Dinami R, et al. SFPQ and NONO suppress RNA:DNA-hybrid-related telomere instability. *Nat Commun* (2019) 10(1):1001. doi: 10.1038/s41467-019-08863-1

19. Xia QY, Wang Z, Chen N, Gan HL, Teng XD, Shi SS, et al. Xp11.2 translocation renal cell carcinoma with NONO-TFE3 gene fusion: morphology, prognosis, and potential pitfall in detecting TFE3 gene rearrangement. *Mod Pathol* (2017) 30(3):416–26. doi: 10.1038/modpathol.2016.204

20. Weterman MA, van Groningen JJ, Tertoolen L, van Kessel AG. Impairment of MAD2B-PRCC interaction in mitotic checkpoint defective t(X;1)-positive renal cell carcinomas. *Proc Natl Acad Sci U.S.A.* (2001) 98(24):13808–13. doi: 10.1073/pnas.241304198

21. Chen X, Yang Y, Gan W, Xu L, Ye Q, Guo H. Newly designed break-apart and ASPL-TFE3 dual-fusion FISH assay are useful in diagnosing Xp11.2 translocation renal cell carcinoma and ASPL-TFE3 renal cell carcinoma: a STARD-compliant article. *Med (Baltimore)* (2015) 94(19):e873. doi: 10.1097/MD.0000000000000873

22. Xiong L, Chen X, Liu N, Wang Z, Miao B, Gan W, et al. PRCC-TFE3 dual-fusion FISH assay: A new method for identifying PRCC-TFE3 renal cell carcinoma in paraffin-embedded tissue. *PloS One* (2017) 12(9):e0185337. doi: 10.1371/journal.pone.0185337

23. Macher-Goeppinger S, Roth W, Wagener N, Hohenfellner M, Penzel R, Haferkamp A, et al. Molecular heterogeneity of TFE3 activation in renal cell carcinomas. *Mod Pathol* (2012) 25(2):308–15. doi: 10.1038/modpathol.2011.169

24. Malouf GG, Monzon FA, Couturier J, Molinie V, Escudier B, Camparo P, et al. Genomic heterogeneity of translocation renal cell carcinoma. *Clin Cancer Res* (2013) 19(17):4673–84. doi: 10.1158/1078-0432.CCR-12-3825

25. Argani P, Olgac S, Tickoo SK, Goldfischer M, Moch H, Chan DY, et al. Xp11 translocation renal cell carcinoma in adults: expanded clinical, pathologic, and genetic spectrum. *Am J Surg Pathol* (2007) 31(8):1149–60. doi: 10.1097/PAS.0b013e318031ffff

26. Gandhi JS, Malik F, Amin MB, Argani P, Bahrami A. MiT family translocation renal cell carcinomas: A 15th anniversary update. *Histol Histopathol* (2020) 35(2):125–36. doi: 10.14670/HH-18-159

27. Wang XT, Xia QY, Ni H, Ye SB, Li R, Wang X, et al. SFPQ/PSF-TFE3 renal cell carcinoma: a clinicopathologic study emphasizing extended morphology and reviewing the differences between SFPQ-TFE3 RCC and the corresponding mesenchymal neoplasm despite an identical gene fusion. *Hum Pathol* (2017) 63:190–200. doi: 10.1016/j.humpath.2017.02.022

28. Wang XT, Xia QY, Zhou XJ, Rao Q. Xp11 translocation renal cell carcinoma and the mesenchymal counterparts: An evolving concept with novel insights on clinicopathologic features, prognosis, treatment, and classification. *Crit Rev Oncog* (2017) 22(5-6):481–97. doi: 10.1615/CritRevOncog.2017020558

29. Song Y, Yin X, Xia Q, Zheng L, Yao J, Zeng H, et al. Xp11 translocation renal cell carcinoma with morphological features mimicking multilocular cystic renal neoplasm of low malignant potential: a series of six cases with molecular analysis. *J Clin Pathol* (2021) 74(3):171–6. doi: 10.1136/jclinpath-2020-206681

30. Argani P. MiT family translocation renal cell carcinoma. *Semin Diagn Pathol* (2015) 32(2):103–13. doi: 10.1053/j.semdp.2015.02.003

31. Rao Q, Williamson SR, Zhang S, Eble JN, Grignon DJ, Wang M, et al. TFE3 break-apart FISH has a higher sensitivity for Xp11.2 translocation-associated renal cell carcinoma compared with TFE3 or cathepsin K immunohistochemical staining alone: expanding the morphologic spectrum. *Am J Surg Pathol* (2013) 37(6):804–15. doi: 10.1097/PAS.0b013e31827e17cb

32. Takayama KI. Splicing factors have an essential role in prostate cancer progression and androgen receptor signaling. *Biomolecules* (2019) 9(4). doi: 10.3390/biom9040131

33. Geller JI, Argani P, Adeniran A, Hampton E, De Marzo A, Hicks J, et al. Translocation renal cell carcinoma: lack of negative impact due to lymph node spread. *Cancer* (2008) 112(7):1607–16. doi: 10.1002/cncr.23331

34. Marcon J, DiNatale RG, Sanchez A, Kotecha RR, Gupta S, Kuo F, et al. Comprehensive genomic analysis of translocation renal cell carcinoma reveals copy-number variations as drivers of disease progression. *Clin Cancer Res* (2020) 26(14):3629–40. doi: 10.1158/1078-0432.CCR-19-3283

35. Calio A, Segala D, Munari E, Brunelli M, Martignoni G. MiT family translocation renal cell carcinoma: from the early descriptions to the current knowledge. *Cancers* (2019) 11(8). doi: 10.3390/cancers11081110

36. Qu Y, Wu X, Anwaier A, Feng J, Xu W, Pei X, et al. Proteogenomic characterization of MiT family translocation renal cell carcinoma. *Nat Commun* (2022) 13(1):7494. doi: 10.1038/s41467-022-34460-w

37. Pan CC, Sung MT, Huang HY, Yeh KT. High chromosomal copy number alterations in Xp11 translocation renal cell carcinomas detected by array comparative genomic hybridization are associated with aggressive behavior. *Am J Surg Pathol* (2013) 37(7):1116–9. doi: 10.1097/PAS.0b013e318293d872

38. McKay RR, Bosse D, Xie W, Wankowicz SAM, Flaifel A, Brandao R, et al. The clinical activity of PD-1/PD-L1 inhibitors in metastatic non-clear cell renal cell carcinoma. *Cancer Immunol Res* (2018) 6(7):758–65. doi: 10.1158/2326-6066.CIR-17-0475

39. Boileve A, Carlo MI, Barthelemy P, Oudard S, Borchiellini D, Voss MH, et al. Immune checkpoint inhibitors in MITF family translocation renal cell carcinomas and genetic correlates of exceptional responders. *J Immunother Cancer* (2018) 6(1):159. doi: 10.1186/s40425-018-0482-z

40. Hou MM, Hsieh JJ, Chang NJ, Huang HY, Wang HM, Chuang CK, et al. Response to sorafenib in a patient with metastatic xp11 translocation renal cell carcinoma. *Clin Drug Investig* (2010) 30(11):799–804. doi: 10.2165/11537220-000000000-00000

frontiers | Frontiers in Oncology

TYPE Systematic Review
PUBLISHED 07 March 2023
DOI 10.3389/fonc.2023.1104242

OPEN ACCESS

EDITED BY
Dingwei Ye,
Fudan University, China

REVIEWED BY
Orazio Caffo,
Santa Chiara Hospital, Italy
Enrique Gonzalez Billalabeitia,
Hospital Universitario 12 de Octubre, Spain

*CORRESPONDENCE
Feng Sun
sunfeng@bjmu.edu.cn
Jin Gu
zlgujin@126.com
Ningchen Li
wjpurologycenter@sina.com

†These authors have contributed equally to this work and share first authorship

SPECIALTY SECTION
This article was submitted to Genitourinary Oncology, a section of the journal Frontiers in Oncology

RECEIVED 21 November 2022
ACCEPTED 20 February 2023
PUBLISHED 07 March 2023

CITATION
Wang L, Li C, Zhao Z, Li X, Tang C, Guan Z, Sun F, Gu J and Li N (2023) Comparison of doublet and triplet therapies for metastatic hormone-sensitive prostate cancer: A systematic review and network meta-analysis.
Front. Oncol. 13:1104242.
doi: 10.3389/fonc.2023.1104242

Comparison of doublet and triplet therapies for metastatic hormone-sensitive prostate cancer: A systematic review and network meta-analysis

Lei Wang[1†], Chunxing Li[2†], Zichen Zhao[1], Xiaojian Li[1], Chong Tang[3], Zhenpeng Guan[3], Feng Sun[4*], Jin Gu[5,6*] and Ningchen Li[1*]

[1]Wu Jieping Urology Center, Peking University Shougang Hospital, Beijing, China, [2]Department of Pharmacy, Aerospace Center Hospital, Beijing, China, [3]Department of Orthopedics, Peking University Shougang Hospital, Beijing, China, [4]Department of Epidemiology and Biostatistics, School of Public Health, Peking University Health Science Center, Beijing, China, [5]Gastrointestinal Cancer Center, Peking University Cancer Hospital, Key Laboratory of Carcinogenesis and Translational Research (Ministry of Education), Beijing, China, [6]Department of Gastrointestinal Surgery, Peking University Shougang Hospital, Beijing, China

Background: The best choice of first-line treatment for metastatic hormone-sensitive prostate cancer (mHSPC) is unclear. We aimed to compare the effectiveness and safety determined in randomized clinical trials of doublet and triplet treatments for mHSPC.

Methods: Medline, Embase, Cochrane Central and ClinicalTrials.gov were searched from inception through July 01, 2022. Eligible studies were phase III randomized clinical trials evaluating androgen deprivation treatment (ADT) alone, doublet therapies [ADT combined with docetaxel (DOC), novel hormonal agents (NHAs), or radiotherapy (RT)], or triplet therapies (NHA+DOC+ADT) as first-line treatments for mHSPC. Outcomes of interest included overall survival (OS), progression-free survival (PFS) and grades 3-5 adverse events (AEs). Subgroup analyses were performed based on tumor burden. The effects of competing treatments were assessed by Bayesian network meta-analysis using R software.

Results: Ten trials with 12,298 patients comparing nine treatments were included. Darolutamide (DARO) +DOC+ADT ranked best in terms of OS benefits (OR 0·52 [95% CI 0·39–0·70]), but its advantages were all statistically insignificant compared with other therapy options except for DOC+ADT (OR 0·68 [95% CI 0·53–0·88]) and RT+ADT (OR 0·57 [95% CI 0·40–0·80]). In terms of PFS, enzalutamide(ENZA)+DOC+ADT (OR 0·32 [95% CI 0·24–0·44]) and abiraterone and prednisone (AAP) +DOC+ADT (OR 0·33 [95% CI 0·25–0·45]) ranked best. For patients with high volume disease (HVD), low volume disease (LVD), and visceral metastases, the optimal therapies were AAP+DOC+ADT (OR 0·52 [95% CI 0·33–0·83]), apalutamide+ADT (OR 0·52 [95% CI 0·26–1·05]) and DARO+DOC+ADT (OR 0·42 [95% CI 0·13–1·34]), respectively. For safety, AAP

+DOC+ADT (OR 3·56 [95% CI 1·51–8·43]) ranked worst with the highest risk of grade 3–5 AEs.

Conclusions: Triple therapies may further improve OS and PFS but may be associated with a decrease in safety. Triplet therapies could be suggested for HVD patients, while doublet combinations should still be preferred for LVD patients.

Systematic Review Registration: https://www.crd.york.ac.uk/PROSPEROFILES/303117_STRATEGY_20220202.pdf, identifier CRD4202303117.

KEYWORDS

prostate cancer, chemotherapy, hormonal therapy, radiation therapy, combination therapy

Introduction

Prostate cancer (PCa) is one of the most common malignant tumors in men worldwide (1). Distant metastasis often indicates a poor prognosis (2). For metastatic hormone-sensitive prostate cancer (mHSPC), androgen-deprivation therapy (ADT) has been regarded as the standard of care (SOC) and the only systematic treatment option for a long time (3). However, patients receiving ADT will inevitably gradually resist the treatment and enter the stage of castration resistance (mCRPC), which will significantly worsen the prognosis (4–6). Delaying the progression of metastatic prostate cancer to mCRPC has always been an important topic in the field of prostate cancer treatment.

In recent years, the emergence of many novel therapies has greatly improved the prognosis of patients with mHSPC (7–9). These therapies consist of ADT combined with another therapeutic agent. The earlier agent was the docetaxel (DOC) chemotherapy (10–12), followed by the androgen synthesis inhibitor abiraterone acetate (13, 14) and the new androgen receptor inhibitors enzalutamide (ENZA) (15, 16) and apalutamide (APA) (17). The above three drugs and darolutamide (DARO) are also known as novel hormonal agents (NHAs) to distinguish them from traditional endocrine therapeutic drugs such as goserelin and bicalutamide. In addition, ADT combined with radiotherapy (RT) (18) is considered to provide survival benefits for mHSPC patients with low volume disease (LVD). The emergence of these novel combination therapies is significantly changing the previous standard of care for mHSPC using ADT alone, but the advantages and disadvantages of these combination therapies are controversial due to the lack of head-to-head comparisons (4, 7, 8, 19–24).

Recent reports of triplet therapies for mHSPC have made the situation even more confusing. The earliest reports of triplet therapy can be traced back to a subgroup analysis reported in the ENZAMET study in 2019 (15), where up to 44.7% of enrolled patients received docetaxel chemotherapy just before or concurrently with the experimental intervention. Data from this subgroup could be used to analyze the efficacy of ENZA+DOC +ADT versus DOC+ADT, but there was no significant difference in the final overall survival (OS) results. However, the PEACE-1 study (25) published positive results on triplet therapy in 2021, and OS in patients receiving abiraterone combined with DOC+ADT was significantly better than that in patients receiving DOC+ADT. The results from another well-designed phase III clinical study, ARASENS (26), further showed that patients who received the novel hormonal agent darolutamide in combination with DOC +ADT also had a longer OS than patients receiving DOC+ADT.

The emergence of new effective treatment options is beneficial, but for clinical oncologists, understanding the pros and cons of different treatment options is clinically important. This study aimed to conduct a network meta-analysis (NMA) of the efficacy and safety of doublet and triplet therapies for mHSPC identified in phase III randomized clinical trials (RCTs) in recent years to compare the efficacy and safety of different treatments in mHSPC according to the current data.

Methods

The study protocol was registered with the International Prospective Register of Systematic Reviews (PROSPERO), registration number CRD4202303117.

Search strategy

According to the Preferred Reporting Items for Systematic Reviews and Meta-Analyses (PRISMA) specification, a systematic search was conducted for RCT studies published prior to and including July 01, 2022. Databases searched included Medline, Embase, Cochrane Central, and ClinicalTrials.gov. The main search terms included prostate cancer, hormone sensitive, clinical trial, docetaxel, abiraterone, enzalutamide, apalutamide, darolutamide, radiotherapy, etc. Different combinations and strategies were applied during different database retrievals (Appendix P 1-4). Only the results of RCTs published in English were included in this article,

and a search was performed before the final statistical analysis to avoid omitting the latest published results.

Study selection

The literature was screened according to the principles of Participants, Interventions, Comparisons and Outcomes (PICO). Inclusion criteria were as follows: study population: 1) Adult patients with mHSPC, aged ≥18 years; 2) Patients with initial onset or those who progressed after previous local therapy; 3) The duration of ADT treatment allowed in the stage of localized prostate cancer was no more than three years, and in the stage of metastatic prostate cancer was no more than six months; 4) Data from phase III RCTs. Interventions: 1) First-line treatments for mHSPC recommended in the latest guidelines of EAU and NCCN, including ADT combined with docetaxel, abiraterone acetate, enzalutamide, apalutamide, and RT+ADT (for LVD patients); 2) Recently reported triplet therapies, mainly NHAs+DOC+ADT. Control group: 1) According to the design of different studies, treatments in control groups included ADT alone, ADT plus placebo, or ADT plus traditional nonsteroidal antiandrogens (NSAA) (27, 28); 2) In studies with triplet therapies, the treatment in control groups was DOC+ADT. Outcomes: The main outcome was OS, and the secondary outcomes were progression-free survival (PFS) and safety indicators of high-grade AEs. Exclusion criteria: 1) Patients with metastatic or nonmetastatic castration-resistant prostate cancer; 2) Nonrandomized controlled studies or phase I/II RCTs; 3) Research that could not extract relevant data; 4) Duplicate studies.

Risk of bias assessment

The methodological quality of each study was independently assessed by two independent investigators using the revised Cochrane Collaboration Risk of Bias tool RoB1.0, and differences of opinion were resolved by consultation. The overall bias of the trial was assessed for each study from the following seven domains: random sequence generation (selection bias), allocation concealment (selection bias), blinding of participants and personnel (performance bias), blinding of outcome assessment (detection bias), incomplete outcome data (attrition bias), selective reporting (reporting bias), and other biases. The study as a whole was deemed as having a "low risk of bias" if all terms were at low risk of bias. The study as a whole was judged to be at high risk of bias if either item was judged to be at high risk of bias. Other conditions were judged to be at moderate risk of bias. We also assessed the certainty of evidence using the Confidence in Network Meta-Analysis framework (CINeMA).

Data extraction

Two independent researchers followed a preplanned search strategy that required each researcher to perform his research separately according to PRISMA guidelines (29). When multiple papers reported results from the same study at different stages, data was only extracted for the most recent results. Any discrepancies were resolved by consensus. Two investigators used predesigned forms for data extraction and recording. The characteristics of the included patients, including ECOG performance score, age, PSA value, Gleason score, visceral metastasis, tumor burden, proportion of patients with primary metastasis, previous ADT use, and previous/concurrent use of docetaxel, were recorded in detail. In terms of related efficacy results, HR values for OS and PFS were recorded, as well as HR values for different tumor burden subgroups. For safety outcomes, the number of patients with high-grade AEs were recorded, and OR values were calculated.

Data synthesis strategy

Three similar indicators related to PFS were used in different studies, including PFS (12, 13, 18, 30–32), radiographic progression-free survival (rPFS) (11, 14, 16, 17, 25, 33–36), and clinical progression-free survival (cPFS) (10, 11, 15). Since the three were similar in definition, and in most cases the imaging progression was earlier than the aggravation of clinical symptoms and death, we unified the three into one "generalized PFS" in the present meta-analysis (7). Traditional nonsteroidal antiandrogens (NSAA) have long been considered to result in no or very little improvement in OS in patients with metastatic prostate cancer (27, 28); therefore, we considered NSAA+ADT as the same treatment as ADT alone to pool more data in the present review. In the subgroup analysis, we focused on tumor burden (high- versus low-volume disease), as most RCTs suggested that tumor burden was a feature that influenced the efficacy of interventions. Following the CHAARTED study criteria (11, 36, 37), high volume disease (HVD) was defined as the presence of visceral metastases and/or four or more bone metastases, with at least one bone metastasis located outside the spine and pelvis. We also made subgroup analyses for de novo patients and patients with previous local treatment.

Statistical analysis

The network meta-analysis was performed using the "gemtc" and "rjags" packages of the R 4·0·5 software using the Monte Carlo Markov Chain (McMc) method in a Bayesian framework (38, 39). A network diagram was drawn for each intervention. The original hazard ratio (HR) values and 95% confidence intervals (CIs) of each RCT study (or their subgroup data) were extracted, and the consistency model was used (40). The number of model chains was 3, the initial value was 2·5, the sampling number was 10,000, and the number of iterations was 100 000 with a step size of 10. For closed-loop studies with both direct evidence and indirect evidence, the node-splitting model was used to test the consistency of closed-loop studies, and $P<0·05$ was considered statistically significant. The "mtc.anohe" command in the "gemtc" package was used to assess overall heterogeneity and was recorded with the variance parameter I^2. Heterogeneity was assessed visually using forest plots and I^2 statistics. If the heterogeneity was large ($I^2>50\%$, $P<0·1$), the source of heterogeneity was further analyzed.

The trace plotting method and density plotting method were used to evaluate the convergence of the model. The rank probability was calculated to determine the level of superiority and inferiority of different treatments according to P scores (41). We extracted the "number of patients with grade 3-5 AEs/total patients" in each group and calculated the odds ratio (OR) and 95% CI.

Results

Characteristics of eligible studies

A total of 5138 articles and 169 clinical trials were retrieved from the literature search, and 68 of them were read in full text after browsing the titles and abstracts. Finally, ten multicenter phase III randomized controlled trials (21 references) (10–18, 25, 26, 30–37, 42, 43) were included in the analysis (Figure 1). A total of 12,298 patients were included, with a median number of patients of 1,069 (range, 385-2061), median follow-up time of 44·6 months (range, 34-84 months), and publication years between 2013 and 2022. The ten trials involved a total of nine treatments, including ADT alone, DOC+ADT, abiraterone and prednisone(AAP)+ADT, ENZA +ADT, APA+ADT, RT+ADT, ENZA+DOC+ADT, AAP+DOC +ADT, and DARO+DOC+ADT. For OS, the overall risk of bias was low in five trials (CHAARTED, STAMPEDE-arm C, TITAN, HORRAD and ARASENS), while the remaining trials raised some concerns. All trials raised some concerns regarding generalized PFS except for the TITAN trial (Appendix P 5-6).

The STAMPEDE study (12, 13, 18, 30, 31) allowed the recruitment of localized high-risk patients, and we only extracted data from mHSPC patients in this analysis. In the multiarm, multiphase STAMPEDE study, there was a period of overlap in the recruitment timing of arm C and arm G; thus data from this period could be used to directly compare AAP+ADT and DOC +ADT (32). The PEACE-1 study (25) used a 2 × 2 factorial design for newly diagnosed mHSPC patients. Only the data of the docetaxel population was extracted, and the triplet therapy "AAP +DOC+ADT" and the doublet therapy "DOC+ADT" were compared. The baseline characteristics of all included studies are listed in Table 1 and Appendix (P 7-8).

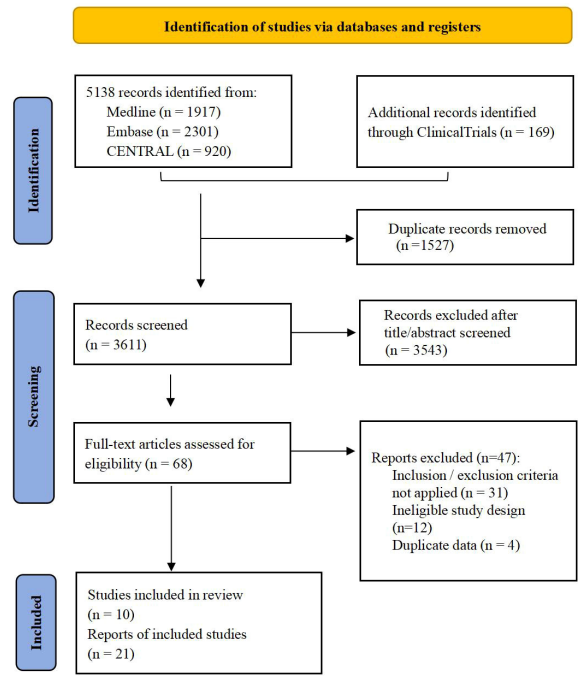

FIGURE 1
Literature screening flow chart.

There was a certain proportion of patients with "early planned docetaxel used" in ENZAMET (15), ARCHES (16, 42), TITAN (17, 33) and STAMPEDE arm H (18) trials. There were obvious differences in HR values for OS between the docetaxel population and the population that did not use docetaxel (Table 2), which suggested that the treatment sequence of docetaxel followed by NHAs may limit the effectiveness of NHAs (15, 16, 18, 33, 42). Thus, in our review, we strictly evaluated the impact of "planned docetaxel use" on the efficacies of NHAs or radiotherapy in relevant studies (15, 16, 18, 33, 42). We strictly excluded data from the docetaxel population in effectiveness assessment, unless data extraction was difficult in some subgroups. In the ENZAMET and ARCHES studies, 44·7% and 17·8% of patients received "early planned docetaxel chemotherapy", respectively, and these patients actually received triplet therapy. We extracted data from these docetaxel populations and made an exploratory analysis on the comparative efficacy of triplet therapy of "ENZA+DOC+ADT" and doublet therapy of "DOC+ADT". For similar data of the docetaxel population in the TITAN and STAMPEDE arm H studies, we did not conduct a similar analysis due to the small number of patients and incomplete data (Appendix P 9).

OS for the overall population

Figure 2 shows a network diagram comparing different treatment options. Only data from 342 mHSPC patients from arms C and G of the STAMPEDE study, a multiarm, multistage RCT, were extracted for a head-to-head comparison (32). Consistency tests for this closed-loop comparison suggested that p values were all >0.1 (Appendix P 11). The results of the heterogeneity test indicated that I^2 = 60.1% for the comparison of abiraterone and docetaxel, and the heterogeneity was derived from the direct comparison between the two agents (Appendix P 12-18).

The STAMPEDE study had four comparison groups, arm C (12), arm G (13), and arm H (18), and a head-to-head subgroup (32). While in both ENZAMET (15) and ARCHES (16, 42) studies, independent analyses of the "docetaxel population" were performed. Therefore, a total of 15 comparison groups were obtained from the ten trials (Appendix P 9), and the data of these 15 groups were all included in the network meta-analysis of OS. The forest plot demonstrated a comparison with ADT alone or DOC +ADT and is shown in Figures 3A, B.

Except for radiotherapy (HR 0·92, 95% CI 0·76-1·11), the other seven treatment options were all significantly better than ADT in terms of OS benefits. Compared with docetaxel chemotherapy, only the triplet therapies of DARO+DOC+ADT (HR 0·68, 95% CI 0·53-0·88) had significant OS benefits. Additionally, the triplet therapy of

TABLE 1 Characteristics of included trials.

Trial	Population	Enrollment	Treatment added to ADT	mHSPC cases No. (Exp. *vs.* Ctrl)	Inclusion of interest	Primary endpoint	Secondary endpoint (with interest)	Follow -up, mo
GETUG -AFU15 [10,37]	France and Belgium	Oct. 2004-Dec. 2008	Docetaxel *vs.* no treatment	385 (192 *vs.* 193)	1) no previous chemotherapy; 2) previous hormone therapy in metastatic setting within the past 2 months allowed; 3) 29% with metastases after previous radical treatment; 4) 48% with HVD; 5) daily prednisone use not needed; 6) 66% received ADT combined with NSAA.	OS	cPFS, bPFS, rPFS	84
CHAARTED[11,38]	USA	July 2006-Dec. 2012	Docetaxel *vs.* no treatment	790 (397 *vs.* 393)	1) no previous chemotherapy; 2) no previous hormone therapy in metastatic setting; 3) 27% with metastases after previous radical treatment; 4) 65% with HVD; 5) daily prednisone use not needed.	OS	cPFS, time to CRPC	54
STAMPEDE-arm C [12] [31]	UK and Swiss	Oct.2005-Mar.2013	Docetaxel *vs.* no treatment	1086 (362 *vs.* 724)	1) no previous chemotherapy; 2) 5% with metastases after previous radical treatment; 3) 56% with HVD; 4) daily prednisone use needed (5mg, bid); 5) 7% with planned SOC radiotherapy.	OS	FFS, PFS, time to any treatment after progression	78
STAMPEDE-arm G [13,30]		Nov. 2011-Jan. 2014	AAP *vs.* no treatment	1002 (500 *vs.* 502)	1) no prior chemotherapy; 2) no previous long-term hormone therapy; 3) 5% with metastases after previous radical treatment; 4) 55% with HVD; 5) 30% with planned SOC Radiotherapy.	OS	FFS, PFS, symptomatic SRE, adverse events, QOL, PCa-specific survival	42
STAMPEDE-arm H [18]		Jan. 2013-Sep.2016	Radiotherapy *vs.* no treatment	2061 (1032 *vs.* 1029)	1) 18% with planned DOC chemotherapy (≤6 cycles and without disease progression); 2) 100% newly diagnosed mPCa; 3) 58% with HVD.	OS, FFS	PFS, mPFS, prostate cancer-specific survival, and symptomatic local event-free survival	37
LATITUDE [14,36]	Worldwide (34 countries)	Feb. 2013-Dec.2014	AAP *vs.* placebo	1199 (597 *vs.* 602)	1) no prior chemotherapy, radiation therapy, or surgery; 2) previous hormone therapy in metastatic setting within the past 3 months allowed;	OS, rPFS	Time to PSA progression, Time to next symptomatic SRE, Time to subsequent PCa therapy	52

(Continued)

TABLE 1 Continued

Trial	Population	Enrollment	Treatment added to ADT	mHSPC cases No. (Exp. *vs.* Ctrl)	Inclusion of interest	Primary endpoint	Secondary endpoint (with interest)	Follow -up, mo
					3) 100% newly diagnosed mPCa; 4) mHSPC with two of three high risk factors, 80% with HVD.			
ENZAMET [15]	6 countries, maily Australian and Canada	Mar.2014-Mar.2017	Enzalutamide *vs.* NSAA	1125 (563 *vs.* 562)	1) 16% with DOC chemotherapy (≤2 cycles and without disease progression) before randomization; 2) previous hormone therapy in metastatic setting within the past 3 months allowed; 3) 39% with metastases after previous radical treatment; 4) 52% with HVD; 5) 44.7% with planned early DOC used.	OS	cPFS, adverse events	34
ARCHES [16,33,35]	Worldwide (24 countries)	Mar. 2016-Jan.2018	Enzalutamide *vs.* placebo	1150 (574 *vs.* 576)	1) 18% with previous chemotherapy (≤6 cycles and without disease progression); 2) no previous hormone therapy in metastatic setting; 3) 26% with metastases after previous radical treatment; 4) 63% with HVD; 5) 435(38%) had received prior AA. 5) 6.7% received concomitant antiandrogens.	OS, rPFS	time to PSA progression, time to initiation of new antineoplastic therapy, objective response	44.6
TITAN [17,34]	Worldwide (23 countries)	Dec.2015-July 2017	Apalutamide *vs.* placebo	1052 (525 *vs.* 527)	1) 10.7% with previous chemotherapy (≤6 cycles and without disease progression); 2) previous hormone therapy in metastatic setting within the past 3 months allowed; 3) 16% with metastases after previous radical treatment; 4) 63% with HVD; 5) NSAA allowed before randomization.	OS, rPFS	Time to chemotherapy, time to pain progression, time to chronic opioid use, time to SRE.	44
HORRAD [43]	Netherlands	Nov. 2004-Sep.2014	Radiotherapy *vs.* no treatment	432 (216 *vs.* 216)	1) no previous chemotherapy; 2) 100% newly diagnosed mPCa; 3) 83% with high burden in HORRAD definition.	OS	PSA-PFS	47
PEACE-1 (Docetaxel population) [25]	7 European countries	Nov. 2013-Dec. 2018	AAP+DOC *vs.* DOC	710 (355 *vs.* 355)	1) 100% *de novo* mHSPC; 2) no previous long-term	rPFS; OS	CRPC-free survival, cPFS, Prostate	42

(Continued)

TABLE 1 Continued

Trial	Population	Enrollment	Treatment added to ADT	mHSPC cases No. (Exp. *vs.* Ctrl)	Inclusion of interest	Primary endpoint	Secondary endpoint (with interest)	Follow -up, mo
					hormone therapy; 3) 64% with HVD; 4) Concomitant DOC and abiraterone use; 5) Full 6 cycles of DOC administered in 100% of patients; 6) ± radiotherapy allowed.		cancer specific survival, Toxicity	
ARASENS [26]	Worldwide (23 countries)	Nov. 2016-June 2018	DARO+DOC *vs.* DOC	1306 (651 *vs.* 654)	1)100% *de novo* mHSPC. 2) No previous chemotherapy, 2nd AR inhibitor, immunotherapy, or radiotherapy within 2 weeks before randomization; 3) NSAA allowed but should be discontinued before randomization.	OS	CRPC-free survival, time to pain progression, time to initiation of new antineoplastic therapy, safety	43.7 (DARO) 42.4 (Ctrl)

AA, antiandrogen drugs; AAP, abiraterone acetate+prednisone; ADT, androgen deprivation therapy; AR, androgen receptor; bPFS, biochemical progression free survival; cPFS, clinical progression free survival; CRPC, castration resistant prostate cancer; Ctrl, control group; DARO, darolutamide; DOC, docetaxel; Exp., experimental group; FFS, failure free survival; HVD, high volume disease in CHAARTED definition; mHSPC, metastatic hormonal-sensitive prostate cancer; mPCa, metastatic prostate cancer; mPFS, metastatic progression free survival; NSAA, non-steroidal anti-androgen; including nilutamide, flutamide or bicalutamide; OS, overall survival; QOL, quality of life; rPFS, radiographic progression free survival; SRE, skeletal related events; SOC, standard of care.

TABLE 2 Clinical trials or subgroups related to mHSPC's triplet therapies.

Study	Available comparison	Patients in available subgroups (n, %)	*de novo* mHSPC	Start of DOC use to NHA or RT	Proportion of pts with full 6 cycles of DOC administered	OS for DOC population (HR, 95% CI)	OS for non-DOC population (HR, 95% CI)	Generalized PFS for Doc population (HR,95% CI)
ENZAMET [15]	ENZA+DOC +ADT *vs.* DOC+ADT	503(44.7%)	61%	Prior (35%) and Concomitant (65%)	71% (65% in ENZA group and 76% in control group)	0.90 (0.62-1.31)	0.53, 0.37-0.75	cPFS: 0.48 (0.37-0.62)
ARCHES [16,33,35]	ENZA+DOC +ADT *vs.* DOC+ADT	205(17.8%)	67%	Prior	86%	0.74 (0.46-1.20)	0.64, 0.51-0.81	rPFS 0.52 (0.30-0.89)
TITAN[17,34]	APA+DOC +ADT *vs.* DOC+ADT	113(10.7%)	81%	Prior	NR (In median, 6 cycles administered)	1.12 (0.59-2.12)	0.61, 0.50-0.76	NR
STAMPEDE -RT [18]	RT+DOC +ADT *vs.* DOC+ADT	367(17.8%)	100%	Prior	NR	0.81 (0.49-1.34)	0.93, 0.80-1.08	NR
PEACE-1[25]	AAP+DOC +ADT *vs.* DOC+ADT	710(60.5%)	100%	Concomitant	100%	0.75 (0.59-0.95)	NA	rPFS: 0.50 (0.40-0.62)
ARASENS[26]	DARO+DOC +ADT *vs.* DOC+ADT	1306(100%)	86%	Concomitant	86.6%	0.68 (0.57-0.80)	NA	NR

AAP: abiraterone and prednisone; ADT: androgen deprivation therapy; APA: apalutamide; CI: confidence interval; cPFS: clinical progression free survival; DARO: darolutamide; DOC: docetaxel; ENZA: enzalutamide; HR: hazard ratio; NA: not applicable; NHA: novel hormonal agent; NR: not reported; PFS: progression free survival; rPFS: radiographic progression free survival; RT: radiotherapy.

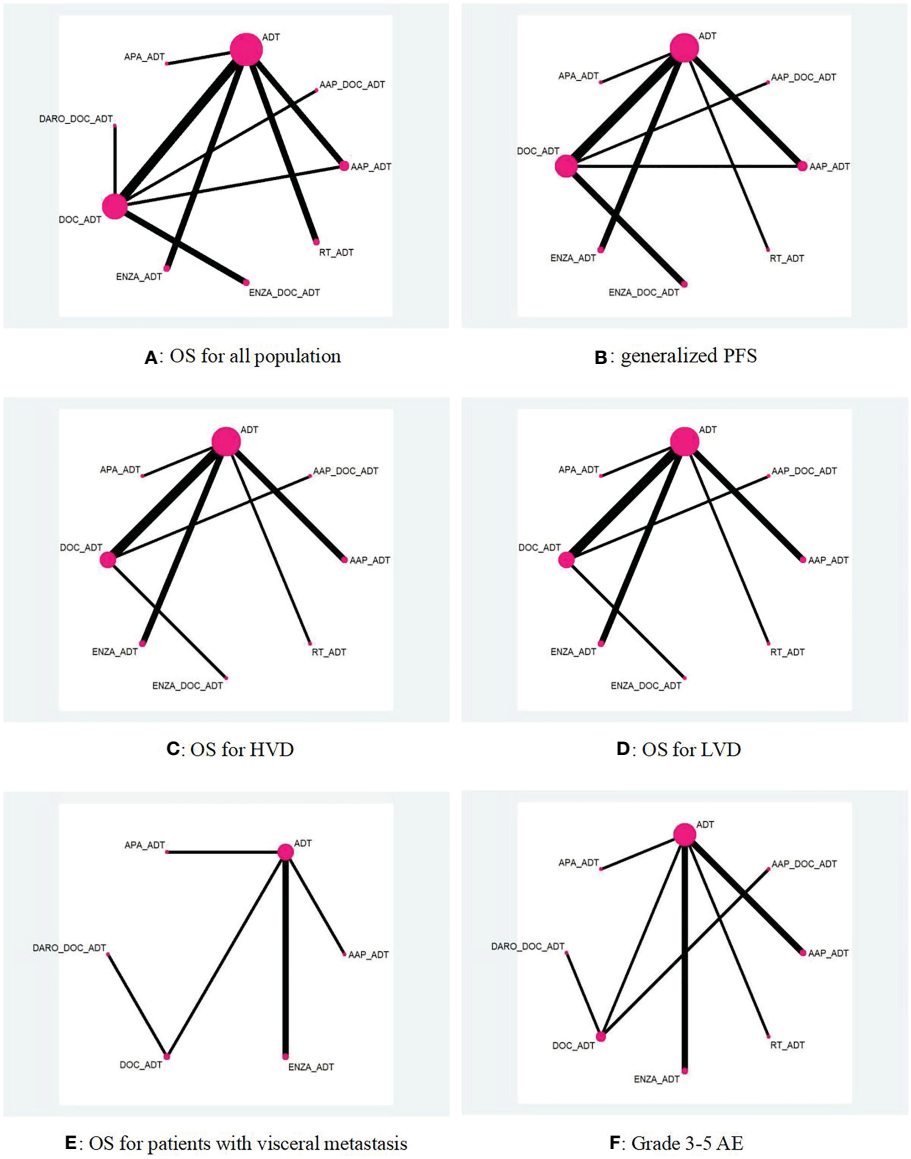

FIGURE 2
Network diagram of different treatment options for mHSPC **(A–F)**. AAP, abiraterone acetate and prednisone; ADT, androgen deprivation treatment; APA, apalutamide; DARO, darolutamide; DOC, docetaxel; ENZA, enzalutamide; HVD, high volume disease; LVD, low volume disease; OS, overall survival; PFS, progression free survival; RT, radiotherapy; The connector line "_" represents combination of different treatment regimens.

ENZA+DOC+ADT was not superior to ENZA+ADT (HR 1·07, 95% CI 0·70-1·64). The detailed HR data of the comparison between each two treatment groups can be found in Appendix (P 21-24). The ranking and ranking probability of competing interventions are shown in Appendix (P 25-32). The triplet treatment DARO+DOC +ADT had the highest probability of ranking the best. The convergence of the models was well according to trace and density plots (Appendix P 33-34).

Generalized PFS for the overall population

In addition to the HORRAD (43) and ARASENS (26) trials, 13 of the 15 comparison groups reported results of PFS or similar indicators (Appendix P 9). Specifically, six comparison groups (GETUG-AFU15 (10, 36), LATITUDE (14, 35), ARCHES (16, 42) and its docetaxel subgroup, TITAN (17, 33), and PEACE-1 (25) reported results of rPFS, four comparison groups (STAMPEDE arm C (12), arm G (13), arm H (18), and AAP-DOC head-to-head comparison subgroup (32) reported results of PFS, and cPFS was reported in four comparison groups (GETUG-AFU15 (10), CHAARTED (11), ENZAMET (15), and ENZAMET's docetaxel subgroup). We unified these indicators as a "generalized PFS" (We chose rPFS, rather than cPFS, in GETUG-AFU15 for subsequent comparison).

The results showed that except for radiotherapy (HR 0·96, 95% CI 0·80-1.16), all other measures were significantly better than ADT (Figures 3C, D). In addition, except for ADT (HR 1·50, 95% CI 1·32-1·72) and radiotherapy (HR 1·44, 95% CI 1·14-1·83), which were inferior to docetaxel chemotherapy, other treatments were all superior to docetaxel chemotherapy. The ranking probability and

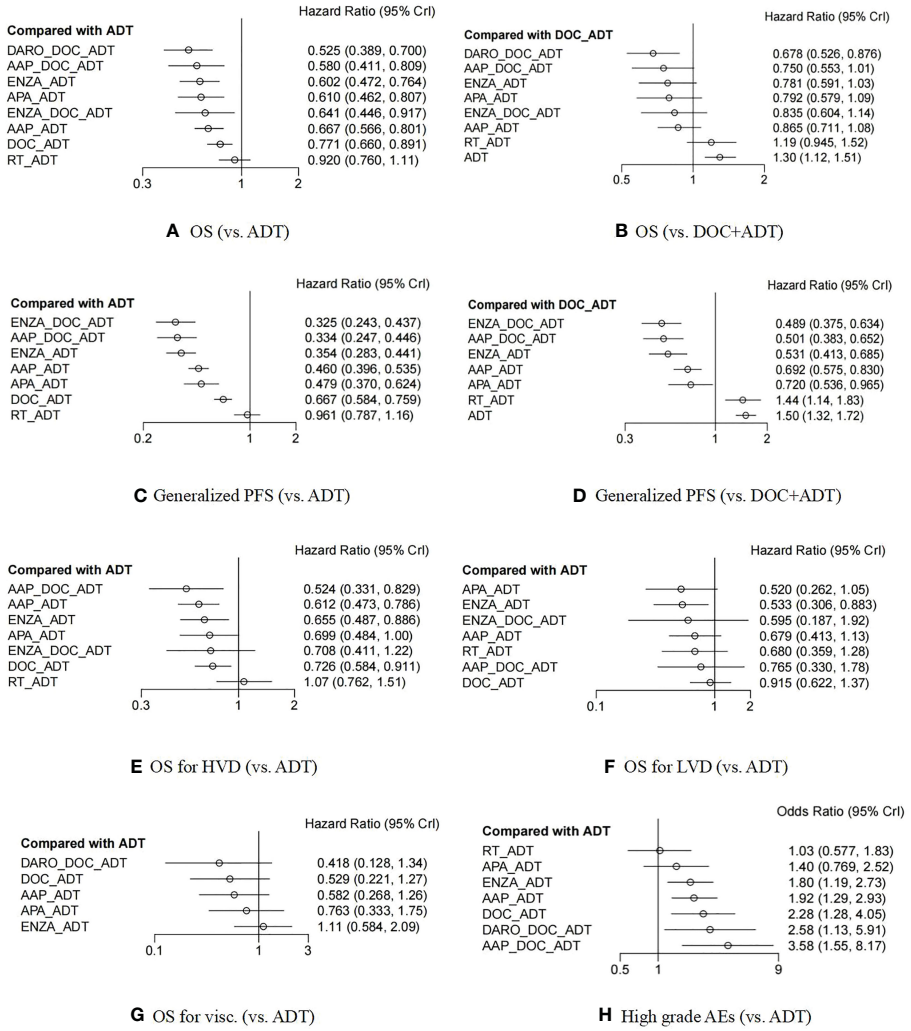

FIGURE 3
Forest plot between different treatment options and ADT monotherapy (or DOC+ADT) in patients with metastatic hormonal-sensitive prostate cancer **(A–H)**. ADT, androgen deprivation treatment; DOC, docetaxel; AAP, abiraterone acetate and prednisone; ENZA, enzalutamide; APA, apalutamide; RT, radiotherapy; DARO, darolutamide; OS, overall survival; PFS, progression free survival; HVD, high volume disease; LVD, low volume disease; Visc., patients with visceral metastasis; AEs, adverse events. The connector line "_" represents combination of different treatment regimens.

HR values for the pairwise comparisons of each treatment measure can be found in Appendix (P 21-32). The triplet therapy ENZA +DOC+ADT had the highest probability of ranking the best. Besides, we also made respective analyses for rPFS, PFS and cPFS (The forest plots can be seen in Appendix P 20).

OS for the population in subgroups

OS data of high- or low- volume subgroups were extracted from 11 of the 15 comparison groups and 8 treatments were included (Appendix P 9). The analysis results of mHSPC with high volume disease (HVD) showed that radiotherapy (HR 1·07, 95% CI 0·76-1·51) had no benefit compared with ADT, the benefit of ENZA +DOC+ADT (HR 0·71, 95% CI 0·41-1·22) had no significant difference compared with ADT, while the other five treatments all had significant benefits compared to ADT (Figure 3E). In terms of possible ranking, the best was AAP+DOC+ADT (HR 0·52, 95% CI 0·33-0·83), followed by AAP+ADT (HR 0·61, 95% CI 0·47-0·79). The results of low tumor disease (LVD) showed that APA+ADT (HR 0·52, 95% CI 0·26-1·05) and ENZA+ADT (HR 0·53, 95% CI 0·31-0·88) possibly ranked the highest (Figure 3F). However, it has to be emphasized that ARASENS trial did not stratify the patients according to disease volume.

Only six studies reported HR data in patients with visceral metastases, involving five interventions (Appendix P 9). The results suggested that DARO+DOC+ADT (HR 0·42, 95% CI 0·13-1·34) had the highest probability of ranking the best, while the new antiandrogens, especially enzalutamide (HR 1·11, 95% CI 0·58-2·09), performed less well. (Figures 3G and Appendix P 25-32)

Safety

In terms of safety indicators, we selected grade 3-5 AEs, as there were more studies reporting grade 3-5 AEs than serious adverse

events (SAEs). In particular, two important trials related to triplet therapies, PEACE-1 (25) and ARASENS (26), both reported grade 3-5 AEs. The CHAARTED study (11) reported grade 3-5 AEs in the docetaxel group, but corresponding data in the control group were lacking; thus, these data were not used. No data from GETUG -AFU15 (10, 36) were used, as they reported a different safety indicator of "AE events/person month". Finally, we included a meta-analysis of grade 3-5 AEs from nine studies (Appendix P 45) involving eight different interventions.

The results showed that the risk of grade 3-5 AEs in triplet therapies was relatively high, especially that of AAP+DOC+ADT (Figure 3H). The order of security was: ADT alone (comparator) > RT+ADT (1·03, 0·57-1·87) > APA+ADT (1·39, 0·76-2·55) > ENZA +ADT (1·81, 1·18-2·77) > AAP+ADT (1·92, 1·27-2·95) > DOC +ADT (2·28, 1·26-4·16) > DARO+DOC+ADT (2·59, 1·11-6·09) > AAP+DOC+ADT (3·56, 1·51-8·43).

The certainty of the evidence for outcomes of interest as measured with CINeMA varied from high to very low. Full information on CINeMA is described in the appendix (Appendix P 46–64).

Discussion

We performed a comprehensive network meta-analysis on the first-line therapies for mHSPC recommended by major guidelines such as EAU (2) and NCCN (44). Compared with previous similar meta-analyses, our paper not only included the final OS data of the ARCHES (42) and TITAN (33) trials but also conducted an in-depth analysis of three different triplet therapies: the darolutamide triplet therapy and the abiraterone triplet therapy came from newly reported outcomes of ARASENS (26) and PEACE-1 (25) trials, while data of the third therapy, the enzalutamide triplet therapy, were extracted from the docetaxel population from previous ENZAMET (15) and ARCHES (16, 34, 42) studies.

This paper has two features in data extraction. First, in the OS analysis, the docetaxel population in multiple studies (including ENZAMET (15), ARCHES (16, 34, 42), TITAN (17, 33), and STAMPEDE arm-H (18) was excluded, as we found that the HRs for OS of interventions in the docetaxel population in the above trials were significantly different from those of the nondocetaxel population. The use of docetaxel was likely to affect the accurate evaluation of the efficacy of interventions. Second, we reintegrated and utilized the docetaxel population data in the ENZAMET (15) and ARCHES (16, 34, 42) trials to evaluate whether enzalutamide triple therapy was superior to docetaxel treatment.

Our results showed that triplet therapies with darolutamide or abiraterone were likely to further improve OS benefits. However, ENZA+DOC+ADT did not show an OS benefit compared with ENZA+ADT or DOC+ADT, and the possible explanations might be as follows: 1) In the ENZAMET and ARCHES studies, whether patients chose to accept "planned early docetaxel use" was not random but mainly dependent on the judgment of the attending doctors, while the ENZAMET study was also not blinded; 2) In the docetaxel population of the ENZAMET study, there was a certain difference between the enzalutamide group and the control group in the proportion of patients receiving six complete courses of chemotherapy, which were 65% and 76%, respectively; 3) A considerable proportion of patients received docetaxel before enzalutamide (35% in ENZAMET, 100% in ARCHES), rather than receiving novel hormonal agents and docetaxel chemotherapy concurrently as in the PEACE-1 and ARASENS studies. However, in the comparison of "generalized FPS" benefits, enzalutamide triplet therapy was "unexpectedly" ranked first. Since the orders of pros and cons of several other interventions in terms of PFS were almost exactly the same as those in terms of OS, we highly suspected that the poor performance of triplet therapy with enzalutamide in terms of OS was more likely to be influenced by external factors such as patient baseline and medication use.

For different tumor burden or visceral metastasis subgroups, the rankings of interventions fluctuate greatly. For example, ENZA +ADT ranked almost highest for LVD patients but lowest for patients with visceral metastasis. This suggests that we should consider a variety of factors when choosing treatment for mHSPC patients, especially the burden and location of metastasis.

In the PEACE-1 trial, AAP+DOC+ADT had a significant advantage over DOC+ADT in overall OS, and in STAMPEDE arm H, RT+ADT had a significant advantage over ADT in OS for low volume disease. However, treatment superiority in these randomized controlled trials became insignificant in our meta-analysis. Considering the power of indirect comparison of network metastasis, when this happens, the results of RCTs are more reliable. However, we also look forward to direct comparisons from more RCTs to further clarify the superiority of the above treatment combinations.

There are some deficiencies in this meta-analysis: 1) We considered "ADT+NSAA" therapy (27, 28) in the control group of the ENZAMET trial the same and analyzed it consolidated with "ADT+placebo" or "ADT+ no treatment" in other trials to make the interpretation of the results more concise and to make it possible to combine docetaxel populations in the ENZAMET and ARCHES trials. However, it will be questioned in terms of rigor. 2) Strictly speaking, PFS, rPFS and cPFS are not the same indicators. Once they are combined into "generalized PFS" for analysis, caution should be taken in the interpretation of the results. 3) For the studies of ENZAMET, ARCHES, TITAN and STAMPEDE arm H, we excluded the data of the docetaxel population in the comparison of HRs (OS) to ensure that HR data were not affected by docetaxel chemotherapy. However, in the analysis of some HRs for OS and PFS of high/low volume disease subgroups, due to the difficulty of data acquisition, we did not exclude the data of the docetaxel population. 4) In triplet therapies, many drugs were given sequentially rather than concurrently (Table 2), these differences could reduce the reliability of our network meta-analysis. 5) According to CINeMA, we rated many comparisons as low or very low quality, especially for OS in subgroups analysis, which restricts the interpretation of our results. The reasons for downgrading mainly come from items of imprecision and incoherence, and the low quality may be related to small sample size of included trials and too many indirect comparisons.

Conclusion

Our results showed that compared with ADT alone, ADT combined with docetaxel, abiraterone acetate, enzalutamide or apalutamide had significant benefits for OS, and the newly emerging triplet therapies may further increase the benefits of OS but at the expense of a certain decrease in safety. Our results suggested that the standard treatment of mHSPC could be considered transferring to the triple therapy of NHAs+DOC +ADT after the transition from ADT alone to NHA/DOC+ADT, especially for patients with high volume disease. However, in most cases, the differences in efficacy between the different interventions are not significant, and they show different efficacy profiles when considering different subgroups, which allows clinicians considerable flexibility in choosing treatment options for individual patients.

Data availability statement

The original contributions presented in the study are included in the article/Supplementary Material. Further inquiries can be directed to the corresponding authors.

Author contributions

Conceptualization: LW and FS. Data curation: LW, CL, ZZ, and XL. Formal statistical analysis: LW, CL, and FS. Methodology: LW and CL. Software: CT. Validation: ZG and FS. Writing-original draft: LW and CL. Writing-review and editing: JG and NL. All authors had full access to all of the data, and the corresponding authors had the final responsibility to submit for publication. All authors contributed to the article and approved the submitted version.

Acknowledgments

Thanks to the "Lancet Club" of Peking University Shougang Hospital for all the help in the conception and writing of this paper.

Conflict of interest

The authors declare that the research was conducted in the absence of any commercial or financial relationships that could be construed as a potential conflict of interest.

Publisher's note

Supplementary material

The Supplementary Material for this article can be found online at: https://www.frontiersin.org/articles/10.3389/fonc.2023.1104242/full#supplementary-material

References

1. Sung H, Ferlay J, Siegel RL, Laversanne M, Soerjomataram I, Jemal A, et al. Global cancer statistics 2020: GLOBOCAN estimates of incidence and mortality worldwide for 36 cancers in 185 countries. *CA Cancer J Clin* (2021) 71(3):209–49. doi: 10.3322/caac.21660

2. Cornford P, van den Bergh RCN, Briers E, Van den Broeck T, Cumberbatch MG, De Santis M, et al. EAU-EANM-ESTRO-ESUR-SIOG guidelines on prostate cancer. part II-2020 update: Treatment of relapsing and metastatic prostate cancer. *Eur Urol* (2021) 79(2):263–82. doi: 10.1016/j.eururo.2020.09.046

3. Pagliarulo V, Bracarda S, Eisenberger MA, Mottet N, Schröder FH, Sternberg CN, et al. Contemporary role of androgen deprivation therapy for prostate cancer. *Eur Urol* (2012) 61(1):11–25. doi: 10.1016/j.eururo.2011.08.026

4. Chen J, Zhang Y, Zhang X, Zhao J, Ni Y, Zhu S, et al. Comparison of systemic treatments for metastatic castration-resistant prostate cancer after docetaxel failure: A systematic review and network meta-analysis. *Front Pharmacol* (2021) 12:789319. doi: 10.3389/fphar.2021.789319

5. Galletti G, Leach BI, Lam L, Tagawa ST. Mechanisms of resistance to systemic therapy in metastatic castration-resistant prostate cancer. *Cancer Treat Rev* (2017) 57:16–27. doi: 10.1016/j.ctrv.2017.04.008

6. Sartor O, de Bono JS. Metastatic prostate cancer. *N Engl J Med* (2018) 378(7):645–57. doi: 10.1056/NEJMra1701695

7. Wang L, Paller CJ, Hong H, De Felice A, Alexander GC, Brawley O. Comparison of systemic treatments for metastatic castration-sensitive prostate cancer: A systematic review and network meta-analysis. *JAMA Oncol* (2021) 7(3):412–20. doi: 10.1001/jamaoncol.2020.6973

8. Sathianathen NJ, Koschel S, Thangasamy IA, Teh J, Alghazo O, Butcher G, et al. Indirect comparisons of efficacy between combination approaches in metastatic hormone-sensitive prostate cancer: A systematic review and network meta-analysis. *Eur Urol* (2020) 77(3):365–72. doi: 10.1016/j.eururo.2019.09.004

9. Menges D, Yebyo HG, Sivec-Muniz S, Haile SR, Barbier MC, Tomonaga Y, et al. Treatments for metastatic hormone-sensitive prostate cancer: Systematic review, network meta-analysis, and benefit-harm assessment. *Eur Urol Oncol* (2022) 5 (6):605–616. doi: 10.1016/j.euo.2022.04.007

10. Gravis G, Fizazi K, Joly F, Oudard S, Priou F, Esterni B, et al. Androgen-deprivation therapy alone or with docetaxel in non-castrate metastatic prostate cancer (GETUG-AFU 15): A randomised, open-label, phase 3 trial. *Lancet Oncol* (2013) 14 (2):149–58. doi: 10.1016/S1470-2045(12)70560-0

11. Sweeney CJ, Chen YH, Carducci M, Liu G, Jarrard DF, Eisenberger M, et al. Chemohormonal therapy in metastatic hormone-sensitive prostate cancer. *N Engl J Med* (2015) 373(8):737–46. doi: 10.1056/NEJMoa1503747

12. James ND, Sydes MR, Clarke NW, Mason MD, Dearnaley DP, Spears MR, et al. Addition of docetaxel, zoledronic acid, or both to first-line long-term hormone therapy in prostate cancer (STAMPEDE): Survival results from an adaptive, multiarm, multistage, platform randomised controlled trial. *Lancet* (2016) 387(10024):1163–77. doi: 10.1016/S0140-6736(15)01037-5

13. James ND, de Bono JS, Spears MR, Clarke NW, Mason MD, Dearnaley DP, et al. Abiraterone for prostate cancer not previously treated with hormone therapy. *N Engl J Med* (2017) 377(4):338–51. doi: 10.1056/NEJMoa1702900

14. Fizazi K, Tran N, Fein L, Matsubara N, Rodriguez-Antolin A, Alekseev BY, et al. Abiraterone plus prednisone in metastatic, castration-sensitive prostate cancer. *N Engl J Med* (2017) 377(4):352–60. doi: 10.1056/NEJMoa1702900

15. Davis ID, Martin AJ, Stockler MR, Begbie S, Chi KN, Chowdhury S, et al. Enzalutamide with standard first-line therapy in metastatic prostate cancer. *N Engl J Med* (2019) 381(2):121–31. doi: 10.1056/NEJMoa1903835

16. Armstrong AJ, Szmulewitz RZ, Petrylak DP, Holzbeierlein J, Villers A, Azad A, et al. ARCHES: A randomized, phase III study of androgen deprivation therapy with enzalutamide or placebo in men with metastatic hormone-sensitive prostate cancer. *J Clin Oncol* (2019) 37(32):2974–86. doi: 10.1200/JCO.19.00799

17. Chi KN, Agarwal N, Bjartell A, Chung BH, Pereira de Santana Gomes AJ, Given R, et al. Apalutamide for metastatic, castration-sensitive prostate cancer. *N Engl J Med* (2019) 381(1):13–24. doi: 10.1056/NEJMoa1903307

18. Parker CC, James ND, Brawley CD, Clarke NW, Hoyle AP, Ali A, et al. Radiotherapy to the primary tumour for newly diagnosed, metastatic prostate cancer (STAMPEDE): a randomised controlled phase 3 trial. *Lancet* (2018) 392(10162):2353–66. doi: 10.1016/S0140-6736(18)32486-3

19. Wang Y, Gui H, Wang J, Tian J, Wang H, Liang C, et al. Comparative efficacy of combined radiotherapy, systemic therapy, and androgen deprivation therapy for metastatic hormone-sensitive prostate cancer: A network meta-analysis and systematic review. *Front Oncol* (2020) 10:567616. doi: 10.3389/fonc.2020.567616

20. Marchioni M, Di Nicola M, Primiceri G, Novara G, Castellan P, Paul AK, et al. New antiandrogen compounds compared to docetaxel for metastatic hormone sensitive prostate cancer: Results from a network meta-analysis. *J Urol* (2020) 203(4):751–9. doi: 10.1097/JU.0000000000000636

21. Kinsey EN, Zhang T, Armstrong AJ. Metastatic hormone-sensitive prostate cancer: A review of the current treatment landscape. *Cancer J* (2020) 26(1):64–75. doi: 10.1097/PPO.0000000000000418

22. Chen J, Ni Y, Sun G, Liao B, Zhang X, Zhao J, et al. Comparison of current systemic combination therapies for metastatic hormone-sensitive prostate cancer and selection of candidates for optimal treatment: A systematic review and Bayesian network meta-analysis. *Front Oncol* (2020) 10:519388. doi: 10.3389/fonc.2020.519388

23. Wallis CJD, Klaassen Z, Bhindi B, Goldberg H, Chandrasekar T, Farrell AM, et al. Comparison of abiraterone acetate and docetaxel with androgen deprivation therapy in high-risk and metastatic hormone-naïve prostate cancer: A systematic review and network meta-analysis. *Eur Urol* (2018) 73(6):834–44. doi: 10.1016/j.eururo.2017.10.002

24. Mori K, Mostafaei H, Sari Motlagh R, Pradere B, Quhal F, Laukhtina E, et al. Systemic therapies for metastatic hormone-sensitive prostate cancer: network meta-analysis. *BJU Int* (2022) 129(4):423–33. doi: 10.1111/bju.15507

25. Fizazi K, Foulon S, Carles J, Roubaud G, McDermott R, Fléchon A, et al. Abiraterone plus prednisone added to androgen deprivation therapy and docetaxel in *de novo* metastatic castration-sensitive prostate cancer (PEACE-1): a multicentre, open-label, randomised, phase 3 study with a 2×2 factorial design. *Lancet* (2022) 399(10336):1695–707. doi: 10.1016/S0140-6736(22)00367-1

26. Smith MR, Hussain M, Saad F, Fizazi K, Sternberg CN, Crawford ED, et al. Darolutamide and survival in metastatic, hormone-sensitive prostate cancer. *N Engl J Med* (2022) 386(12):1132–42. doi: 10.1056/NEJMoa2119115

27. Akaza H, Hinotsu S, Usami M, Arai Y, Kanetake H, Naito S, et al. Combined androgen blockade with bicalutamide for advanced prostate cancer: Long-term follow-up of a phase 3, double-blind, randomized study for survival. *Cancer* (2009) 115 (15):3437–45. doi: 10.1002/cncr.24395

28. Maximum androgen blockade in advanced prostate cancer: an overview of the randomised trials. prostate cancer trialists' collaborative group. *Lancet* (2000) 355 (9214):1491–8. doi: 10.1016/S0140-6736(00)02163-2

29. Page MJ, McKenzie JE, Bossuyt PM, Boutron I, Hoffmann TC, Mulrow CD, et al. The PRISMA 2020 statement: An updated guideline for reporting systematic reviews. *BMJ* (2021) 372:n71. doi: 10.1136/bmj.n71

30. Hoyle AP, Ali A, James ND, Cook A, Parker CC, de Bono JS, et al. Abiraterone in "High-" and "Low-risk" metastatic hormone-sensitive prostate cancer. *Eur Urol* (2019) 76(6):719–28. doi: 10.1016/j.eururo.2019.08.006

31. Clarke NW, Ali A, Ingleby FC, Hoyle A, Amos CL, Attard G, et al. Addition of docetaxel to hormonal therapy in low- and high-burden metastatic hormone sensitive prostate cancer: Long-term survival results from the STAMPEDE trial. *Ann Oncol* (2019) 30(12):1992–2003. doi: 10.1093/annonc/mdz396

32. Sydes MR, Spears MR, Mason MD, Clarke NW, Dearnaley DP, de Bono JS, et al. Adding abiraterone or docetaxel to long-term hormone therapy for prostate cancer: Directly randomised data from the STAMPEDE multi-arm, multi-stage platform protocol. *Ann Oncol* (2018) 29(5):1235–48. doi: 10.1093/annonc/mdy072

33. Chi KN, Chowdhury S, Bjartell A, Chung BH, Pereira de Santana Gomes AJ, Given R, et al. Apalutamide in patients with metastatic castration-sensitive prostate cancer: Final survival analysis of the randomized, double-blind, phase III TITAN study. *J Clin Oncol* (2021) 39(20):2294–303. doi: 10.1200/JCO.20.03488

34. Azad AA, Armstrong AJ, Alcaraz A, Szmulewitz RZ, Petrylak DP, Holzbeierlein J, et al. Efficacy of enzalutamide in subgroups of men with metastatic hormone-sensitive prostate cancer based on prior therapy, disease volume, and risk. *Prostate Cancer Prostatic Dis* (2021) 25(2):274–82. doi: 10.1038/s41391-021-00436-y

35. Fizazi K, Tran N, Fein L, Matsubara N, Rodriguez-Antolin A, Alekseev BY, et al. Abiraterone acetate plus prednisone in patients with newly diagnosed high-risk metastatic castration-sensitive prostate cancer (LATITUDE): Final overall survival analysis of a randomised, double-blind, phase 3 trial. *Lancet Oncol* (2019) 20(5):686–700. doi: 10.1016/S1470-2045(19)30082-8

36. Gravis G, Boher JM, Joly F, Soulié M, Albiges L, Priou F, et al. Androgen deprivation therapy (ADT) plus docetaxel versus ADT alone in metastatic non castrate prostate cancer: Impact of metastatic burden and long-term survival analysis of the randomized phase 3 GETUG-AFU15 trial. *Eur Urol* (2016) 70(2):256–62. doi: 10.1016/j.eururo.2015.11.005

37. Kyriakopoulos CE, Chen YH, Carducci MA, Liu G, Jarrard DF, Hahn NM, et al. Chemohormonal therapy in metastatic hormone-sensitive prostate cancer: Long-term survival analysis of the randomized phase III E3805 CHAARTED trial. *J Clin Oncol* (2018) 36(11):1080–7. doi: 10.1200/JCO.2017.75.3657

38. Dias S, Sutton AJ, Ades AE, Welton NJ. Evidence synthesis for decision making 2: a generalized linear modeling framework for pairwise and network meta-analysis of randomized controlled trials. *Med Decis Making* (2013) 33(5):607–17. doi: 10.1177/0272989X12458724

39. van Valkenhoef G, Lu G, de Brock B, Hillege H, Ades AE, Welton NJ. Automating network meta-analysis. *Res Synth Methods* (2012) 3(4):285–99. doi: 10.1002/jrsm.1054

40. Woods BS, Hawkins N, Scott DA. Network meta-analysis on the log-hazard scale, combining count and hazard ratio statistics accounting for multi-arm trials: A tutorial. *BMC Med Res Methodol* (2010) 10:54. doi: 10.1186/1471-2288-10-54

41. Rücker G, Schwarzer G. Ranking treatments in frequentist network meta-analysis works without resampling methods. *BMC Med Res Methodol* (2015) 15:58. doi: 10.1186/s12874-015-0060-8

42. Armstrong AJ, Azad AA, Iguchi T, Szmulewitz RZ, Petrylak DP, Holzbeierlein J, et al. Improved survival with enzalutamide in patients with metastatic hormone-sensitive prostate cancer. *J Clin Oncol* (2022) 40(15):1616–22. doi: 10.1200/JCO.22.00193

43. Boevé LMS, Hulshof M, Vis AN, Zwinderman AH, Twisk JWR, Witjes WPJ, et al. Effect on survival of androgen deprivation therapy alone compared to androgen deprivation therapy combined with concurrent radiation therapy to the prostate in patients with primary bone metastatic prostate cancer in a prospective randomised clinical trial: Data from the HORRAD trial. *Eur Urol* (2019) 75(3):410–8. doi: 10.1016/j.eururo.2018.09.008

44. Schaeffer E, Srinivas S, Antonarakis ES, Armstrong AJ, Bekelman JE, Cheng H, et al. Prostate cancer, version 1.2021: Featured updates to the nccn guidelines. *JNCCN J Natl Compr Cancer Network* (2021) 19(2):134–43. doi: 10.6004/jnccn.2021.0008

frontiers | Frontiers in Oncology

TYPE Original Research
PUBLISHED 22 March 2023
DOI 10.3389/fonc.2023.1067987

OPEN ACCESS

EDITED BY
Dingwei Ye,
Fudan University, China

REVIEWED BY
Zeyan Li,
Shandong University, China
Wangrui Liu,
Shanghai Jiao Tong University, China

*CORRESPONDENCE
Zhongqing Wei
weizq1@163.com

†These authors have contributed equally to this work and share first authorship

SPECIALTY SECTION
This article was submitted to Genitourinary Oncology, a section of the journal Frontiers in Oncology

RECEIVED 17 October 2022
ACCEPTED 10 March 2023
PUBLISHED 22 March 2023

CITATION
Fan Z, Xu H, Ge Q, Li W, Zhang J, Pu Y, Chen Z, Zhang S, Xue J, Shen B, Ding L and Wei Z (2023) Identification of an immune subtype-related prognostic signature of clear cell renal cell carcinoma based on single-cell sequencing analysis. *Front. Oncol.* 13:1067987. doi: 10.3389/fonc.2023.1067987

Identification of an immune subtype-related prognostic signature of clear cell renal cell carcinoma based on single-cell sequencing analysis

Zongyao Fan[1,2†], Hewei Xu[1,2†], Qingyu Ge[1,2†], Weilong Li[1,2], Junjie Zhang[1,2], Yannan Pu[3], Zhengsen Chen[1,2], Sicong Zhang[1,2], Jun Xue[1,2], Baixin Shen[1,2], Liucheng Ding[1,2] and Zhongqing Wei[1,2*]

[1]Department of Urology, The Second Affiliated Hospital of Nanjing Medical University, Nanjing, China, [2]Department of Urology, The Second Clinical Medical College of Nanjing Medical University, Nanjing, China, [3]Department of Rehabilitation Medicine, The Second Affiliated Hospital of Nanjing Medical University, Nanjing, China

Background: There is growing evidence that immune cells are strongly associated with the prognosis and treatment of clear cell renal cell carcinoma (ccRCC). Our aim is to construct an immune subtype-related model to predict the prognosis of ccRCC patients and to provide guidance for finding appropriate treatment strategies.

Methods: Based on single-cell analysis of the GSE152938 dataset from the GEO database, we defined the immune subtype-related genes in ccRCC. Immediately afterwards, we used Cox regression and Lasso regression to build a prognostic model based on TCGA database. Then, we carried out a series of evaluation analyses around the model. Finally, we proved the role of VMP1 in ccRCC by cellular assays.

Result: Initially, based on TCGA ccRCC patient data and GEO ccRCC single-cell data, we successfully constructed a prognostic model consisting of five genes. Survival analysis showed that the higher the risk score, the worse the prognosis. We also found that the model had high predictive accuracy for patient prognosis through ROC analysis. In addition, we found that patients in the high-risk group had stronger immune cell infiltration and higher levels of immune checkpoint gene expression. Finally, cellular experiments demonstrated that when the VMP1 gene was knocked down, 786-O cells showed reduced proliferation, migration, and invasion ability and increased levels of apoptosis.

Conclusion: Our study can provide a reference for the diagnosis and treatment of patients with ccRCC.

KEYWORDS

ccRCC, single-cell sequencing analysis, immune, prognostic signature, vmp1

1 Introduction

Renal cell carcinoma (RCC) is one of the most common and deadly malignancies of the urinary tract, with an annual morbidity rate of 2.2% and a mortality rate of 1.8% (1). Clear cell renal cell carcinoma (ccRCC) is the most common histological type of RCC, making up about 80% of all cases (2, 3). Currently, the preferred clinical treatment is partial or radical nephrectomy for patients with stage I or II renal cell carcinoma (4). However, about 30% of patients have metastasized at first diagnosis and the 5 years survival rate for this group of patients is low because ccRCC is not sensitive to radiotherapy and chemotherapy (5, 6). Therefore, it is important to find new therapeutic tactics to improve the prognosis of ccRCC.

The tumor microenvironment (TME) is a complex dynamic multicellular ecosystem consisting of a variety of components such as immune cells, stromal cells, cancer cells, neuronal cells, blood vessels, and various growth factors (7, 8). Immune cells in the TME have been considered a key and central area of oncology research, playing a valuable role in the prognosis of malignancies, and in treatment resistance (9). Obradovic et al. demonstrated that TREM2/APOE/C1Q-positive macrophage infiltration is a potential prognostic biomarker for ccRCC recurrence, as well as a candidate therapeutic target (10), and Errarte et al. proved the implication of CAF (cancer-associated fibroblasts) in the proliferation, angiogenesis, metastasis development and drug resistance during RCC tumourigenesis. This fact assumes that CAF is a potential clinical tool for the diagnosis, prognosis and treatment of ccRCC (11). Furthermore, TME-related biomarkers were found to predict prognosis for ccRCC patients as novel targets for immunotherapy (12). In recent years, various immunotherapeutic strategies, comprising anti-PD-1, anti-PD-L1 and anti-CTLA-4, are recommended as the mainstay of treatment for advanced RCC. However, the majority of patients who receive immunotherapy experience primary and acquired drug resistance, which ultimately causes treatment failure (13, 14). Therefore, the discovery of new targets for immunotherapy is of great importance.

Single-cell RNA sequencing (SCQ) is used to study cell heterogeneity and to identify different cell types within heterogeneous cell populations. Unlike traditional RNA sequencing, SCQ will help to understand the differences between different cells at the gene and gene expression levels during disease progression (15, 16). SCQ is now widely used in the study of various diseases, and results have been achieved (17, 18).

In our study, we first performed dimensionality reduction, clustering and cell type annotation analysis on the SCQ data of ccRCC. Through these analyses, we classified the different tumor cells as immune and non-immune components and successfully obtained marker genes for cells in the immune group. A prognostic model for ccRCC patients was constructed based on these genes and clinical information and transcriptome sequencing of ccRCC patients from the The Cancer Genome Atlas (TCGA) database. This model precisely assesses the prognosis of ccRCC patients and is associated with the immune microenvironment. Finally, we validated the role of VMP1, the important gene in the model, through cellular experiments. Our study offers novel ideas for the diagnosis and treatment of ccRCC.

Abbreviations: ccRCC, Clear cell renal cell carcinoma; RCC, Renal cell carcinoma; TME, The tumor microenvironment; SCQ, Single-cell RNA sequencing; TCGA, The Cancer Genome Atlas; PCA, principal component analysis; WGCNA, Weighted gene co-expression network analysis; TOM, topological overlap matrix; AUC, area under the curve; ROC, receiver operating characteristic curve; VMP1, vacuole membrane protein 1; IFI30, Interferon γ-inducible protein 30; CEBPB, CCAAT/enhancer-binding protein B; FKBP11, FK506 binding protein 11; ATP1B1, ATPase Na/K transporting subunit beta 1.

2 Methods

A flowchart of our work was shown in Figure 1.

2.1 Data source and preprocessing

The ccRCC SCQ dataset GSE152938 was downloaded from the GEO database, including 1 normal kidney sample, 2 ccRCC samples, 1 chromophobe renal cell carcinoma sample and 1 papillary renal cell carcinoma sample. Because this article was designed to study the prognosis of patients with ccRCC, we removed other types of samples. Next, we perform quality control on the SCQ data, we selected genes expressed in at least three cells and cells with total gene expression between 300 and 3000 for the next analysis. And, cells with mitochondrial gene expression greater than 5% of total gene expression were also excluded. The transcriptome RNA-seq data and its corresponding clinical information were acquired from the TCGA database, comprising 539 ccRCC data and 72 normal data. And, to ensure the accuracy of the study, 530 ccRCC samples that included complete clinical information were selected for further analysis.

2.2 SCQ data analysis

First, we normalized the ccRCC SCQ data filtered in the previous step by the method of "LogNormalize". Then, due to the sheer volume of cells, we classified them by the marker genes expressed by each cell, and merged the similar categories, through the method of principal component analysis (PCA) dimension reduction. Finally, with the help of the function of "SingleR", we annotated cell types according to their marker genes, and we used the "FindAllMarkers" function to obtain marker genes for different cell types.

2.3 Weighted gene co-expression network analysis

WGCNA is a systematic statistical approach that can group genes with analogous expression patterns and illustrate the relationship between genes of a particular group and specific traits (19). In our study, we used this method to obtain the set of genes associated with clinical traits. First, we performed an initial screening of the samples,

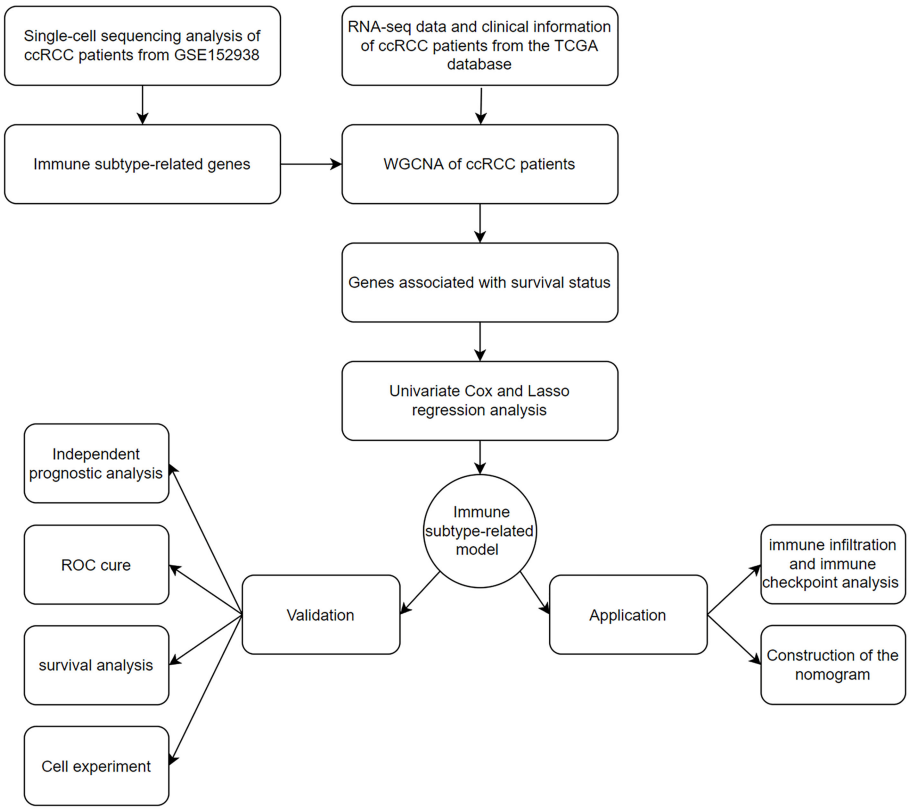

FIGURE 1
The flowchart of data collection and analysis in this study.

excluding non-renal cancer patients and genes with small fluctuations. Then, to improve the accuracy of the screening, we transformed the adjacency matrix into a topological overlap matrix (TOM) and set the minimum group size to 30. Finally, we merge similar groups and output the resulting graph and data.

2.4 Construction of the immune subtype-related prognostic model

Firstly, we combined the above-obtained genes with TCGA transcriptome data to obtain the immune subtype-related gene expression data. Subsequently, we merged the expression data with their survival status and performed a univariate Cox analysis to identify genes associated with prognosis. Then, the genes were further selected by the way of Lasso regression analysis, and through this we can get the model genes. Finally, we calculated the risk score for each ccRCC patient based on the formula and with the help of the median risk score, we were able to classify the patients into two risk groups.

2.5 Evaluation of the model

We analyzed whether the risk score was an independent prognostic factor by the measure of Cox analysis. Then, we assessed the predictive effect of the model by plotting the survival curves of the ccRCC patients, and we make the most of the ROC curve to evaluate the accuracy and sensitivity of this model. In the last, we plot the patient's survival status on an axis with the risk score as the horizontal coordinate to give a better visualisation of each patient's survival status.

2.6 Analysis of immune function

With the help of the results of 7 kinds of immune infiltration in ccRCC downloaded from the TIMER database, we showed the difference in the level of immune infiltration between ccRCC patients in two groups. Meanwhile, we also investigated the difference in the expression level of immune checkpoint-related genes between ccRCC patients in two groups.

2.7 Construction of the nomogram

In our study, by combining each patient's risk score of our model with clinical information, we successfully constructed a nomogram that can predict the patient's risk of death. Then we used ROC to assess the accuracy of nomogram in predicting patient outcomes

2.8 Cell culture and transfection

CcRCC cell-lines 786-O was purchased from the Chinese Academy of Sciences Committee on Type Culture Collection Cell

Bank (Shanghai, China) and were cultured in RPMI-1640 medium (Gibco, USA) supplemented with 10% FBS (Gibco, USA). siRNA VMP1 and siRNA negative control were purchased from RiboBio (Guangzhou, China), and transfected with Lipofectamine 2000 reagent (Invitrogen, CA, USA).

2.9 RNA extraction and quantitative real-time polymerase chain reaction

Total RNAs of 786-O were extracted using the TRIzol reagent. Then, we made use of a reverse transcription kit from (vazyme, China) to obtain cDNA. We detected the relative expression level of the target gene by the measure of qRT-PCR based on the 2-ΔΔCt method.

2.10 Cell proliferation analysis

5-ethynyl-29-deoxyuridine (EdU) assay was performed based on the manufacturer's instructions (RiboBio, Guangzhou, China). The 786-O cells were first inoculated in 24-well plates, followed by incubation with EdU reagent for 2h. Finally, after labelling the DNA with 2-(4-Amidinophenyl)-6-indolecarbamidine dihydrochloride (DAPI), the cell images were inspected under a fluorescent microscope.

2.11 Transwell assay

To assess the migratory capacity of the cells, we adjusted the 24-well plates (Nset, China) by transwell culture chambers (Corning, USA). Cells were inoculated into 200μL of the medium in the upper chambers without serum. The lower layer of the chamber is 700μL of medium containing 10%FBS. For cell invasion ability, pre-lay a layer of Matrigel over the chambers, the rest of the steps are the same as above. After 24h incubation in the cell incubator, the medium was discarded and the cells were wiped from the inside of the bottom of the chambers using a cotton swab. Finally, after fixing them with methanol and staining the cells at the bottom of the chamber with crystal violet, images of the cells were taken using a microscope.

2.12 Scratch wound healing assay

Cells in logarithmic growth phase were inoculated in 6-well plates. When the cells reached about 90%, 200μL tips were used to draw 2 vertical lines along the vertical direction, and after washing out the cell debris, the complete medium was replaced with a medium containing 1% FBS. After 24 hours, the distance the cells migrated to the scratched area was carefully observed under the microscope and this was used to test the migration ability of the cells.

2.13 Apoptosis detection using flow cytometry

Cells were first digested with trypsin and washed twice with PBS. Then, according to the Annexin V-FITC/PI Apoptosis Detection Kit (vazyme, China) guidelines, cells were incubated with Annexin V-FITC and PI in a dark environment for 10 minutes. Finally, the rate of apoptosis was measured using flow cytometry.

2.14 Statistical analysis

Bioinformatics analysis was conducted using the R software (V. 4.1.2). The quantification and graphing of the experiment data was conducted using Image J software (V.1.8.0) and GraphPad Prism (V.9.0). All measurement data are shown as the mean ± SD. The data differences between the two groups were analyzed by Student's t-test and P-values less than 0.05 were considered significant in all tests.

3 Results

3.1 SCQ data analysis and identification of immune-related genes

As illustrated in Figure 2A, we found a relatively even distribution of cells with gene expression levels between 300 and 3000, and the mitochondrial genes of the majority of cells were <5%. Using the above criteria to screen the cells, we successfully obtained 1759 cells. Figure 2B showed that these cells were uniformly distributed in the ccRCC samples and that the gene expression levels were positively associated with the amount of gene expression (0.88). This indicated that the screened cells are suitable for further analysis. Figure 2C showed the ten most variable genes in selected cells, including JCHAIN, RGS5, ENPP2 and MZB1.

After PCA descending treatment, these cells were divided into 11 clusters. In Figure 3A, we could find 10 highest expressed genes in each cluster. In Figure 3B, we could find the distribution of these 11 clusters. With the help of the function of "SingleR", we annotated cell types according to their marker genes, and the clusters associated with immune cells are 0, 1, 4, 6, 7, 9 (Figure 3C). We then used the "FindAllMarkers" function to acquire 858 immune subtype-related genes.

3.2 Weighted gene co-expression network analysis

In TCGA cohort, with the help of WGCNA, we got the gene modules related to the patient's survival status. By using a soft threshold of 4 and a minimum module gene count of 30, we succeeded in obtaining 3 modules related to clinical traits (Figures 3D, E). Because we wanted to analyze patients' prognosis, we selected genes associated with the patients' survival status for further analysis.

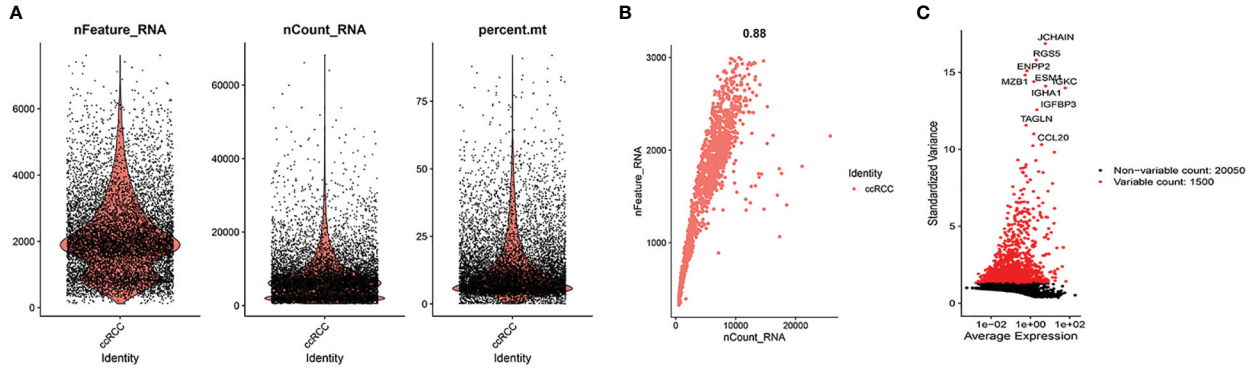

FIGURE 2
Quality control. **(A)** When gene expression levels in cells of ccRCC samples were in the range of 300-3000, the distribution of each cell was relatively even. At the same time, we also found the mitochondrial genes of the majority of cells were <5%. **(B)** The cells were uniformly distributed in the ccRCC samples and the gene expression levels were positively associated with the amount of gene expression (0.88). **(C)** 10 hypervariable genes.

3.3 Construction of the immune subtype-related prognostic model

First, a differential analysis was performed based on genes obtained in the previous step in the TCGA cohort to obtain the differential genes in the tumor and normal groups. Then, as shown in Figure 4A, we succeeded in obtaining 66 genes related to the prognosis of ccRCC patients through univariate Cox analysis, 63 of which had a hazard ratio (HR) > 1. In the last, after randomizing patients into the training and validation set, we carried out Lasso regression analysis on these 64 genes, and the result showed when the number of genes included is 5, the gene contraction tended to be stabilized and the partial likelihood deviation was minimized (Figures 4B, C). We finally obtained 5 model genes, including IFI30, CEBPB, VMP1, ATP1B1, and FKBP11, and we found that gene ATP1B1 was highly expressed in normal patients, while IFI30, CEBPB, VMP1, and FKBP11 were highly expressed in ccRCC patients (Figure 4D). The names and the coefficients of the prognostic genes were listed in Table 1. Risk score =

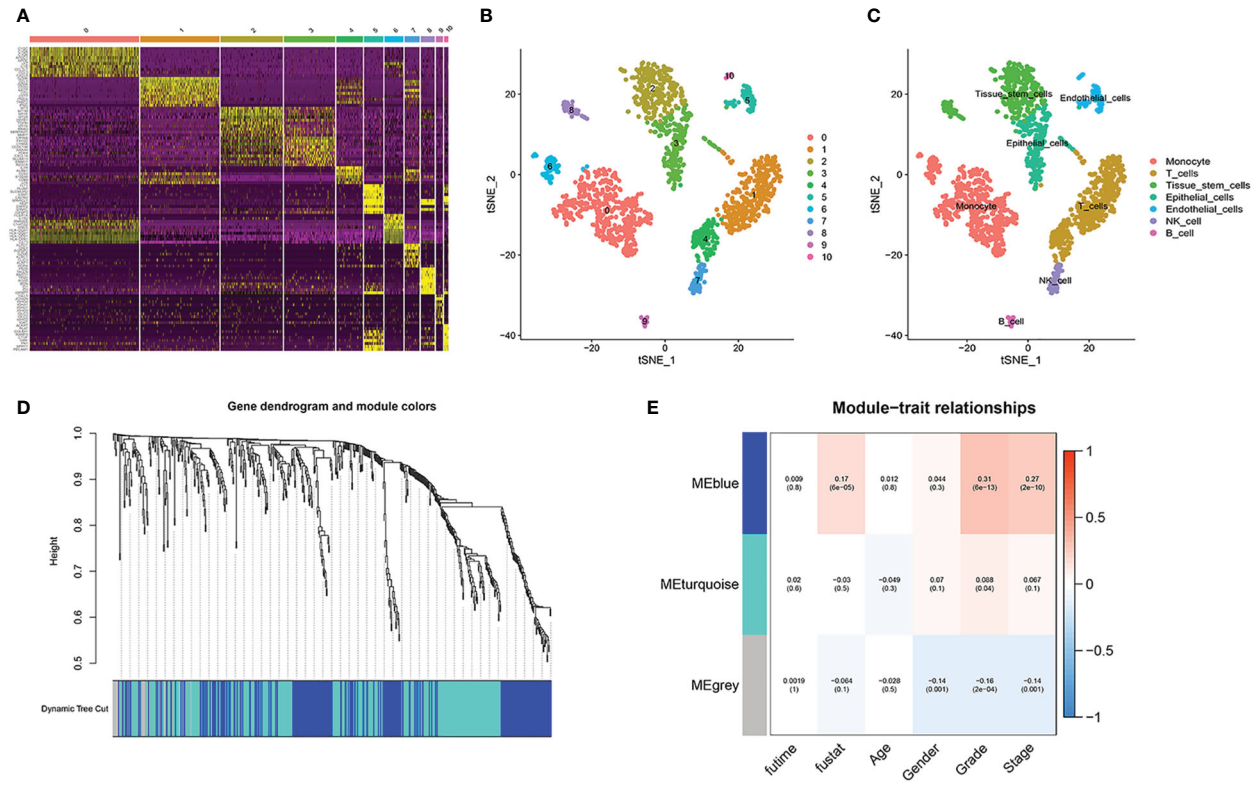

FIGURE 3
Single-cell sequencing analysis. **(A)** 10 highest expressed genes in each cluster. **(B, C)** the distribution and annotations of these 11 clusters. **(D, E)** WGCNA found that MEblue was closely related to the score of survival status.

10.3389/fonc.2023.1067987

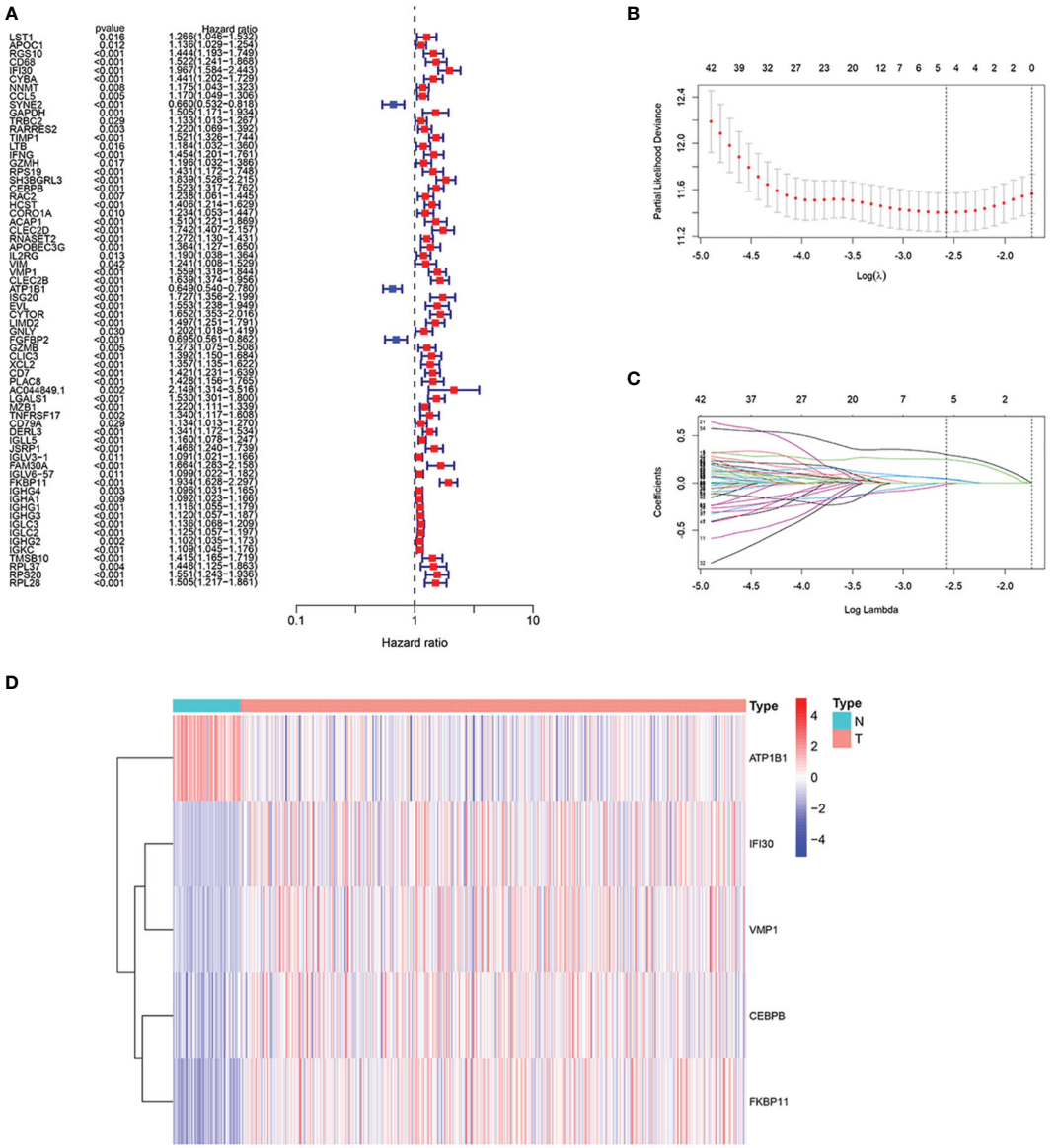

FIGURE 4
Construction of the prognostic model. **(A)** We succeeded in obtaining 66 genes associated with the prognosis of the patients through the univariate Cox analysis, 63 of which had a hazard ratio (HR) > 1. **(B, C)** 5 genes were selected to construct the prognostic model by Lasso regression. **(D)** Expression of 5 model genes in the transcriptome sequencing of normal and ccRCC patients.

TABLE 1 Genes used for model building and their Coefficients.

Gene	Coefficients
IFI30	0.251764
CEBPB	0.049804
VMP1	0.041372
ATP1B1	-0.007404
FKBP11	0.301602

Genes and their coefficients used to construct prognostic models. The risk score = IFI30*0.251764 + CEBPB *0.049804 + VMP1*0.041372 + ATP1B1*(-0.007404) + FKBP11*0.301602.

IFI30*0.252 + CEBPB *0.050 + VMP1*0.041 + ATP1B1*(-0.007) + FKBP11*0.302. We then used median patient risk values to classify patients into two groups for further analysis.

3.4 Validation of the immune subtype-related prognostic model

First, to explore whether risk scores were an independent factor of influence for ccRCC patients, we performed univariate and multivariate Cox regression on age, gender, grade, stage and risk score in ccRCC patients. The presentation of the results showed that in both the training

and validation sets, the risk score was an independent prognostic factor (Figure 5). We then examined the relationship between patients' risk scores and survival status. In Figures 6A, B, we could find the distribution of patients' risk scores in ccRCC patients. And, with increasing risk scores, the chance of patient death increased (Figures 6C, D). Next, to validate the accuracy of the model, we plotted ROC curves for 1, 2, 3, 4 and 5 years for both datasets. We found the area under the curve (AUC) was found to be almost greater than 0.7 for both datasets from 1 to 5 years, suggesting that the model had good stability and accuracy in predicting patient prognosis (Figures 6E, F). Finally, to further test the credibility of the model, we performed a survival analysis in the ccRCC patients (Figures 7A, B). At the same time, a further, more specific categorical survival analysis was carried out for all ccRCC patients. The results showed a more rapid decline in survival of ccRCC patients in the high-risk group, irrespective of age, gender grade and stage (Figures 7C–J).

3.5 Evaluation of immune infiltration and immune checkpoint

As shown in the above analysis, patients in the high-risk group had significantly poorer survival. We therefore wanted to investigate whether there were differences in immune function in order to guide the treatment of the disease in some sense. The results showed more immune cell infiltration in the high-risk group, consisting of T cells, B cells and macrophage cells (Figure 8A). Furthermore, almost all immune checkpoint genes were also more highly expressed in the high-risk group (Figure 8B), indicating that it is possible that high-risk group ccRCC patients may receive more benefit from immunotherapy.

3.6 Construction of the nomogram

In order to better predict the prognosis of ccRCC patients, a nomogram was constructed including clinical information and risk score. In Figure 9A, with the use of gender, age, total stage, M stage, grade and risk score values for the patient "TCGA-CZ-4853", we predicted his mortality rates of 0.0804, 0.207 and 0.325 at 1, 3 and 5 years. Next, we constructed a calibration curve (Figure 9B) and found that the nomogram was a good predictor of prognosis at 1, 3 and 5 years for ccRCC patients. In addition, ROC analysis was carried out to better assess the accuracy of the nomogram. The results showed that both the 1 year, 3 year, and 5 years, nomogram was more accurate than clinical information (Figures 9C–E).

3.7 Effect of VMP1 knockdown on the proliferation of ccRCC cells

To assess the knockdown efficiency of the VMP1 in 786-O cells, we examined the expression of the VMP1 in the 786-O cell line by qRT-PCR. Figure 10A showed significant downregulation of VMP1

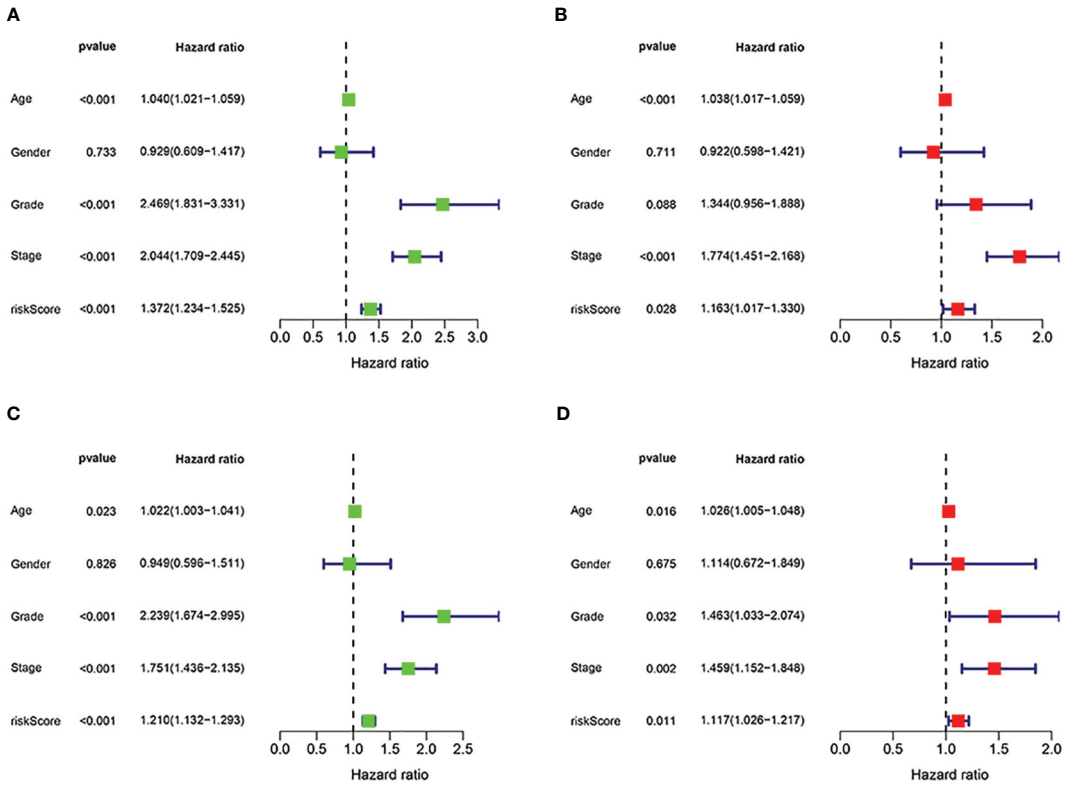

FIGURE 5
Independent prognostic analysis of the signature. **(A, B)** Cox regression revealed that the risk score was an independent prognostic factor in ccRCC patients in training group. **(C, D)** Cox regression revealed that the risk score was an independent prognostic factor in ccRCC patients in validation group.

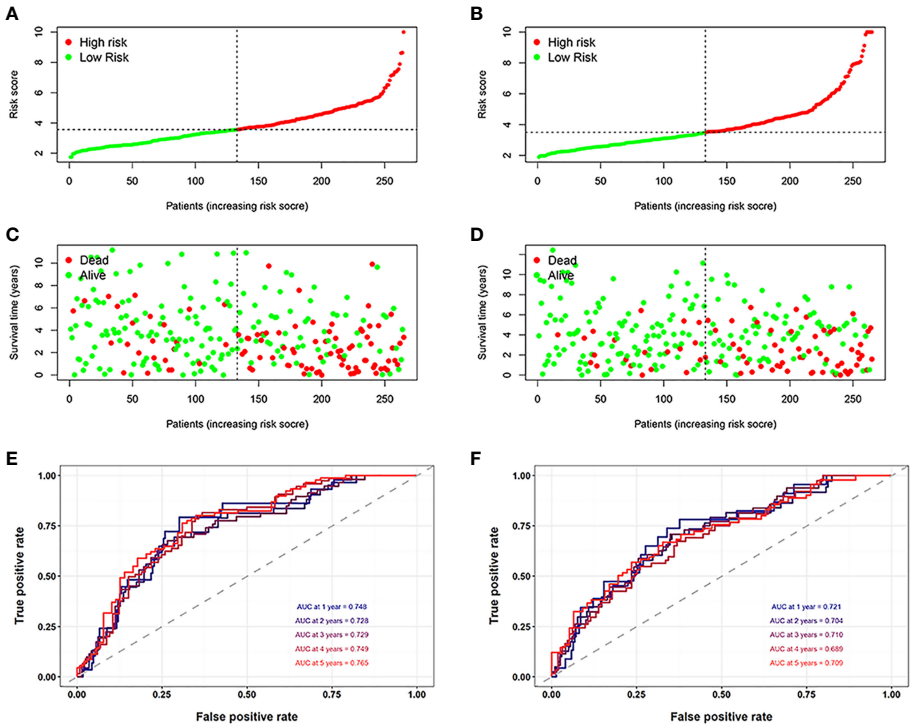

FIGURE 6
Assessment of the model. **(A, B)** The distribution of patients' risk scores in the training and validation groups. **(C, D)** With increasing risk scores, the chance of patient death increased. **(E, F)** The ROC curves for 1, 2, 3, 4 and 5 years for both datasets.

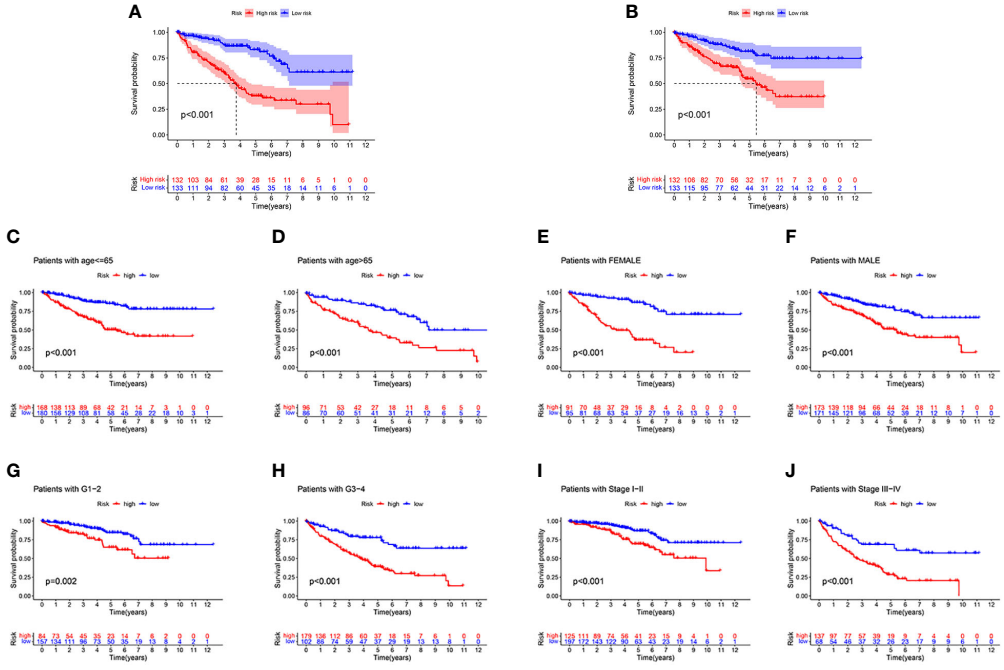

FIGURE 7
The survival analysis. **(A, B)** The survival analysis between high-risk groups and low risk groups between the training cohort and the validation cohort. **(C–J)** A more rapid decline in survival in the high-risk group than in the low-risk group, irrespective of age, gender grade and stage.

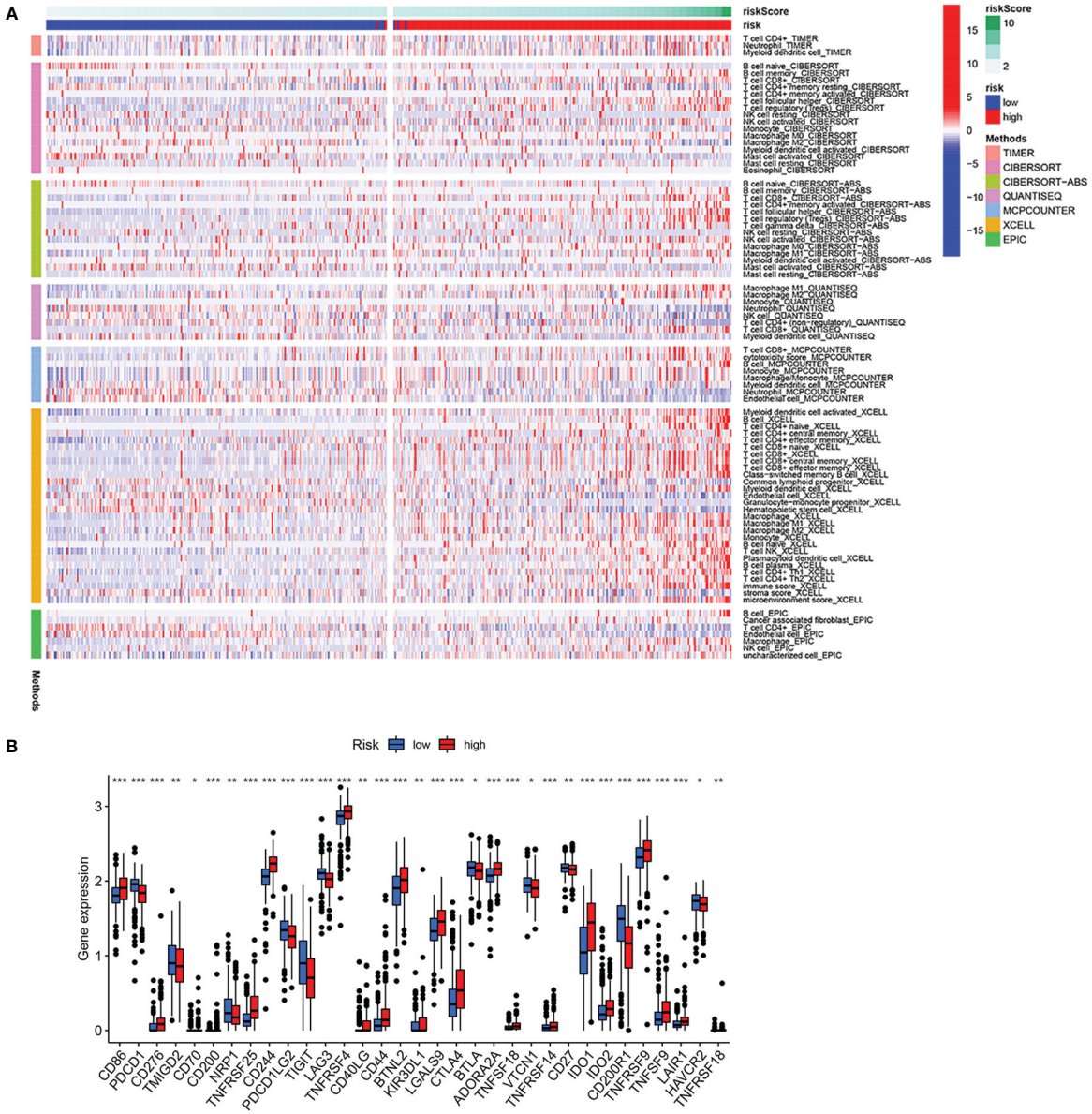

FIGURE 8
Analysis of immune infiltration and immune checkpoint. **(A)** Heatmap of immune cell infiltration in high-risk group and low-risk group. **(B)** Differential expression of immune checkpoint genes in high-risk group and low-risk group. *p<0.05, **p<0.01, ***p<0.001.

expression levels in the 786-O cells after siRNA transfection, suggesting that further studies are feasible and meaningful. The EdU assay was used to test whether VMP1 knockdown had an effect on the proliferation of 786-O cells, which showed that the proliferation of cells was suppressed after the vmp1 gene was knocked down (Figure 10B).

3.8 Effect of VMP1 knockdown on the migration and invasion of ccRCC cells

The effect of decreased VMP1 expression on cell migration and invasion was examined by the transwell method. Results displayed that the decreased expression of VMP1 also impaired cell migration and invasion (Figures 10C, D). Scratch healing assays also showed a significantly slower wound healing rate in 786-O cells with a decreased expression of the VMP1 (Figures 10E, F).

3.9 Effect of VMP1 knockdown on the apoptosis of ccRCC cells

We analyzed the influence of VMP1 on the apoptosis of 786-O cells. The results indicated that the apoptosis level in the low VMP1 expression group was significantly higher compared to NC group (Figures 10G, H).

4 Discussion

As the most common and malignant subtype of RCC, the main treatment options for advanced ccRCC consist of palliative tumor

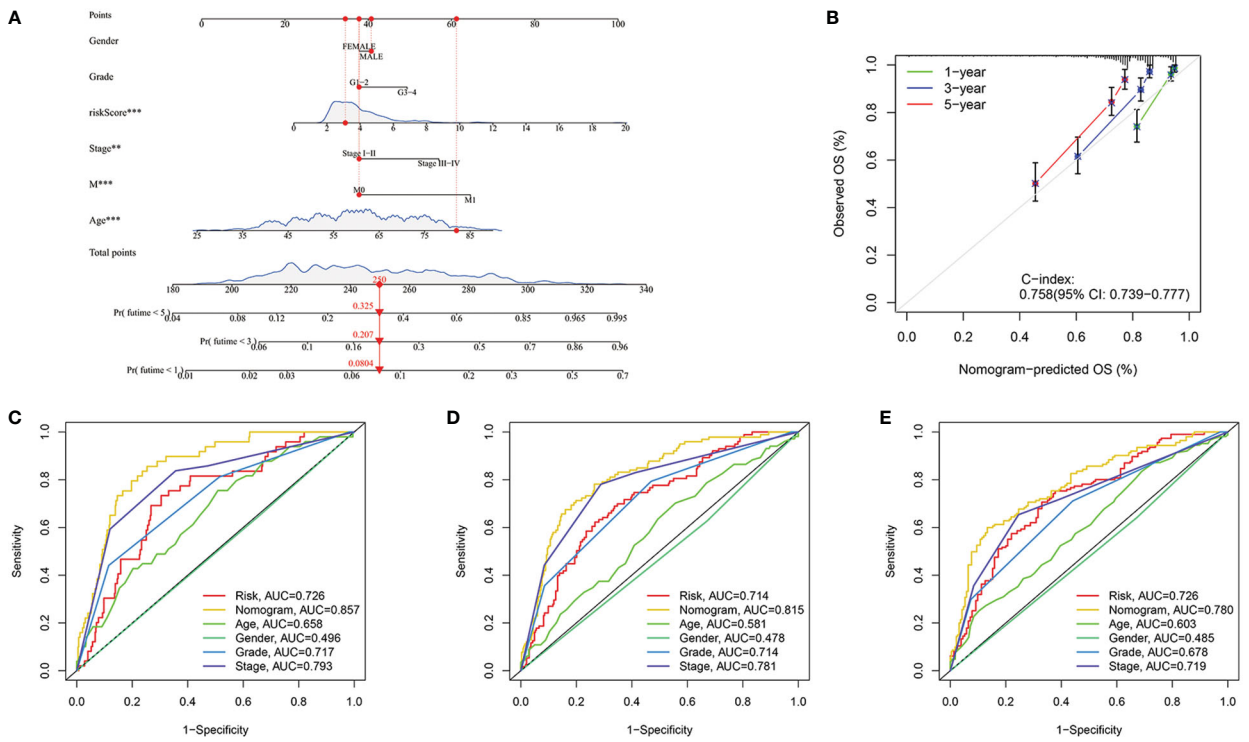

FIGURE 9
Construction of the nomogram. **(A)** Nomogram to predict the probability of mortality at 1, 3, and 5 years. **(B)** The C-index of the nomogram. **(C–E)** ROC curve of the nomogram in 1, 3 and 5 years were 0.857, 0.815 and 0.780 respectively. **p<0.01, ***p<0.001.

resection, targeted therapy and immunotherapy due to its insensitivity to radiotherapy and chemotherapy (20). Although a large number of ccRCC patients currently have improved overall survival rates as a result of immunotherapy, there are still some patients who have poor outcomes (21). These suggest that our understanding of the immune microenvironment of ccRCC is far from adequate and we need to continue to explore its mechanisms and find new prognostic markers and therapeutic targets.

In this study, we analyzed SCQ data from ccRCC to classify cells into immune and non-immune groups and extracted marker genes from the immune group. We then performed Cox and Lasson regression analyses based on these marker genes and constructed an immune subtype-related prognostic model. Each patient was then divided into two groups by calculating risk scores, and the model was found to be an accurate predictor of patient prognosis through survival analysis, AUC and other analyses. We next found higher levels of immune infiltration and immune checkpoint genes expression in the high-risk group, indicating that patients in the high-risk group are able to receive more benefits from immunotherapy. Finally, our cellular experiments displayed that the proliferation and migration of kidney cancer cells were reduced and apoptosis levels were increased after vacuole membrane protein 1 (VMP1) knockdown, revealing that it may be a key oncogene and a possible breakthrough point for treatment.

Our risk model includes 5 genes, all of which take part in the regulation of cancer. Interferon γ-inducible protein 30 (IFI30) is a reductase localized in lysosomes and expressed mainly in antigen-presenting cells, including B cells, T cells and macrophages, that catalyzes the reduction of disulfide bonds (22, 23). IFI30 can promote breast cancer proliferation, migration and invasion through cellular autophagy, and promote melanoma development by modulating tolerance to autoantigens (23, 24). CCAAT/enhancer-binding protein B (CEBPB)is a member of the family of transcription factors of the basic-leucine zipper class. When subjected to external stimuli, its expression can be increased, promoting the expression of downstream inflammatory factors and thus promoting the proliferation and migration of glioblastoma cells (25). FK506 binding protein 11 (FKBP11) has been reported to be highly expressed in melanoma, hepatocellular carcinoma and oral cancer and to promote the development of oral cancer by regulating the cell cycle and apoptosis through the P53 pathway (26–28). As ccRCC progresses, increased methylation of the promoter of ATPase Na/K transporting subunit beta 1 (ATP1B1) decreases its expression in cancer, thereby inhibiting tumor progression and acting as a cancer suppressor (29, 30). VMP1, previously thought to be a pancreatitis-associated protein (31), has recently been demonstrated to promote glioma development and Kras-mediated pancreatic cancer initiation by regulating cellular autophagy (32, 33). In addition, in acute myeloid leukemia, HER2 positive breast cancer and ovarian cancer, the poor prognosis of patients is strongly associated with high expression of VMP1 (34–36). However, overexpression of VMP1 inhibited the metastasis, proliferation and increased their sensitivity to chemotherapeutic drug, 5-fluorouracil, in colorectal cancer cells (37). There are no similar studies in ccRCC patients, so this paper focused on VMP1. We found that poor prognosis in ccRCC patients

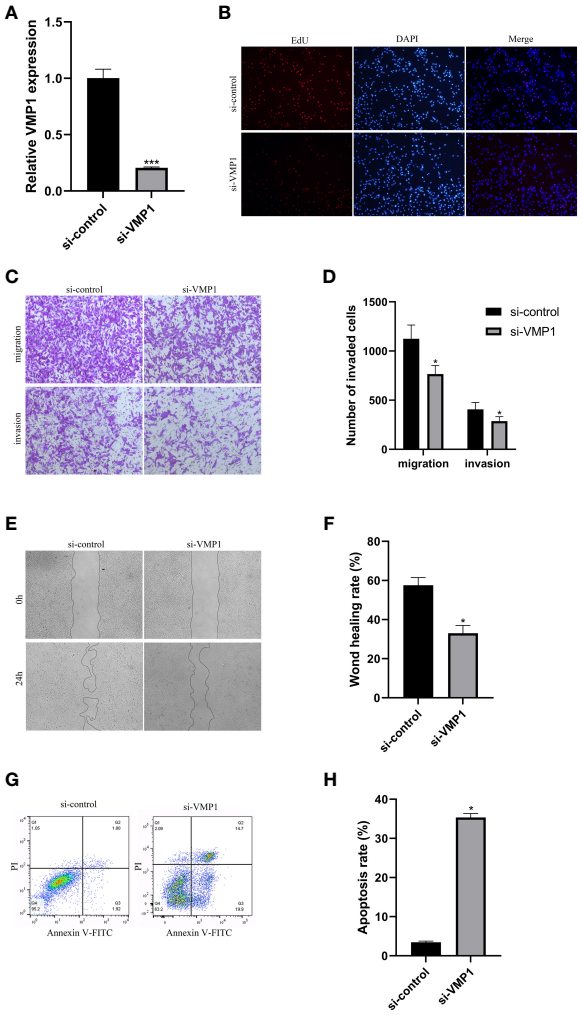

FIGURE 10
Cell experiments. **(A)** qRT-PCR analysis was performed to confirm the knockdown of gene VMP1. **(B)** EdU assay suggested that the proliferation ability of 786-O cells was reduced with VMP1 knockdown. **(C, D)** Transwell assay showed that the migration and invasion of 786-O cells were reduced with VMP1 knockdown. **(E, F)** Scratch assay showed that the migration of 786-O cells was reduced with VMP1 knockdown. **(G, H)** Cell apoptosis assay showed that the apoptosis rate of 786-O cells was Increased with VMP1 knockdown. *p<0.05, ***p<0.001.

was related to high VMP1 expression and that knockdown of VMP1 inhibited cell growth and induced apoptosis.

CcRCC is one of the most immunologically infiltrative tumors of the urinary tract and immunotherapy is the main treatment option for advanced kidney cancer (38). Therefore, it is important to know the immune function of each patient to control the progression of the tumor and prolong the prognosis of the patient and to look for new prognostic markers to extend the survival time of patients. We propose a new model for immune subtypes with the help of SCQ analysis of ccRCC. Patients in the high-risk group have higher levels of immune infiltration, which has implications for guiding treatment.

In summary, we have developed a new prognostic model based on the results of single-cell analysis, which can accurately predict the survival time of ccRCC patients and has implications for guiding immunotherapy. We have initially validated the effect of VMP1 on ccRCC cell function, and we will further explore the specific mechanisms of VMP1 at the cellular level to provide new targets for the diagnosis and treatment of ccRCC.

5 Conclusions

We constructed an immune subtype-related prognostic signature of ccRCC, and demonstrated the role of VMP1 in ccRCC by cellular assays. These can accurately assess the prognosis of patients with ccRCC and provide a new target for treatment.

Data availability statement

The original contributions presented in the study are included in the article/supplementary material. Further inquiries can be directed to the corresponding author.

Author contributions

ZF, HX and QG were responsible for the design of this study. WL, JZ, YP, ZC, SZ and JX were involved in database search and

statistical analyses. ZF, HX, QG, LD and BS were involved in the writing of manuscript. ZW was responsible for the submission of the final version of the paper. All authors contributed to the article and approved the submitted version.

Funding

This work was supported by the National Key Technology R&D Program of China (nos. 2018YFC2002204).

Acknowledgments

We are very grateful for data provided by databases such as TCGA, GEO.

Conflict of interest

The authors declare that the research was conducted in the absence of any commercial or financial relationships that could be construed as a potential conflict of interest.

Publisher's note

All claims expressed in this article are solely those of the authors and do not necessarily represent those of their affiliated organizations, or those of the publisher, the editors and the reviewers. Any product that may be evaluated in this article, or claim that may be made by its manufacturer, is not guaranteed or endorsed by the publisher.Abbreviation

References

1. Sung H, Ferlay J, Siegel RL, Laversanne M, Soerjomataram I, Jemal A, et al. Global cancer statistics 2020: GLOBOCAN estimates of incidence and mortality worldwide for 36 cancers in 185 countries. *CA Cancer J Clin* (2021) 71:209–49. doi: 10.3322/caac.21660

2. Linehan WM, Ricketts CJ. The cancer genome atlas of renal cell carcinoma: findings and clinical implications. *Nat Rev Urol* (2019) 16:539–52. doi: 10.1038/s41585-019-0211-5

3. Capitanio U, Montorsi F. Renal cancer. *Lancet* (2016) 387:894–906. doi: 10.1016/S0140-6736(15)00046-X

4. Chowdhury N, Drake CG. Kidney cancer: An overview of current therapeutic approaches. *Urol Clin North Am* (2020) 47:419–31. doi: 10.1016/j.ucl.2020.07.009

5. Moch H, Cubilla AL, Humphrey PA, Reuter VE, Ulbright TM. The 2016 WHO classification of tumours of the urinary system and Male genital organs-part a: Renal, penile, and testicular tumours. *Eur Urol* (2016) 70:93–105. doi: 10.1016/j.eururo.2016.02.029

6. Lee MH, Jarvinen P, Nisen H, Bruck O, Ilander M, Uski I, et al. T And NK cell abundance defines two distinct subgroups of renal cell carcinoma. *Oncoimmunology* (2022) 11:1993042. doi: 10.1080/2162402X.2021.1993042

7. Fridman WH, Pages F, Sautes-Fridman C, Galon J. The immune contexture in human tumours: impact on clinical outcome. *Nat Rev Cancer* (2012) 12:298–306. doi: 10.1038/nrc3245

8. Kim S, Kim A, Shin JY, Seo JS. The tumor immune microenvironmental analysis of 2,033 transcriptomes across 7 cancer types. *Sci Rep* (2020) 10:9536. doi: 10.1038/s41598-020-66449-0

9. Bai D, Feng H, Yang J, Yin A, Qian A, Sugiyama H. Landscape of immune cell infiltration in clear cell renal cell carcinoma to aid immunotherapy. *Cancer Sci* (2021) 112:2126–39. doi: 10.1111/cas.14887

10. Obradovic A, Chowdhury N, Haake SM, Ager C, Wang V, Vlahos L, et al. Single-cell protein activity analysis identifies recurrence-associated renal tumor macrophages. *Cell* (2021) 184:2988–3005 e2916. doi: 10.1016/j.cell.2021.04.038

11. Errarte P, Larrinaga G, Lopez JI. The role of cancer-associated fibroblasts in renal cell carcinoma. an example of tumor modulation through tumor/non-tumor cell interactions. *J Adv Res* (2020) 21:103–8. doi: 10.1016/j.jare.2019.09.004

12. Zhang Z, Li Z, Liu Z, Zhang X, Yu N, Xu Z. Identification of microenvironment-related genes with prognostic value in clear cell renal cell carcinoma. *J Cell Biochem* (2020) 121:3606–15. doi: 10.1002/jcb.29654

13. Ito M, Mimura K, Nakajima S, Saito K, Min AKT, Okayama H, et al. Immune escape mechanism behind resistance to anti-PD-1 therapy in gastrointestinal tract metastasis in malignant melanoma patients with multiple metastases. *Cancer Immunol Immunother* (2022) 71:2293–300. doi: 10.1007/s00262-022-03154-z

14. Zabransky DJ, Danilova L, Leatherman JM, Lopez-Vidal TY, Sanchez J, Charmsaz S, et al. Profiling of murine syngeneic HCC tumor models as a framework to understand anti-PD-1 sensitive tumor microenvironments. *Hepatology* (2022) 10:1002. doi: 10.1002/hep.32707

15. Gonzalez-Silva L, Quevedo L, Varela I. Tumor functional heterogeneity unraveled by scRNA-seq technologies. *Trends Cancer* (2020) 6:13–9. doi: 10.1016/j.trecan.2019.11.010

16. Hernandez Martinez A, Madurga R, Garcia-Romero N, Ayuso-Sacido A. Unravelling glioblastoma heterogeneity by means of single-cell RNA sequencing. *Cancer Lett* (2022) 527:66–79. doi: 10.1016/j.canlet.2021.12.008

17. Hao D, Han G, Sinjab A, Gomez-Bolanos LI, Lazcano R, Serrano A, et al. The single-cell immunogenomic landscape of b and plasma cells in early-stage lung adenocarcinoma. *Cancer Discovery* (2022) 12:2626–45. doi: 10.1158/2159-8290.CD-21-1658

18. Baslan T, Hicks J. Unravelling biology and shifting paradigms in cancer with single-cell sequencing. *Nat Rev Cancer* (2017) 17:557–69. doi: 10.1038/nrc.2017.58

19. Langfelder P, Horvath S. WGCNA: an r package for weighted correlation network analysis. *BMC Bioinf* (2008) 9:559. doi: 10.1186/1471-2105-9-559

20. Ljungberg B, Albiges L, Abu-Ghanem Y, Bedke J, Capitanio U, Dabestani S, et al. European Association of urology guidelines on renal cell carcinoma: The 2022 update. *Eur Urol* (2022) 82:399–410. doi: 10.1016/j.eururo.2022.03.006

21. Benhamouda N, Sam I, Epaillard N, Gey A, Phan L, Pham HP, et al. Plasma CD27, a surrogate of the intratumoral CD27-CD70 interaction, correlates with immunotherapy resistance in renal cell carcinoma. *Clin Cancer Res* (2022) 28:4983-94. doi: 10.1158/1078-0432.CCR-22-0905

22. West LC, Cresswell P. Expanding roles for GILT in immunity. *Curr Opin Immunol* (2013) 25:103–8. doi: 10.1016/j.coi.2012.11.006

23. Fan Y, Wang X, Li Y. IFI30 expression predicts patient prognosis in breast cancer and dictates breast cancer cells proliferation *via* regulating autophagy. *Int J Med Sci* (2021) 18:3342–52. doi: 10.7150/ijms.62870

24. Rausch MP, Meador LR, Metzger TC, Li H, Qiu S, Anderson MS, et al. GILT in thymic epithelial cells facilitates central CD4 T cell tolerance to a tissue-restricted, melanoma-associated self-antigen. *J Immunol* (2020) 204:2877–86. doi: 10.4049/jimmunol.1900523

25. Lei K, Xia Y, Wang XC, Ahn EH, Jin L, Ye K. C/EBPbeta mediates NQO1 and GSTP1 anti-oxidative reductases expression in glioblastoma, promoting brain tumor proliferation. *Redox Biol* (2020) 34:101578. doi: 10.1016/j.redox.2020.101578

26. Lin IY, Yen CH, Liao YJ, Lin SE, Ma HP, Chan YJ, et al. Identification of FKBP11 as a biomarker for hepatocellular carcinoma. *Anticancer Res* (2013) 33:2763–9.

27. Hagedorn M, Siegfried G, Hooks KB, Khatib AM. Integration of zebrafish fin regeneration genes with expression data of human tumors in silico uncovers potential novel melanoma markers. *Oncotarget* (2016) 7:71567–79. doi: 10.18632/oncotarget.12257

28. Qiu L, Liu H, Wang S, Dai XH, Shang JW, Lian XL, et al. FKBP11 promotes cell proliferation and tumorigenesis *via* p53-related pathways in oral squamous cell carcinoma. *Biochem Biophys Res Commun* (2021) 559:183–90. doi: 10.1016/j.bbrc.2021.04.096

29. Selvakumar P, Owens TA, David JM, Petrelli NJ, Christensen BC, Lakshmikuttyamma A, et al. Epigenetic silencing of Na,K-ATPase beta 1 subunit gene ATP1B1 by methylation in clear cell renal cell carcinoma. *Epigenetics* (2014) 9:579–86. doi: 10.4161/epi.27795

30. Inge LJ, Rajasekaran SA, Yoshimoto K, Mischel PS, McBride W, Landaw E, et al. Evidence for a potential tumor suppressor role for the Na,K-ATPase beta1-subunit. *Histol Histopathol* (2008) 23:459–67. doi: 10.14670/HH-23.459

31. Dusetti NJ, Jiang Y, Vaccaro MI, Tomasini R, Azizi Samir A, Calvo EL, et al. Cloning and expression of the rat vacuole membrane protein 1 (VMP1), a new gene

activated in pancreas with acute pancreatitis, which promotes vacuole formation. *Biochem Biophys Res Commun* (2002) 290:641–9. doi: 10.1006/bbrc.2001.6244

32. Lin W, Sun Y, Qiu X, Huang Q, Kong L, Lu JJ. VMP1, a novel prognostic biomarker, contributes to glioma development by regulating autophagy. *J Neuroinflamm* (2021) 18:165. doi: 10.1186/s12974-021-02213-z

33. Loncle C, Molejon MI, Lac S, Tellechea JI, Lomberk G, Gramatica L, et al. The pancreatitis-associated protein VMP1, a key regulator of inducible autophagy, promotes Kras(G12D)-mediated pancreatic cancer initiation. *Cell Death Dis* (2016) 7:e2295. doi: 10.1038/cddis.2016.202

34. Zheng L, Chen L, Zhang X, Zhan J, Chen J. TMEM49-related apoptosis and metastasis in ovarian cancer and regulated cell death. *Mol Cell Biochem* (2016) 416:1–9. doi: 10.1007/s11010-016-2684-3

35. Folkerts H, Wierenga AT, van den Heuvel FA, Woldhuis RR, Kluit DS, Jaques J, et al. Elevated VMP1 expression in acute myeloid leukemia amplifies autophagy and is protective against venetoclax-induced apoptosis. *Cell Death Dis* (2019) 10:421. doi: 10.1038/s41419-019-1648-4

36. Amirfallah A, Arason A, Einarsson H, Gudmundsdottir ET, Freysteinsdottir ES, Olafsdottir KA, et al. High expression of the vacuole membrane protein 1 (VMP1) is a potential marker of poor prognosis in HER2 positive breast cancer. *PloS One* (2019) 14: e0221413. doi: 10.1371/journal.pone.0221413

37. Wang C, Peng R, Zeng M, Zhang Z, Liu S, Jiang D, et al. An autoregulatory feedback loop of miR-21/VMP1 is responsible for the abnormal expression of miR-21 in colorectal cancer cells. *Cell Death Dis* (2020) 11:1067. doi: 10.1038/s41419-020-03265-4

38. Senbabaoglu Y, Gejman RS, Winer AG, Liu M, Van Allen EM, de Velasco G, et al. Tumor immune microenvironment characterization in clear cell renal cell carcinoma identifies prognostic and immunotherapeutically relevant messenger RNA signatures. *Genome Biol* (2016) 17:231. doi: 10.1186/s13059-016-1092-z

Frontiers in Oncology

Advances knowledge of carcinogenesis and tumor progression for better treatment and management

The third most-cited oncology journal, which highlights research in carcinogenesis and tumor progression, bridging the gap between basic research and applications to imrpove diagnosis, therapeutics and management strategies.

Discover the latest Research Topics

See more →

Frontiers

Avenue du Tribunal-Fédéral 34
1005 Lausanne, Switzerland
frontiersin.org

Contact us

+41 (0)21 510 17 00
frontiersin.org/about/contact